DOT/FAA/AR-97/100

Office of Aviation Research
Washington, D.C. 20591

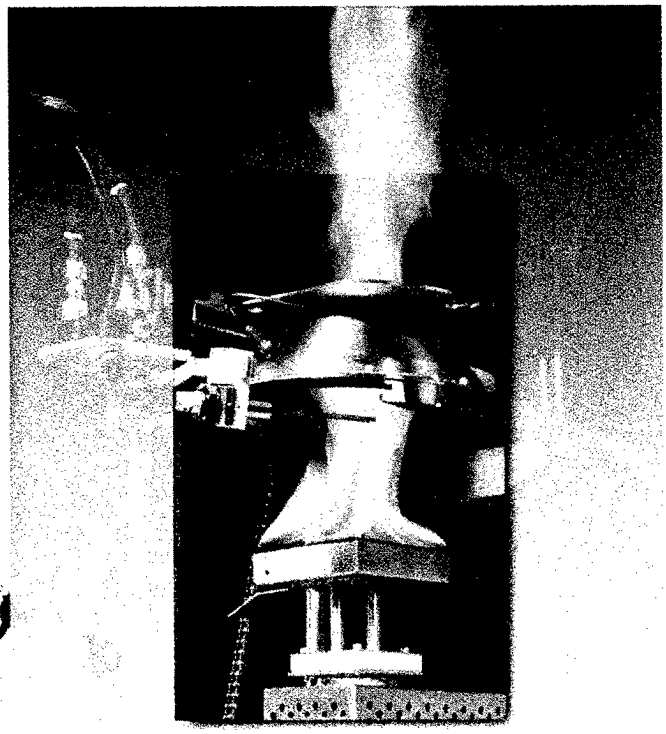

Fire-Resistant Materials: Progress Report

November 1998

Final Report

U.S. Department of Transportation
Federal Aviation Administration

NOTICE

Technical Report Documentation Page

1. Report No.	2. Government Accession No.	3. Recipient's Catalog No.
DOT/FAA/AR-97/100		

4. Title and Subtitle	5. Report Date
FIRE-RESISTANT MATERIALS: PROGRESS REPORT	Novemer 1998
	6. Performing Organization Code: AAR-422
7. Author(s): Edited by Richard E. Lyon	8. Performing Organization Report No.
9. Performing Organization Name and Address: Federal Aviation Administration, Airport and Aircraft Safety, Research and Development, William J. Hughes Technical Center, Atlantic City International Airport, NJ 08405	10. Work Unit No. (TRAIS)
	11. Contract or Grant No.
12. Sponsoring Agency Name and Address: U.S. Department of Transportation, Federal Aviation Administration, Office of Aviation Research, Washington, DC 20591	13. Type of Report and Period Covered: Final Report
	14. Sponsoring Agency Code

15. Supplementary Notes

16. Abstract

This report details the research being conducted by the Federal Aviation Administration (FAA) to develop fire-safe cabin materials for commercial aircraft. The objective of the Fire-Resistant Materials program is to eliminate burning cabin materials as a cause of death in aircraft accidents. Long-term activities include the *synthesis* of new, thermally stable, low fuel value organic and inorganic polymer systems. The synthesis effort is supported by fundamental research to understand polymer combustion and fire resistance mechanisms using numerical and analytic *modeling* and the development of new *characterization* techniques. Aircraft materials which are targeted for upgraded fire resistance are (1) thermoset resins for interior decorative panels, secondary composites, and adhesives; (2) thermoplastics for decorative facings, telecommunication equipment, passenger service units, molded seat parts, transparencies, and electrical wiring; (3) textile fibers for upholstery, carpets, decorative murals, tapestries; and (4) elastomers/rubber for seat cushions, pillows, and sealants. During the first 2 years of the program (1995-1996) we have made significant progress in achieving our interim goal of a 50 percent reduction in the heat release rate of cabin materials by 2005 and zero heat release rate cabin materials by 2018 with respect to the 1996 baseline for new aircraft.

A previous report, Fire-Resistant Materials: Research Overview, DOT/FAA/AR-97/99, summarizes the background and technical objectives of the program and serves as an introduction to the present document.

17. Key Words	18. Distribution Statement
Fire, Aircraft, Cabin materials, Flammability, Heat release rate, Polymer, Plastic, Resin, Rubber	This document is available to the public through the National Technical Information Service (NTIS), Springfield, Virginia 22161.

19. Security Classif. (of this report)	20. Security Classif. (of this page)	21. No. of Pages	22. Price
Unclassified	Unclassified	295	

Form DOT F1700.7 (8-72) Reproduction of completed page authorized

TABLE OF CONTENTS

Page

EXECUTIVE SUMMARY vii

MATERIALS 1

Development and Molecular Characterization of Polybenzoxazines: A New Class of Versatile, High-Performance Phenolic Resins for Flame-Retardant Applications
Hatsuo Ishida 3

Phosphine Oxide Copolymers: The Synthesis and Characterization of New Thermoplastic Fire-Resistant Materials
James E. McGrath, Ph.D. 11

Phosphine Oxide Copolymers: Synthesis and Characterization of Advanced Fire-Resistant Engineering Thermoplastic
James E. McGrath, Ph.D. 21

Poly-X™ Self-Reinforced Polyphenylenes: New High-Performance, Fire-Resistant Materials for Aircraft Cabin Interiors
Mark S. Trimmer, Mark R. Isomaki, and Mike Ulman 27

Enediynes and Fullerenes
Synthesis and Characterization of New Flame-Resistant Materials
James M. Tour 35

Polyphosphazenes: Flame Retardants for Aircraft Applications
Harry R. Allcock 43

Flame-Retardant Precursors to Heterocyclic Polymers
Chunping Gao and Simon W. Kantor 51

Thermally Stable Silphenylene Vinyl Siloxane Elastomers and Their Blends
H. Dennis, Zhu, Simon, W. Kantor, and William J. MacKnight 59

Thermally Labile Polymers that Release Radical Traps: Polycarbodiimides
Bruce Novak 76

Preparation of Cyanate Ester Monomers
Ada Casares, Ph.D. 83

Environmentally Friendly Inorganic Additives
Nanocomposites: A Revolutionary New Flame-Retardant Approach
Jeffrey W. Gilman and Takashi Kashiwagi 92

Surface-Active Flame Retardants
Wei Chen and Thomas J. McCarthy 105

Mutually Interpenetrating Organic-Inorganic Networks
Bruce Novak 111

Organic-Inorganic Hybrid Polymers From Renewable Sources
S. Baliat, S.L. Jouppi, R.M. Laine, R. Tamaki, D.R. Treadwell,
C. Zhang, R. Baranwal, and C. Worthen 117

Fire-Resistant Aluminosilicate Composites
Richard E. Lyon 126

Development of Silicone Resins for Use in Fabricating Low-Flammability
Composite Materials
Timothy C. Chao, Gary T. Burns, Dimitris E. Katsoulis, and William C. Page 141

Fire-Retardent Polyetherimide Nanocomposites
Jongdoo Lee, Tohru Takekoshi, and Emmanuel P. Giannelis 149

Polyphosphazene Blends
Michael M. Coleman and Paul C. Painter 155

MODELING 167

Molecular Dynamics Modeling of Thermal Degradation in Polymers
Marc R. Nyden 169

Molecular Modeling and Microcalorimetry for Polymer Pyrolysis and Flammability
Phillip R. Westmoreland, Karin Rotem, and Taline Inguilizian 181

Atomistic Molecular Models of Amorphous Polybenzoxazine at Bulk Density and
as a Thin Film
Won-kook Kim and Wayne L. Mattice 187

A Pyrolysis Model for Char-Forming Polymers
Richard E. Lyon 193

Computational Model of Intumescent Char Formation
Kathryn M. Butler 206

CHARACTERIZATION 215

Polyimides
Stephen Z. D. Cheng 217

Thermomechanical Stability of Resins and Composites
A. J. Lesser, G. Schueneman, and C. Comeaux 229

A Microscale Combustion Method for Determining Flammability Parameters of Polymers
Richard N. Walters and Richard E. Lyon 241

Integral Method of Nonisothermal Kinetic Analysis
Richard E. Lyon 245

In Situ Flame Chemistry by Remote Spectroscopy
S. Michael Angel 259

Flame-Retarding Properties of Phosphorus Containing Poly(amic acid)
Byung-Wook Jo, Jin-Hae Chang, and Richard J. Farris 266

Fire Calorimetry of Flame-Retarded Polymers
D.J. Priest 279

EXECUTIVE SUMMARY

Forty percent of the passengers who survive the impact of an aircraft accident subsequently die in a postcrash fire. Unless this percentage is reduced or the accident rate decreases, the number of fire fatalities will increase by 4 percent each year with the expected growth in passenger air traffic. Compounding the upward trend in aircraft fire fatalities is the additional fire load associated with the 1 percent annual growth in the use of lightweight, combustible polymers and composites for aircraft interiors and structures. Current aircraft utilize several tons of combustible plastics for cabin interior components (figures 1 and 2). This is a fire load comparable to the equivalent weight of aviation fuel. The cabin fire load will approximately double in the very large (800 passenger) airplanes under development by airframe manufacturers unless ultra fire-resistant materials become available. The use of materials with improved fire resistance (relative to commodity plastics) was mandated by the Federal Aviation Administration (FAA) in 1987 with requirements for the burning rate and flame spread of seat cushions and in 1990 with the establishment of regulations limiting the heat release rate of large area cabin interior components. These regulations provide for an additional 2-4 minutes of cabin escape time in the event of an aircraft accident involving a postcrash fuel fire outside the cabin. Further improvement in cabin material fire-safety is unlikely without government-sponsored research because the market is limited to passenger aircraft cabins and does not justify the research investment by private industry. In response to this situation, the FAA has initiated a proactive, long-range research effort in Fire-Resistant Materials to identify and develop the enabling materials technology for a cost-effective, fireproof passenger aircraft cabin. In combination with other fire-safety system improvements, ultra-fire-resistant materials will eliminate catastrophic inflight fuselage fires and provide a minimum of 10 minutes of passenger escape time in a postcrash fire.

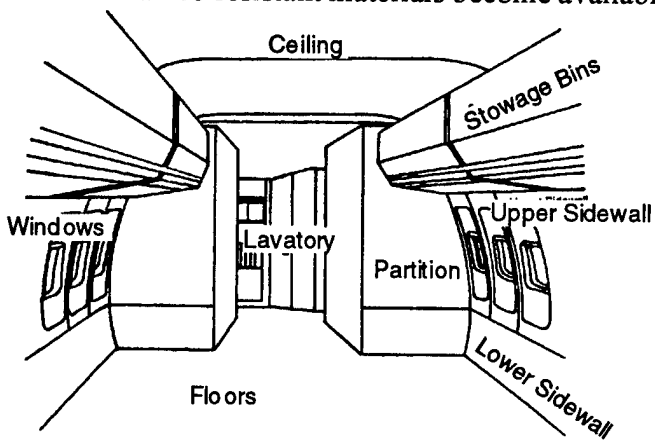

FIGURE 1. FLAMMABLE CABIN COMPONENTS

The objective of the Fire-Resistant Materials program is to eliminate burning cabin materials as a cause of death in aircraft accidents. The research is basic in nature and focuses on the synthesis, modeling, processing, and characterization of new materials and materials combinations. In accord with the recommendations of the National Research Council's Materials Advisory Board in their report "Fire- and Smoke-Resistant Interior Materials for Commercial Transport Aircraft," (NMAB-477-1, National Academy Press, 1995) near term technical approaches include modification of specialty and commodity polymers using additives and processing routes. Databasing of materials' fire performance in micro-, bench-, and full-scale testing supports science-based studies of polymer combustion and identifies critical fire performance properties to guide development. Long-term activities include the synthesis of new, thermally stable, low fuel value organic/inorganic polymer systems. The synthesis effort is supported by fundamental research to understand polymer combustion and fire resistance mechanisms using numerical and analytic modeling and the development of new characterization techniques.

The output of this research will be an order-of-magnitude reduction in cabin fire hazards relative to current cabin materials at comparable cost and functionality. Since the heat release rate of burning materials is the primary fire hazard indicator, the technical objective is to develop low-cost, lightweight, serviceable polymers and composite materials with zero heat release rate as measured by FAR 25.853(a-1), "Heat Release Rate Test for Cabin Materials." Materials with a zero heat release rate will provide sufficient passenger escape time in a postcrash fuel fire to ensure survivability. With respect to the 1996 baseline for new aircraft, individual fire-resistant materials will demonstrate a 50 percent reduction in heat release rate by the year 2002. Prototype cabin components fabricated from combinations of fire-resistant materials will demonstrate zero heat release rate by the year 2010. The potentially higher initial cost of fire-resistant cabin materials will be offset by user financial incentives which include shorter process cycles, better durability, and lower heat release rate.

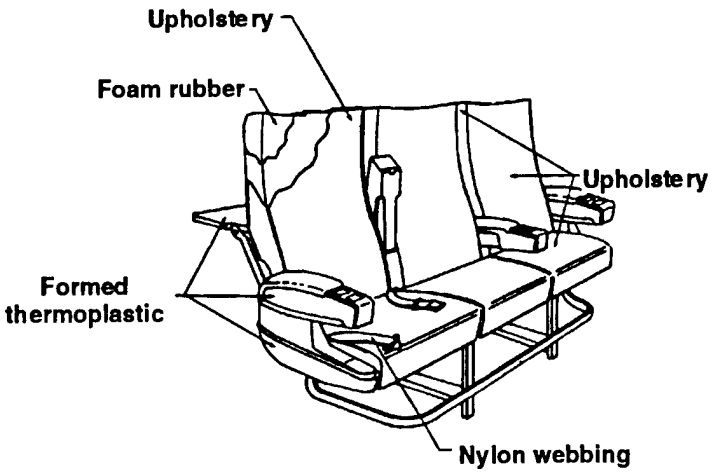

FIGURE 2. FLAMMABLE SEAT COMPONENTS

The fire-resistant materials program is executed from an in-house technology base at the William J. Hughes Technical Center, Atlantic City International Airport, NJ, through FAA-industry partnerships and university-based research consortia. Direct funding by several Fortune 100 aircraft and chemical companies to the FAA-university-industry consortia covers about 30 percent of research costs for fire safe materials. During the first 2 years of the program (1995-1996) we have made significant progress in achieving our interim goal of a 50 percent reduction in the heat release rate of cabin materials by 2005 and zero heat release rate cabin materials by 2018. The progress to date in this program reflects the commitment of Congress, the FAA, and the materials and aircraft industries to improving the safety of air transportation. This collaboration has resulted in the outstanding technical work which is summarized in this report. The FAA is grateful to all of the participating researchers in government, industry, and academia whose ideas and hard work are creating the enabling technology for a fireproof passenger aircraft cabin.

MATERIALS

DEVELOPMENT AND MOLECULAR CHARACTERIZATION OF POLYBENZOXAZINES: A NEW CLASS OF VERSATILE, HIGH-PERFORMANCE PHENOLIC RESINS FOR FLAME-RETARDANT APPLICATIONS

Hatsuo Ishida
The NSF Center for Molecular and Micro Structure of Composites (CMMC)
Department of Macromolecular Science
Case Western Reserve University
Cleveland, Ohio 44106-7202

ABSTRACT

A new class of phenolic resins has been developed. As a result of ring-opening benzoxazine chemistry rather than the traditional condensation phenolic chemistry, many problems associated with the traditional phenolic materials have been minimized or eliminated. The rich molecular design flexibility allows mechanical and physical properties to be tailored to specific needs. A wide variety of raw materials offers opportunities for economical advantages and for the optimization of their mechanical and physical properties. Polybenzoxazines show a wide spectrum of mechanical and physical properties. Their char yields are inherently very high, ranging from 35% to 87%. Near zero shrinkage upon polymerization, low water uptake, and excellent process ability offer a good balance in properties for structural applications.

INTRODUCTION

Thermosetting resins undergo a volumetric shrinkage during polymerization in the range of 2% to 6% even for relatively low-shrinkage materials. Examples of a few higher-shrinking materials include volumetric shrinkage of methyl methacrylate by 21% and that of propylene oxide by 17% upon polymerization. Materials that exhibit zero shrinkage or expansion would possess attractive opportunities for mechanical interlocking to a substrate which would be suitable for adhesives, sealants, and coatings. Resins without shrinkage would also be advantageous for such applications as precision casings, dental composites, and high-strength composites. Poor fiber-matrix adhesion or the voids and micro cracks within the matrix often lead to premature failure in composite materials. Poor interfacial adhesion can be traced to the formation of residual stresses which are at least partially caused by cure shrinkage[1]. However, until Bailey and his coworkers introduced and developed their series of spiro-orthocarbonates, spiro-orthoesters, and other strained bicyclic compounds, no material with these characteristics was known[1-5]. These materials have been shown to polymerize with either zero shrinkage or even a slight expansion. A volumetric expansion of up to 17% has been demonstrated for amorphous polymers cured from crystalline monomers[5].

Practical applications of Bailey's materials have been limited to cases where they are co-polymerized with epoxy resins[6-14]. The spiro-orthoesters and orthcarbonates have been shown

to improve bonding strength in adhesives and improve mechanical strength in composites as volume control additives copolymerized with epoxies[11-14]. But, others have failed to see these improvements[13] and have reported that the reduced shrinkage is to a large extent caused by a lowering of the glass transition of the epoxy by the addition of these materials rather than the reported expansion upon polymerization[15, 16]. These expanding spiro-orthoester polymers seem to have quite limited utility as homopolymers for mechanically demanding structural materials.

Recently, however, a family of benzoxazine-based phenolic resins have been developed in our laboratory that appear to display not only apparent expansion or zero shrinkage upon polymerization, but also properties as homopolymers that equal or exceed the performance values established by conventional phenolic and epoxy resins.

Materials and Chemistry of Traditional Phenolics

An ordinary phenolic resin utilizes either acid or base catalyzed reaction products of phenol and formaldehyde. The acid catalyzed phenolic resins tend to form linear oligomers:

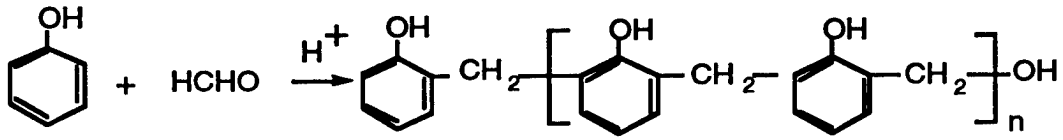

On the other hand, base catalyzed phenolic resins tend to form highly substituted compounds:

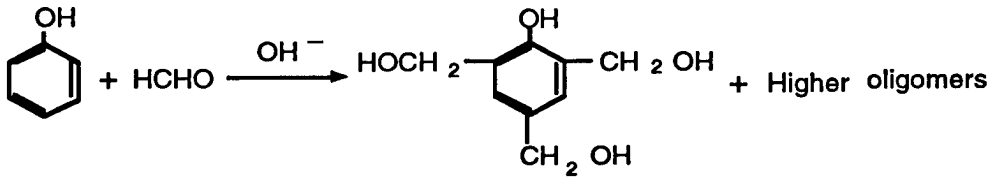

With acid acting as a further catalyst, the phenolic resins undergo curing reactions through condensation polymerization, liberating water molecules. Due to the complex reaction route, the molecular structure of the final polymer is poorly understood. Although the mechanical properties of the cured phenolic resins depend strongly on the conditions employed, phenolic resins give a high char yield on combustion typically ranging 35% to 55%. Decomposition begins at 350°C and continues up to 600°C. Auto ignition temperature in air is above 900°C (see Table 2 for additional properties).

Chemistry of Polybenzoxazines, a New Class of Phenolic Resins

The chemistry of the new phenolic system is based on benzoxazine. The chemistry of monomeric systems[17-23] and attempts to produce polymers[24-26] have been reported in the literature, although no mechanical and physical properties have been discussed. The basic chemistry is described as follows:

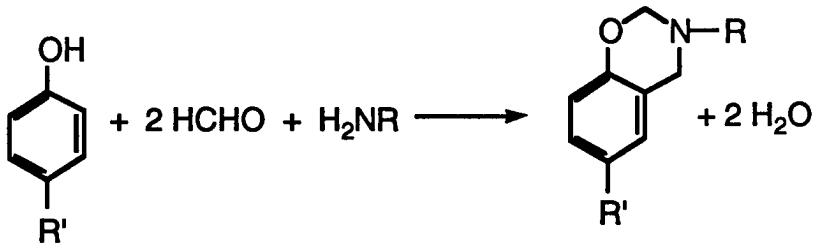

There are many phenolic derivatives available which provide great flexibility in molecular design of this phenolic resin. The amine component allows additional molecular design flexibility. Indeed, if the OH functionality is exchanged with a primary amine, the same compound can be used for the amine part of the ingredient. Even more abundant selections of amine compounds are available as potential candidates for the comonomer.

The synthesized compound is then subjected to thermal polymerization with or without a mild catalyst and the reaction chemistry is expressed below:

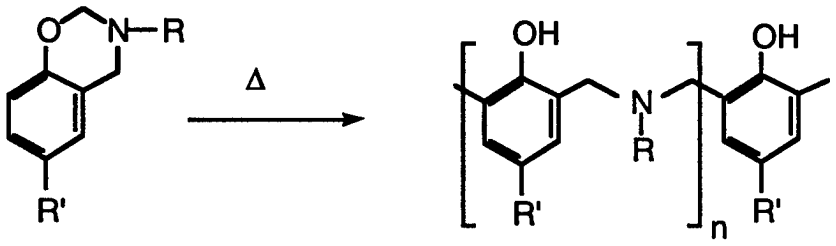

The ring-opening polymerization takes place with purified monomer (99 + %) typically in the range between 140°C and 220°C through the opening of the benzoxazine ring[27, 28]. The fundamental polymerization mechanism appears to be ionic polymerization; however, detailed molecular mechanisms have not been deduced yet. In the presence of phenol, which can act as an initiator and a catalyst, the polymerization temperature can be reduced by approximately 30-60°C[29].

The *monofunctional* benzoxazine leads to essentially a *linear polymer*, though the molecular weight is only on the order of 500-2000 g/mol[26]. The polymers of interest for structural applications are the *difunctional or polyfunctional benzoxazine* resins which lead to *cross-linked polymers.* The difunctional benzoxazine monomers have tetra-functionality in terms of the number of reaction sites[4] per monomer.

While the use of phenolic derivatives, formaldehyde, and amines is not immune to the toxicity argument, the phenolic derivatives are somewhat less toxic than phenol, and the release of by-products, such as formaldehyde or amine, during benzoxazine polymerization is substantially less than those released during the traditional phenolic curing process. It should be emphasized that *the ring-opening polymerization mechanism produces no water,* unlike the water-producing condensation polymerization of ordinary phenolic resins. *An extremely unusual aspect of this resin is the near-zero shrinkage after polymerization*[30, 31]. No such monomers which exhibit this behavior other than spiro-ortho compounds have been reported in the literature. Some examples of volumetric expansion or near-zero shrinkage of polybenzoxazines are listed in Table 1[31]. It should be noted that the density of the monomer listed in Table 1 is

that of the amorphous state, thus eliminating the contribution from the expansion due to the crystalline-to-amorphous transition. The monomer was polymerized at 150°C and the monomer and polymer densities were measured at room temperature.

Table 1. Volumetric Changes From Amorphous Monomer to Amorphous Polymer

Abbreviation*	Phenol	Amine	Density of Monomer	Density of Polymer	Volume Increase (%)
B-m	bisphenol-A	methylamine	1.159 ± 0.001	1.122 ± 0.002	3.2
B-e	bisphenol-A	ethylamine	1.109 ± 0.001	1.104 ± 0.002	0.41
B-c	bisphenol-A	cyclohexylamine	1.123 ± 0.003	1.118 ± 0.0006	0.43
B-a	bisphenol-A	aniline	1.200 ± 0.001	1.195 ± 0.002	0.40
B-c	4,4¢-dihy-droxylben-zophenone	methylamine			0.40

* All benzoxazine resins use formaldehyde as the common component.

Synthesis of the monomer generally shows yields of nearly 70%-95% depending on the component, temperature, time, solvent, and synthetic procedure. However, an as-synthesized product leads to a polymerized product in a manner similar to epoxy resins where a mixture of monomer and higher oligomers are used as initial resin. The oligomers can participate in the polymerization process. The polymerized products from the purified and as-synthesized mixture show similar mechanical properties. Thus, 100% of the reaction products from monomer synthesis other than the solvent and water can be used (water is produced during the monomer synthesis, although it is not produced during the polymerization process). Use of the as-synthesized products is especially attractive for industrial application where purification is an undesirable additional step. Attempts to scale up the production of benzoxazine resins in the 20-100 kg quantities have been successful. We have recently developed a solventless method for benzoxazine resin preparation. This new synthetic method eliminates the use of dioxane or any other undesirable solvents[32]. Furthermore, some of the benzoxazine resins use economically comparable raw materials to ordinary phenolic resins.

Molecular design flexibility deserves some mention. Traditional phenolic resin starts either with novolac or resols. The monofunctional phenol can be substituted with various groups to add some property changes. However, the property ranges achieved by this approach are limited. Another approach is to use multifunctional phenols as in the benzoxazine chemistry. Unfortunately, the novolacs made by this method will lead to unacceptably high viscosity which develops processability problems, although the property ranges that can be achieved by this approach are much wider than simple substitution of monofunctional phenols. Benzoxazine chemistry combines the best of both above strategies. It can lead to an extremely wide property range while maintaining low viscosities (about 0.1-0.2 Pa-s at 150°C) during processing[33, 34]. The oligomers that contain phenolic groups can act as latent catalysts, if catalysts are desired, though the as-synthesized benzoxazine resins are quite stable below 100°C[35]. The benzoxazine polymerization is autocatalyzed. Other catalysts, such as weak acids and amines, can also be used as catalysts. Thus, benzoxazine resins exhibit superb processability that leads to very low void contents (typically less than 1.0%) when made into fiber-reinforced composites[36, 37].

At a first glance, the thermal stability of this class of Mannich base polymers might seem problematic since it is well known that the Mannich bridge, $-CH_2-N(R)-CH_2-$, shows either thermal degradation or a reverse Mannich reaction at moderate temperatures around 100-120°C. Unexpectedly, however, TGA results of many polybenzoxazines do not show any evidence of low-temperature thermal degradation. This surprisingly good thermal stability is possibly due to the stabilization of the Mannich bridges by the very strong intramolecular hydrogen bonding between the phenolic OH groups and the nitrogen atom of the Mannich bridges[38]. A TGA curve of the polybenzoxazine based on 4,4′-dihydroxybenzophenone and aniline is shown in Figure 1[37]. The decomposition temperature as defined by the 5% reduction of the weight is above 400°C. No effect of oxygen is seen until 560°C in the short-term test. The mechanical properties of this resin and its carbon fiber composite are shown in Tables 2 and 3, respectively, for comparison to traditional materials.

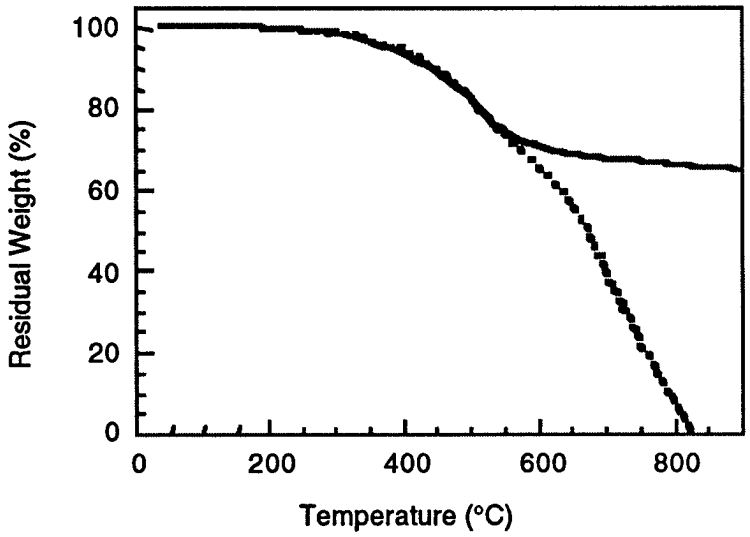

Figure 1. TGA Curves of Benzophenone/Aniline Based Polybenzoxazine. Experiments were performed under nitrogen (solid curve) and air (dotted curve).

Table 2. The Physical and Mechanical Properties of the Polybenzoxazines (PBZ's) and the General References of Other Resins

Materials	Tensile Strength (MPa)	Tensile Modulus (GPa)	Strain at break, Tensile (%)	Density (g/cm^3)	T_g (°C)
44Oa PBZ*	62	>6	2.3	1.250	340
Phenolics**	35 - 62	2.7 - 4.8	1.5 - 2.0	1.24 - 1.32	~ 175
Epoxies	28 - 90	2.4	3 - 6	1.11 - 1.40	150 - 261
Polyimides, thermoset***	56	3.8	~ 1.0	1.41 - 1.90	230 - 380

* Cured at 290°C for 1 hr
** ref (39, 40)
*** ref (41, 42)

Table 3. The Mechanical Properties of Carbon Fiber-Reinforced Polybenzoxazine Composites and PMR-15 Thermosetting Polyimide Composites

Carbon Fibers***	Resins	Curing Conditions	Flexural Strength MPa, (s*)	Flexural Modulus GPa, (s*)	Flexural Toughness kJ/m^2, (s*)	Interlaminar Shear Strength MPa, (s*)
T-650/42, 6K	44Oa PBZ**	260°C for 1 h	2160 (318)	230 (27)	52 (8.5)	81 (10.0)
T-650/35, 6K	PMR-15 polyimide	288°C for 16 h	1650 (-)	140 (-)	-	105 (-)

* standard deviation

** 4,4'–dihydroxybenzophenone/aniline based polybenzoxazine

*** optimum surface treatment of carbon fibers for polybenzoxazine is not yet known, thus the sizing that is used for polyimide is also used for polybenzoxazine.

It should be emphasized that the mechanical and physical properties can be tailored in a very wide range by changing the structure of the phenolic derivative and the primary amine. Saturation water uptake of bisphenol-A/aniline or bisphenol-A/methylamine-based polybenzoxazines are 1.9% and 1.3% by weight, respectively, after more than 1600 days of immersion in water at room temperature. This is less than the majority of epoxy resins. The dielectric constant is 3.5 or less and the loss factor is less than 0.01. A comparison of the characteristics of ordinary phenolic resins and polybenzoxazine resins is listed below.

- Advantages of Traditional Phenolics
  - — Nonflammable
  - — Inexpensive
  - — High thermal and chemical resistance
- Disadvantages of Traditional Phenolics
  - — Produces water and other small molecules during cure
  - — Very brittle
  - — Short shelf life
  - — Very poor molecular design flexibility
- Advantages of Benzoxazine Chemistry
  - — Near-zero shrinkage during polymerization
  - — No catalyst needed (thermal initiation, but catalyst can be used)
  - — No water produced (ring-opening polymerization)
  - — Excellent mechanical properties
  - — Low water uptake and low dielectric constants
  - — Long shelf life
  - — High char yield
  - — Extremely versatile molecular design flexibility
  - — Excellent processability

In addition, all the advantages of the traditional phenolics are preserved.

CONCLUSIONS

Polybenzoxazines have shown a good balance of the mechanical and physical properties that are suitable for structural applications. Unusual properties have been observed. These include very high char yield, near-zero shrinkage or expansion of volume upon polymerization, low water absorption, and high thermal properties. With excellent processability and molecular design flexibility, polybenzoxazines offer strong potential in many structural and other applications.

REFERENCES

1. Bailey and R.L. Sun, *Amer. Chem. Soc., Div. Polym. Chem. Prepr.*, **13**, 281 (1972).
2. Bailey, H. Katsuki, and T. Endo, *Amer. Chem. Soc., Div. Polym. Chem., Prepr.*, **14**, 1679 (1973).
3. Bailey, H. Iwama, and R. Tsushima, *J. Polym. Sci.*, **56**, 117 (1976).
4. Bailey and T. Endo, *J. Polym. Sci.*, **64**, 17 (1978).
5. Bailey and H. Katsuki, *Amer. Chem. Soc., Div. Polym. Chem., Prepr.*, **14**, 1169 (1973).
6. Shimbo, M. Ochi, and Y. Shigeta, *J. Appl. Polym. Sci.*, **26**, 2265 (1981).
7. Lim, M.R. Piggot, and W.J. Bailey, *SAMPE Q.*, **15**, 25 (1984).
8. Piggot and T. Pyshnov, *Polym. Mat. Sci. Eng.*, **54**, 18 (1986).
9. Pingsheng, Z. Shiquiang, and P. Caiyaun, *J. Mat. Sci.*, **24**, 1528 (1989).
10. Bailey, M.J. Amone, B. Issari, Y.-N. Lin, K. No, C.-Y. Pan, K. Saigo, J. Stanbury, S.-R. Tan, C. Wu, N. Yamakazi, and J. Zhou, *Polym. Mat. Sci. Eng.*, **54**, 23 (1986).
11. Cohen, C. Bluestein, R. Kozic, and D. Fergesen, *Polym. Mat. Sci. Eng.*, **54**, 12 (1986).
12. Thompson, E.F. Williams, and W.J. Bailey, *J. Dent. Res.*, **58**, 1522 (1979).
13. Pingsheng and Z. Zhou, *J. Mat. Sci.*, **26**, 3792 (1991).
14. Bailey, *Mat. Sci. Eng.*, **A126**, 271 (1990).
15. Shimbo, M. Ochi, T. Inamura, and M. Inoue, *J. Mat. Sci.*, **20**, 2965 (1985).
16. Ishida and J. Nigro, in "Polymer Characterization: Physical Property, Spectroscopic and Chromatographic Methods," C.D. Craver and T. Provder, Eds., Advanced Chemistry Series 227, Am. Chem. Soc., Washington D.C. (1990) p. 259.
17. Caldwell and T.R. Thompson, *Am. Chem. Soc.*, **61**, 765 (1939).
18. Bruson and C.W. McMullen, *J. Am. Chem. Soc.*, **63**, 270 (1941).
19. Cope and F.W. Holly, *J. Am. Chem. Soc.*, **66**, 1875 (1944).
20. Burke, *J. Am. Chem. Soc.*, **71**, 609 (1949).
21. Lane, Brit. Pat. No. 694,489 (1953).
22. Burke and E.L. Mortensen, *J. Org. Chem.*, **29**, 909 (1964).

23. Burke, J.L. Bishop, E.L. Mortensen, and W.N. Bauer, *J. Org. Chem.*, **30**, 3423 (1965).

24. Schreiber, German Offen. No. 2,255,504 (1973).

25. Schreiber, German Offen. No. 2,323,936 (1973).

26. Riess, J.M. Schwob, G. Guth, M. Roche, and B. Laude in "*Advances in Polymer Synthesis*," Polymer Science & Technology, Vol. 31, B. M. Culbertson and J.E. McGrath, Eds., Plenum, New York (1985) p. 27.

27. X. Ning and H. Ishida, *J. Polym. Sci. -Phys.*, **32**, 921 (1994).

28. X. Ning and H. Ishida, *J. Polym. Sci. Chem. Ed.*, **32**, 1121 (1994).

29. H. Ishida and Y. Roduriguez, *J. Appl. Polym. Sci.*, **58**, 1751 (1995).

30. H. Ishida and D.J. Allen, *J. Polym. Sci. Phys. Ed.*, **34**, 1019 (1996).

31. H. Ishida and H.Y. Low, *ACS Polym. Mat. Sci. Eng.*, (1996).

32. H. Ishida, U.S. Pat. No. 5,543,516, Aug. 6 (1996).

33. "Rheological Characterization of Curing of Benzoxazine Resins," H. Ishida and D. Allen, *ACS Polym. Mat. Sci. Eng.*, **73**, 496 (1995).

34. N. Suprapakorn, S. Dhumrongvaraporn, and H. Ishida, Polymer Composites (submitted).

35. H. Ishida and Y. Rodriguez, *Polymer* , **36**, 3151 (1995).

36. S.B. Shen and H. Ishida, *J. Mat. Sci.* (in press).

37. S.B. Shen and H. Ishida, *Polym. Comp.*, **17**, 710 (1996).

38. Dunkers, E.A. Zarate, and H. Ishida, *J. Phys. Chem.*, (in press).

39. Patridge in "Advanced Composites," I.K. Patridge Ed., Elsevier Applied Science, New York (1989) Chap. 2.

40. Suzuki, A. Nagai, M. Suzuki, and A. Takahashi, *J. Appl. Polym. Sci.*, **44**, 1807 (1992).

41. Kopf, in "Encyclopedia of Polymer Science and Engineering," Vol. 7, John Wiley & Sons, New York (1985) pp. 639-665.

42. "Encyclopedia '94," Modern Plastics, New York (1994) pp. 185-191.

PHOSPHINE OXIDE COPOLYMERS: THE SYNTHESIS AND CHARACTERIZATION OF NEW THERMOPLASTIC FIRE-RESISTANT MATERIALS

James E. McGrath, Ph.D.
Dept. of Chemistry
2108 Hahn Hall
Virginia Tech
Blacksburg, VA 24061-0344

September 1995 through October 1996

INTRODUCTION

Organic materials are widely utilized in aircraft interiors for various important functions such as carpets, seats, bins, appliance housings, communication devices, etc. The relevance of the fire safety of these materials to airline transportation is well acknowledged but poorly understood. There is an important need to further identify fundamental relationships between the molecular structure of the materials and their behavior in fires. This should assist in the rational design of fire-resistant cabins for commercial aircraft. It is considered that basic research on synthesis, characterization, and processing of new materials will be necessary to improve the fire performance of material systems. A summary of these features has recently been provided[1].

Thermoplastic materials offer attractive advantages including rapid processability by methodologies such as injection molding, film extrusion, and fiber spinning.[2] In addition, the likelihood of generating recyclable materials is recognized to be more straightforward than for the other option, e.g., thermosetting network systems. The author and his colleagues have been involved in novel phosphorus containing polymers now for over 5 years. Emphasis has been placed upon hydrolytically stable melt-processable high-performance polymeric materials that are capable of demonstrating either high glass-transition temperatures and/or high semicrystalline melting points. The latter are of interest for applications requiring excellent chemical resistance such as for textile fibers and many engineering thermoplastic applications. Amorphous high glass-transition temperature materials are an alternate possibility, and such systems would be favored where transparency and exceptionally high impact strength are sought. Both morphologies are possible in the systems investigated thus far. The triphenyl phosphine oxide unit is inherently non-coplanar and leads, in general, to amorphous homopolymers which display high transition temperatures, good optical transparency, very high char yields when exposed to either nitrogen or air (TGA experiments), ductile mechanical behavior, and good adhesion characteristics (especially to metals). Many of these same characteristics can be applied to semicrystalline copolymers where the composition of the triaryl phosphine oxide structure is limited to about 50 mole percent or less. Examples of systems already demonstrated include the poly(arylene ether ketone)s, polyimides, polybenzoxazoles, as well as polycarbonates, polyesters, and polyamides. In addition, poly(thioarylene phosphine oxides), which are analogous to polyphenylene sulfides, have also been synthesized.

Initial characterization of the homo- and copolymers was limited to thermogravimetric analysis (TGA) and rather crude laboratory Bunsen burner testing. However, these preliminary evaluations repeatedly demonstrated significant qualitative, but apparently fundamental, differences between the high-performance aromatic polymers which contained hydrolytically stable phosphorus and their controls.

Some of the homo- and copolymers, as mentioned earlier, showed remarkably high weight retention in both inert atmospheres, such as nitrogen, as well as more aggressive air or oxygen systems.

Physical addition or chemical incorporation of phosphorus into polymeric materials is a long-standing industrial approach for improving fire-resistant properties. Our previous papers have described synthesis procedures[4] and the preparation of novel monomers[5,6] as well as new functionalized oligomers and polymers[3,7-9]. In particular, several important features of the hydrolytically stable phosphorus carbon containing materials have been identified, including oxygen plasma resistance[10-12], polymer supported catalysis[13], structural adhesive[14], radiation resistance[15], and polymer blends[16]. One of our current research thrusts is to develop candidate adhesive and composite material systems based on polyimides. Such polyimides are anticipated to have excellent physical and mechanical properties, solvent resistance, and attractive fire resistance. We here describe the synthesis and characterization of linear diphenyl methyl phosphine oxide containing polyimides. The phosphine oxide groups in the backbone was expected to improve fire resistance. The important monomer bis(*m*-aminophenyl) methyl phosphine oxide (DAMPO), shown below, was prepared by an improvement of a literature method[17]. The synthesis and characterization of controlled thermoplastic and high gel fraction containing thermosetting network systems based on this diamine are reported herein.

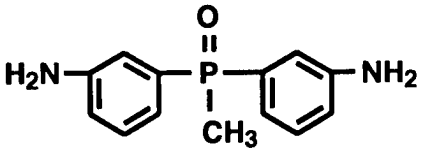

DAMPO

EXPERIMENTAL

Materials

1-Methyl-2-pyrrolidone (NMP), *o*-dichlorobenzene (*o*-DCB), triethylamine (Et_3N), ethanol, and methanol were purchased from Aldrich and used as received. Methyl triphenyl phosphonium bromide (Aldrich) was used as received. 2,2'-Bis[4-(3,4-dicarboxyphenoxy)phenyl]propane dianhydride (bisphenol-A dianhydride, BPADA, Ultem™ precursor) was kindly provided by General Electric and was dried at ~170°C under vacuum prior to use. Pyromellitic dianhydride (PMDA) was purchased from Allco and was dried at ~140°C under vacuum prior to use. Phthalic anhydride (PA, from Aldrich) was sublimed prior to use. The chemical structures of all monomers and endcappers utilized are listed in Table 1.

Scheme 1. Synthesis of Bis(M-Aminophenyl)Methyl Phosphine Oxide (DAMPO)

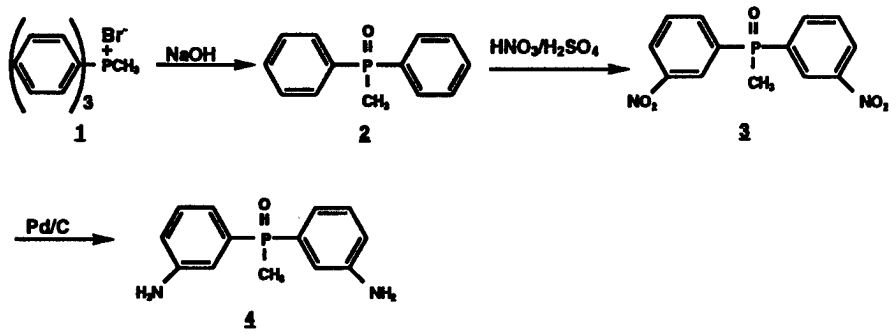

1 2 3 4

Table 1. Polyimide Monomers and Endcappers

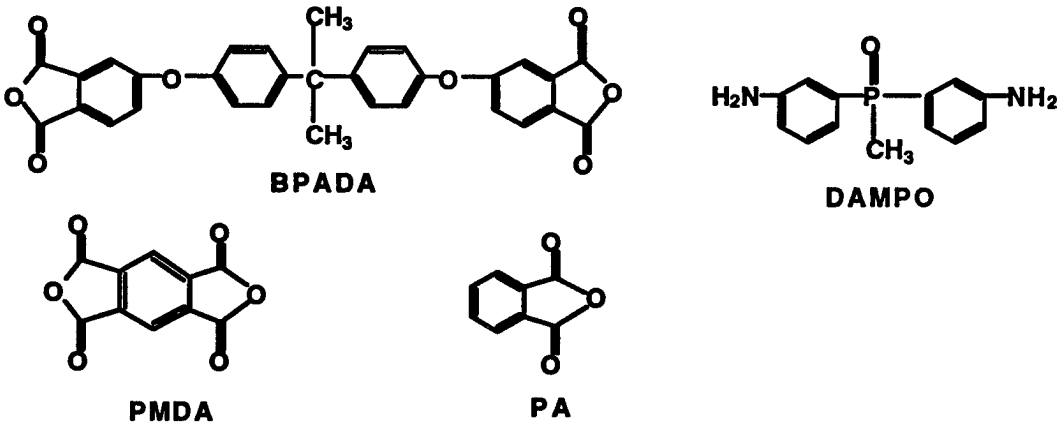

Bis(*m*-aminophenyl) Methyl Phosphine Oxide (DAMPO) Synthesis

Bis(*m*-aminophenyl) methyl phosphine oxide (DAMPO) was prepared following a modified literature method[17].

Polymer Synthesis

The polymers were synthesized via a previously described ester acid route[4]. The polymer was coagulated by slowly dripping the cooled polyimide solution into methanol in a high-speed blender. The polymer was collected by vacuum filtration and washed with excess methanol and with excess anhydrous diethyl ether. It was then air dried for 6-8 hours and vacuum dried at ~160°C for 24 hours. Copolyimides were synthesized according to the same procedure described above except where a mixture of dianhydrides or diamines were used instead of pure monomers.

Preparation of Polymer Films

Solvent Cast Films. Polymer solution (15% wt/vol) in chloroform was used to cast films on a clean glass plate. The glass plate was then air dried for 2 hours and slowly heated to 170°C (2 hours) and dried for another 12 hours. Films were carefully peeled off from the glass plate and were used for refractive index measurements.

Compression Molded Films. Polymer powder was placed between two steel plates which were wrapped with aluminum foil and had previously applied release agents. The plates were then placed into a preheated (250°C) smart press and 0.2 kpsi contact pressure was applied to the plates for 10-15 minutes. A pressure of 1.2 kpsi was then applied for another minute, and the plates were released and cooled in another cooling press for 1-2 minutes. A film with a thickness of 10-15 mils was obtained and used for tensile tests.

Characterization

Fourier transform infrared spectra were obtained with a Nicolet Impact 400 FT infrared spectrometer and were used to determine the presence of ethynyl groups in the polyimide oligomers. Nuclear magnetic resonance (^{1}H, ^{13}C, and ^{31}P NMR) spectra were obtained with a Varian Unity 400 spectrometer and used to confirm the monomer and polymer structures and the number average molecular weights of the oligomers via end group analysis. The solid state ^{31}P NMR spectra was obtained with a Brucker 270 spectrometer.

Intrinsic Viscosity

Intrinsic viscosity measurements were conducted in NMP at 25°C using a Canon-Ubbelohde viscometer.

Gel Permeation Chromatography (GPC)

GPC measurements were performed on a Waters 150-C ALC/GPC instrument which was equipped with a viscosity detector; M_n and M_w/M_n values for the polyimide samples were determined using universal calibration procedures previously developed[18].

Thermal Analysis

Glass-transition temperatures and cure exotherms were determined by differential scanning calorimetry (DSC) using a Perkin Elmer DSC 7 Differential Scanning Calorimeter. Scans were run at a heating rate of 10°C/minute and reported values were obtained from a second heat after quick cooling. Thermogravimetric analyses (TGA) were performed dynamically on a Perkin Elmer TGA 7 Thermogravimetric Analyzer at 10°C/minute in air. The char was collected and ground to a fine powder for solid state ^{31}P NMR analysis.

Tensile Property Measurements

Tensile property measurements were taken on an Instron Model 1123 following the ASTM D638 method. The measurements were conducted at a strain rate of 0.05 in/minute at room temperature. Samples were cut with a dog bone die conforming to ASTM D368 type V. All values are the average of 4-5 runs per specimen.

RESULTS AND DISCUSSIONS

The BPADA/DAMPO amorphous polyimides were successfully synthesized via an ester-acid route *(Scheme 2)* in high yields and purity. When equal molar amounts of BPADA and DAMPO were used in the polymerization without endcapper (uncontrolled MW), very high MW homopolyimide was obtained, e.g., [h]=2.95 (dL/g) and Mn=98,000 (g/mole) by GPC (Table 2). Previous workers[18] reported that only low MW homopolyimide was obtained in their 6FDA/DAMPO polymerization, and this was attributed to the low reactivity of DAMPO. In contrast, our results indicated that this was not true if the DAMPO was pure and the reaction conditions were suitable (e.g., concentration and temperature, etc.). Thus, this paper appears to be the first to describe a DAMPO-based high MW homopolyimide.

Scheme 2. Synthesis of Phosphorus Containing Polyimides

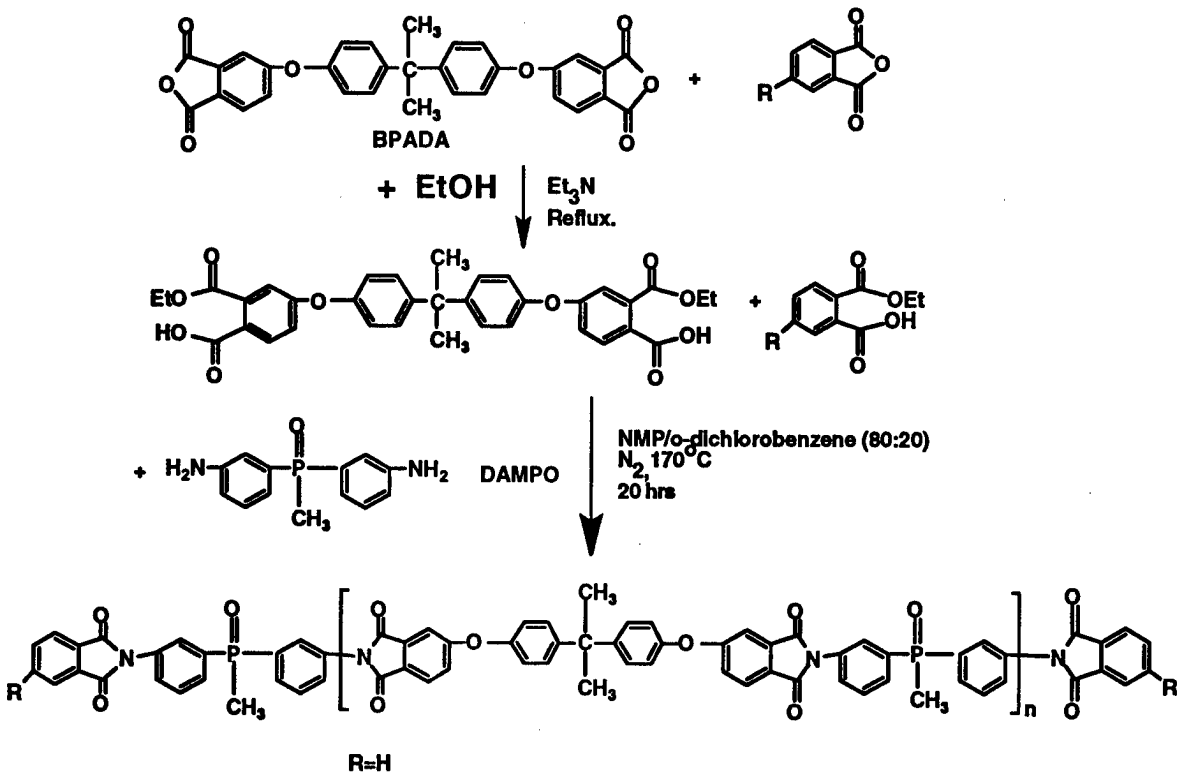

Table 2. Characterization of BPADA/DAMPO Thermoplastic Polyimides

Target Mn (g/mole)	[η] (dlg^{-1}, NMP 25°C)	Tg (°C)[a]	5% wt. loss (°C)[b]	750°C Char Yield in Air (%)[b]
5.0K, PA endcap	0.15	197	493	42
30.0K, PA endcap	0.47	215	519	58
1:1 Stoichiometry	2.95	221	509	62

[a]Heating rate of 10°C/minute in nitrogen
[b]Measured in air at 10°C/minute

Controlled MW polyimide thermoplastics were prepared by the reaction of dianhydride with a stoichiometric excess of diamine and phthalic anhydride (PA) endcapper. The BPADA/DAMPO PA capped (Mn=30,000 g/mole) polyimide compression moldable thermoplastic displayed a T_g value of 215°C (Table 2). All of these polyimides are soluble in NMP, DMAc, and $CHCl_3$, and no melting endothermic peak can be detected by DSC, which demonstrates that the systems are amorphous. The BPADA/DAMPO-based thermoplastic had a high (54%) char yield at 750°C in air (Figure 1) by dynamic thermogravimetric analysis. The control BPADA/*m*-PDA-based polyetherimide thermoplastic did not show any char in air at 750°C. Careful examination of the TGA pan after heating the phosphorus containing imide film in air to 800°C suggested that the film expanded, possibly indicating intumescence during char formation. The residue char was collected for solid state ^{31}P analysis which showed that the char contained some inorganic phosphorus compounds (Figure 2). Such char forming character is considered to be very important for fire resistance since the char can insulate the underlying polymer and restrict flammable volatiles from diffusing through the char and feeding the flame. This may explain the apparent excellent self-extinguishing character of these phosphine oxide containing polyimides relative to other engineering thermoplastics.

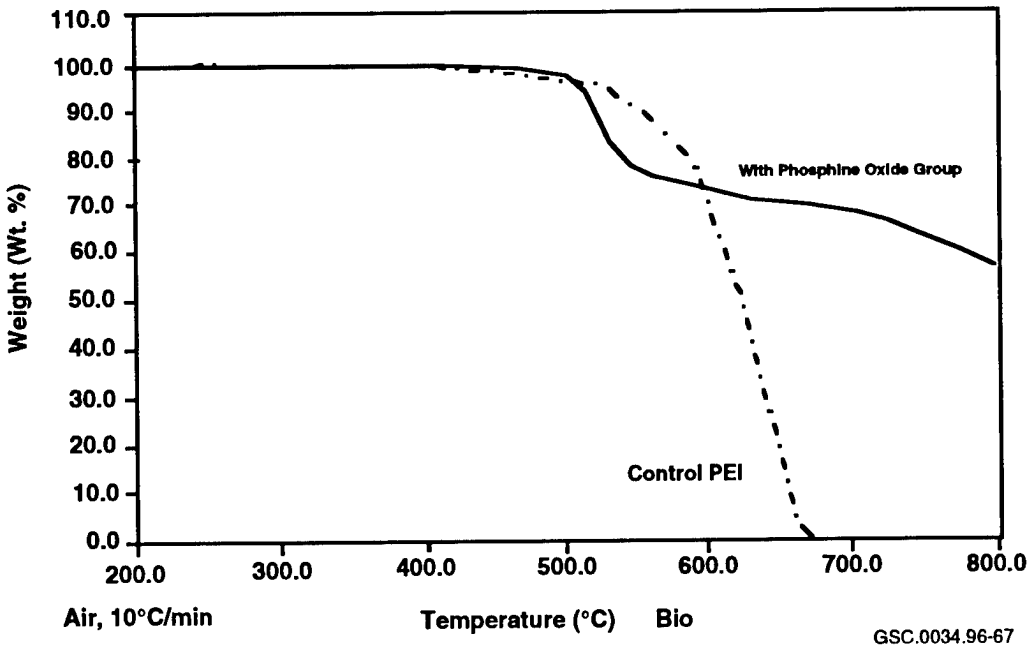

Figure 1. Influence of Phosphine Oxide Group on the TGA of Polyetherimides Char Yield in Air

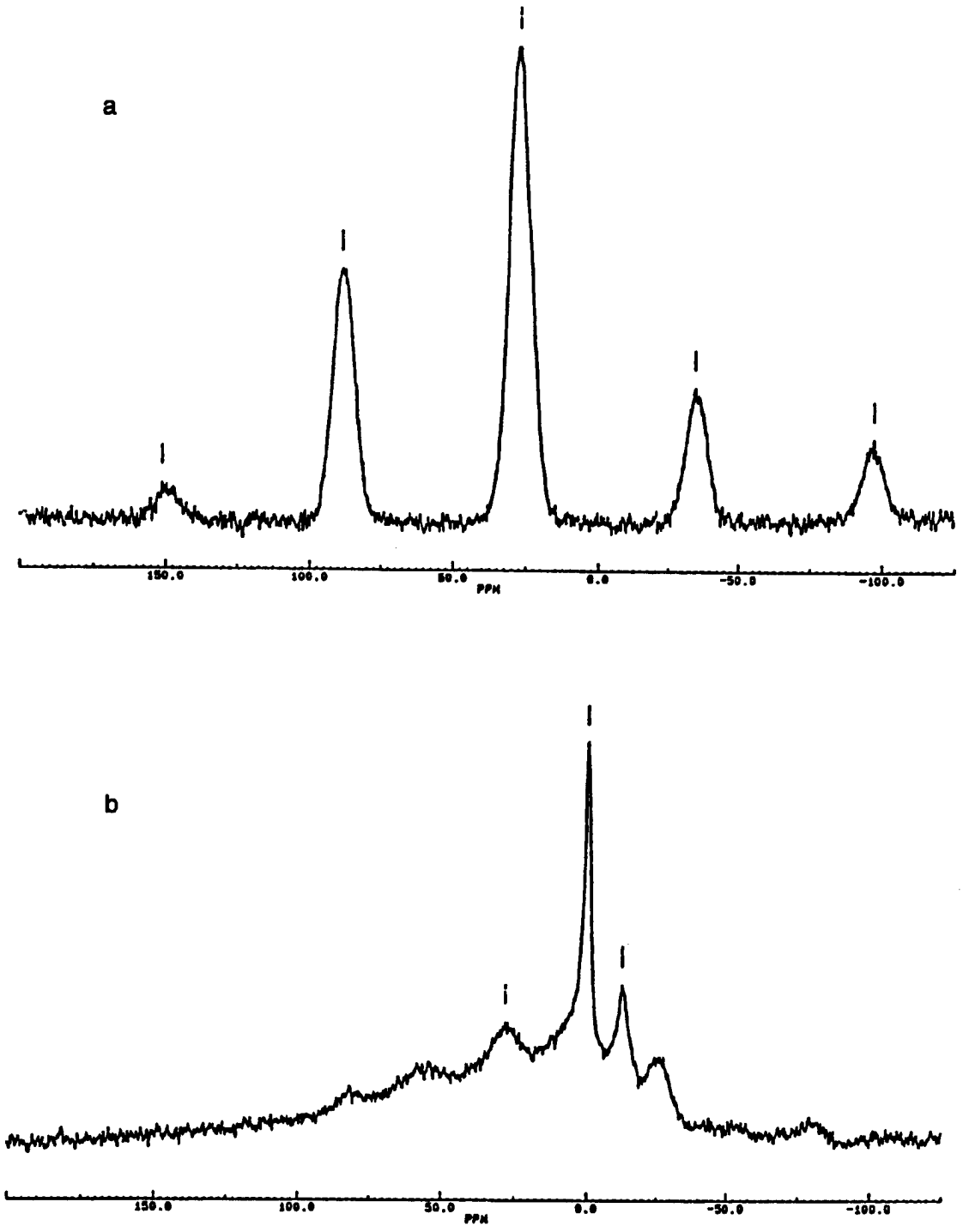

a: before heating, polyimide
b: after heating to 800°C, polyimide char

Figure 2. ^{31}P NMR of BPADA/DAMPO Polyimide Before and After Heating to 800°C in Air

Several thermoplastic copolyimides were synthesized. Interestingly, both homo- and copolyimide thermoplastic materials showed better tensile properties than an Ultem™ control (Table 3). Thus, the modulus and yield stress increased and the yield strain was almost the same compared to Ultem™ When 10 mole% of PMDA was incorporated into the BPADA/DAMPO system, T_g slightly increased (223°C) and the tensile modulus increased to 670±50 ksi. The increase of modulus may be due to enhanced intermolecular forces resulting from the polar phosphine oxide group in the imide backbones. T_g values were also increased by incorporating 50% *p*-PDA into the BPADA/DAMPO system. All these copolymers were soluble in NMP, DMAc, and $CHCl_3$, and no melting endothermic peaks were found by DSC.

Table 3. Tensile Properties of BPADA/DAMPO-Based Polyimides

System	T_g (°C)	5% wt. Loss (°C)	750°C Char Yield in Air (%)	Modulus (ksi)	Yield Stress (ksi)	Yield Strain (%)
Mn=30,000 g/mole PA capped	215	519	58	610±60	20±2	7.1±0.3
Mn=30,000 g/mole, 10% PMDA PA capped	223	507	58	670±50	20±1	6.6±0.5
Ultem™	217		0	530±40	17±1	6.9±0.1

CONCLUSIONS

The BPADA/DAMPO-based polyimide thermoplastics and thermosets were synthesized via an ester-acid route with good molecular weight control. Thermoplastic systems displayed high char yield and good thermooxidative properties. The high MW thermoplastic homopolyimides and copolyimides had good tensile properties.

REFERENCES

1. R. E. Lyon and T. E. Lund, Advanced Aircraft Materials Research and Development Plan, pp. 345-364, Proceedings of the International Conference for the Promotion of Advanced Fire-Resistant Aircraft Interior Materials, Atlantic City, New Jersey, February 1993; R. E. Lyon, Polymeric Materials: Science and Engineering, 71, 26, 1994.

2a. D. Wilson, P. Hergenrother, and H. Stenzenberger, Editors, *Polyimides*, Chapman and Hall, 1990.

2b. P. M. Hergenrother, Editor, *Adv. in Polym. Sci.: High Performance Polymer*, Vol. 117, Springer-Verlag, 1994.

3. G. W. Meyer, B. Tan, and J. E. McGrath, *High Perfm. Polym.* 6, 423, 1994.

4. T. M. Moy, C. D. DePorter, and J. E. McGrath, *Polymer* 34, 819, 1993.

5. H. Yang, M. E. Rogers, and J. E. McGrath, *Polym. Prep.* 36 (1), 205, 1994.

6. M. F. Martinez-Nunez, V. N. Sekharipuram, and J. E. McGrath, *Polym. Prep* 35 (2), 709, 1994; H. Ghassemi, et al., manuscript in preparation.

7. I. Wan, J. McGrath, and T. Kashiwagi, p. 29; D. Knauss, J. McGrath, and T. Kashiwagi, p. 41, G. L. Nelson, editor, *Fire and Polymers II*, ACS symposium Series 599, 1995.

8. G. W. Meyer, T. E. Glass, H. J. Grubbs, and J. E. McGrath, *Polym. Sci., Part A: Polym.Chem.*, 33, 2141, 1995.

9. S. J. Mecham, S. Jayaraman, Y. J. Lee, J. P. Mecham, D. J. Riley, T. E. Glass, and J. E. McGrath, *Polym. Prep.* 36 (1), 789, 1994.

10. C.D. Smith, H. Grubbs, H.F. Webster, A. Gungor, J.P. Wightman, and J.E. McGrath, *High Perfm. Polym.* 3, 211, 1991.

11 E. Bonaplata, H. Ding, B.E. Hanson, and J.E. McGrath, Polymer, 36 (15), 3035, 1995.

12. Y.J. Lee, A. Gungor, T.H. Yoon, and J.E. McGrath, *J. Adhs.*, 55 (1-2), 167, 1995.

13. J.E. McGrath and C.D. Smith, U.S. patent #5,079,333 to Virginia Tech, 1992; C.D. Smith, H. Grubbs, H.F. Webster, J.P. Wightman, and J.E. McGrath, *Polym. Mater. and Sci. Eng.*, 65, 113, 1991.

14. J. W. Connell, J. G. Smith, Jr., and P.M. Hergenrother, *Polymer*, 36(1), 5, 13, 1995.

15. J.L. Hopewell, D.J.T. Hill, J.H. O'Donnell, P.J. Pomery, D.B. Priddy, Jr., C.D. Smith, and J.E. McGrath, *Polymer Deg. and Stabl.*, 45, 293-299, 1994.

16. K. G. Gravalos, *J. Polym. Sci., Part A: Polym. Chem.* 30, 2521, 1992.

17. M. Konas. T. M. Moy, M. E. Rogers, A. R. Shultz, T. C. Ward, and J. E. McGrath, *J. Polym. Sci.: Part B: Polym. Phys.* 33, 1429, 1995.

18. I. K. Varma and B. S. Rao, *J. Appl. Polym. Sci.* 28, 2805, 1983.

PHOSPHINE OXIDE COPOLYMERS: SYNTHESIS AND CHARACTERIZATION OF ADVANCED FIRE-RESISTANT ENGINEERING THERMOPLASTIC

James E. McGrath, Ph.D.
Dept. of Chemistry
2108 Hahn Hall
Virginia Tech
Blacksburg, VA 24061-0344

INTRODUCTION

Polyphenylene sulfide (PPS)[1,2] (**1**) is an important engineering polymer which has been the focus of intensive research for the past two decades. It is a semicrystalline polymer with T_g around 85°C and a T_m of about 285°C. Early versions of PPS were known to undergo curing reactions which increased its molecular weight, toughness, ductility, and solvent resistance[3]. Due to this overall combination of properties, PPS is an important, relatively new, molding resin and has been used as a matrix material for thermoplastic composites. PPS has long been believed to possess a rather "inherent" fire-resistant behavior, but there are relatively few examples of where this characteristic has been demonstrated. Remarkably high limiting oxygen index values for PPS have been reported[3]. Incorporation of a triarylphosphine oxide moiety into the polymer backbone generally enhances fire resistance[4] and it is proposed that the interactions of these materials with functionalized carbon or glass fibers will be improved due to the very polar phosphine oxide group. Copolymers can be designed to be either totally amorphous with high concentrations of triaryl phosphine oxide or semicrystalline with modest phosphorus containing compositions. A related sulfide sulfone (**2**) has been investigated relatively briefly in the literature, and references to its investigation are mostly limited to either patent literature or commercial trade literature[5]. PPSS has been described as an amorphous material with a T_g around 217°C. This paper focuses on the synthesis and properties of polyphenylene sulfide copolymers containing either triaryl phosphine oxide or diarylsulfone in modest concentrations. The structure of triaryl phosphine oxide monomer utilized is shown below (**3**).

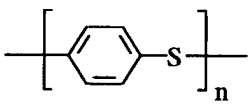

PPS (**1**)

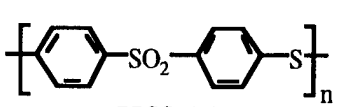

PPSS (**2**)

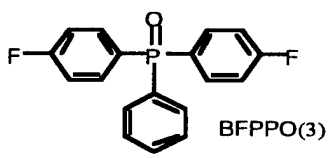

EXPERIMENTAL

Materials

Monomer grade p-dichlorobenzene was kindly supplied by PPG Industries. N-Methyl pyrrolidinone and sodium hydrosulfide were obtained from Aldrich and were used as received. Sodium hydroxide was obtained from Mallinckrodt. Anhydrous lithium benzoate was received from Acros.

Synthesis of PPS

Preparation of PPS homopolymer is described in the patent literature and elsewhere.[6,7] The reactions were conducted in a stainless steel pressure reactor equipped with a reflux condenser, liquids charging tube, stirrer, and appropriate gas inlet and outlet ports. The reactions were conducted at 225°C for 1 hour and then the temperature was raised to 265°C for an additional 4 hours. The pressures at this temperature ranged from 80-120 psi.

Synthesis of PPSS

Preparation of high molecular weight polyphenylene sulfide sulfone is described in the patent literature[5] and elsewhere[8] in our initial preprints.

Preparation of 4,4'-Difluorodiphenyl Phenylphosphine Oxide (3)

The monomer was prepared and purified by a variation of a known Grignard technique.[5]

Synthesis of PPS-Phosphine Oxide Copolymer

Copolymers containing 2 mole% of **(3)** or DCDPS were prepared by modifying the general procedure of Campbell.[6]

Characterization

Glass-transition temperatures were measured using a Perkin Elmer DSC 7 at a heating rate of 10°C per min. in nitrogen. PPS and copolymers of PPS were compression molded into tough ductile films at 300°C, and IR spectra were obtained using a Nicolet Impact 400 FT-IR. Cone Calorimetry was performed at the NIST Laboratories by Dr. T. Kashiwagi. The samples were in the form of films (10 cm x 10 cm x 3 mm) and were tested using a heat flux of 70 KW/m^2.

RESULTS AND DISCUSSIONS

PPS and copolymers of PPS containing triaryl phosphine oxide or arylsulfone groups were prepared (Scheme 1) in an analogous manner as reported in the patent literature[5]. The endgroups were designed to be principally chlorophenyl, which enhances the melt stability by using a 1 mole% excess of the halogenated monomer(s). The other choice, mercaptide-type endgroups, are generally less desirable for stability concerns. The reaction was conducted in a pressure reactor at elevated temperatures. These materials were isolated in the form of small beads.

The polymer was found to be insoluble in common organic solvents both at room temperature and at elevated temperature. PPS homopolymer is reported to be insoluble in solvents below 200°C. Thermal transitions of the homo- and copolymers, which were obtained from the heating cycle after quench cooling from melt, are presented in Table 1. Preliminary results from DSC measurements suggest that minor incorporation of the triaryl phosphine oxide moiety, which has a non-coplanar structure, surprisingly has little influence on the melting endotherms of these materials. The PPS copolymer containing low concentrations of diphenyl sulfone displays similar melting behavior. The glass-transition temperature of these materials are in the range of 92-95°C.

Scheme 1

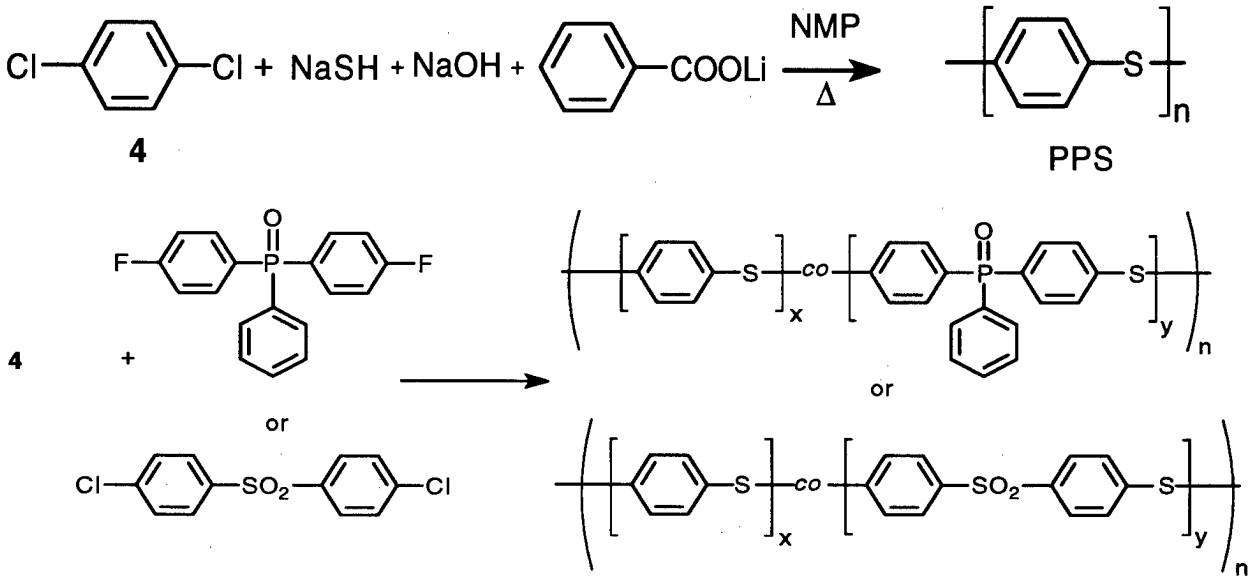

Table 1. Thermal Transitions of PPS Homo- and Copolymers

Polymer	T_g (°C)	T_c (°C)	T_m (°C)
PPS	95	140	285
PPS-co-PO	93	127	286
PPS-co-S	92	140	289

Tough, ductile films indicative of high molecular weight were prepared by compression molding at 300°C followed by quench cooling. These films were utilized to record the IR spectra which is presented in Figure 1. An examination of the infrared region from 1400-500 cm^{-1} shows clearly the presence of an absorption band at 1203 cm^{-1} which is assigned to an aryl phosphine oxide group. Similarly, an absorption band at 1159 cm^{-1}, characteristic of a sulfone group, is evident. Furthermore, these absorbances are not present in the PPS spectrum. Therefore, these preliminary findings suggest that the copolymers containing triaryl phosphine oxide or arylsulfone at modest concentrations can be prepared. Due to the insolubility of these materials, traditional NMR techniques could not be utilized to determine their microstructure. High-temperature NMR studies have been used for determining the microstructure of PPS homo-

polymers.[9] Currently, similar studies, along with elemental analysis are underway to determine how quantitative the incorporation of these comonomers is in the copolymers.

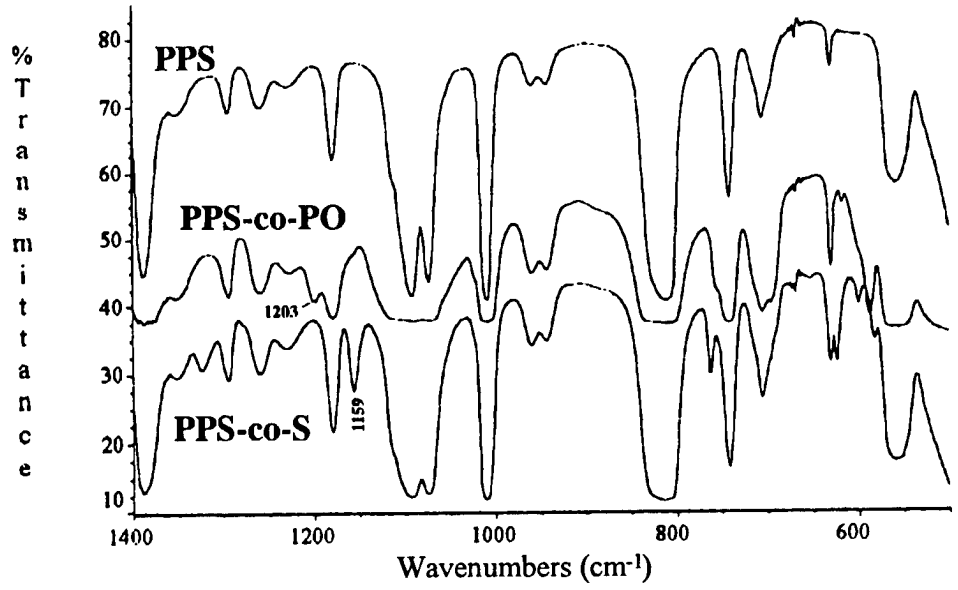

Figure 1. IR Spectra of Homo- and Copolymers

High molecular weight PPSS was prepared (Scheme 2) in an analogous manner as reported elsewhere.[5,8] Molecular weights have been achieved that range from 14,000 to 49,000 number average molecular weight. The weight-to-number average ratio appears to be in the expected range of about 2.0. The glass-transition temperatures for PPSS are about 215-220°C.

Scheme 2

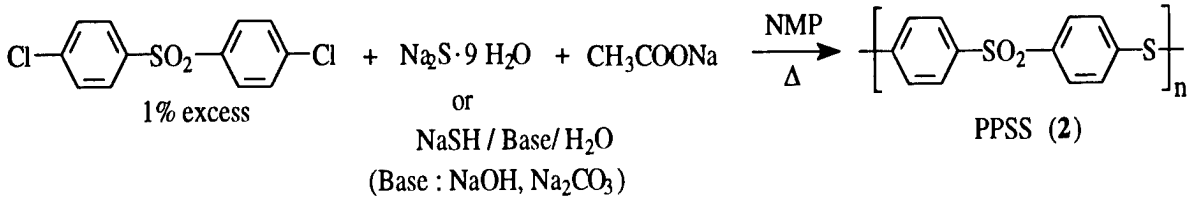

The flammability behavior of PPSS and PPS was examined by Cone Calorimetry at the NIST Laboratories by Dr. T. Kashiwagi. Experiments were performed at a heat flux of 70 KW/m^2. The results will be presented more completely elsewhere. The heat release rate (HRR) results for flaming cumbustion in the cone calorimetry are presented in Figure 2. Commercial Udel and Victrex polyarylene ether sulfone controls showed the highest heat release rate. Both PPS and PPSS homopolymer, desirably, showed a much lower heat release rate, indicating superior fire resistance.

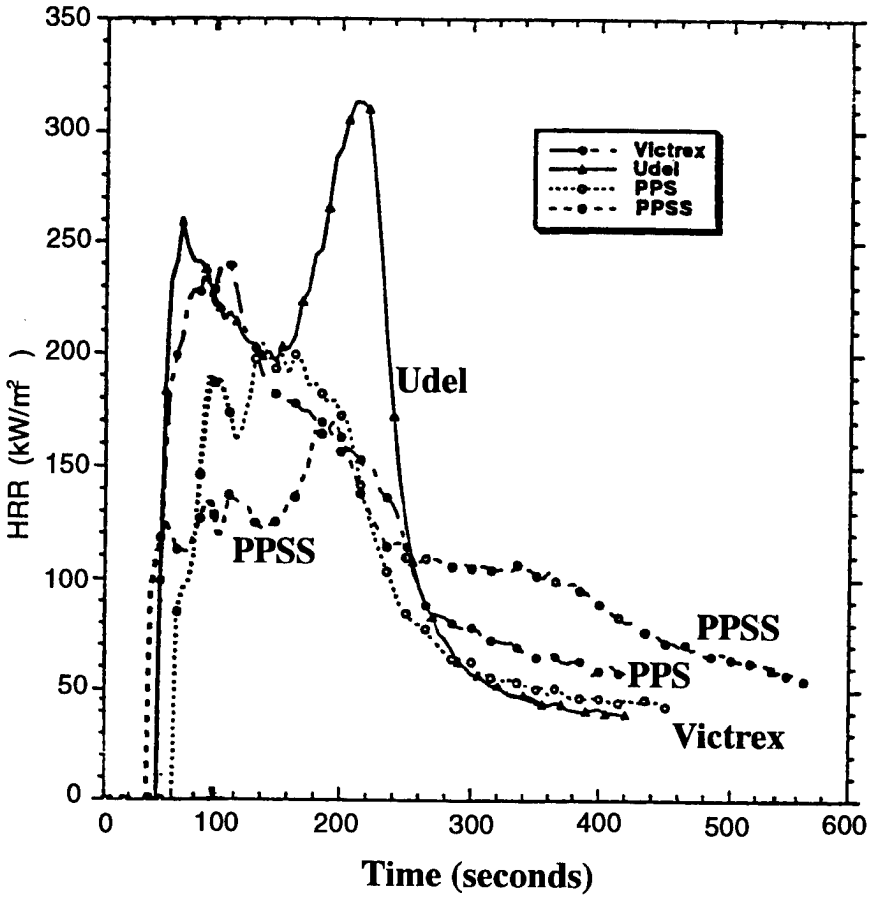

Figure 2. Cone Calorimetry Results (70 KW/m²)

CONCLUSIONS

High molecular weight PPS and PPSS homopolymers were prepared. PPS copolymers containing modest concentrations of triaryl phosphine oxide or arylsulfone units were successfully prepared which may improve interfacial properties in fiber reinforced composites. The incorporation of phosphine oxide and sulfone into the PPS backbone was ascertained via IR spectroscopy. These materials can be compression molded to produce tough, ductile films. PPSS and PPS homopolymers exhibit low heat release rates as judged by Cone Calorimetry experiments. Currently, research efforts are being focused on the preparation of high molecular weight PPS copolymers containing controlled concentrations of triaryl phosphine oxide or diphenyl sulfone moeities. High-temperature NMR and GPC studies are also underway. Carbon fiber composite panels using PPSS are being prepared.

ACKNOWLEDGMENTS

The authors wish to acknowledge financial support of this project by USDOT/FAA, Grant Number 95-G-051 and the NSF Science and Technology Center (DMR-91-20004). They also wish to thank Dr. T Kashiwagi of NIST Laboratories for the Cone Calorimetry experiments.

REFERENCES

1. J. F. Geibel and R. W. Campbell in *Comprehensive Polymer Science*, Pergamon Press, Vol. 5, 1989, p. 543.
2. L.C. Lopez and G. L. Wilkes, *J. Macromol. Sci., Rev. Macromol. Chem. Phys.*, **C29**, 1989, 83.
3. H. W. Hill, Jr.; *Ind. Eng. Chem. Prod. Res. Dev.*, **18**, 1979, 4.
4. C. D. Smith, H. J. Grubbs, A. Gungor, J. Wescott, S. C. Liptak, P. A. Wood, and J. E. McGrath; *Proceedings of the International Conference for Promotion of Advanced Fire-Resistant Aircraft Interior Materials*, Atlantic City, NJ, p. 159-174, Feb. 1993.
5. (a) R. L. Bobsein and E. Clark, Jr.; *US Patent 4,808,698*; **1989** (To Phillips Petroleum Company); (b) R. W. Campbell; *US Patent 4,301,274*; **1981** (To Phillips Petroleum Company); (c) H. Tamada, S. Okita and K. Kobayashi; *Polym. J.*, **25**, 1993, 339;(d) E. A. Gladkova, V. I. Nedel'kin, S. I. Ovsyannikova, O. B. Andrianova, Y. V. Genin, L. I. Komarova, S. S. A. Pavlova, L. V. Dubrovina, and V. A. Sergeev; *Polym. Sci.*, **34**, 1992, 1053.
6. (a) R. W. Campbell, *US Patent 3,919,177*; **1975** (To Phillips Petroleum Company); (b) J. T. Edmonds and H. W Hill, *US Patent 3,354,129*; **1967** (To Phillips Petroleum Company).
7. (a) D. R. Fahey and C. E. Ash; *Macromolcules*, **24**,1991, 4242; (b) D. R. Fahey, H. D. Hensley, C. E. Ash, and D. R. Senn; *Macromolecules*, **30**, 1997, 387.
8. (a) Y. N. Liu, A. Bhatnagar, Q. Ji, H. Zhuang, J. F. Geibel, and J. E. McGrath, *Polymer Preprints*, **38(1)**, 1997, 109; (b) A. Bhatnagar, Y. N. Liu, M. Muggli, T. C. Ward, D. A. Dillard, H. Parvatareddy, and J. E. McGrath, *Polymer Preprints*, **38(1)**, 1997, 111.
9. B. Wade, A. S. Abhiraman, S. Wharry, and D. Sutherlin, *J. Polym. Sci., Part B: Polym. Phys.*, **28**, 1990, 1233.

POLY-X™ SELF-REINFORCED POLYPHENYLENES: NEW HIGH-PERFORMANCE, FIRE-RESISTANT MATERIALS FOR AIRCRAFT CABIN INTERIORS

Mark S. Trimmer, Mark R. Isomaki, and Mike Ulman
Maxdem Incorporated, 140 East Arrow Highway, San Dimas, CA 91773-3336

ABSTRACT

There is a need for new fire-resistant polymers to make safer aircraft components while meeting ever more stringent mechanical performance requirements. Poly-X™ resins are a recently developed family of self-reinforced polymers (SRPs) based on rigid-rod polyphenylene backbones (the reinforcement) with sidechain appendages. These unique materials combine exceptional strength, stiffness, and scratch resistance with thermoplastic processability. An initial screening of the fire resistance characteristics of a few examples of these SRP resins was performed and demonstrated extremely promising fire-resistant characteristics as well. Measurements included limiting oxygen index (with and without a selection of flame retardants), smoke emission, vertical ignition, heat release rate, and thermal analyses. Although complete structure-property understanding has yet to be realized, the results do appear to correlate with the chemical and physical characteristics of the new polymers; thus, it may be possible to rationally design improved SRP materials. The observed attributes are ideal for applications where low weight, durability, fire safety, and moderate cost are critical factors, including aircraft structures; boat and submarine components; fire-resistant industrial, office, and household equipment and structures; and components for mass transit vehicles and automobiles.

INTRODUCTION

Self-reinforced polymers (SRPs) may be considered to be a special class of molecular composites[1] in which only a single component serves as both the reinforcing rigid-rod polymer (the molecular fiber) and the matrix resin, thus alleviating phase separation problems. Processable rigid-rod SRPs can be achieved with rigid-flexible block copolymeric structures, by the utilization of carefully chosen sidechain substituents (thereby yielding what is sometimes referred to as "hairy-rod" polymers), and/or by utilizing a carefully controlled number of "kinked" comonomer units. Poly-X™ resins are a new family of SRPs based on rigid-rod polyarylenes that possess a unique combination of high-performance mechanical properties along with good processibility[2,3]. Research largely inspired and supported by Wright-Patterson AFB has demonstrated that rigid-rod polymers possess exceptional mechanical properties[4], but most are either intractable (e.g., polyparaphenylene[5] or aromatic polypyromellitimides[6]) or are soluble only in strong acids (e.g., polybenzazoles[7] and polyquinolines[8]). Poly-X™ SRPs have been designed to overcome the processing deficiencies of rigid-rod polybenzazoles and polyquinolines via the use of carefully chosen pendant sidechains to impart solubility and thermal processability to the normally intractable rigid-rod polyparaphenylene backbone (Figure 1). Thus, they are soluble in a variety of common organic solvents (methylene chloride,

N-methylpyrrolidinone, *m*-cresol, phenyl ethers, etc.) and, most importantly, can be thermally processed (compression molded, extruded, injection molded, etc.) into a variety of product forms.

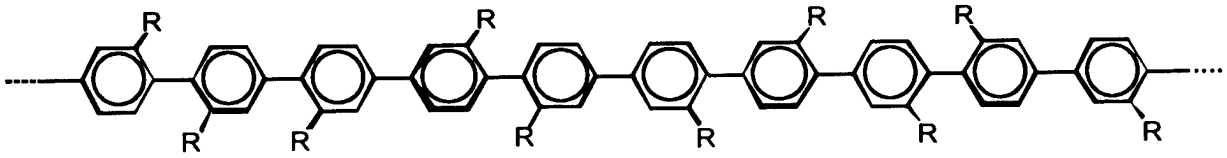

Figure 1. General Poly-X™ SRP Structure

SRP homopolymers or copolymers of controlled composition and isomer configuration can be prepared. Since a variety of substituent groups (R) can be utilized, Poly-X™ SRP resins comprise a class of polymers, like polyimides, polyesters, and polyamides, within which exists a wide range of structural variation (i.e., there are many different derivatives possible). The most well-studied materials (Figure 2) are the rigid-rod PX™-1000 (benzoyl sidechain) and PX™-2000 (4-phenoxybenzoyl sidechain) homopolymers and the "tougher" PX™-1200 series of "kinked-SRP" copolymers, that are based on the PX™-1000 backbone modified with occasional *m*-linkages ("kinks"). The Poly-X™ SRPs appear very promising for a variety of high-performance applications because of their unique combination of chemical, physical, and mechanical properties combined with their good processability and potential low cost. A particularly interesting application is aircraft interior components that would benefit from the lightweight and durability provided by the SRPs. However, such uses have strict fire safety requirements and, while these highly aromatic materials were expected to be fire resistant, no quantitative characterization had been done previously. The following work describes the results of initial flammability studies performed with these interesting new plastics.

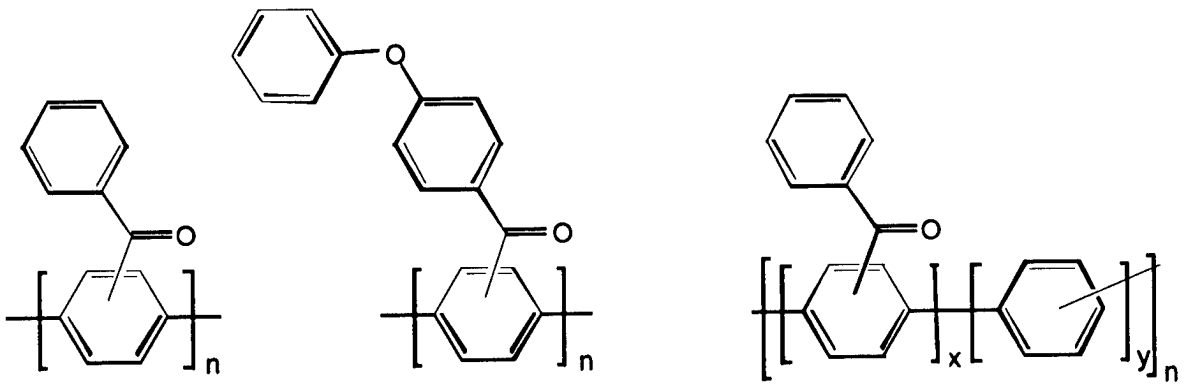

PM™-1000 PX™-2000 PX™-1200

Figure 2. Best Studied Poly-X™ SRP Derivatives

EXPERIMENTAL

The Poly-X™ resins used in this study were prepared via Maxdem's proprietary processes. Formulations containing flame retardants were prepared by either physically mixing the two solids (resin powder and solid additive) or by impregnating the resin powder with a solution of

hydroxide (Lonza Inc.), zinc borate (zinc hexaborate), and Reoflam™ PB-460™ (FMC Corporation) proprietary brominated aromatic phosphate ester.

Thermogravimetric analyses (TGAs) were performed using a Perkin-Elmer TGA-7 instrument at a heating rate of 10°C/min under either air or argon atmospheres. All flammability measurements except cone calorimetry were obtained at Delsen Testing Laboratories (Glendale, CA). Limiting oxygen index (LOI) was measured in accordance with the methods of ASTM-D-2863-91 using compression molded specimens of approximate dimension 6.3 x 3 x 125 mm which were preconditioned for a minimum of 24 hours at 23°C and 50% relative humidity and are reported as the average of the results for three specimens. Flaming-mode smoke emission was measured in accordance with FAR 25.853(c), Amendment 25-72, Appendix F, Part V, Paragraph (b). Samples were compression molded and machined to approximate dimensions 76 x 76 x 3.25 mm (PX™-1000) or 74 x 74 x 6.35 mm (PX™-1200) and preconditioned for a minimum of 24 hours at 21°C and 50% relative humidity. The results are reported as the average of the specific optical smoke density (D_s) for three specimens. Vertical ignition was measured according to FAR 25.853(a), Amendment 25-72, Appendix F, part I, Paragraph (b)(1-4). Samples were compression molded and machined to approximate dimensions 76 x 254 x 5 mm and preconditioned for a minimum of 24 hours at 21°C and 50% relative humidity. Test results are reported as the average for three samples using CP-grade methane as the ignition source with a flame temperature of 971 ± 56°C and a flame height of 38 mm. One end of the specimen was utilized for the 12-second experiment and the other end (completely unaffected by the first test) was utilized for the 60-second test. No dripping of flaming particles was observed in any case.

Heat release rate (OSU method) was measured at Delsen according to FAR 25.853(c), Amendment 25-72, Appendix F, Part IV using compression molded specimens of approximate dimension 150 x 150 x 3.8 mm preconditioned for a minimum of 24 hours at 21°C and 50% relative humidity. The results are reported as the average for three specimens exposed to a radiant heat flux density of 35 kW/m^2. Cone calorimetry was performed by FAA personnel using facilities available at NIST. Specimens were compression molded with approximate dimensions 100 x 100 x 6.35 mm. These results are reported from a single measurement only and should be considered preliminary.

RESULTS AND DISCUSSION

The rigid-rod polyparaphenylene backbone of the Poly-X™ SRPs is the reinforcing component of these materials and imparts high mechanical strength and stiffness. The comparative data in Figure 3 demonstrates the superior mechanical properties relative to other engineering thermoplastics. It is clearly evident from this data that the materials exhibit unprecedented strength and especially stiffness for unreinforced, unoriented polymeric resins (high-performance engineering thermoplastics typically have moduli around 3.5 GPa and strengths around 100 MPa). It has also been found that additives (e.g., plasticizers or flame retardants) can be utilized in reasonable proportion without totally sacrificing the desirable mechanical properties of the SRP materials. For example, addition of 10 phr (parts per hundred of resin) of triphenylphosphate (TPP) decreases the modulus of PX™-1000 resin from about 10 GPa to about 8.5 GPa, but this value is still well above those for other unfilled engineering thermoplastics.

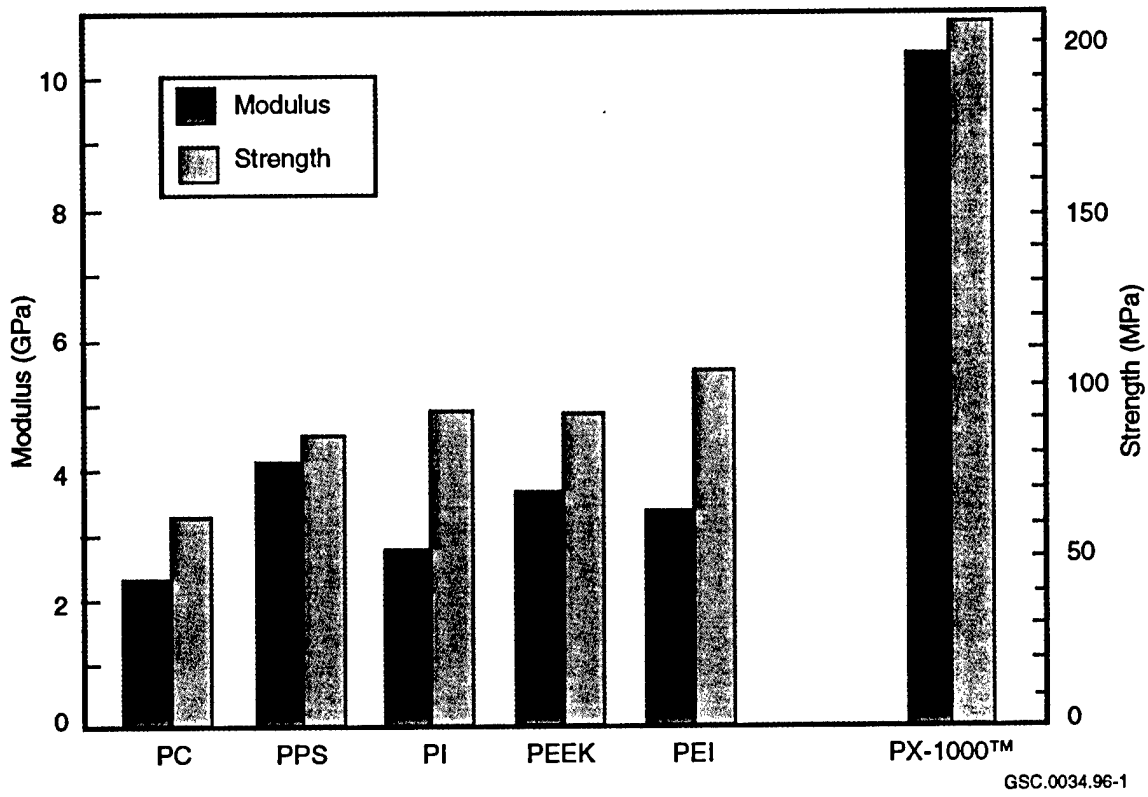

Figure 3. Comparative Tensile Properties of Various Engineering Thermoplastics

The intrinsically high aromatic content of the polyphenylenes imparts high thermal stability to these materials. The results of thermogravimetric analyses (TGA) experiments are shown in Figure 4 for the PX™-1000 derivative (PX™-1200 and PX™-2000 behave similarly) . The materials show very high weight retention to around 500°C even in air. Such behavior places these materials into the upper echelon of high-temperature stable polymers, although there are some heteroaromatic and polyimide materials that may be slightly better. The aromatic structure and high thermooxidative stability of the polymers also lead to high fire resistance. A first indication of this can be seen in the limiting oxygen index (LOI) data summarized in Table 1, with the SRPs typically showing LOI values in the 40% range (very good for organic polymers that usually burn at or below atmospheric oxygen concentrations). Although a complete study has not yet been performed, an initial screening indicates that these polymers also respond well to flame-retardant additives, with LOI values commonly around 50% for formulations including approximately 10 phr of additive.

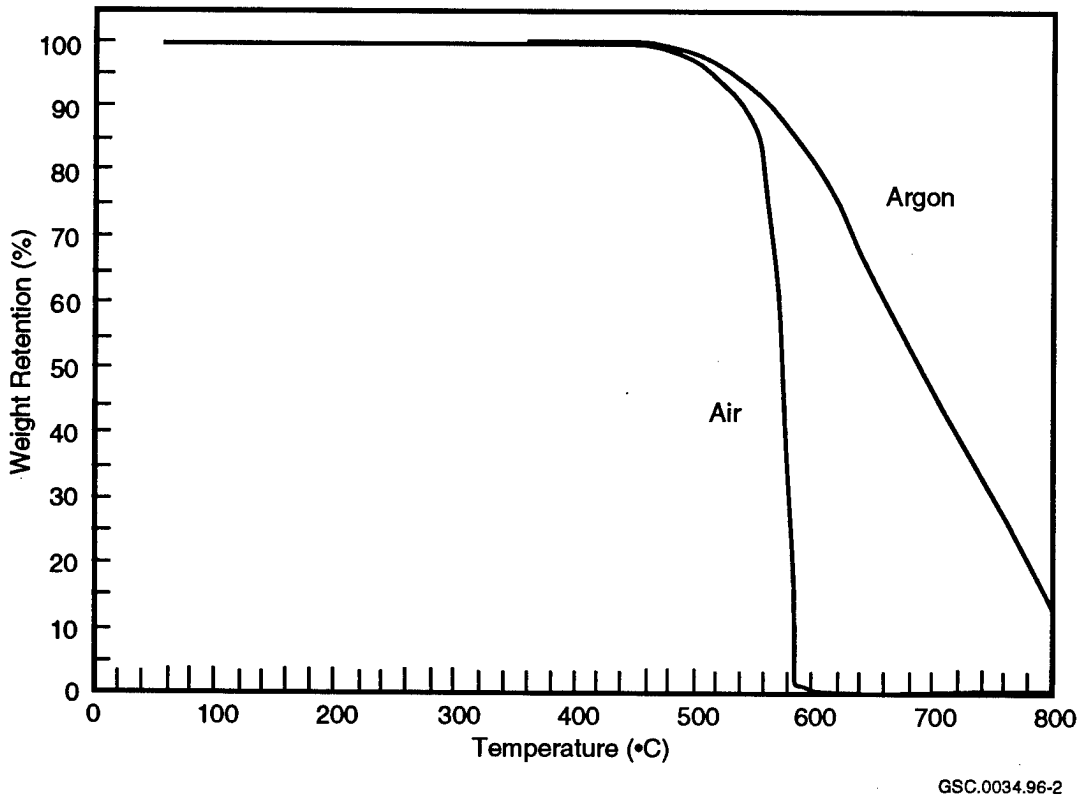

Figure 4. TGA of PX™-1000 SRP Resin in Air and Argon Atmospheres

Along with thermal stability and flame resistance, the materials also do not emit significant quantities of smoke during combustion. Under standard flaming-mode smoke emission conditions, the baseline PX™-1000 and PX™-1200 derivatives emit virtually no smoke. Low emission of smoke and toxic gases is important for aircraft and fire safety since smoke inhalation is probably a more significant killer than fire itself.[9] These SRP materials perform at least as well as any other organic polymer of which we are aware. We still need to measure emission of potentially toxic gasses, but expect this to be less of a problem than for many other fire-resistant plastics including chlorinated, fluorinated, or heteroaromatic polymers. We also need to determine how smoke emission might be affected by incorporation of flame-retardant additives.

Table 1. Limiting Oxygen (LOI) Data for Poly-X™ SRP Compositions

Derivative	Additive (10 phr)	Limiting Oxygen	Burn Time	Burn Length
PX™-1000	none	41%	180 s	<50 mm
PX™-1200	none	42%	180 s	<50 mm
PX™-2000	none	32%	180 s	<50 mm
PX™-1000	Saytex® 102E	52%	180 s	<50 mm
PX™-1000	TPP	52%	180 s	≈55 mm
PX™-1000	Magnifin® H10	49%	180 s	<50 mm
PX™-1000	Zinc Borate	42%	180 s	<50 mm

The high modulus, and corresponding high viscosity, of SRP materials, along with their tendency to char at high temperature, also contributes to their fire safety characteristics. The results of vertical ignition experiments with PX™-1000 and PX™-1200 are summarized in Table 2. The materials show excellent behavior, especially since they show no tendency to drip or shed flaming particles that can contribute to fire spread. We believe that this attribute can also be utilized in blends and alloys of the SRP materials, since the rigid-rod component will help to increase modulus and prevent dripping under fire conditions.

Table 2. Twelve- and Sixty-Second Vertical Ignition (VI) Data for Poly-X SRPs

Derivative	12-Second VI		60-Second VI	
	Extinguish Time	Burn Length	Extinguish Time	Burn Length
PX™-1000	<1 s	2.5 mm	1.6 s	15 mm
PX™-1200	<1 s	2.5 mm	1.3 s	20 mm

An initial measurement of heat release rate was performed for a sample of the PX™-1000 material via the OSU method with interesting results. While the peak heat release rate (110 kW/m^2) was higher than allowed, the time for the heat release to peak was very long at 290 seconds. Correspondingly, there was essentially no heat release at 2 minutes (measured total heat release value was -7 kW•min/m^2).

FAA researchers also carried out preliminary cone calorimetry experiments with SRP samples using the equipment available at NIST. The data in Table 3 summarizes the behavior observed for the baseline PX™-1000 and PX™-1200 derivatives exposed at several different levels of heat flux. In general, the materials exhibit a relatively long-time ignition at all except the highest flux values. The data also shows the effect when relatively low levels (10 phr) of flame-retardant chemicals are added to the PX™-1000 derivative. In general, a decrease in mass loss is observed

Table 3. Cone Calorimeter Results for Poly-X™ SRP Compositions

Sample	Heat Flux (kW/m)	Ignition Time (s)	Heat Release (MJ/m^2)	Peak Mass Loss g/s•m^2
PX™-1000	35	647	38.6	11.3
	50	203	49.6	15.1
	75	92	54.6	17.3
PX™-1200	35	1,032	27.1	5.7
	50	214	43.6	9.1
	75	86	50.5	13.4
PX™-1000 + 10 phr Saytex® 102E	50	196	48.4	12.9
PX™-1000 + 10 phr Zinc Borate	50	204	47.3	11.1
PX™-1000 + 10 phr Magnifin® H10	50	209	47.5	8.8
PX™-1000 + 10 phr Reoflam™ PB-460™	50	383	22.0	4.5

with the addition of the additives, but ignition time and heat release show smaller effects. However, in this rather limited sampling, the PB-460™ additive (a brominated aromatic phosphate material) appeared to have a more significant effect, almost doubling the ignition time and halving the heat release. Clearly, the interaction of these new polymers with different flame-retardant additives needs to be more fully explored.

CONCLUSIONS

The initial flammability results summarized herein suggest that the polyphenylene SRPs are indeed inherently very fire-resistant materials. Combined with their high strength, stiffness, modulus, and low density, they appear ideal for aircraft interior applications, where low weight, durability, fire safety, and moderate cost are critical factors. Further work will focus on more fully understanding the chemistry of these novel materials under fire conditions, on developing structure-property relationships, and on characterizing their interaction with various types of flame-retarding additives. This information can then be used to prepare optimized formulations with maximum fire safety characteristics. Important applications of these materials are expected to include lightweight, secondary structures for aircraft (for both new aircraft and retrofit of existing planes); boat and submarine components; fire-resistant industrial, office, and household equipment and structures; and components for mass transit vehicles and even automobiles.

NOMENCLATURE

PC	bisphenol-A polycarbonate
PEEK	polyetheretherketone
PEI	polyetherimide
phr	parts per hundred resin
PI	thermoplastic polyimide
PPS	polyphenylene sulfide
TPP	triphenylphosphate

ACKNOWLEDGMENTS

This work was funded by Phase I SBIR contract DTRS-57-95-C-00022 from the U.S. Department of Transportation (DOT), Volpe National Transportation Systems Center, 55 Broadway, Kendall Square, Cambridge, MA 02142 under the technical supervision of the Federal Aviation Administration (FAA). We would like to thank Richard Lyon, Fred Arnold, and Joni Arnold at FAA for obtaining heat-release data using the cone calorimeter at NIST and for providing corroborating thermal analysis data.

REFERENCES

1. W.-F. Hwang and T.E. Helminiak, *Mat. Res. Soc. Symp. Proc.*, 134, 507 (1989).
2. M. Marrocco, M.S. Trimmer, L.-C. Hsu, R.R. Gagné, and R.R. *Proc. Int. SAMPE Symp.*, 39, 1063 (1994).
3. R.R. Gagné, S.A. Harding, M. Marrocco, M. Trimmer, and Y. Wang, *Polymer Preprints, Japan*, 42(1), 138 (1993).
4. "The Materials Science and Engineering of Rigid-Rod Polymers," W.W. Adams, R.K. Eby, and D.E. McLemore, Eds., *Mat. Res. Soc. Symp. Proc.* Volume 134 (1989).
5. P. Kovacic and M.B. Jones, *Chem. Rev.*, 87, 357 (1987)
6. C.E. Sroog, *J. Polym. Sci., Macromol. Rev.*, 11, 161 (1976).
7. F.E. Arnold, *Mat. Res. Soc. Symp. Proc.*, 134, 75 (1989).
8. J.K. Stille, *Macromolecules*, 14, 870 (1981).
9. B.C. Levin, R.G. Gann, *ACS Symp. Ser.*, 425, 3 (1990).

ENEDIYNES AND FULLERENES

SYNTHESIS AND CHARACTERIZATION OF NEW FLAME-RESISTANT MATERIALS

Principal Investigator: James M. Tour, University of South Carolina
Department of Chemistry and Biochemistry, Columbia, SC 29208
Email: tour@psc.sc.edu

Graduate Assistant: Alexander B. Morgan

ABSTRACT

This paper describes the synthesis and characterization achieved to date of new non-halogenated, flame-resistant polymer additives based on alkynes. These materials are synthesized simply in a one-step reaction using a bimetallic catalyst system from commercially available brominated aromatic flame retardants. Practical flame testing of these alkynylated materials in polystyrene and high-impact polystyrene has been performed with some interesting results. These results show that these materials have promise towards combating fire in other less flammable plastics due to their high char forming properties.

INTRODUCTION

Previously, two non-halogenated materials were synthesized in our laboratory. These were enediynes and alkynylated polyphenylenes. Both of these materials show promise towards combating flame propagation. The alkynylated polyphenylenes are high char forming polymers due to the cross-linking alkyne. Enediynes are very similar in reactivity to alkynes and may be able to perform the same cross-linking effect as alkynes. Enediynes, upon heating, go through the Bergman cyclization to form a 1,4-benzenoid compound, which is a very reactive radical system(1). These diradicals can act as radical traps and stop the radical depolymerization which occurs at the surface of the plastic. Enediynes may also have this high char effect due to their potential to cross-link via the 1,4-diradical, which is formed upon thermal initiation of the Bergman cyclization.

These cross-linking units, either alkyne or enediyne, may prevent depolymerization of the plastic, slow the rate of fuel release, and form a char. Char is a carbon-based soot/residue which undergoes very little oxidative degradation. This char would form an outer carbon layer which would keep in fuel (monomers), thus preventing flame propagation. Enediynes and polyphenylenes may work effectively by themselves, but together they could solve the previously stated problems and prevent the fatalities created by fire during aircraft crashes. These materials are synthesized from brominated aromatic starting materials, which are common organics in today's chemical market.

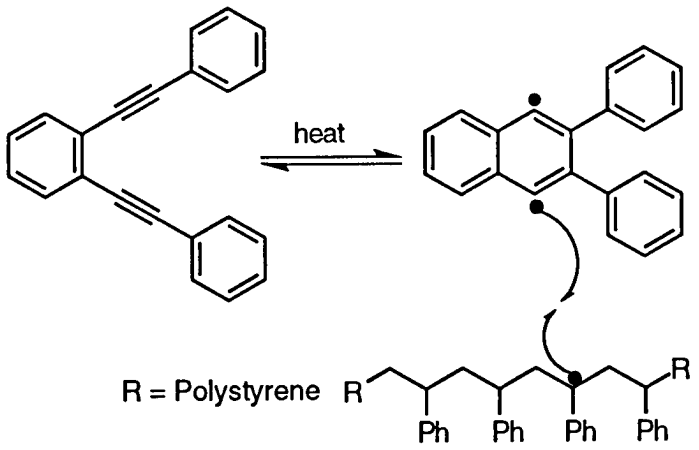

One class of widely used flame retardants, as mentioned before, are the brominated organic flame retardants. There is a wide range of brominated flame retardants, from fully aromatic to fully aliphatic small molecules to brominated polymer monomers, oligomers, and polymers. Each of these materials is ideally suited for one polymer resin or another. There are several companies around the world which manufacture these compounds, so there is a very wide market for these compounds. Our method of making alkyne-based flame retardants utilizes brominated aromatics as starting materials. Such a wide selection of these brominated aromatics leads to a wide selection of alkyne-based flame retardants. Therefore, our approach offers four key advantages in making alkyne-based flame retardants from currently existing brominated flame retardants. The first advantage is the variety of compounds that can be made. This gives these additives more flexibility as far as the type of polymer resin in which they can be used effectively. The second advantage is the main reaction used in the synthesis of these flame retardants. The reaction is a simple one-step reaction, using a bimetallic catalyst system, leading to the consumption only of the added alkyne added, *with little or no bromide remaining after our reactions*. The other reactants can be recycled through careful engineering, leading to conservation of materials and low cost for the additive. The third advantage is that these alkyne based compounds would either be halogen (bromine) free or low in halogen content. This is desirable as the goal is to avoid halogenated materials due to environmental concerns. The final advantage is quite industrially attractive. Since the synthesis of these alkyne based materials relies upon brominated organics, the chemical industry would not have to heavily retool to make these compounds. It could continue to make them as starting materials and then simply add another part to the process to complete the reaction to the alkyne-based flame retardant. It is our hope that these four advantages will make alkyne-based flame retardants, if successful, a practical and commercially viable solution to preventing fires in aircraft accidents and any accident where fire and plastics are involved.

SYNTHESIS, RESULTS, AND DISCUSSION

The best way to synthesize these alkynylated materials and enediynes is through the use of a cross-coupling reaction between an aromatic halide and the desired acetylene. There were two cross-coupling reaction protocols used. The first reaction protocol utilizes a palladium/copper cross coupling, also known as a Sonogoshira or a Castro-Stephans coupling[2]. The second reaction protocol utilizes a palladium/zinc cross coupling, also known as a Negishi coupling[3].

Each of these particular protocols has been modified and optimized through experimentation to provide the best conditions for synthesizing these materials. These two general synthetic protocols are shown below.

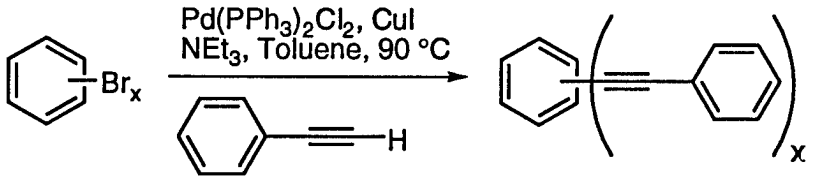

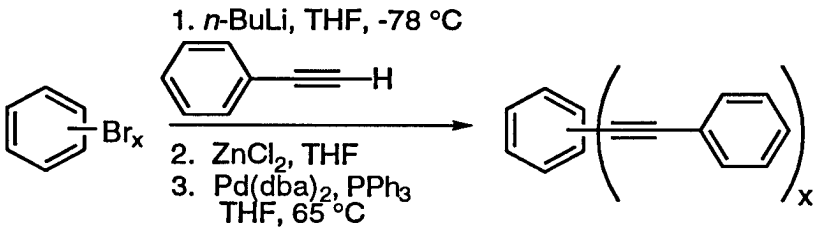

Enediynes

Various enediynes have been made in our lab to be used as precursors for substituted poly-phenylenes[4]. It was thought that these materials may be useful as flame retardants by themselves. However, this was not the case. 1,2-Di(phenylethynyl)benzene was blended with Ultem™[5], a polyetherimide engineering plastic, and tested for its flame retardancy in a cone calorimeter[6]. A large initial exothermic event was seen at ignition of the plastic. This was interpreted as a flash point for the enediyne, 1,2-di(phenylethynyl) benzene, due to its relatively low boiling point. To determine whether or not enediynes would be effective thermally, initiated cross-linking units, larger molecular weight, higher boiling point molecules with enediyne functionalities were needed.

Multialkynylated Materials

The first general class of compounds made were the multialkynylated diphenyl ethers. They were made from either decabromodiphenyl ether or octabromodiphenyl ether, respectively, and phenylacetylene. The two compounds which show great promise are deca(phenylethynyl)-diphenyl ether (**DPEDPE**) and octa(phenylethynyl)diphenyl ether (**OPEDPE**).

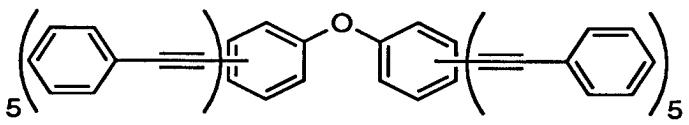

DPEDPE

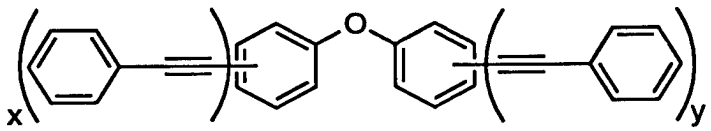

x + y = 8 (Avg.)

OPEDPE

Neither of these compounds began to decompose until 300°C, and both gave very good char yields. Another multialkynylated material was made from tetrabromophthalic anhydride to give tetra(phenylethynyl)phthalic anhydride (**TPEPA**).

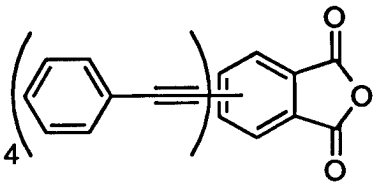

TPEPA

A table containing thermal gravimetric analysis (TGA) data showing onset temperatures of decomposition and %wt loss at 900°C (N_2, 10°C min^{-1}) for each of these three compounds is shown below. Differential scanning calorimetry (DSC) data are also included in this table with the peak temperatures of observed exothermic events listed.

Compound	TGA: Onset	%wt. loss at 900°C	DSC Exotherms
DPEDPE	300°C	22.5	240, 310, 350°C
OPEDPE	300°C	22.3	225°C
TPEPA	300°C	35.4	275°C

Polymeric and Oligomeric Alkynylated Materials

This category of alkyne-based flame retardants is synthesized from brominated polymeric and oligomeric materials. One polymeric compound made as a potential flame retardant was poly(di-(phenylethynyl)styrene) (**PDPES**).

This polymer was made from a commercial flame retardant, Great Lakes Chemical Corporation PDBS-80 [poly(dibromostyrene)]. According to data from NIST and Great Lakes Chemical, PDBS-80 is a mixture of 43% 3,4-dibromo isomer (seen below), 28% 2,4-dibromo isomer, 15% 4-monobromo isomer, 10% 2,5-dibromo isomer, and 5% 2,4,5-tribromo isomer. All of these percentages are accurate to +/- 1%. Thus 48% of the polymer would contain the enediyne unit, and the rest would contain cross-linking phenylethynyl units and some remaining unreacted ortho bromide. **PDPES** would have two potential flame-retarding abilities. It could act as a radical trap (from the enediynes and unreacted bromine) and as a cross-linking agent (from the nonadjacent phenylethynyl units).

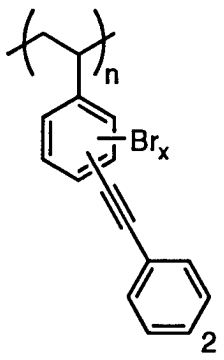

PDPES

One problem with enediynes has been seen so far and that is the major heat release caused by the exothermic Bergman cyclization forming the 1,4-diradical benzenoid. Preliminary Cone Calorimetry data showed that a great amount of heat was released when the enediyne materials were present — almost more heat than combustion of the polymer without the enediyne material added. This exothermic event, which occurs with alkynes as well as enediynes, needs to be addressed so that the heat release can be countered with some other material which endothermically cools the system. This could probably be done with materials which give off nonflammable gases, such as nitrogen or carbon dioxide. So a final area to explore is nonflammable gas releasers, particularly materials which release carbon dioxide. Carbonates are the desired material for this purpose. Existing phenolics could be turned into carbonates with the use of phenyl chloroformate, as was done with tetrabromobis phenol A, following cross coupling with phenylacetylene to give tetra(phenylethynyl)bis phenol A phenyl carbonate (**TPEBPAPC**).

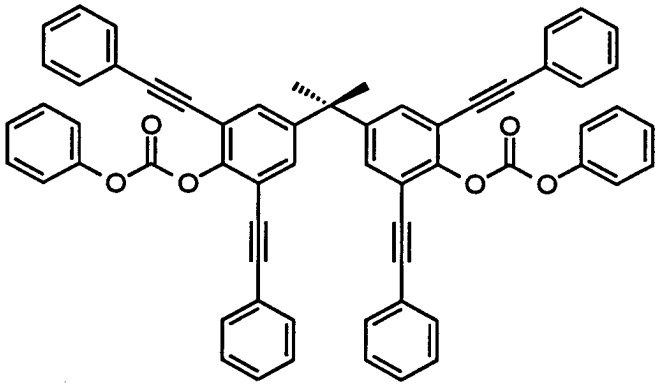

TPEBPAPC

The other materials synthesized were phenylethynylated oligomeric carbonates, synthesized from Great Lakes Chemical Corporation brominated oligomeric carbonates, a tetramer which produced phenylethynylated carbonate tetramer (**PECT**), and a pentamer capped with 2,4,6-tribromophenyl groups to produce phenylethynylated carbonate pentamer (**PECP**).

Both of these oligomeric carbonates have many desirable properties. They are easily synthesized and purified in high yields. Also, they are very lightly colored, which is important to consider so that the additive does not greatly discolor the polymer into which it is blended. They also have high thermal resistance and the ability not only to be a cross-linking additive, but also to emit a

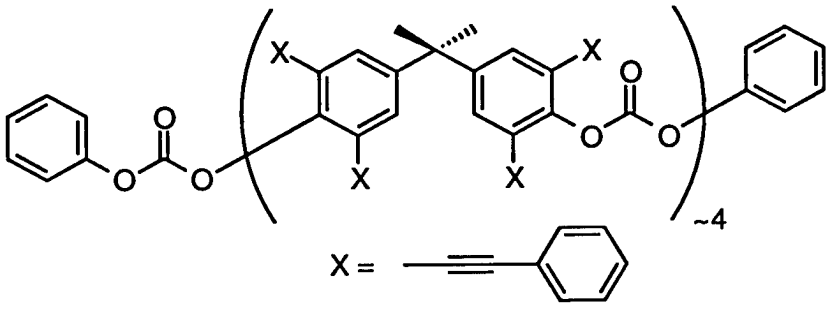

PECT

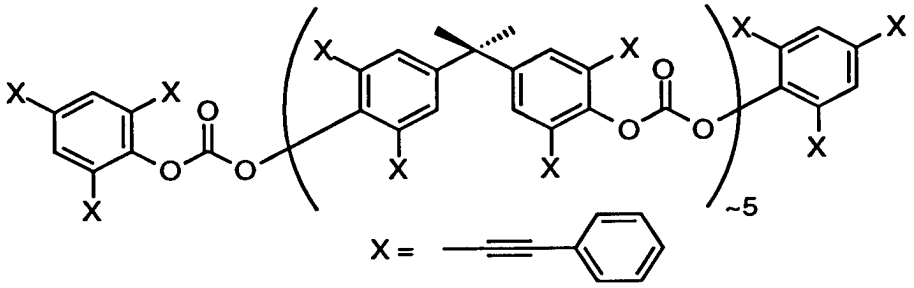

PECP

nonflammable gas, carbon dioxide upon decomposition. Clearly, thermal stability has been improved with the addition of the cross-linking alkynes, as shown by the following TGA data. These oligomeric carbonates have had some success at flame retardancy. They were blended 10 wt% into HIPS and then subjected to a UL-94 burn test. After the first 10-sec ignition, the plastic self-extinguished at 23 seconds via dripping of the molten flaming plastic. After the second ignition, the remainder of the bar burned. While this is only a V-2 result as far as the UL-94 test is concerned, *it is impressive that a nonhalogenated material was able to provide that result in a very flammable polymer*. One other interesting result was seen during these burns: the formation of char was seen during the burning of the plastic. *This char could not be reignited and only glowed red upon further exposure to an open flame*. This shows that these additives do indeed form glassy carbon char during the burning process, which shows promise for our additives in engineering plastics.

A table containing thermal gravimetric analysis (TGA) data showing onset temperatures of decomposition and %wt. loss at 900°C (N_2, 10°C min^{-1}) for each of the above mentioned compounds is shown below. Differential scanning calorimetry (DSC) data are also included in this table, with the peak temperatures of observed exothermic events listed.

Compound	TGA: Onset	%wt. loss at 900°C	DSC Exotherms
PDPES	300°C	24.4	275, 325, 375°C
PECT	300°C	32.5	375°C
PECP	300°C	28.2	375°C
TPEBPAPC	300°C	42.4	395°C

FUTURE WORK AND CONCLUSIONS

At this time, a large number of alkyne-based flame retardants have been synthesized from existing commercially available brominated aromatics. One definite advantage to these materials is that the cross-linking they perform will help slow the burning of the plastic as well as prevent the molten plastic dripping that occurs during fires. Even though these materials have shown no real practical effectiveness in bulk commodity plastics, such as polypropylene (PP) and polystyrene (PS), they still have great promise. It is very difficult to prevent bulk plastics like PP and PS from burning, so difficult that these polymers have been dubbed "gasoline" polymers by many researchers. Engineering plastics could be the best place for these additives, since many are already thermally stable but still burn, and the combination of an engineering plastic and a high-char material could meet the FAA's desired goal of a fire-resistant cabin interior. The phenylethynylated oligomeric carbonates show the most promise towards this goal and will be tested in polycarbonate in the near future. Further research in this area should answer these questions and determine whether or not these materials are practical solutions to preventing fire fatalities in airline crashes and other accidents where fire rears its incandescent head.

ACKNOWLEDGMENTS

Decabromodiphenyl ether (Saytex 102E), octabromodiphenyl ether (Saytex 111), tetrabromo bisphenol-A (Saytex RB-100), ethylene bis(tetrabromophthalimide) (Saytex BT-93), and flame-retardant testing assistance (UL-94, LOI) were provided by Albemarle Corporation's Technical Center in Baton Rouge, Louisiana. Brominated oligomeric carbonates (Great Lakes BC-58 and BC-52), polydibromostyrene (Great Lakes PDBS-80), 2,6-(dibromo)poly phenylene oxide (Great Lakes PO-64P), and 2,4,6-tribromophenol (Great Lakes PH-73) were provided by Great Lakes Chemical Corporation. High-impact polystyrene and polycarbonate resins were provided by Dow Plastics. Flame-retardant testing (Cone Calorimetry) was provided by the National Institute of Standards and Technology (Dr. Jeff Gilman).

NOMENCLATURE, SYMBOLS, ABBREVIATIONS

HIPS	High-Impact Polystyrene
Ph	Phenyl
PDPES	Polydi(phenylethynyl)styrene
THF	Tetrahydrofuran
DSC	Differential Scanning Calorimetry
TGA	Thermal Gravimetric Analysis
LOI	Limiting Oxygen Index
HVUL-94	Horizontal/Vertical Underwriters Laboratory-94 Flame Test
DPEDPE	Deca(phenylethynyl)diphenyl ether
OPEDPE	Octa(phenylethynyl)diphenyl ether
PECT	Phenylethynylated carbonate tetramer
PECP	Phenylethynylated carbonate pentamer
TPEPA	Tetra(phenylethynyl)phthalic anhydride
TPEBPAPC	Tetra(phenylethynyl)bis phenol A phenyl carbonate

REFERENCES

1. (a) Bergman, R. G. *Acc. Chem. Res.* **1973**, *6*, 25. (b) Bergman, R. G., Lockhart, T. P., and Comita, P. B. *J. Am. Chem. Soc.* **1981**, *103*, 4082. (c) Bergman, R. G. and Lockhart, T. P., *J. Am. Chem. Soc.* **1981**, *103*, 4091. (d) Bergman, R. G., Bharucha, K. N., Marsh, R. M., and Minto, R. E. *J. Am. Chem. Soc.* **1992**, *114*, 3120.
2. (a) Sonogashira, K., Tohda, Y., and Hagihara, N. *Tetrahedron Lett.* **1975**, 4467. (b) Stephans, R. D., and Castro, C. E. *J. Org. Chem.* **1963**, *28*, 3313. (c) Suffert, J. and Ziessel, R. *Tetrahedron Lett.* **1991**, *32*, 757. (d) Blum, J., Baidossi, W., Badrieh, Y., Hoffman, R. E., and Shumann, H. *J. Org. Chem.* **1995**, *60*, 4738
3. Negishi, E., Takahashi, T., Baba, S., Van Horn, D. E., and Okukado, N. *J. Am. Chem. Soc.* **1987**, *109*, 2393.
4. John, J. A. and Tour, J. M. *J. Am. Chem. Soc.* **1994**, *116*, 5011.
5. General Electric trade name.
6. Cone calorimetry data provided by Dr. Jeff Gilman - NIST.

POLYPHOSPHAZENES: FLAME RETARDANTS FOR AIRCRAFT APPLICATIONS

Harry R. Allcock
Department of Chemistry
The Pennsylvania State University
University Park, PA 16802

ABSTRACT

Polyphosphazenes are among the most fire-resistant and fire-retardant polymers known. The facile synthesis of polyphosphazenes by the macromolecular substitution route allows the modification of the polymers to produce specific property combinations including polymer-polymer compatibility. Thus, these polymers may be incorporated into other polymeric materials without compromising the overall structural and mechanical properties. Our goal is to develop an understanding of the mechanism by which polyphosphazenes are fire resistant and fire retardant and to determine the structure-property relationship. Also of interest is the development of an alternative synthesis route which would lower the costs and thus make polyphosphazenes commercially feasible on a large scale. Here we report our initial results in the development of an alternative synthesis route as well as our examination of the thermal stability of a specific polyphosphazene and its effect on the fire resistance and fire-retardant properties of a polyurethane.

INTRODUCTION

A need exists for major advances in the reduction of fire hazards in civil aircraft. Most organic polymers used in commercial aircraft have desirable structural and mechanical properties but have low thermal-oxidative stability. These materials are highly combustible in the presence of a heat source and also can generate dense toxic smoke.

Polyphosphazenes are almost ideal species to impart fire resistance and fire-extinguishing properties to other polymers via polymer blends or IPN's. This would allow the continued use of conventional polymers that are currently in widespread use in civil aircraft. We have already carried out preliminary research into the incorporation of different polyphosphazenes into polymer grafts, blends, and IPN's.[1-3]

Polyphosphazenes form a class of more than 700 high molecular weight macromolecules comprised of an alternating phosphorus and nitrogen backbone which serves as a platform for a wide variety of organic side groups.[4-5] The phosphorus-nitrogen backbone is inherently, thermally, and oxidatively stable. This underlies the fact that polyphosphazenes are among the most fire-resistant and fire-retardant polymers known. Small-molecule compounds that contain phosphorus and nitrogen have been known for at least 30 years to be unusually fire resistant and fire retardant and some have been used commercially for this purpose. However, small-molecule additives have several disadvantages which make them undesirable for long-term fire-retardant applications. Typically, they volatilize at elevated temperatures and low pressures and also leach

from the flammable material over long periods of time. On the other hand, polymeric fire retardants are nonvolatile and essentially nonmigratory. Therefore, for long-term applications, fire-retardant polymers offer the possibility of improved properties for incorporation into seat cushions, carpets, fuel hoses, sound insulation, and other materials used in the aircraft interior. The structural and mechanical properties of polyphosphazenes are determined by both the backbone and the choice of side groups. Thus, polyphosphazenes may be readily modified in order to control specific properties such as solubility, miscibility, glass-transition temperature, flexibility, elasticity, rigidity, or adhesion and their suitability for incorporation into composites, alloys, blends, IPN's, laminates, and so on. It is the choice of the side group that determines the overall thermal stability of the polyphosphazene. For example, poly[*bis*(p-R-phenoxy) phosphazenes], where R is a polar groups, typically undergo side group condensation reactions to form a highly cross-linked ultrastructure.[6-10] Therefore, it is possible to develop polyphosphazenes to be used as fire retardants without compromising the overall properties of the materials.

Polyphosphazenes may be among the most fire-resistant and flame-extinguishing polymers known, but their high cost of production limits their use in nonmilitary applications. Therefore it is not only necessary to develop polyphosphazenes with specific properties for fire-retardant applications, but also to develop new synthetic methods which will lower the cost of manufacture for commercial use. To this end, our research has two overall objectives. First, the development of a potentially inexpensive route to the formation of the starting polymer, poly(dichlorophosphazene) (**2**). Second, the development of specific polymers produced from poly(dichlorophosphazene) to solve flammability problems in civil aircraft.

ALTERNATIVE SYNTHESIS ROUTE FOR POLYPHOSPHAZENES

The relative high cost of polyphosphazenes is the main hindrance to the commercial use of polyphosphazenes as fire retardants. This is not a result of the cost of the starting materials but of the challenging reaction conditions and engineering involved in the large-scale synthesis of poly(dichlorophosphazene) (**2**). Typically, poly(dichlorophosphazene) (**2**) is prepared by the thermal ring-opening polymerization of hexachlorocyclotriphosphazene (**1**) either in the melt at elevated temperatures and reduced pressure or in solution at elevated temperatures utilizing a catalyst and solvents such as *o*-dichlorobenzene (see Scheme 1). Custom-designed polyphosphazenes are then synthesized by the replacement of all the chlorine atoms in poly(dichlorophosphazene) by a wide variety of side groups. We have recently reported the ambient temperature synthesis of poly(dichlorophosphazene) by a living cationic synthesis, which provides excellent molecular weight control.[11] The general reaction is illustrated in *Scheme 2*. This is a more direct route to the synthesis of poly(dichlorophosphazene), and this could provide the key to lowering the costs of polyphosphazenes in general. This route is based on the PCl_5-initiated polymerization of the phosphoranimine, trichloro(trimethylsilyl)phosphoranimine ($Cl_3P{=}NSiMe_3$, **3**). This polymerization proceeds with the elimination of Me_3SiCl, which could be recycled to prepare more of the phosphoranimine. Ideally, the ambient temperature used, the low cost of starting materials, and the potential complete recyclability of the Me_3SiCl could result in the feasible commercial large-scale production of poly(dichlorophosphazene).

Scheme 1

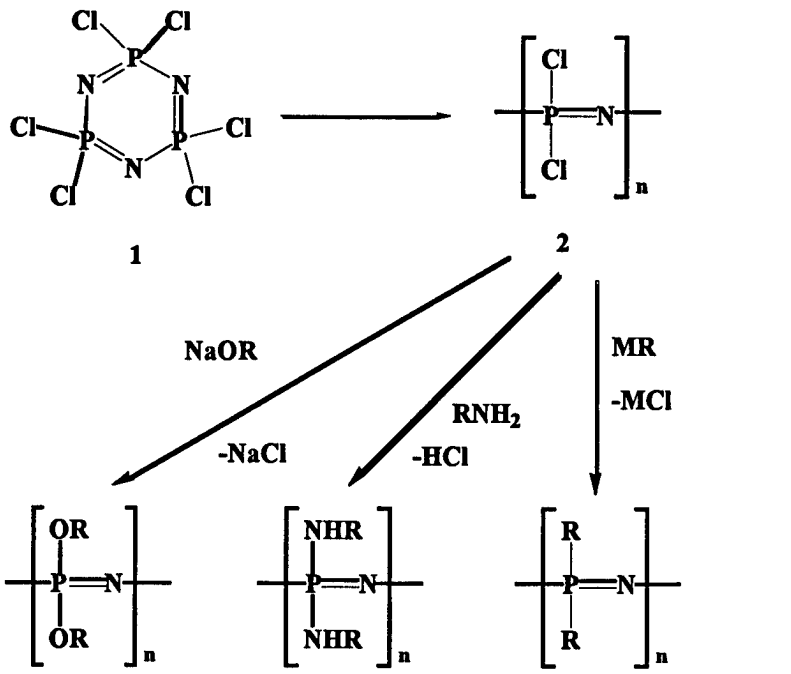

n ~ 15,000 MR = Organometallic Reagent

Scheme 2

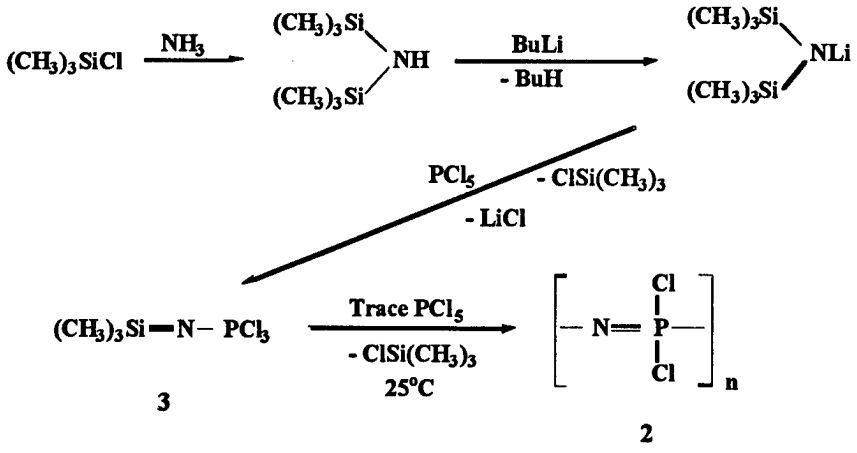

Since our initial communication in 1995, we have continued to study this synthesis route to poly-(dichlorophosphazene).[12-14] One aspect of particular interest is in the ability to control the molecular weights of the resulting polymers, because the molecular weight influences solubility

and miscibility with other polymers. We have examined the effect of varying the monomer **3** to PCl_5 molar ratio. It was found that an increase in the ratio of monomer **3** to PCl_5 results in an increase in molecular weight while still maintaining a low polydispersity. Moreover, once the reaction had proceeded to completion, the polymer molecular weight continues to increase following the addition of more monomer.[12] Thus, the polymerization displays "living" characteristics which opens new opportunities for the of development for polyphosphazenes.

FIRE RESISTANCE AND FIRE RETARDANCY OF POLYPHOSPHAZENES

This research is aimed at answering several questions in order to develop an understanding of the influence of phosphorus and nitrogen compounds on the fire-resistant and fire-retardant properties of other materials.

1. It is known that polyphosphazenes undergo several degradation mechanisms at elevated temperatures. These processes can include backbone cleavage, depolymerization, cross-linking via the side groups, or a combination of these mechanisms. Therefore, it is necessary to understand the degradation mechanisms of those polyphosphazenes which exhibit fire resistance and fire-retardant properties. Also of interest is the identification of the volatile products given off and their role in the fire-retardant behavior.

2. A need exists to understand the structural relationship between polyphosphazenes and their fire-retardant and self-extinguishing properties.

3. Will specific polyphosphazenes which exhibit fire resistance and fire retardance be able to impart these properties to materials formed with other polymers? What degree of loading of polyphosphazene would be required to impart these properties?

4. How can polyphosphazenes be combined with other commercial polymers into polymer blends and IPN's without compromising the structural and mechanical properties?

The polyphosphazene chosen for the initial work is poly[*bis*(carboxylatophenoxy)phosphazene] (**4**).[15] This polymer was chosen for several reasons . First, the fire-retardant properties of poly(aryloxyphosphazenes) are known. Second, carboxylic acid groups are known to react with

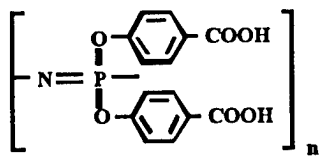

4

isocyanates to form amide linkages, and this allows for the grafting of the polyphosphazene to polyurethanes. Polyurethanes constitute an important class of polymers in the civil aircraft

industry. Third, a recently developed facile synthesis route for the polyphosphazene makes the polymer readily available.[16-17]

A study of the thermal stability of poly[*bis*(carboxylatophenoxy)phosphazene] (**4**) has been carried out.[18] It was found that, at temperatures above 200°C, polymer **4** undergoes cross-linking and condensation reactions with concurrent release the noncombustible gases, water, and carbon dioxide. This also results in the formation of an ultrastructure with a 50% char yield at 850°C which could quench further combustion. It is these features which make polymer **4** a good candidate for incorporation into polymer blends or IPN's as a potential fire retardant. Thus, we have investigated the incorporation of polymer **4** into polyurethane blends. Typically, polyurethanes for commercial applications are formed by the reaction of two prepolymers, one with terminal alcohol groups and the other with terminal isocyanate groups which are mixed to form the higher molecular weight polyurethanes, Scheme 3. Polymer **4** was grafted into a polyurethane blend during the reaction between two standard polyurethane prepolymers, Scheme 4. The effect of polymer **4** on the thermal decomposition of the polyurethane was then examined by thermogravimetric analysis (TGA) and differential weight analysis (DTG), see Figure 1. A flammability test was also performed to determine the effect of polymer **4** on the average burning time and extent of combustion of the polyurethane.

It was found by TGA and DTG experiments that the presence of 20 wt% of polymer **4** in a blend with the polyurethane interferes with the degradation mechanism and maximum rate of degradation of the polyurethane. Additional interactions between the two polymers is evident in the appearance of a maximum in the DTG curve which is not associated with either of the polymers individually. In collaboration with the research groups of Professors Coleman and Painter at Penn State, horizontal flame tests were carried out on a series of sample bars of a pure polyurethane foam and one incorporating 20 wt% of chemically bonded polymer **4**. Polyurethanes are known to be extremely combustible, which was evident from control experiments in which the polyurethane was completely consumed within 40 sec. The sample with 20 wt% of polymer **4** exhibited self-extinguishing properties. The sample was exposed to the flame for the total allowed time of 30 sec and was then removed. It self-extinguished after a total of 55 sec. When examined, it was found that the outer third of the sample had charred and this had protected the inner portion of the sample from further combustion. We attribute this self-extinguishing property to the fact that polymer **4** releases water and carbon dioxide during cross-linking to form the high char yielding ultrastructure. This char appears to be a low thermal conductor which results in a large thermal gradient thoughout the sample to limit heat transfer to the remaining sample.

Scheme 3

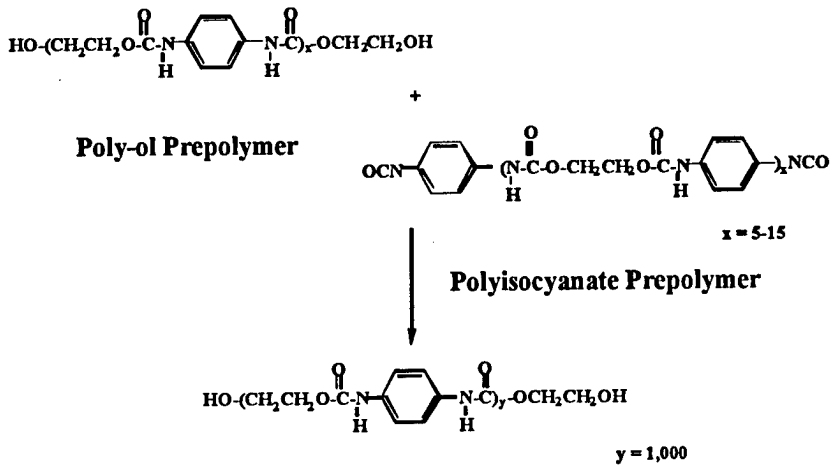

Scheme 4

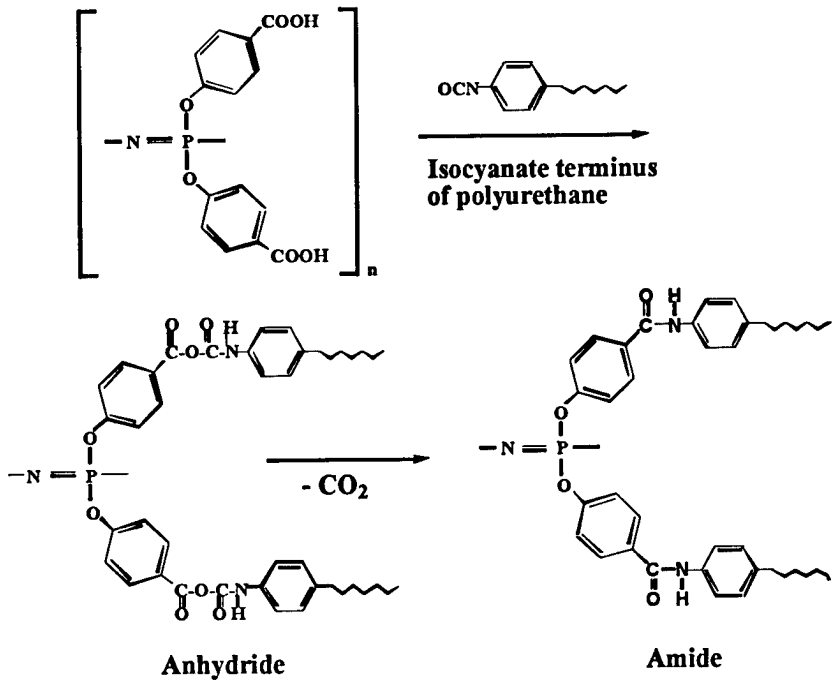

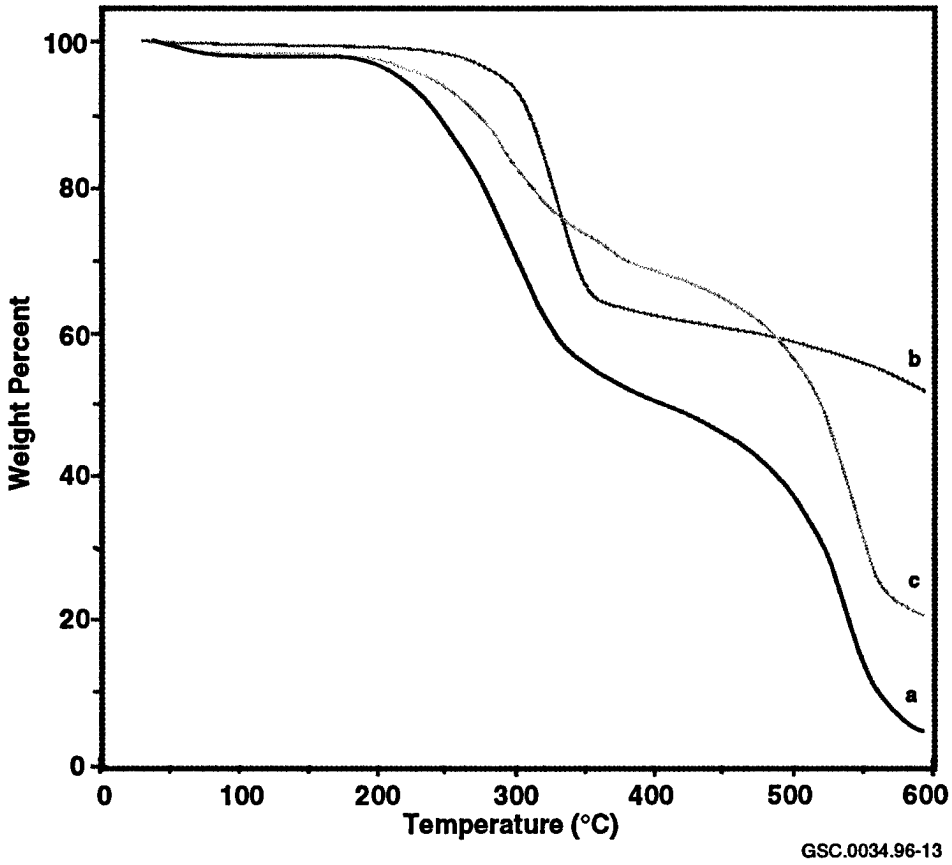

Figure 1. The TGA Curve for Samples of (a) Polyurethane, (b) Polyphosphazene, and (c) Blend With a 20 wt% of Polyphosphazene

FUTURE WORK

A summary of ongoing research is as follows: (1) the investigation of other reactive polyphosphazenes for grafting not only to polyurethanes but also to other important classes of commercial polymers such as polyamides, polyesters, phenolics, and ABS; (2) the design and synthesis of polyphosphazenes for blends with polyolefins and polyvinyl materials; (3) the development of a fundamental basis of compatibility between polyphosphazenes and organic polymers in blends and IPN's; (4) to continue investigating the mechanism of fire resistance and fire retardance of polyphosphazenes as a means for improving material performance; (5) to continue investigating the use of the new "living" cationic ambient temperature synthesis of polyphosphazenes and the implementation of the process on a large scale; and (6) to continue investigation of the new "living" cationic ambient temperature synthesis route for the development of block co-polymers, which could form more compatible blends and IPN's with classical combustible organic polymers.

REFERENCES

1. H.R. Allcock and K.B. Visscher, *Chem. Mater.*, 4, 1182 (1992).
2. H.R. Allcock, K.B. Visscher, and I. Manners, *Chem Mater.*, 4, 1188 (1992).
3. K.B. Visscher, I. Manners, and H.R. Allcock, *ACS Div. PMSE Prepr.*, 65, 3 (1991).
4. H.R. Allcock, *Adv. Maer.*, 6, 106 (1994).
5. J.E. Mark, H.R. Allcock, and R. West, "Inorganic Polymers," Prentice Hall, New Jersey (1992).
6. T.N. Bowmer, R.C. Haddon, S. Chichester-Hicks, M.A. Gomez, and J.G. Fatou, *Macromolecules*, 24, 4827 (1991).
7. S.J. Maynard, T.R. Sharp, and J.F. Haw, *Macromolecules*, 24, 2794 (1991).
8. H.R. Allcock, G.S. McDonnell, G.H. Riding, and I. Manners, *Chem. Mater.*, 2, 425 (1990).
9. L. Goldfarb, N.D. Hann, R.L. Dieck, and D.C.J. Messersmith, *Polym. Sci., Polym. Chem.*, 16, 1505 (1978).
10. H.R. Allcock, G.Y. Moore, and W.J. Cook, *Macromolecules*, 7, 571 (1974).
11. C.H. Honeyman, I. Manners, C.T. Morrissey, and H.R. Allcock, *J. Am. Chem. Soc.*, 117, 7035 (1995).
12. H.R. Allcock, C.A. Crane, C.T. Morrissey, C.H. Honeyman, and I. Manners, *Macromolecules*, in press.
13. H.R. Allcock, S.D. Reeves, J.M. Nelson, and C.A. Crane, manuscript in preparation.
14. H.R. Allcock, J.M. Nelson, and S.D. Reeves, manuscript in preparation.
15. C.S. Reed, J.P. Taylor, K.S. Guigley, K.S. Kully, K.A. Bernheim, M.M. Coleman, P.C. Painter, and H.R. Allcock, manuscript in preparation.
16. H.R. Allcock and S. Kwon, *Macromolecules*, 22, 75 (1989).
17. H.R. Allcock and S. Kwon, U.S. Patent 5,053,451.
18. C.S. Reed, K.S. TenHuisen, P.W. Brown, and H.R. Allcock, *Chem. Mater.*, 8, 440 (1995).

FLAME-RETARDANT PRECURSORS TO HETEROCYCLIC POLYMERS

Chunping Gao and Simon W. Kantor

Department of Polymer Science and Engineering
University of Massachusetts at Amherst
Amherst, MA 01003

ABSTRACT

Heterocyclic precursor polymers, polyhydroxyamides (PHA's), were prepared via low-temperature condensation routes. These polymers can be derivatized with phosphorous compounds to form the phosphorous containing PHA derivatives. Model compounds for the cyclization of the functionalized PHA were prepared to select the most efficient cyclization chemistry which preferably involved an endothermic formation of Polybenzoxazoles, PBO. Both PHA and their phosphorous derivatives cyclize above 200°C to form PBO endothermically and generate flame-retardant molecules such as water or phosphorous compounds.

INTRODUCTION

To eliminate fire as a cause of death in aircraft accidents, a long-range research effort is needed to develop new advanced materials and materials combinations that resist ignition and burning in a high heat flux environment.[1] New high-performance, rigid-rod poly(benzobisoxazole)s are promising materials which are a class of heat-resistant, high-strength, high-modulus polymers that have received much attention from academia and industry.[2] Poly(benzobisoxazole) is the only organic material tested which meets the FAA fire performance goal of no piloted ignition at 50 kw/m^2 incident heat flux when tested in accordance with ASTM E-1354.[1,3]

The synthesis of poly(benzoxazole)s, PBO, often involve low-temperature solution polycondensation of bis(o-aminophenol)s with dicarboxylic acid chlorides or diimidate esters, melt polycondensation of bis(o-aminophenol)s with dicarboxylic acids or diphenylesters, and high-temperature solution polycondensation of bis(o-aminophenol)s with dicarboxylic acids or their derivatives in poly(phosphoric acid) as a reaction medium.[4-7] The melt or condensation in polyphosphoric acid does not generate the desired precursors but rather, the fully cyclized PBO.

It has been reported that PBO can be prepared from the cyclization of their precursors polyhydroxyamides, PHAs, which are our target polymers to be synthesized by low-temperature routes.[8,9] In these studies, films and fibers of PHA, which were prepared by the solution condensation of 3,3′-dihydroxybenzidine and aromatic dicarboxylic acid chlorides, were converted to polybenzoxazole-imides by heat treatment under nitrogen at 370°C for 1 hour.

This investigation is concerned with the synthesis and characterization of PHA and their phosphorous-containing derivatives as the precursors to PBO. We are exploring low-temperature solution polymerizations to prepare heterocyclic precursor polymers which, by themselves, will possess excellent physical properties. These stable precursor polymers may be used as high-performance fire-retardant fibers, composites, and coatings at temperatures up to about 150°C. Above these temperatures and under fire conditions, the precursor polymers will cyclize to form stable aromatic heterocyclic polymers with the simultaneous release of small flame extinguishing phosphorous or brominated molecules.

RESULTS AND DISCUSSION

Synthesis of 3,3′-Dihydroxybenzidine

3,3′-Dihydroxybenzidine (**2**) (**Scheme I**) was prepared by demethylation of 3,3′-dimethoxbenzidine (**1**) with hydriodic acid according to the method reported by Burkhardt and Harold with some modification.[10] In this reaction, with good mixing and proper refluxing, the conversion can reach 100 percent in less than 24 hours. As long as the demethylation reaction is complete, a pure product is readily achieved after recrystallization. 3,3′-Dihydroybenzidine (**2**) is very soluble in alcohols, dipolar aprotic solvents, and aqueous basic solution.

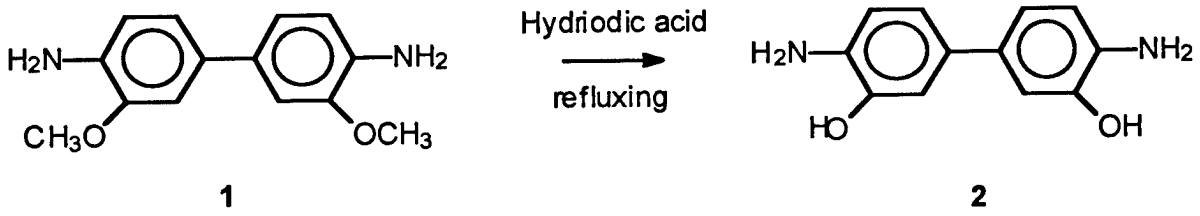

1 **2**

Scheme 1

Synthesis of Aromatic PHA

Fully aromatic PHA **3** of the structures shown in **Scheme II** were prepared by the condensation of 3,3′-dihydroxybenzidine with isophthaloyl chloride or terephthaloyl chloride at 0°C to room temperature using N,N-dimethylacetamide (DMAc) with or without pyridine. Since the polymerization is exothermic, the reaction mixture initially was cooled with ice. The polymers were characterized by NMR to confirm their structures.

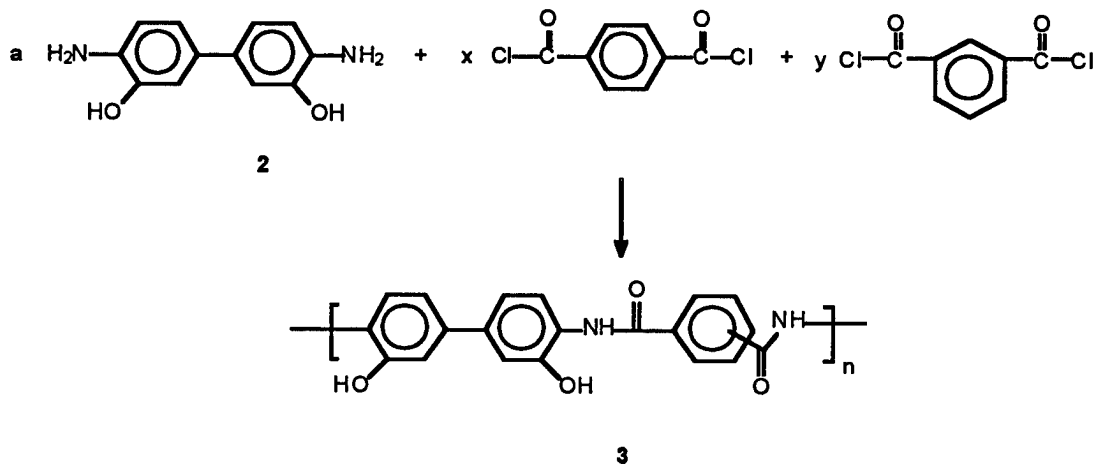

2

3

	3a	3b	3c	3d	3e
x/y	1/0	0/1	1/1	1/4	1/9

Scheme II

Model Reactions for Derivatization of PHA

Our primary goal is to prepare phosphorous containing polyhydroxyamide derivatives via functionalization of PHA with diphenyl chlorophosphate or diphenyl phosphinic chloride. In order to determine the best reaction conditions leading to high yield, the model reactions (**Scheme III**) were carried out. N-(2-hydroxyphenyl)benzamide (**4**) was obtained from the condensation of 2-hydroxyaniline and benzoyl chloride at room temperature in DMAc. N′-(2-hydroxyphenyl)-benzamide **4** was used to react with diphenyl chlorophosphate or diphenyl phosphinic chloride. It was found that an interfacial method at room temperature gave quantitative conversion. Water and chloroform were used as solvents, with sodium hydroxide as a base, and sodium dodecyl sulfate as the surfactant.

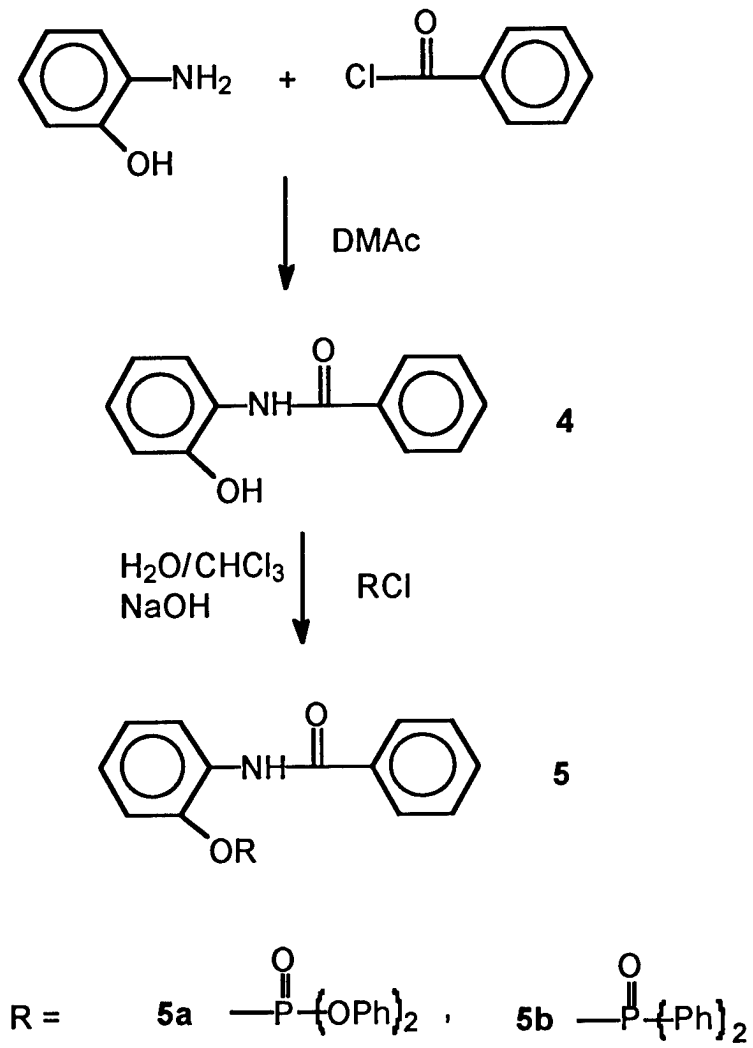

Scheme III

PHA **3** (Scheme IV) were successfully derivatized with diphenyl chlorophosphate or diphenyl phosphinic chloride at room temperature using water and chloroform as solvents in the presence of sodium hydroxide and sodium dodecyl sulfate in quantitative yield. The derivatization reaction takes only 30-60 minutes in a mixing blender at high speed. Without surfactant, the reaction does not proceed or does so at a very low rate. The higher the surfactant concentration, the higher the reaction rate. The base can be sodium hydroxide or potassium hydroxide. The concentration of base in the reaction does not have significant effect on the reaction rate or conversion. It was also found that reaction rate and conversion would be low if too much water was used. Therefore, the volume of water should be kept to the minimum needed to completely dissolve the PHA. Chloroform, methylene chloride, benzene, or toluene can be used as the solvents for this reaction. An optimized amount of the best solvent, chloroform, is needed to make a solution of diphenyl chlorophosphate or diphenyl phosphinic chloride with concentrations in the range of 0.1 to 0.5 M. All phosphorous containing polyhydroxyamide derivatives were characterized by solution NMR.

Derivatization of PHA

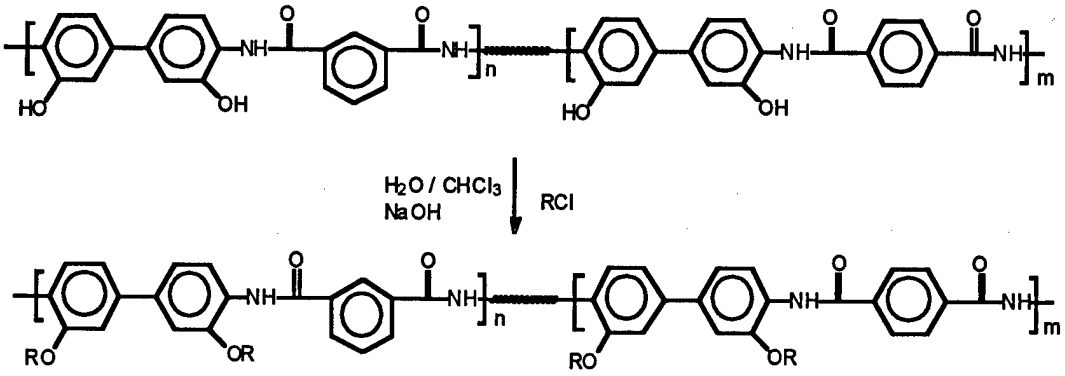

6

	6a	6b	6c	6d	6e	6f
n/m	1/0	1/0	0/1	0/1	1/1	1/1
R	$-P(=O)-(OPh)_2$	$-P(=O)-(Ph)_2$	$-P(=O)-(OPh)_2$	$-P(=O)-(Ph)_2$	$-P(=O)-(OPh)_2$	$-P(=O)-(Ph)_2$

Scheme IV

Model Reactions for Cyclization of PHA Derivatives

The phosphorous PHA derivatives **6** were designed to cyclize at high temperature to form PBO and simultaneously generate phosphorous flame retardants. To confirm this cyclization, the model reactions (Scheme V) were carried out. The phosphorous model compounds **5** cyclize at temperatures above 300°C and form phenyl benzoxazole and phosphorous compounds.

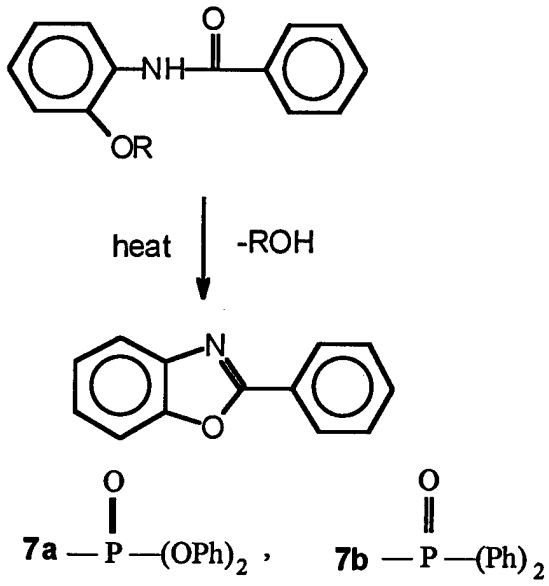

Scheme V

Characterization of PHA and Their Derivatives

PHA **3a-e** are soluble in aqueous basic solution which are stable at least for 24 hours at room temperature, since the inherent viscosities of PHA in aqueous basic solution remained unchanged for 24 hours at room temperature (Figure 1). Hydrolysis of PHA started to occur above 50°C. The inherent viscosities of PHA decreased by 50% after refluxing at 100°C for 30 minutes. The properties of PHA and their phosphorous containing derivatives are summarized in Table 1. The inherent viscosities of the polymers in DMAc at 25°C were in a range of 1.46-3.41 dL/g.

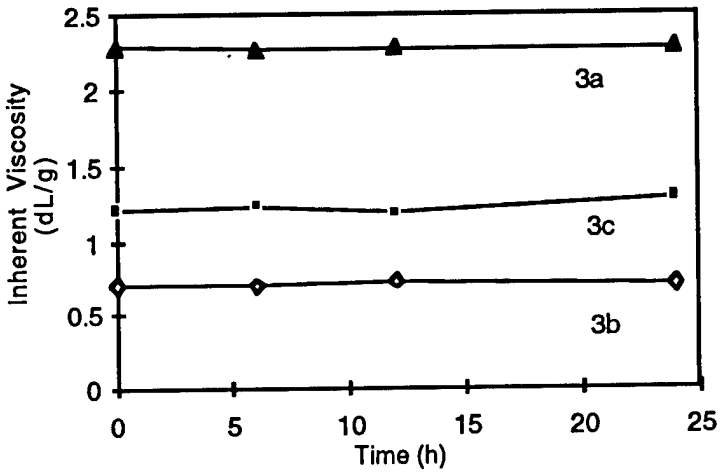

Figure 1. Inherent Viscosity of PHA in Aqeous Basic Solution

Table 1. Properties of PHA and Functionalized Derivatives

Polymers	η_{inh}[a] (dL/g)	T_{onset}[b] (°C)	WLC (%)[c] Obs.	WLC(%) Cal	Char Yield[d] (%)
3a	2.10	200	13	10	49
3b	1.52	220	12	10	50
3c	3.41	215	12	10	52
6a	1.35	253	38	60	40
6b	1.89	259	39	60	40
6c	2.61	255	40	60	42
6d	1.46	248	35	57	33
6e	1.90	245	35	57	35
6f	2.70	250	36	57	38

[a] Inherent viscosity in DMAC at room temperature. [b] Onset temperature of cyclization of the polymers observed in DSC, 10°C/min. [c] Weight loss associated with the cyclization of the polymers, 20°C/min under nitrogen. [d] TGA, 20°C/min under nitrogen.

Figure 2 shows the typical DSC scans of PHA **3a** and **3b**. An endothermic peak, starting about 200°C, was observed for **3a** or **3b**. Similar results (Table 1) were obtained for the other polymers. This endothermic phenomenon is associated with the cyclization of PHA to form PBO. The advantage of an endothermic cyclization is that the reaction acts as a heat sink to further slow down combustion.

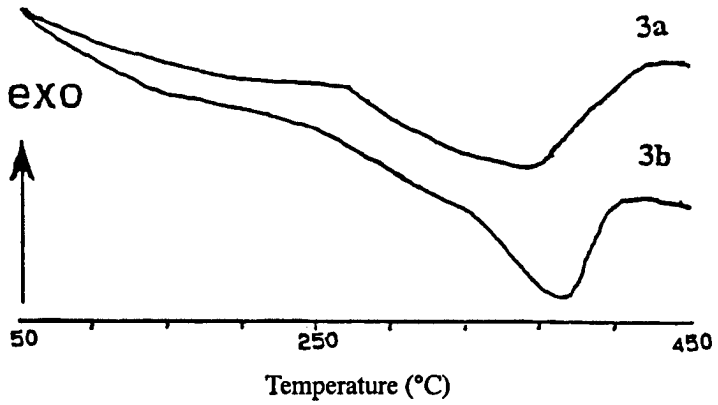

Figure 2. DSC Scans of Polyhydroxyamides 3a, 3b

Thermogravimetric analysis of PHA **3b** (Figure 3) shows a weight loss between 200 to 374°C for the loss of water formed in the cyclization to PBO. After cyclization, no significant weight loss was observed before 550°C with a char yield of 50% at 900°C. For phosphorous containing derivative **6a,** TGA exhibits a weight loss between 310 to 350°C for the loss of phosphorous compounds generated in the cyclization reaction to PBO. The char yield of **6a** at 900°C is 40%. Similar results (Table 1) were observed for other polymers. PHA cyclize at lower temperatures than their phosphorous derivatives. In the case of PHA, the observed weight loss for the loss of water generated from the cyclization is very close to the calculated value. The observed weight loss of the phosphorous derivatives for the loss of phosphorous compounds is lower than the calculated value. The phosphorous compounds generated from the cyclization probably self-condense to form higher molecular weight compounds and remain in the system.

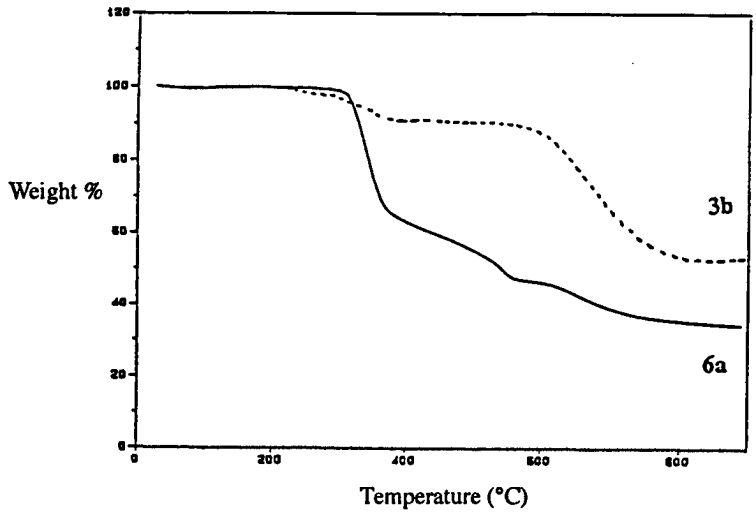

Figure 3. TGA of Polyhydroxyamide 3b and its Derivatives 6a

PHA prepared from 3,3′dihydroxybenzidine and isopathaloyl- or terephthaloyl-chloride are not only soluble in aqueous alkali but also in dipolar aprotic solvents such as DMAc, DMF, DMSO, and NMP. The phosphorous PHA derivatives are soluble in dipolar aprotic solvents. Lithium chloride can increase the solubility of PHA and their derivatives in dipolar aprotic solvent. The

PHA from isophthaloyl chloride is more soluble than similar polymers from terephthaloyl chloride. Flexible, tough films were cast from the solution of the polymers in dipolar aprotic solvent by evaporating the solvent slowly at 100°C.

CONCLUSIONS

Novel flame-retardant heterocyclic polymer precursors were synthesized by a new method. Fully aromatic PHA's were prepared from the condensation of 3,3′-dihydroxybenzidine with isophthaloyl chloride or terephthaloyl chloride at room temperature using N,N-dimethylacetamide as a solvent with or without pyridine. These polymers were successfully derivatized in quantitative yield with diphenyl chlorophosphate or diphenyl phosphinic chloride at room temperature using water and chloroform as solvents in the presence of sodium hydroxide and a surfactant.

PHA's are soluble in aqueous alkali to form a stable solution that may be used for processing. Fully aromatic PHAs and their derivatives are also soluble in dipolar aprotic solvents such as N,N-dimethylacetamide, N,N-dimethylformamide, and dimethyl sulfoxide. The resulting solution may be processed through solution processing methods to yield films, fibers, and coatings. The processing studies are currently under investigation.

PHAs and their derivatives were quantitatively cyclized at temperatures above 200°C or under fire conditions to form thermally stable PBO with the simultaneous release of water or phosphorous compounds which are well known flame retardants. These cyclization reactions to form PBO are endothermic and very efficient. The advantage of an endothermic cyclization is that the reaction acts as a heat sink to further slow down combustion. Another possible advantage of having the volatile flame suppressant liberated is that, as the polymer is cyclized to form a heterocyclic fire-resistant polymer, a foam may be formed with voids full of gaseous flame suppressant molecules to inhibit the fire and also act as a fire retardant for other adjacent structures.

REFERENCES

1. R. E. Lyon, PMSE, 71, 26 (1994), "Advanced Fire Safe Aircraft Materials Research Program," DOT/FAA/AR-95/98.
2. M. W. Ranney, Flame-Retardant Polymers, Noyes Data Corporation, New Jersey (1970).
3. P. K. Kim, P. Pierin, and R. Wessling, J. Fire Science, 11(4), 296 (1993).
4. J. F. Wolfe, Encyclopedia of Polymer Science and Engineering, Wiley Interscience, 11, 601 (1985).
5. J. F. Wolfe and F. E. Arnold, Macromolecules, 14, 909 (1981).
6. S. W. Kantor and J. Sonnenberg, US Pat. 3,306, 876 (1967).
7. P. E. Cassidy, Thermal Stable Polymers, Marcel Dekker, Inc., New York (1980).
8. J. Preston, W. Dewinter, and W. B. Black, J. Polym. Sci. 10, 1377 (1972).
9. T. Kubota and R. Nakanishi, J. Polm. Sci. B, 2, 655 (1964).
10. G. N. Burkhardt and W. Harold, J. Cheme. Soc., 141 (1929).

THERMALLY STABLE SILPHENYLENE VINYL SILOXANE ELASTOMERS AND THEIR BLENDS

H. Dennis, Zhu, Simon, W. Kantor, and William J. MacKnight
Department of Polymer Science and Engineering, University of Massachusetts, Amherst, MA 01003

ABSTRACT

Vinyl substituted silphenylene siloxane elastomers (VSPSE) with variable vinyl content were synthesized using the disilanol-diaminosilane polycondensation approach. High molecular weight elastomers were obtained by using carefully purified monomers. The polymers were characterized by GPC, DSC, and TGA Analysis by ^{29}Si NMR established that the samples have exactly alternating chemical structures. VSPSEs have low glass transition temperatures (T_g's) ranging from -26 to -63°C. Substitution of the methyl group on silicon with phenyl increases the T_g as well as the TGA residues in both air and nitrogen. TGA experiments showed that the VSPSEs synthesized in this study have the highest degradation temperatures reported so far. The TGA residues at 900°C increased to 70% in nitrogen and 57% in air as the vinyl content increased. Furthermore, remarkable isothermal weight losses were shown by the VSPSEs. For example, the elastomer with one vinyl group per repeating unit had a weight loss of 0.7% in nitrogen and 3% in air after 5 hours at 400°C. Blends of VSPSEs with conventional styrene butadiene rubbers (SBR) and also with styrene-butadiene-styrene triblock copolymers (SBS) were prepared using solution blending. DSC studies indicated that these blends were not miscible. Cross-linking the blends broadened the T_g's for the blend constituents indicating a small degree of interfacial phase mixing. Thermal-oxidative stability of the blends is intermediate between that of the VSPSEs and the SBR or SBS.

INTRODUCTION

Flame-retardant polymers have been developed for many applications including airplanes, cars, textiles, and electrical devices. Traditionally, flame-retardant polymers can be prepared by blending polymers with flame-retardant additives such as halogenated or phosphorous compounds.[1] However, this approach often generates toxic, corrosive, or halogenated gases during combustion. We report here the study of nonhalogenated flame-retardant elastomeric materials based on silphenylene siloxane elastomers containing vinyl substituents on the central silicon atom. Silphenylene siloxane elastomers possess low-temperature flexibility and high-temperature stability.[2] The incorporation of vinyl groups into silphenylene siloxane elastomers (VSPSE) have been reported to yield high char residues upon pyrolysis. While VSPSEs have been synthesized previously by the chlorosilane or ureidosilane condensation route[3-6], we found that the silanol-aminosilane condensation[7] produced superior elastomers with short reaction times and narrower molecular weight distributions. The present study involves the preparation and characterization of purified VSPSE. Blends of VSPSE with SBR or SBS thermoplastic elastomers will also be described. The VSPSE can also be chemically modified

and combined with a variety of other polymers via derivatization of the vinyl group, but this will be the subject of another report.

EXPERIMENTAL

Reagents

1, 4-bis(dimethylsilyl) benzene, bis-(dimethylamino)-dimethyl silane, bis(dimethylamino)-methylvinyl silane, and bis(dimethylamino)-methylphenyl silane were obtained from United Chemical Technologies. The bis(dimethylamino) silanes were purified by distillation under an argon atmosphere. SBR and SBS were obtained from Scientific Polymer Products. They were purified by dissolution in toluene and reprecipitation with methanol which removed inhibitors and stabilizers. All other reagents used were purified using either recrystillization or distillation.

Characterization Methods

The elemental analyses were carried out by the Microanalysis Laboratory at the University of Massachusetts. Inherent viscosities for polymers were determined at 30ϒC in tetrahydrofuran using a Cannon-Ubbelohde viscometer at a polymer concentration of 0.01 g/mL. ^{1}H NMR spectra were obtained with a Bruker/IBM 200AC NMR spectrometer operating at 200 MHz. ^{13}C NMR spectra were obtained with a Varian XL-300 NMR spectrometer operating at 75 MHz in deuterated solvents. ^{29}Si NMR spectra were recorded on a Varian XL-300 NMR spectrometer operating at 60 MHz. GPC measurements were performed on a Waters Model 6000A with a Waters Differential Refractometer using THF as mobile phase. Polystyrene standards were used for calibration.

DSC measurements were conducted with a Perkin-Elmer DSC-7 on samples ranging from 7-10 mg. The temperature and power ordinates of the DSC were calibrated with the known melting point and heat of fusion of a high-purity indium standard supplied by Perkin-Elmer. The glass transition temperature (T_g) was defined as the midpoint of the change in the specific heat. TGA experiments were conducted with a Perkin-Elmer TGA-7 on samples ranging from 10-15 mg.

1, 4-Bis-(hydroxydimethylsilyl) benzene

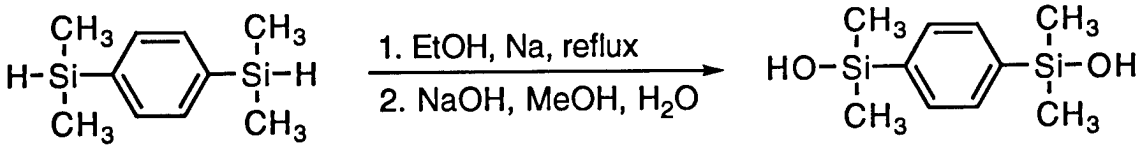

Anhydrous ethanol (10 mL) and a small piece of sodium metal under argon were added to a flame-dried 50 mL three-neck, round-bottom flask equipped with a magnetic stirrer and water condenser. The ethanol was heated to reflux. Then 1, 4-bis(dimethylsilyl)benzene (8.200 g., 42.3 mmol) was added dropwise to the reaction flask with stirring over 10 min. When hydrogen evolution ceased, the reaction mixture was added with vigorous stirring to a mixture of NaOH (5.7 g), CH_3OH (35 mL), and H_2O (4 mL). After standing for 15 min, another solution of NaOH (5.7 g) in H_2O (38 mL) was added to the mixture. The mixture was allowed to stand for 30 min

with occasional shaking and then poured into a vigorously stirred solution of KH_2PO_4 (50 g) in excess ice and H_2O (200 mL). Crude disilanol product was precipitated as a white solid, filtered, dissolved in ethyl ether (50 mL), and washed with an equal volume of water. The ether solution of the product was dried with anhydrous Na_2SO_4 and concentrated to give a white solid. The solid was recrystallized from hot CCl_4 (200 mL) and dried at 70°C overnight in vacuo to provide the final needle like white solid product (8.5 g, yield 89%). ^1H NMR (d_6-DMSO, 200 MHz) d 7.48 (s, -$C_6\underline{H}_4$-aromatic protons), 5.85 (s, -O$\underline{H}$), 0.19 (s, -$C\underline{H}_3$). ^{13}C NMR (d_6-DMSO, 75 MHz) δ 141.2, 132.0, 0.5. Elemental analysis calculated for $C_{10}H_{18}Si_2O_2$: C, 53.05%; H, 8.01%; found: C, 52.71%; H, 8.02%. Melting point (T_m): 137°C.

Poly (1,4-phenylene-hexamethyltrisiloxanyl), VSPSE 1

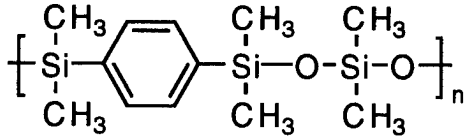

1,4-Bis (hydroxydimethylsilyl) benzene (4.00 g, 17.67 mmol) was added under argon to a flame-dried 50 mL three-neck, round-bottom flask equipped with magnetic stirrer and water condenser. Then dry toluene (6 mL) was transferred into the flask by syringe. With stirring, bis-(dimethyl-amino)-dimethylsilane (2.512 g) was transferred by syringe into the reaction flask. The flask was heated to 105-110°C within 20 min. and the evolution of dimethylamine was noted. After a 1-hour reaction, an additional amount of bis-(dimethylamino)-dimethylsilane (20 μL each time) was added at a time interval of 15 min. until there was no significant gas evolution (total 100 μL) and the reaction mixture gelled. Then, the reaction mixture was precipitated into methanol (40 mL). A transparent gum like elastomer (4.5 g, yield 90%) was obtained after drying in vacuum oven at 70°C for 8 hours. ^{29}Si NMR ($CDCl_3$, 60 MHz) δ -2.62, -19.6. Elemental analysis calculated for $C_{12}H_{22}Si_3O_2$: C, 51.01%; H, 7.85%; found: C, 51.20%; H, 7.67%.

Poly (1,4-phenylene-hexamethyltrisiloxanyl)-co-(1,4-phenylene-1, 1, 3, 5, 5-pentamethyl-3-vinyltrisiloxanyl), VSPSE 2 (Vinyl Content, 10 mol%)

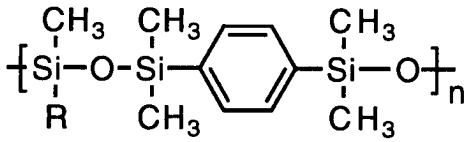

R = -CH_3 (90 mol%) and CH_2=CH- (10 mol%)

1,4-bis (hydroxydimethylsilyl) benzene (4.00 g, 17.67 mmol) was added under argon to a flame-dried 50 mL three-neck, round-bottom flask equipped with magnetic stirrer and water condenser. Then dry toluene (3 mL) was transferred into the flask by syringe. With stirring, a solution of bis(dimethylamino)dimethylsilane (2.268 g) and bis(dimethylamino)-methylvinylsilane (279.7 mg) in toluene (3 mL) was syringe transferred into the reaction flask. The flask was heated to 105-110°C within 20 min., and the evolution of dimethylamine was noted. After a 1-hour reaction, an additional amount of bis(dimethylamino)dimethylsilane (20 μL each time) was added at a time interval of 15 min. until there was no significant gas evolution and the reaction mixture gelled. The reaction mixture was precipitated into methanol (40 mL). A transparent gum like material (4.5 g, yield 90%) was obtained after drying in vacuum oven at 70°C for 8 hours.

Poly (1,4-phenylene-hexamethyltrisiloxanyl)-co-(1,4-phenylene-1, 1, 3, 5, 5-pentamethyl-3-vinyltrisiloxanyl), VSPSE 3 (Vinyl Content, 20 mol%)

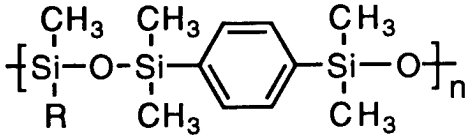

R = -CH_3 (80 mol%) and CH_2=CH- (20 mol%)

The synthesis of VSPSE 3 was similar to that for VSPSE 2. A transparent gum-like material (4.6 g, yield 92%) was obtained after drying in a vacuum oven at 70°C for 8 hours.

Poly (1,4-phenylene-1, 1, 3, 5, 5-pentamethyl-3-vinyltrisiloxanyl), VSPSE 4

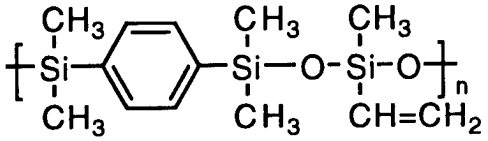

The synthesis of VSPSE 4 was similar to that for VSPSE 1. Bis(dimethylamino)-methylvinyl-silane was used instead of bis(dimethylamino)-dimethylsilane. A transparent gum-like material (4.8 g, yield 92%) was obtained after drying in a vacuum oven at 70°C for 8 hours.

Poly (1,4-phenylene-1, 1, 3, 5, 5-pentamethyl-3-phenyltrisiloxanyl),VSPSE 5

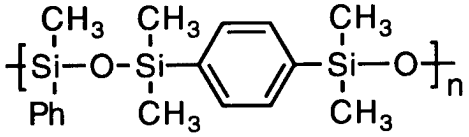

The synthesis of VSPSE 5 was similar to that for VSPSE 1. Bis(dimethylamino)-methylphenyl-silane was used instead of bis(dimethylamino)-dimethylsilane. A transparent gum-like material (5.7 g, yield 93%) was obtained after drying in a vacuum oven at 70°C for 8 hours. ^{29}Si NMR ($CDCl_3$, 60 MHz) δ -1.32, -32.96.

Poly (1,4-phenylene-hexamethyltrisiloxanyl)-co-(1,4-phenylene-1, 1, 3, 5, 5-pentamethyl-3-vinyltrisiloxanyl)-co-(1,4-phenylene-1, 1, 3, 5, 5-pentamethyl-3-phenyltrisiloxanyl), VSPSE 6

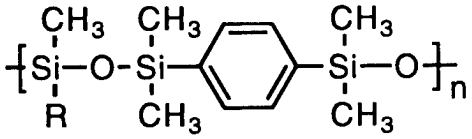

R = Ph (45 mol%), -CH_3 (45 mol%) and CH_2=CH- (10 mol%)

1, 4-bis (hydroxydimethylsilyl) benzene (4.00 g, 17.67 mmol) was added under argon to a flame-dried 50 mL three-neck, round-bottom flask equipped with magnetic stirrer and water condenser

Then dry toluene (3 mL) was transferred into the flask by syringe. With stirring, a solution of bis(dimethylamino)dimethyl silane (1.163 g), bis(dimethylamino)methylphenyl silane (1.654 g), and bis(dimethylamino)-methylvinylsilane (279.7 mg) in toluene (3 mL) was transferred by

syringe into the reaction flask. The flask was heated to 105-110°C within 20 min., and the evolution of dimethylamine was noticed. After a 1 hour reaction, an additional amount of bis-(dimethylamino)dimethyl silane (20 μL each time) was added at a time interval of 15 min. until there was no significant gas evolution and the reaction mixture gelled. The reaction mixture was precipitated into methanol (40 mL). A transparent gum like material (4.8 g, yield 88%) was obtained after drying in a vacuum oven at 70°C for 8 hours.

VSPSEs have been synthesized previously using the chlorosilane or the ureidosilane routes.[3-6] The chlorosilane-silanol condensation reaction will generate HCl which can catalyze the self-condensation of the silanol monomer, thus preventing the formation of exactly alternating polymer structures. Although the ureidosilane approach can produce alternating VSPSE, the reaction times are very long, and broad molecular weight distributions are common. We believe that the presence of ureido end groups would cause lower thermal stability in the VSPSE. For these reasons, we selected the disilanol-diaminosilane polycondensation route in which the by-product amine is generated as a gas providing a clean reaction.[7] The reaction was carried out in toluene at 110°C under argon atmosphere as shown in Scheme 1 below. By careful purification of the starting monomers, either by distillation or recrystallization, all below VSPSEs were obtained as transparent, high molecular weight, gum-like materials with high yields ranging from 88% to 93%. With the use of unpurified monomers, low molecular weight oil-like yellow-colored polymers were obtained. From VSPSE 1 to VSPSE 4 in Scheme 2, the R substituent on the central silicon atom may be either methyl or vinyl or a combination of both with a vinyl content from 10 to 20 mole%. VSPSE 5 has a phenyl group only for the R substituent. For VSPSE 6, the R substituent has a combination of vinyl (10%), methyl (45%) and phenyl groups (45%). The presence of vinyl groups in these elastomers provides a co-vulcanization potential when blended with other unsaturated hydrocarbon rubbers. The phenyl group in VSPSE 6 may also promote some compatibility with SBR type elastomers.

Scheme 1

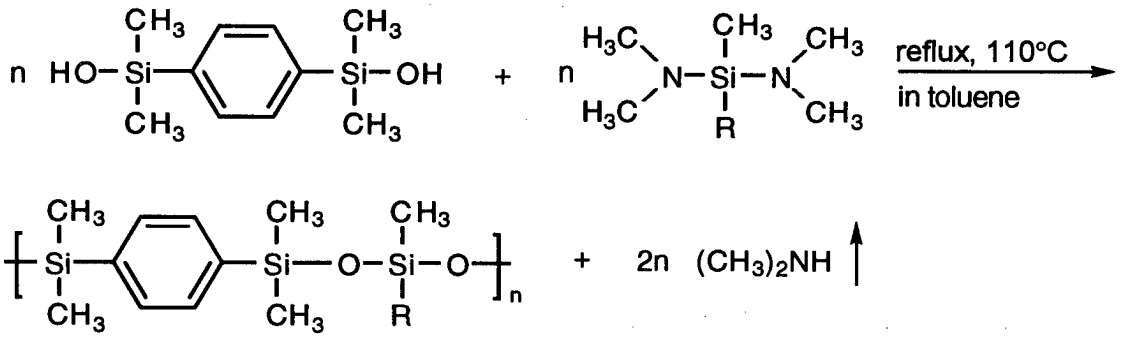

Elastomer Numbers

1	$R = CH_3$
2	$R = 0.9\ CH_3 + 0.1\ -CH=CH_2$
3	$R = 0.8\ CH_3 + 0.2\ -CH=CH_2$
4	$R = -CH=CH_2$
5	$R = -C_6H_5$
6	$R = 0.1\ -CH=CH_2 + 0.45\ CH_3 + 0.45\ -C_6H_5$

Preparation of Uncross-Linked Polymer Blends

A typical procedure for the preparation of an uncross-linked polymer blend is described below and in Scheme 2.

The two elastomers that are to be blended are dissolved together in toluene. The concentration of the blend is less than 5% by weight. Then, it is precipitated by the addition of methanol under vigorous stirring. After decanting the liquid, a wet blend is obtained. Finally, it is washed with methanol and dried in a vacuum oven at 60°C for 8 hours and recovered quantitatively.

Scheme 2. Typical Procedure for Polymer Blend Preparation

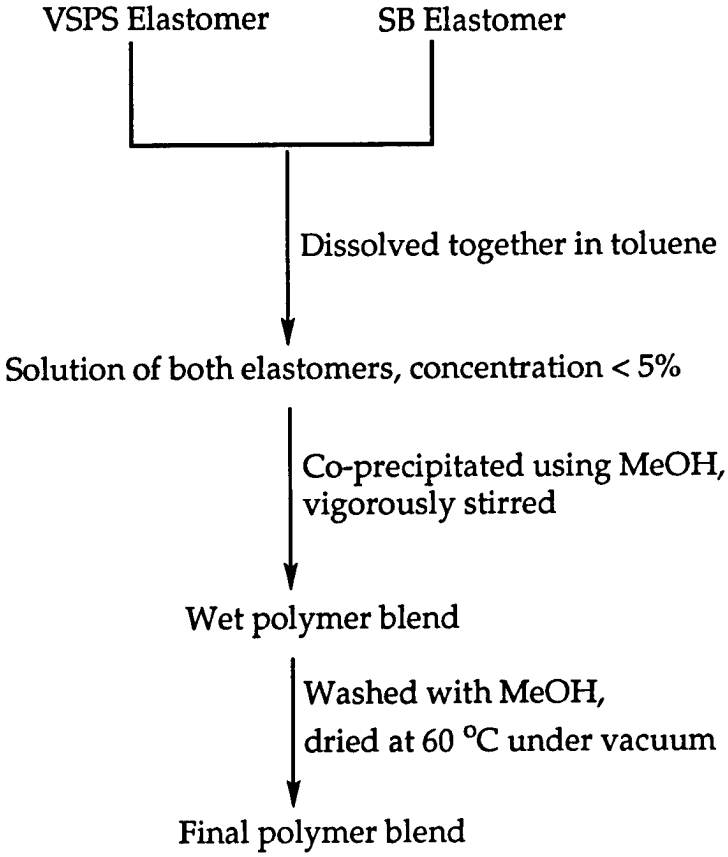

Preparation of Cross-Linked Polymer Blends

A typical procedure for the preparation of a cross-linked polymer blend is described below :

Two polymers to be blended are dissolved first in tetrahydrofuran at a concentration of less than 5% by weight. Then, benzoyl peroxide (BPO, 1% by weight of the blend) is added with stirring into the solution. The blend is obtained by evaporating the THF solvent and drying in a vacuum oven at 30°C for 8 hours. The blend containing 1% BPO was pressure molded at 130°C for 40 min. Then, the cross-linked blend was transferred into a vacuum oven at 30°C for another 3 hours.

RESULTS AND DISCUSSION

Synthesis and Characterization of VSPSE

GPC and DSC techniques were used to characterize the VSPSE. Table 1 summarizes the characterization results. In general, they had relatively high molecular weights ranging from a M_w of 96,000 to 798,000. The molecular weight distribution indexes ranged from 2.3 to 4.8, which is much lower than those attained by the ureido route, which were typically around 10. They exhibited low T_g's, ranging from -26 to -63°C. Substituting the central methyl group with vinyl did not affect the T_g significantly. Substituting the central methyl with phenyl increased Tg by about 40°C. Among the VSPSEs, VSPSE 5 had the highest T_g of -26°C. ^{29}Si solution NMR analyses were also carried out for all VSPSEs. In the case of VSPSEs 1 and 5, only two peaks were observed, which is consistent with the presence of an alternating chemical structure, exhibiting one peak for the silicon atom adjacent to the phenylene ring and a second peak for the central silicon atom. VSPSEs 2, 3, and 6 showed additional peaks due to their more complex compositions since they are copolymers.

^{29}Si NMR spectra for VSPSEs 1 and 5 are shown in Figures 1 and 2 respectively. Table 1 presents a summary of the six elastomers that were prepared by Scheme 2 and includes yields, molecular weights, and glass transition temperatures.

Table 1. VSPSE

VSPSE No.	R	Yield, %	Molecular Weight[1] $M_w \times 10^{-3}$, $M_n \times 10^{-3}$		PDI	T_g[2], °C
1	Me	90	149	64.4	2.3	-59
2	0.9 Me + 0.1 Vi	90	221	66.3	3.3	-59
3	0.8 Me + 0.2 Vi	92	798	168	4.8	-59
4	Vi	92	477	109	4.4	-63
5	Ph	93	96	42.5	2.3	-26
6	0.1Vi + 0.45 Me + 0.45 Ph	88	425	88.7	4.8	-43

1. Polystyrene samples were used as standards and chloroform as solvent.
2. Obtained by DSC measurement.

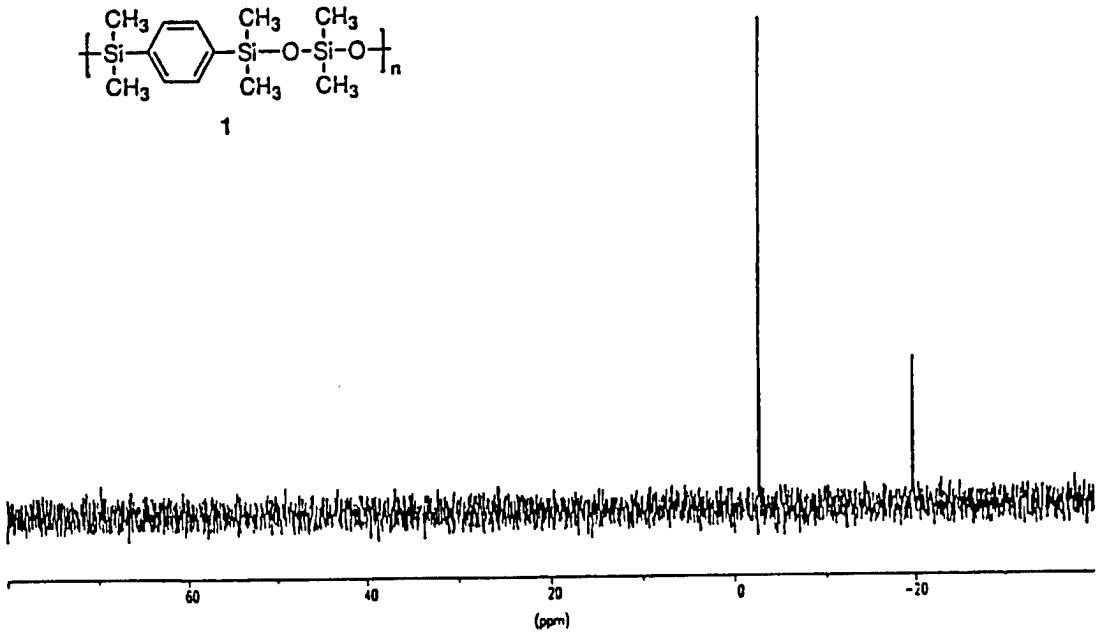

1

Figure 1. Sixty MHz ^{29}Si Solution NMR of VSPSE 1

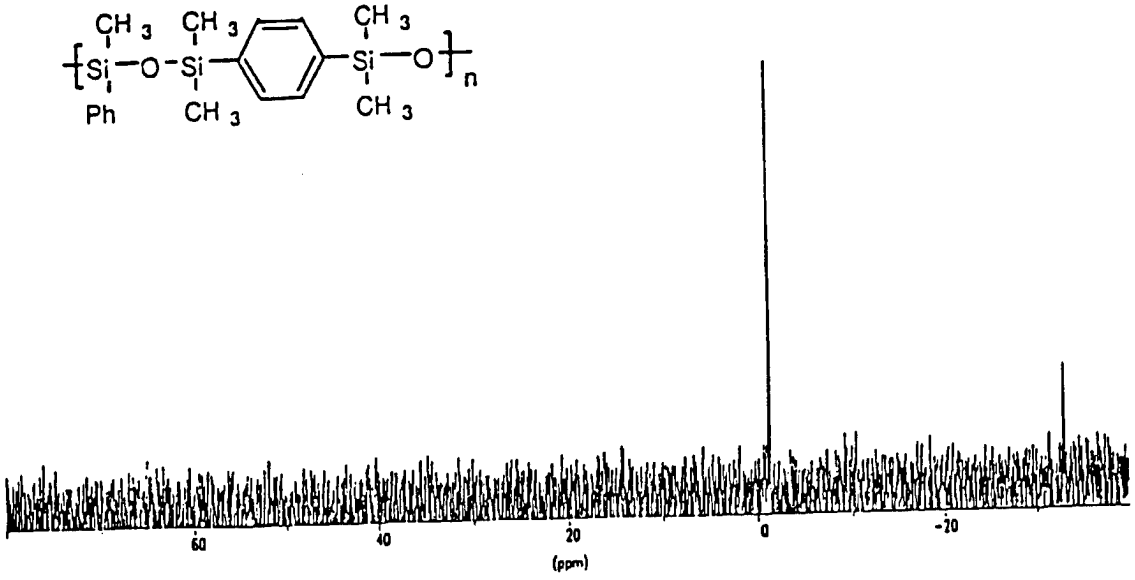

Figure 2. Sixty MHz ^{29}Si Solution NMR of VSPSE 5

Thermal Stability and Decomposition of VSPSE

Figure 3 gives the TGA curves for each VSPSE (1 to 6) under nitrogen atmosphere at a heating rate of 15°C. A summary of the TGA results in nitrogen is given in Table 2. The VSPSEs have high onset degradation temperatures ranging from 395 to 547°C in nitrogen atmosphere, which is from 60°C to more than 100°C higher than decomposition values reported before.[5-6] The temperatures for 50% weight loss are well above 600°C and the end of the major degradation

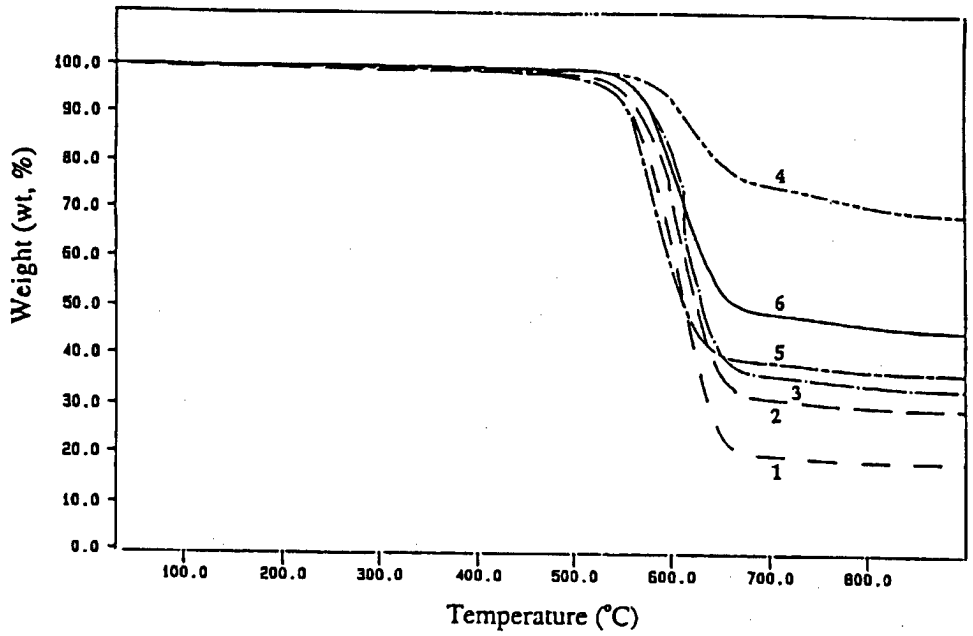

Figure 3. TGA of VSPSE (in N_2, 15°C/Min). Curves 1, 2, 3, 4, 5, and 6 Correspond for VSPSEs 1, 2, 3, 4, 5, and 6, respectively

ranges from 671 to 688°C. From VSPSE 1 to VSPSE 4, the final residue increases from 20% up to 70% as the vinyl content is increased, which has been observed before.[5-6] Comparing VSPSEs 2 and 6, substitution of 50% of the methyl groups with phenyl increases the onset degradation temperature by 42°C and the residue by 14%. In nitrogen, all VSPSEs exhibit a single major break in their decomposition curves before their major weight losses level off at about 670°C. This behavior is indicative of a single mechanism of decomposition which is similar for all the VSPSEs. However, the larger residues for higher vinyl containing compositions also indicate thermally induced vinyl polymerization or aromatization via cyclization reactions.

Table 2. TGA Data of VSPSEs 1-6 in Nitrogen (15°C/M)

VSPSE No.	Onset of degradation T_d (°C)[1]	Temperature for 50% wt. loss (°C)	End of major degradation (°C)	% Residue at 900°C
1	462	614	676	20
2	491	626	686	31
3	517	633	674	33
4	547	--[2]	675	70
5	395	614	671	39
6	523	668	688	45

1. The temperature at which the major degradation starts.
2. Since VSPSE 4 loses only 30% weight at 900°C, the 50% weight loss temperature is clearly considerably above 900°C.

Figure 4 presents the TGA curves of VSPSE 1 to 6 in air at a heating rate of 15°C per minute, and these results are summarized in Table 3. Similar to their decomposition in nitrogen, they exhibit high onset degradation temperatures ranging from 374 to 462°C. As expected, the stability in air is generally less than the corresponding stability in nitrogen, except for VSPSE 5 which is about the same. The temperatures for 50% weight loss are above 600°C and the end of the major degradation temperature ranges from 781 to 883°C. From VSPSEs 1 to 4, the final residue at 900°C is increased from 32% to 57% as the vinyl content is increased. VSPSEs 5 and 6, again, have higher residues and onset degradation temperatures than those of VSPSE 2. The most outstanding thermal and oxidative stability behavior is shown by VSPSE 4, with one vinyl group per repeating unit. This actually corresponds to one vinyl group out of 6 aliphatic substituents, or a 16.7 mole % vinyl content. It will be interesting to examine the thermooxidative behavior of VSPSEs with even higher vinyl content.

One of the most interesting features of the air decomposition curves is the apparent two-step break in the weight loss curves compared to the single-step break in nitrogen. This behavior suggests two distinct and separate decomposition pathways in air, with the second one of these occurring at higher temperatures. At this time, it is not possible to present detailed degradation mechanisms for the decomposition of the VSPSE.

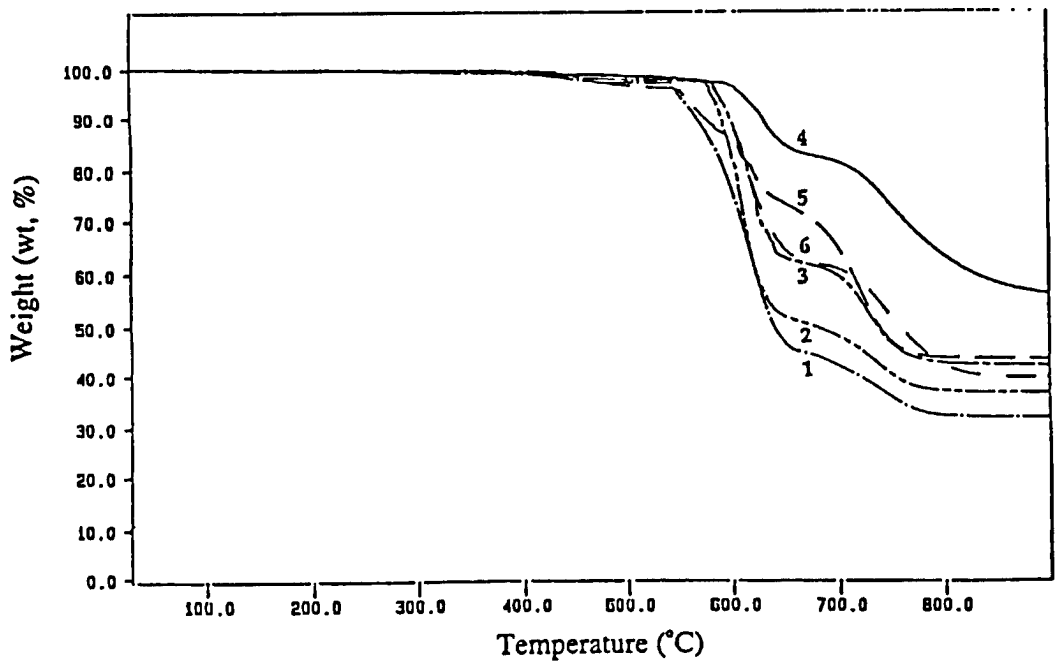

Figure 4. TGA of VSPSE (in air, 15°C/Min). Curves 1, 2, 3, 4, 5, and 6 Correspond to VSPSE 1, 2, 3, 4, 5, and 6, respectively

Table 3. TGA Data of VSPSE 1-6 in Air (15°C/M)

VSPSE No.	Onset of degradation T_d (°C)[1]	Temperature for 50% wt. loss (°C)	End of major degradation (°C)	% Residue at 900°C
1	374	639	787	32
2	419	672	781	37
3	387	736	795	43
4	431	--	883	57
5	396	738	783	44
6	462	756	838	40

1. The temperature at which the major degradation starts.
2. Since VSPSE 4 loses only 57% weight at 900°C, the 50% weight loss temperature is above 900°C.

Figures 5 and 6 show the isothermal decomposition curves for VSPSEs 1 to 6 in nitrogen and air, respectively. All of them are remarkably stable under such conditions. The mass losses summarized in Table 4 range from 0.7% to 10.7% in nitrogen and from 3.0% to 13% in air after 5 hours at 400°C.

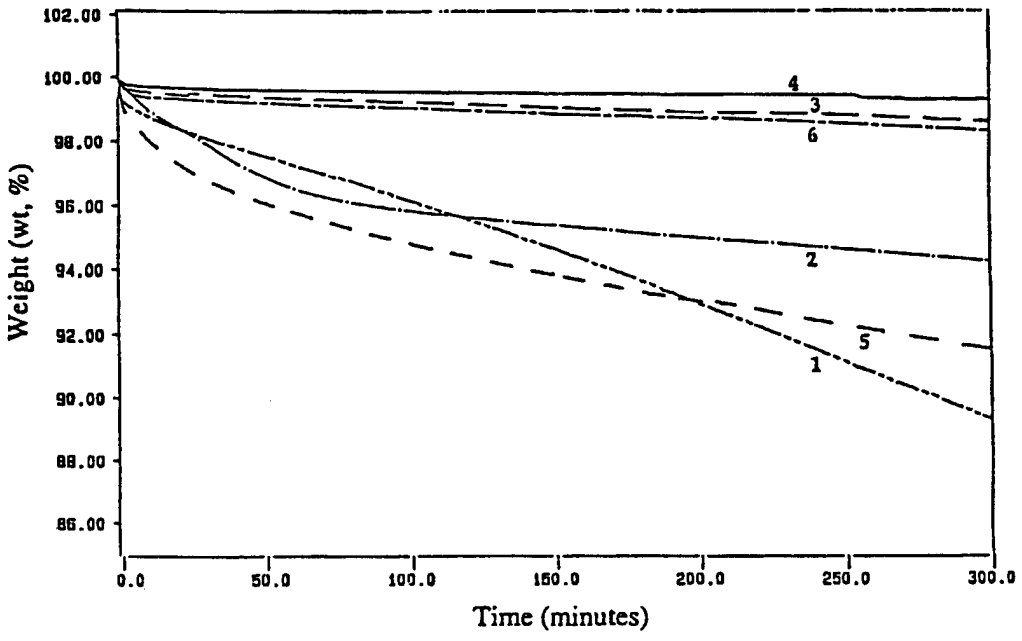

Figure 5. Isothermal Studies of VSPSE (400°C, in N_2). Curves 1, 2, 3, 4, 5, and 6 Correspond to VSPSEs 1, 2, 3, 4, 5, and 6, respectively

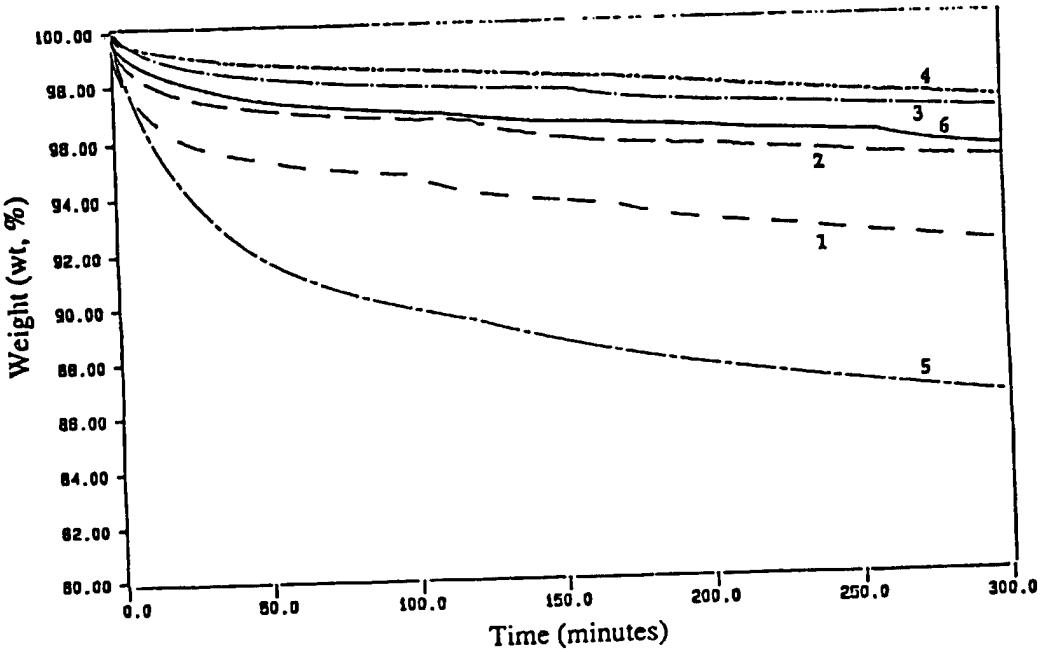

Figure 6. Isothermal Studies of VSPSE (400°C, in air). Curves 1, 2, 3, 4, 5, and 6 Correspond to VSPSEs 1, 2, 3, 4, 5, and 6, respectively

Table 4. Isothermal Weight Loss for VSPSEs in Air and Nitrogen Atmosphere After 5 Hours at 400°C

VSPSE Numbers	1	2	3	4	5	6
in nitrogen, %	10.7	5.9	1.5	0.7	8.0	1.8
in air, %	7.9	5.0	3.5	3.0	13	4.6

These results are unusually low and represent the most thermally stable elastomers reported to date. Previous studies show that 20% mass loss for such elastomers is common.[5-6] We also observed that the isothermal stability for the VSPSE increases from VSPSEs 1 to 4 when the vinyl content is increased. Some VSPSEs such as 6, 3, and 4 have weight losses even less than 2% in nitrogen and VSPSEs 2, 6, 3, and 4 have weight losses less than 5% in air. The most remarkable stability was shown by VSPSE 4, with R = 100% vinyl, which had a weight loss of only 0.7% after 5 hours at 400°C in nitrogen and 3.0% after 5 hours at 400°C in air. When comparing all the dynamic and isothermal TGA studies, VSPSE 4 was consistently the most thermally stable.

Polymer Blends From VSPSE and SBR or SBS

Commercially available SBR and SBS were purified to remove stabilizers and other additives and impurities. These styrene-butadiene rubbers have low glass transition temperatures ranging from -94 to -30°C and high molecular weights as shown in Table 5.

Table 5. Characterization of Commercial SB Elastomers

SB Rubber	Tg (°C)	M_w (x 10^{-3})*	Styrene Content, wt%	1, 2 Addition Content, wt%
SBR-199	-75	838	5%	12
SBR-200	-58	545	23%	9
SBR-201	-30	348	45%	6
SBS-057	-94	131	30%	6
SBS-451	-92	90	28%	4

* Polystyrene samples were used as standards and chloroform as solvent for GPC measurements.

The weight percentage for 1, 2 addition units of 1, 4-butadiene was determined using ^1H NMR integration of olefinic protons. The 1, 2 addition content ranges from 4% to 12% by weight. The 1, 2 addition units of 1, 4-butadiene, corresponding to vinyl content, are preferred for efficient co-vulcanization of the blends.

Uncross-linked polymer blends from VSPSE and SBR or SBS were prepared according to Scheme 2. All the polymer blends listed in Table 6 were prepared. All polymer blends were made either with VSPSE 4 or with VSPSE 6. A weight ratio of 50 to 50 was used for most polymer blends. In all, a total of ten blend compositions, both uncross-linked and cross-linked were prepared.

Table 6. Glass Transition Temperatures of Blends

Elastomers and Blends	Blend Composition	Tg, °C[1] Uncross-Linked	Cross-Linked[2]
VSPSE4	-----	-63	-60
VSPSE6	-----	-43	-42
SBS057	-----	-94	-92
SBS451	-----	-92	-91
SBR199	-----	-75	-74
SBR200	-----	-58	-54
SBR201	-----	-31	-30
VSPSE4/SBS057	50/50	-63, -94	-57, -92
VSPSE4/SBS451	50/50	-63, -92	-57, -91
VSPSE4/SBR199	50/50	-63, -76	-58, -75
VSPSE4/SBR200	50/50	-63, -55	-57
VSPSE4/SBR201	50/50	-65, -28	-59, -26
VSPSE6/SBS057	50/50	-43, -96	-41, -93
VSPSE6/SBS451	50/50	-43, -94	-42, -91
VSPSE6/SBR199	50/50	-43, -76	-41, -74
VSPSE6/SBR200	75/25	-44, -57	-41, -52
VSPSE6/SBR201	50/50	-44, -27	-41, -24

1. For the blend, the first number in the column corresponds to the T_g of the VSPSE and the second number is the T_g of the hydrocarbon elastomer.
2. Cross-linked with benzoyl peroxide, 1% by weight of the blend.

DSC was used to investigate the extent of miscibility for the two constituent polymers in uncross-linked and cross-linked blends. Table 6 shows the T_g results for uncross-linked blends and for uncross-linked individual constituents in these blends. In all cases, two individual unshifted T_g's were observed for VSPSEs 4 and 6 blends indicating their lack of miscibility, which is expected for siloxane and hydrocarbon elastomers. Figure 7 shows the DSC results for the uncross-linked VSPSE4/SBR199 (50/50) blend, which are typical for all uncross-linked blends.

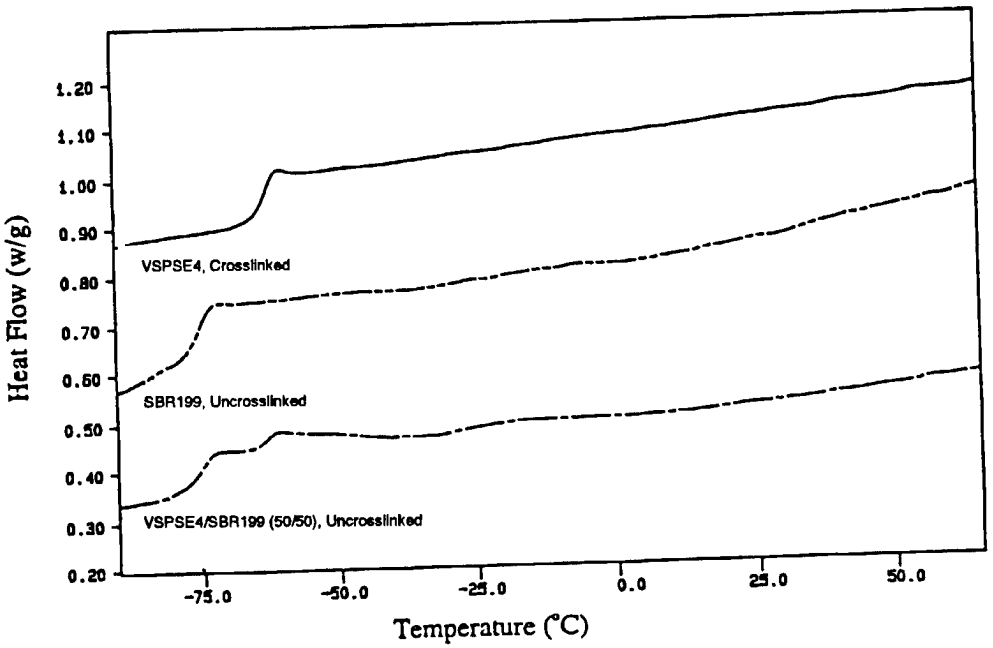

Figure 7. DSC Curves for Uncross-Linked VSPSE 4, SBR199, and VSPSE4/SBR199 (50/50) Blend

The DSC results for the cross-linked blends are also given in Table 6 which also includes the glass transition temperatures of the individual cross-linked blend constituents. It was observed that cross-linking raised the T_g's of the individual polymers in these blends to some degree but did not enhance substantially the miscibility of the blend. The principal effect of cross-linking on the T_g was the broadening of the T_g's of the individual constituents in the blends, which could be due to some degree of phase mixing. This broadening effect is seen in Figure 8. This could be caused by cross-linking some of the chains of the individual components together. The VSPSE4/SBR200 blend shows only one T_g after cross-linking due to the broadening of glass transition peaks. This single T_g was observed because the T_g's of the individual uncross-linked constituents were very close to each other.

In order to determine if there were any synergistic effects of blending on the thermal-oxidative behavior of the blends, TGA experiments were carried out for uncross-linked and cross-linked blends in both nitrogen and air atmosphere. The results for uncross-linked blends are summarized in Table 7.

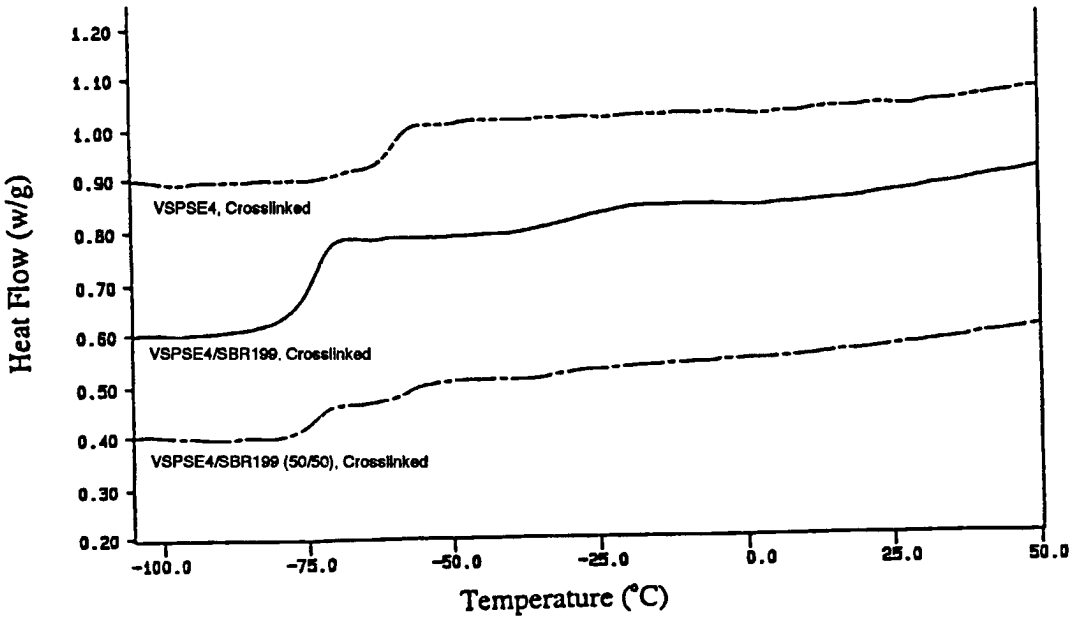

Figure 8. DSC Curves for Cross-Linked VSPSE4, SBR199, and VSPSE4/SBR199 (50/50) Blend

Table 7. TGA Data Summary of Uncross-Linked Polymer Blends (15°C/M)

VSPSE No.	Onset of degradation T_d (°C)* N_2	Air	Temperature for 50% wt. loss (°C) N_2	Air	End of major degradation (°C) N_2	Air	% Residue (900°C) N_2	Air
E4SBR199	370	361	592	485	659	674	32	7
E4SBR200	363	352	601	505	658	774	34	20
E4SBR201	365	364	507	535	642	750	20	23
E4SBS057	365	332	498	492	642	745	09	19
E4SBS451	376	379	525	525	646	663	26	26
E6SBR199	359	358	509	510	652	745	09	19
E6SBR200	384	377	513	624	665	801	12	26
E6SBR201	371	344	496	552	642	740	10	18
E6SBS057	386	330	514	510	650	730	11	15
E6SBS451	384	359	527	571	645	742	14	16

* The temperature at which the major degradation starts.

In nitrogen atmosphere, a two-step degradation was generally observed. The first step corresponded to the degradation of the SB elastomer and the second step corresponded to the VSPSE degradation. In the case of air atmosphere, a three-step degradation was observed in which the first step corresponded to SB elastomer degradation and the other two steps corresponded to the decomposition of the VSPSE. Our data indicated that a "rule of mixtures" behavior was observed for all uncross-linked blends based on TGA experiments.

The cross-linked blends were also characterized by TGA and these results are listed in Table 8.

Table 8. TGA Data Summary of Cross-Linked Polymer Blends (15°C/M)

VSPSE No.	Onset of degradation T_d (°C)*		Temperature for 50% wt. loss (°C)		End of major degradation (°C)		% Residue (900°C)	
	N_2	Air	N_2	Air	N_2	Air	N_2	Air
E4SBR199	380	340	567	603	651	739	27	25
E4SBR200	363	314	495	602	643	746	13	24
E4SBR201	369	301	489	497	640	693	16	15
E4SBS057	380	276	601	547	656	761	36	25
E4SBS451	383	299	588	511	661	741	32	21
E6SBR199	379	347	528	511	655	734	13	13
E6SBR200	371	334	597	662	661	786	27	30
E6SBR201	356	319	476	478	634	717	6	13
E6SBS057	375	313	512	537	648	736	11	16
E6SBS451	373	315	504	509	641	754	11	17

* The temperature at which the major degradation starts.

The degradation temperatures in air for the cross-linked blends are lower than those of the uncross-linked blends. It was also noticed that some blends have higher residues while others have lower residues after cross-linking. Significant increases in the residue amount are observed for VSPSE4/SBS057 blends in both air and nitrogen atmosphere after cross-linking. This effect cannot be explained at this time since there does not appear to be a consistent behavior of the thermal degradation of the blends either before or after cross-linking.

CONCLUSIONS

VSPSEs were successfully synthesized through the disilanol-diaminosilane polycondensation route by using carefully purified starting materials. They were characterized by GPC, DSC, TGA, and ^{29}Si NMR spectroscopy. The results were consistent with the presence of an alternating structure in these polymers. The VSPSEs which were obtained in high yields and with high molecular weights can best be described as stiff gums. They had low T_g's ranging from -26 to -63°C and exhibited the highest degree of thermal and oxidative stability that has been observed so far for any elastomers. The char yield upon pyrolysis increased when the vinyl content increased. Substitution of a methyl group with a phenyl group also increased the final TGA residues. The isothermal weight loss properties for these VSPSEs are exceptional. The 100% vinyl containing VSPSE had a weight loss of only 0.7% after 5 hours at 400°C in nitrogen. Polymer blends were prepared from the VSPE and SBR or SBS with and without cross-linking. The blends showed no evidence of miscibility. Rule of mixtures behavior was observed for the thermal degradation of the blends of VSPSE and either SBR or SBS.

ACKNOWLEDGMENT

The authors express their gratitude to the Federal Aviation Administration for financial support of this project.

REFERENCES

1. M. Lewin, S. M. Atlas, and E. M. Pearce, *Flame-Retardant Polymeric Materials,* Vol. 1 and 2, Plenum Press (Eds.), New York (1975).
2. P. R. Dvornic and R. W. Lenz, in Huthig & Weipf (Eds.), High Temperature Siloxane Elastomers, New York, 1990.
3. Y. C. Lai, P. R. Dvornic, and R. W. Lenz, J. Polym. Sci., Polym. Chem. Ed. 20, 2277 (1982).
4. P. R. Dvornic and R. W. Lenz, J. Polym. Sci., Polym. Chem. Ed. 20, 951 (1982).
5. P. R. Dvornic and R. W. Lenz, Polymer 24, 763 (1983).
6. P. R. Dvornic, H. J. Perpall, P. C. Uden, and R. W. Lenz, J. Polym. Sci., Polym. Chem. Ed. 27, 3503 (1989).
7. (a) R. M. Pike, J. Polym. Sci., 50, 151 (1961). (b) J. E. Curry and J. D. Byrd, J. Appl. Polym. Sci., 9, 295 (1965). (c) R. E. Burks, Jr., E. R. Covington, M. V. Jackson, and J. E. Curry, J. Polym. Sci., Polym. Chem. Ed. 11, 319 (1973). (d) C. U. Pittman, Jr., W. J. Patterson, and S. P. McManus, J. Polym. Sci., Polym. Chem. Ed. 14, 1715 (1976).

THERMALLY LABILE POLYMERS THAT RELEASE RADICAL TRAPS: POLYCARBODIIMIDES

Bruce Novak
Department of Polymer Science and Engineering
University of Massachusetts,
Amherst, MA 01003

OBJECTIVE

Our goal in this facet of the fire-resistant materials program is to identify liquid crystalline polymers that have excellent mechanical properties, yet when put under thermal stress, will decompose cleanly to flame suppressant compounds *(Scheme I).*

Scheme I

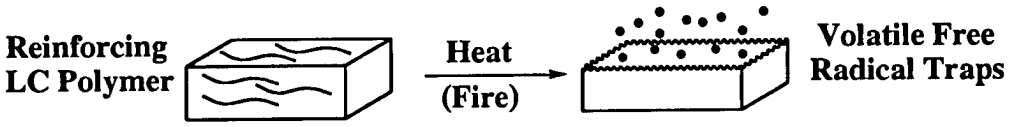

BACKGROUND

Flame suppression by halogenated additives work by trapping radicals and breaking chain propagation. These fillers, however, can leach from materials with time and do not add to the mechanical strength or integrity of the material. Weight requirements dictate that any added components must enhance the mechanical properties of the material. Our approach is to design non-halogenated polymers with superior mechanical properties that can be blended with other common polymers. Upon thermal stress, however, these polymers will be designed to degrade to volatile, non-halogenated, radical scavengers. Unfortunately, most all extended chain, high-performance materials are very expensive and do not decompose in a controlled fashion, and most polymers that undergo controlled decomposition do not have the necessary mechanical properties. We have, however, recently identified a unique class of polymer, the polycarbodiimides, that have both liquid crystalline properties and thermally degrade in a highly controlled fashion back to monomers at appropriate temperature ranges.

Restricting the conformational degrees of freedom within the backbone of a polymer can have the effect of extending the chains and endows the material with a number of interesting properties including high modulus and strength, macromolecular chirality, and liquid crystallinity. In order to access materials with these attributes, we have been interested in developing living routes into extended-chain, helical polymers. We have developed living polymerization catalysts for two different "pro-helical" monomers (i.e., monomers which when polymerized, form helical polymers that adopt stable helical conformations): isocyanides and isocyanates. To a first approximation, the rigidity of the chain is directly proportional to the helix inversion barrier (i.e., the barrier separating right and left handed helices). These two classes of helical polymers,

the polyisocyanides and the polyisocyanates, possess helix inversion barriers ranging from ≥ 27 kcal/mol to 3-5 kcal/mol, respectively (i.e., they range from conformationally locked to highly dynamic). Unfortunately the more rigid (higher barrier) polyisocyanides are thermally unstable and often have defect-riddled structures. We have therefore been interested in designing rigid helical polymers that possess high inversion barriers and good properties. Hence, our synthesis of the polycarbodiimides which, true to our prediction, possess both properties. For purposes of structural materials we are interested in the more rigid materials, the polycarbodiimides.

Polycarbodiimides are a unique class of rigid-chain polymers that adopt 6/1 helical conformations in both solution and the solid phase. Although high molecular weight polycarbodiimides have not been prepared previously, we have recently discovered a class of catalysts that allow carbodiimides to be synthesized in a living manner. Specifically, titanium (IV) amido and alkoxide complexes will initiate the living polymerization of a wide range of carbodiimide monomers (equation 1).[1]

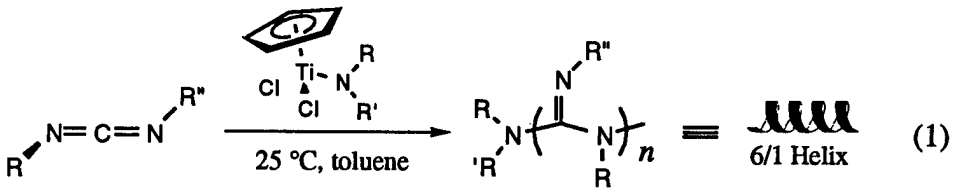

(1)

We have found that these polymers are stiff chain polymers and their stiffness varies from stiff worms to rigid rods depending on the side chain substituents. Some examples are shown in Figure 1.

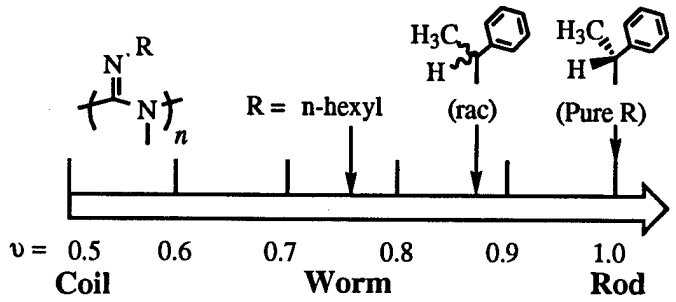

Figure 1. Static Scaling Exponent (υ) Values for Polycarbodiimides With Various Substituents

One interesting feature of the polycarbodiimides is their decomposition behavior. We found that these materials decompose cleanly back to monomer at temperatures of approximately 200°C. Furthermore this decomposition behavior was found to depend on subtle structural features such as chirality of the side chain. For example, the racemic and pure-*R* forms of poly(1-phenylethyl methyl carbodiimide) decompose at 180 and 200°C, respectively. Thus, these polymers offer two attractive and unique features: (1) They adopt rigid rod conformations so they can be used as high-strength components in polymer blends, and (2) they decompose cleanly back to monomers at convenient temperatures. We would like to use this decomposition behavior to our

Scheme II

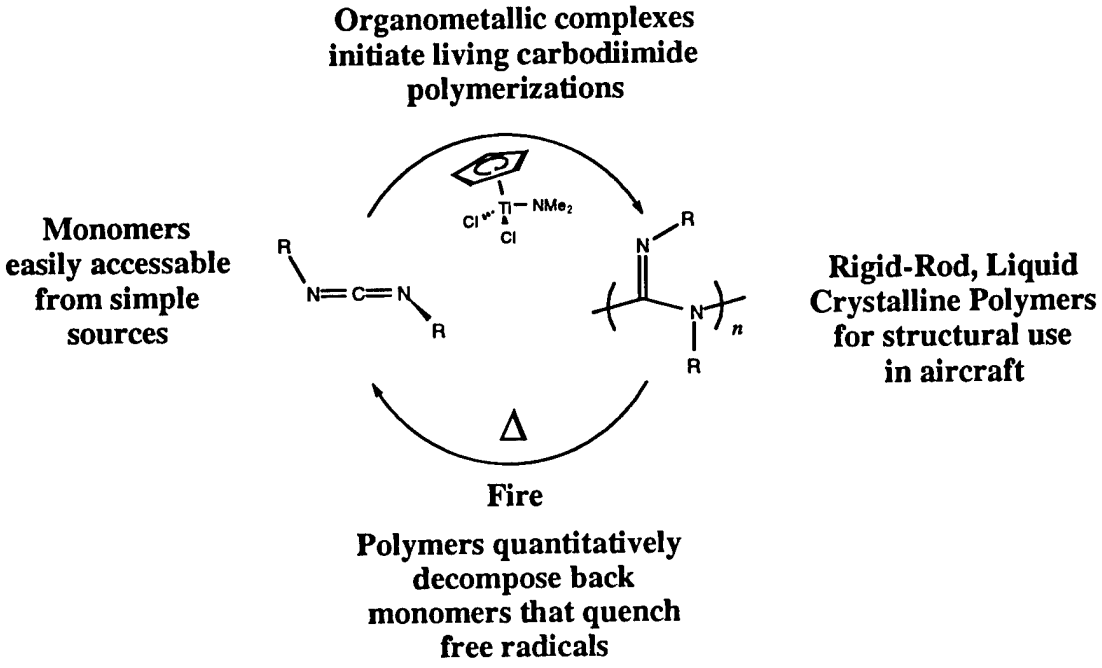

advantage by using the rigid carbodiimide backbone as our liquid crystalline polymer for fire-resistant applications (Scheme II).

In summary, we have discovered an interesting class of new materials that adopt well-ordered, rigid helical conformation and display a number of unusual properties including liquid crystallinity, macromolecular chirality, and rigid-chain solution properties. Furthermore, polycarbodiimides decompose cleanly and quantitatively back to monomer. We wish then to use these materials as a basis for flame-resistant applications. In addition to their structural features, polycarbodiimides possess C–N backbones that lack C–H bonds. By appropriate choice of side chains, polymers with very low hydrogen contents $(C_5H_2N_{10})_n$, high phosphorous/nitrogen contents (organophosphazene materials), or high boron contents (organoborazines) can be prepared.

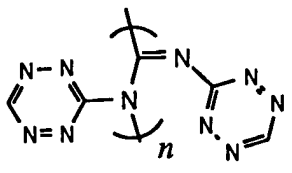

Poly(Carbodiimide Tetrazines)

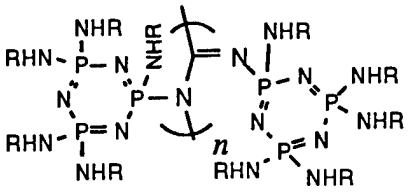

Poly(Carbodiimide Phosphazenes)

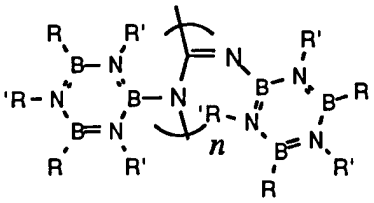

Poly(Carbodiimide Borazines)

We plan to exploit this decomposition behavior by allowing these released carbodiimides to act as radical scavengers (equation 2).

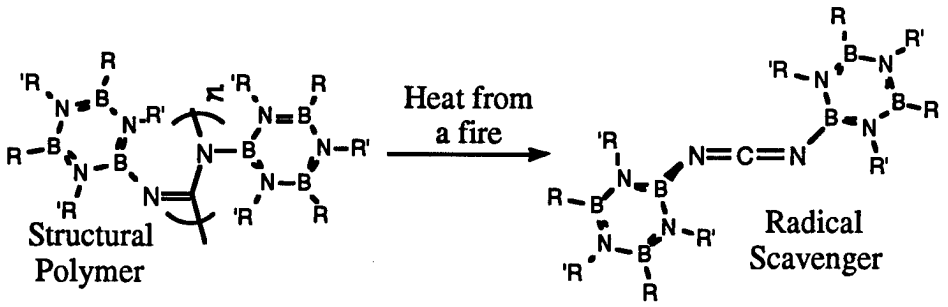

(2)

Other approaches will be the incorporation of stable free radicals into these structures that will act as flame quenching moieties.

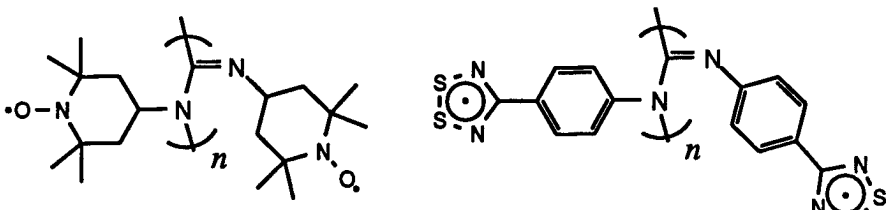

Nitroxyl (TEMPO)
Polycarbodiimide

Thiaazolyl
Polycarbodiimide

THE SYNTHESIS OF PHOSPHAZENE CARBODIIMIDES

In order to synthesize a phosphazene substituted carbodiimide, either 1-aminopentachlorophosphazene (**III**) or 1-isocyanidopentachlorophosphazene or both is needed. We first attempted the synthesis of **III** by allowing hexachlorophosphazene (**1**) to react with excess ammonium hydroxide in refluxing ether for 1 hour to yield the disubstituted product, 1,1-diaminotetrachlorophosphazene (**II**) (equation 3).[2] After work up, the product was purified by recrystallization from ether (35% yield). In order to obtain the monosubstituted product, **II** was heated at reflux in dioxane with two equivalents of HCl for 8 hours. Unfortunately, the reaction was an inseparable mixture of mono- and di-substituted products even after exhaustive purification.

Attempted synthesis of aminophosphazene

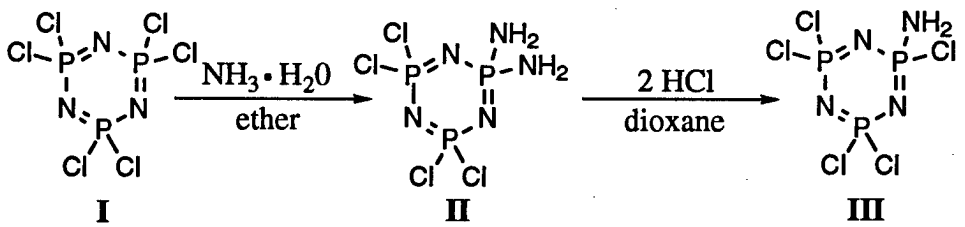

I **II** **III**

(3)

A better procedure for synthesizing a mono-amine substituted phosphazene product involves using hexafluorophosphazene (**IV**) instead of the chloro derivative (equation 4). Hexafluoro-

phosphazene was obtained from the reaction of **I** with excess sodium fluoride (heated at reflux for 14 hours) in acetonitrile.[3] The product was then distilled from the reaction mixture at 50-51°C at atmospheric pressure. The 1-aminopetafluorophosphazene (**V**) obtain by bubbling ammonia through an ether solution of **IV** for 1 hour. After washing with water to remove salts and removing the solvent, a white solid was obtained. The product **V** was sublimed at 40°C under static vacuum. Purity of **V** was verified using GC/MS.

In order to convert **V** into the corresponding urea, **V** was allowed to react with methyl isocyanate in chloroform, but no product was observed to form even after 24 hours of stirring at room temperature. Phosphazene **V** was recovered upon removal of the solvent and isocyanate.

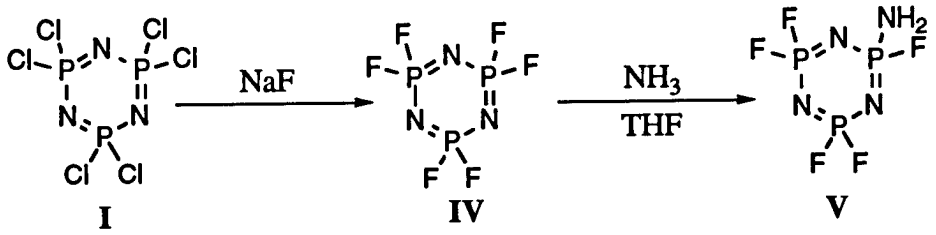

I **IV** **V** (4)

Methyl isocyanate is the most reactive of isocyanates but it has a very low boiling point (32°C). Therefore, *n*-propyl isocyanate was chosen so that the system could be heated. No reaction took place even after 24 hours of refluxing **V** with propylisocyanate in chloroform.

The results above are different from those typically observed for the reaction of amines with isocyanates. The reaction is usually exothermic and complete within a few hours. The reason that the aminophosphazene does not react with isocyanates was most likely due to the strong electron withdrawing effect of the halogenated phosphazene ring. The reactivity of the amine towards nucleophilic attack on the isocyanate can be increased by substituting electron donating groups for the fluorines on the phosphazene (equation 5). We are currently exploring this possibility by substituting either alkoxide or amine groups for the halogens.[4] One possibility is to allow **V** to react with sodium methoxide in methanol to form the 1-aminopentamethoxy-phosphazene. The second possibility is to allow **V** to react with dimethylamine to form the 1-aminopenta(dimethylamino)phosphazene. The product from either reaction will then be converted to the urea by reaction with isocyanate similar to what was discussed previously.

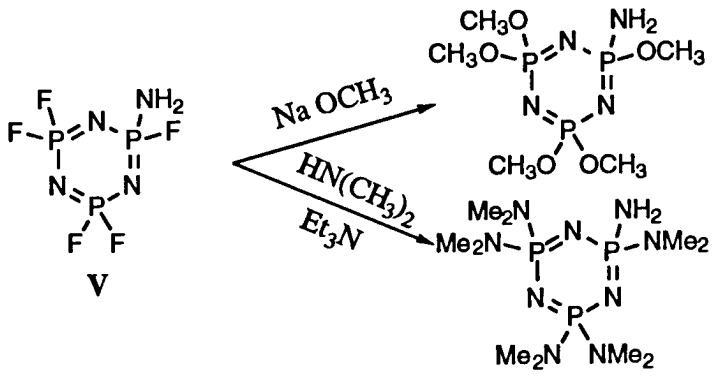

V (5)

THE SYNTHESIS OF TEMPO CARBODIIMIDES

For the purpose of synthesizing a polymer containing stable free radicals, carbodiimides bearing stable nitroxyl radicals were examined. 4-Amino-TEMPO (**VI**) was allowed to react with methylisocyanate in chloroform at room temperature for 12 hours (equation 6).

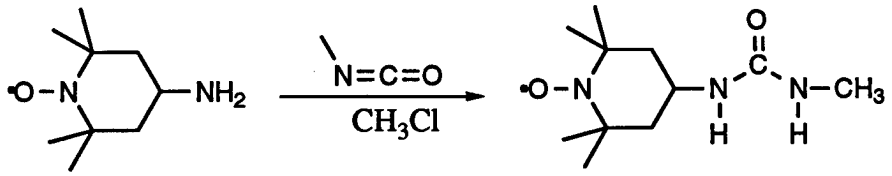

VI **VII** (6)

The resulting urea, **VII**, was isolated as an orange crystalline solid after recrystallization from ethyleneglycoldimethylether (DME). The paramagnetic product was characterized using both IR and elemental analysis.

Methyl TEMPO carbodiimide, **VIII**, was synthesized by dehydrating urea **VII** using triphenylphosphine, bromine, and triethylamine in methylene chloride at room temperature.[5] The reaction was complete within 2 hours (equation 7).

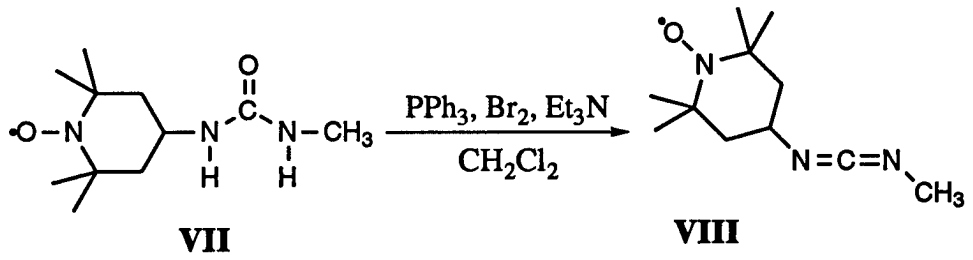

VII **VIII** (7)

The reaction's progress was checked using IR to monitor the appearance of the carbodiimide peak at 2133 cm^{-1}. Monomer **VIII** was isolated as an orange solid and purified by sublimation at 50°C under static vacuum.

THE POLYMERIZATION OF TEMPO CARBODIIMIDE VIII

The polymerization of **VIII** was carried out in a dry box using titanium catalyst 1 (equation 8).[1] Carbodiimide **VIII** was dissolved in a small amount of toluene to give an orange solution which was then added to a stirring solution of the catalyst in toluene. Within 2 days of stirring in the dry box a precipitate was formed. The reaction vessel was removed from the dry box and the reaction stopped by the addition of wet toluene to the solution and the precipitate filtered off. The solid product was a white-orange solid which was not soluble in toluene or THF and was only slightly soluble in chloroform.

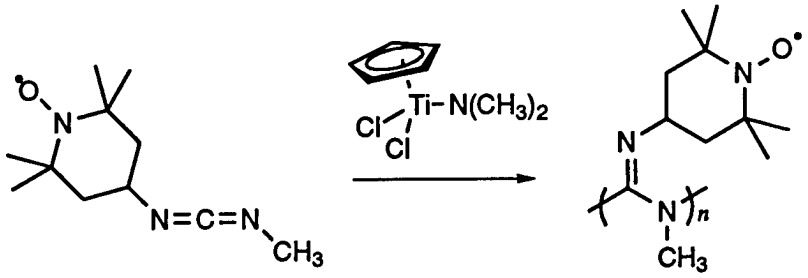

VIII **Poly-VIII** (8)

The general insolubility of poly-**VIII** has precluded its further characterization. In order to improve the solubility of the polymer, a longer alkyl chain will be substituted in place of the methyl group. The general synthetic route outlined for the methyl derivative **VIII** is currently being followed.

REFERENCES

1. Goodwin, A. and Novak, B. M., *Macromolecules*, **1994**, 27, 5520.
2. Feistel, G.R., Feldt, M. K., Dieck, R. L., and Moeller, T., In *Inorganic Syntheses*, Wold, A. and Ruff, J. K., Eds.; **14**, 22.
3. Allcock, H.R., Klingenberg, E.H., and Welker, M.F., *Macromolecules*, **1993**, 26, 5512.
4. Palomo, C. and Mestres, R., *Synthesis*, **1981**, 373.
5. Allcock, H.R., *Phosphorus-Nitrogen Compounds: Cyclic, Linear, and High Polymeric Systems*, Academic Press, New York, 1972, Chapters 6 & 7.

PREPARATION OF CYANATE ESTER MONOMERS

Ada Casares, Ph.D.
Division of Natural Sciences and Mathematics
Richard Stockton College of New Jersey
Pomona, NJ 08240

SUMMARY

Three approaches directed to the synthesis of organic cyanates of interest were studied: (a) phenoxide pathway, (b) cyanuric chloride pathway, and (c) organophosphorous pathway. The preparation of some cyanates described in the literature as well as some new compounds of interest were attempted. A first set of four samples submitted to the FAA consisted of three cyanate monomers and a phosphorous containing a potential additive. Studies by the FAA indicated that the cyanates were of insufficient purity. The study of further purification procedures yielded clean samples.

METHODS

Phenoxide Pathway

General

In a high-efficiency hood, a three-necked, round-bottom flask was equipped with a magnetic stirrer, a low-temperature thermometer, a septum, and a nitrogen/vacuum inlet. The phenol and cyanogen bromide were placed in the flask. The flask was evacuated and charged with nitrogen several times and the mixture was kept under positive nitrogen pressure throughout the reaction. The specified solvent was injected and stirring started. An external dry ice/acetone bath was used to maintain a low reaction temperature. Triethylamine was injected dropwise while maintaining the temperature between -40°C and -10°C; the mixture was then allowed to sit for 45 minutes with stirring and the cold bath allowed to warm up slowly to room temperature. The mixture was then vacuum filtered and the solid (triethyl bromide) was separated. The solution was evaporated in a rotatory evaporator using an ice bath to keep the mixture cold. The residue was prepurified by vacuum distillation for liquids and by repeated low-temperature recrystallization for solids. (Attempts to purify by cold flash chromatography under nitrogen were unsuccessful.) Final products were obtained by rapid cold chromatotron separation on silica gel under nitrogen/crystallization. Purity was monitored by TLC in silica gel. Characterization was done through spectroscopy and when available, described constants.

Phenyl cyanate (4)

Reaction solvent: Acetone Bp: 43-5°C/1mm Hg IR (cm^{-1}): 2200-2300 (CN); 1160-1240 (COC). Proton NMR: 7.35 (s, 5H) TLC: Hexane-Ethyl Acetate 3:1; developing reagents UV and Iodine.

Bisphenyl dicyanate (6)

Reaction solvent: Diethyl ether mp: 74°C (reported, 74°C). IR (cm^1): 2200-2300 (CN); 1160-1240 (COC). Proton NMR: 1.70 (s, 6H); 7.30 (s, 8H) TLC: Hexane-ethyl acetate 3:1; developing reagents UV and iodine.

Biphenyl dicyanate (7)

Reaction solvent THF mp: 128°C (reported, 131°C) IR (cm^{-1}): 2200-2300 (CN); 1160-1240 (COC). Proton NMR: 7.20-7.45 (d, 4H); 7.50-7.70 (d, 4H) TLC: Hexane-ethyl acetate 3:1; developing reagents UV and iodine.

Cyanuric Chloride Pathway

Nucleophilic substitution on cyanuric chloride

In a high-efficiency hood, a three-necked, round-bottom flask was equipped with a magnetic stirrer, a thermometer, and a nitrogen/vacuum inlet. A mixture of 368 mg of cyanuric chloride and 500 mg of potassium cyanate were suspended in 10 mL of ethanol. The system was evacuated and placed under nitrogen several times and the mixture was stirred under nitrogen at room temperature for 40 hr. The ethanol was partially evaporated at room temperature with a rotatory evaporator. Standard workup (methylene chloride, anhydrous sodium sulfate) gave an unstable solid which exothermed with decomposition upon drying under vacuum. No characterization or spectroscopy is available due to the instability of the product.

Nucleophilic substitution on phenyldiazonium chloride

Five hundred mg of aniline were placed in a round-bottom flask in a wet ice/sodium chloride bath. Three mL of 2.0 molar hydrochloric acid were added dropwise, followed by the addition, also dropwise, of 2.0 mL of 3 molar sodium nitrite in water. The temperature was maintained at 5°C throughout. The diazonium salt was filtered and the wet solid was immediately transferred to a clean round-bottom flask in order to remove the acidic water from the previous procedure. A solution of 480 mg of potassium cyanate in ethanol/water was added dropwise with constant stirring at room temperature. TLC (silica gel, hexane-ethyl acetate 3:1, and developing reagents UV and iodine) showed a product with slightly different rf than an authentic sample of pheny cyanate. The reaction was repeated in the presence of 250 mg of 18-crown-6 with identical results.

Organophosphorous Pathway

Tris(phenol)phosphine (13)

In a three-necked, round-bottom flask equipped with a thermometer, a nitrogen inlet, and a septum, 704 mg of tri(4-methoxiphenyl)phosphine (17) were dissolved in methylene chloride, put under stirring, and cooled to -76°C. The mixture was evacuated and charged with nitrogen several times, and 6 mL of one molar boron tribromide in methylene chloride were slowly injected. Stirring was continued at -76°C for 1/2 hour and then allowed to raise to room temperature. The precipitated product was filtered and washed with methylene chloride at

-76°C. TLC (silica gel): hexane-ethyl acetate 1:1 and developing reagents UV and iodine. IR: (cm^{-1}) 3350 (OH) 1500, 1580,and 1600 (aromatic)).

RESULTS

Phenoxide Pathway

It has been well documented in the literature[1,2] that cyanurates (often referred as **s**-triazines) possess fire-retardant properties. Our objective was to produce cyanate ester monomers that could later be polymerized to form useful fire-retardant plastics. These materials are of interest for use in airplanes.

The term "cyanate ester resin" is used to describe both prepolymers and cured resins; the former contain reactive ring-forming cyanate functional groups. During curing, these functional groups form three-dimensional networks of oxygen linked triazine (also termed cyanurate) via a cyclotrimerization reaction.

Polycyanurates are the linking of several cyanurate rings to form the long chain plastics. The products become stable to temperature. We used phenol (1) and triethylamine (2) as a base to remove the hydrogen and produce the phenoxide ion (3) which would then react with cyanogen bromide to form the phenyl cyanate (4). The base was added dropwise to avoid the production of excess phenoxide ion (3). If there is excess phenoxide ion in the presence of the phenyl cyanate (4), imidocarbonates (5) are formed and this is undesirable (Figure 1).

There were three cyanates prepared through this pathway: phenyl cyanate (4), bisphenyl dicyanate (6), and biphenyl dicyanate (7). The later two were difunctional monomers with the potential for polymerization (Figure 2).

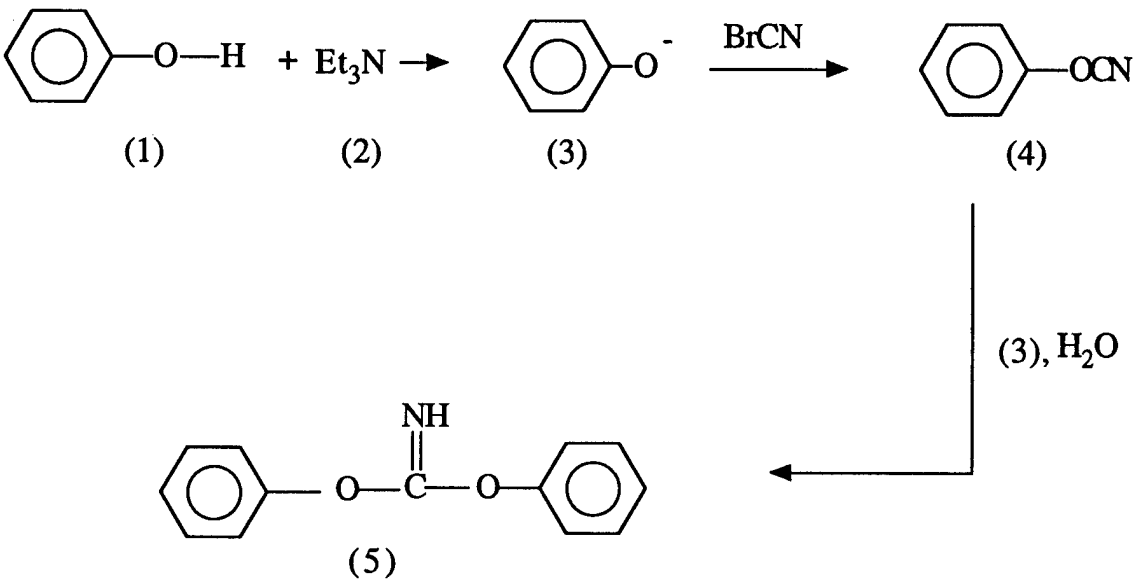

Figure 1. Synthetic Route to Phenyl Cyanate

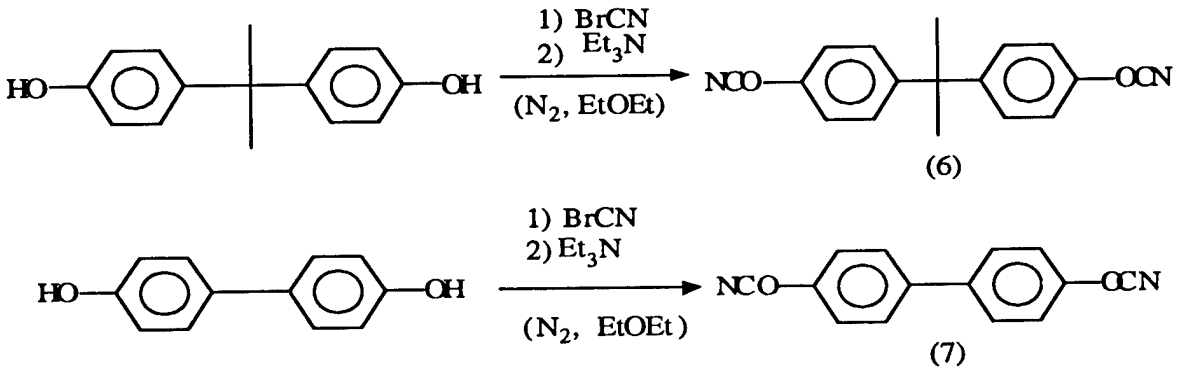

Figure 2. Synthesis of Bisphenyl (6) and Biphenyl Dicyanates (7)

Since phenyl cyanate has only one cyanate group, this compound has no potential for polymerization beyond one triazine ring. It was prepared for the purpose of establishing the conditions for safe handling of the highly toxic cyanogen bromide needed in these reactions. The bisphenol dicyanate (6) is commercially available and was prepared in order to establish conditions for purification and comparison with the known material. When aryl cyanates are contaminated with unreacted phenol, the compounds can't be stored safely due to spontaneous exothermic decomposition. It was important then to achieve a good degree of purity. The biphenyl dicyanate (7) is a research sample not commercially available. Though the samples were purified to a degree where no spontaneous decomposition occurred, when they were analyzed by the FAA the phenolic content was found to be too high. A mixed procedure using crystallization and/or chromatotron separation was developed for further purification. These procedures allowed us to obtain clean samples as indicated by the lack of OH absorption in the IR spectra of the purfied sample.

When the preparation of furylcyanate was attempted the procedure gave no reaction. It was thought that this was due to the nonaromatic nature of the OH group in the starting material. This fact changes the acidity for the generation of the anion. Attempts to generate the anion with butyl lithium and the addition of the mixture resulting from this reaction to cyanogen bromide gave a very complex mixture of products (Figure 2a). This result confirms the known fact that aromatic phenols are more useful than nonaromatic phenols in cyanate formation.

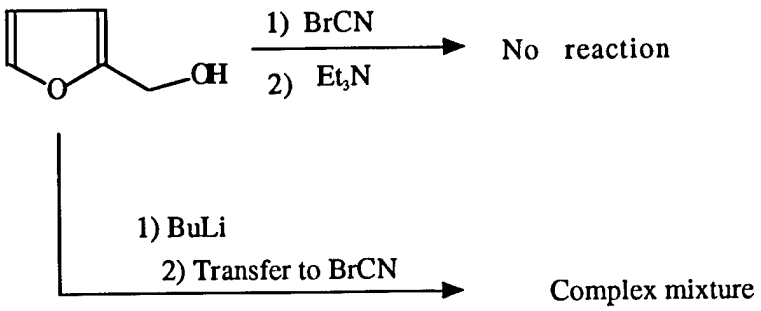

Figure 2a. Synthesis of Furyl Cyanate

Cyanuric Pathway

It has been well documented in the literature[3] that electron withdrawing nitro groups on phenols (8) allow aromatic nucleophilic substitution of halides with mild nucleophiles such as water to form phenols (9). It has also been well documented in the literature[4] that cyanuric chloride (10) will undergo analogous transformation to form cyanuric acid (11) (Figure 3).

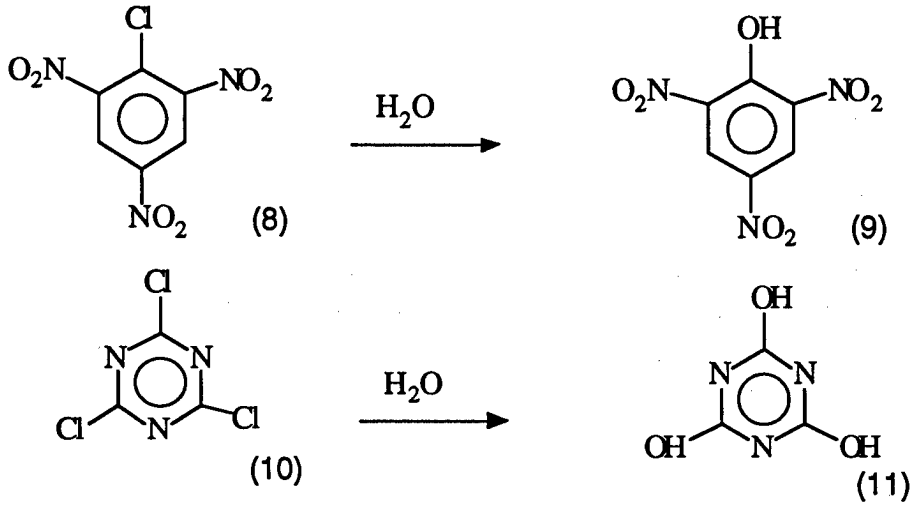

Figure 3. Aromatic Nucleophilic Substitution to Give Phenols

The above information suggested the interesting possibility of using a mild nucleophile such as potassium or sodium cyanate on cyanuric chloride to produce the *s*-triazine-2,4,6-tricyanate (12). This compound, if polymerized, would afford a product with a high density of triazine rings and potentially good fire-retardant properties (Figure 4).

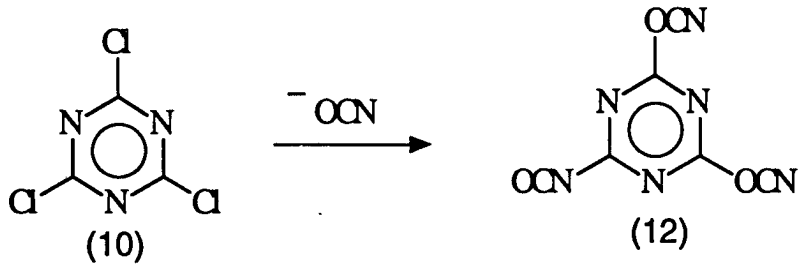

Figure 4. Phenyl Tricyanate from Cyanuric Chloride and Cyanate Salt

When the reaction was performed, the product was unstable and suffered exothermal decomposition before characterization. It is known that the number of cyanate groups per ring is related to the stability of the products. For example, resorcinol dicyanate is quite prone to exothermal decomposition particularly when impure. Since cyanuric acid is stable, the obtained product could not have been the result of hydrolysis of the chloride. This suggests that at least partial nucleophilic substitution took place. In view of the result, an alternative nucleophilic substitution was envisioned. This alternative involved the use of a diazonium salt as the leaving group in a reaction analogous to the Sandmeyer reaction (Figure 5).

Before attempting the reaction with melamine (13), the reaction with aniline (14) was used as a model to determine the viability of the process.

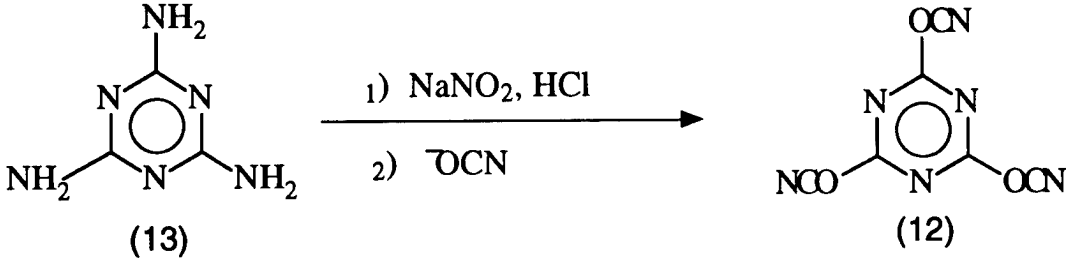

(13) (12)

Figure 5. Melamine Route to Tricyanate Using Diazonium Salt

The nucleophilic displacement with cyanate on phenydiazonium chloride would be the same phenylcyanate (4) of the methoxide pathway. When the reaction was carried out, the resulting thin layer chromatogram was different from that of the phenylcyanate (4). The tentative structure assigned to the reaction product is the isomeric isocyanate (15) (Figure 6). The presence of crown ethers in the reaction did not change the outcome.

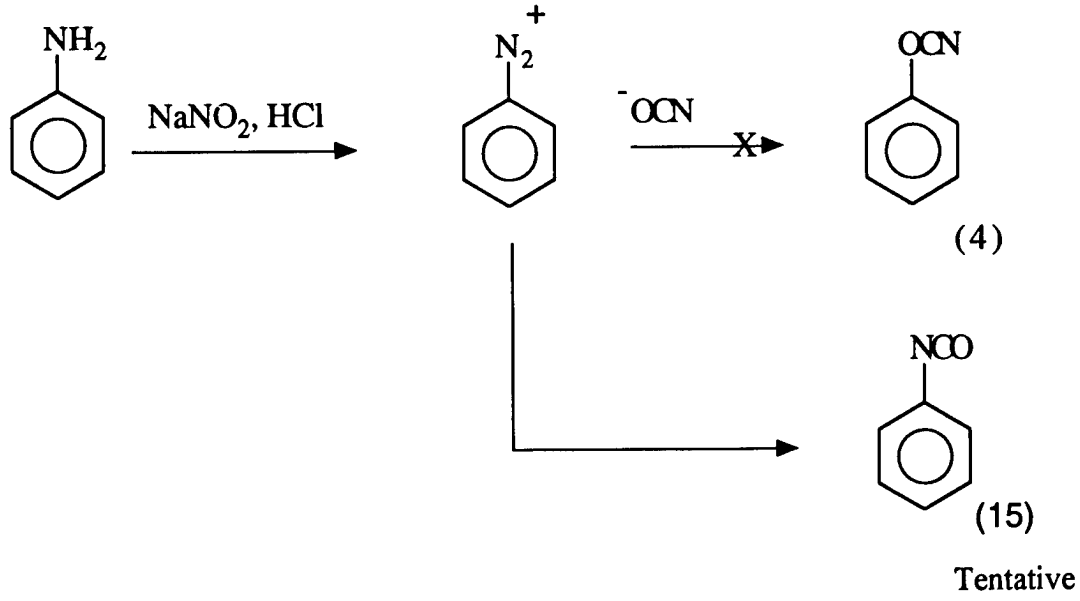

Figure 6. Aniline Route to Phenyl Cyanade Using Diazonium Salt

Organophosphorous Pathway

Compounds containing phosphorous have been known to have fire-retardant properties . Using organophosphorous compounds as an additive or a backbone polymer increases the ability of these plastics to resist combustion[4]. The trisphenolphosphine (16) was envisioned as a potential additive in formulation. Attempts to prepare this compound by a modification of Kashiwashi's[5,6] procedure (Figure 7) failed, probably due to the acidity of the phosphorous trichloride. Protection of the phenol with ethyl vinyl ether also proved inadequate.

Though expensive, the tris(methoxyphenyl)phosphine (17) is commercially available and was cleaved with boron tribromide to provide the desired tris(phenol)phosphine (16) (Figure 8). The conditions for this reaction were first tried on anisol.

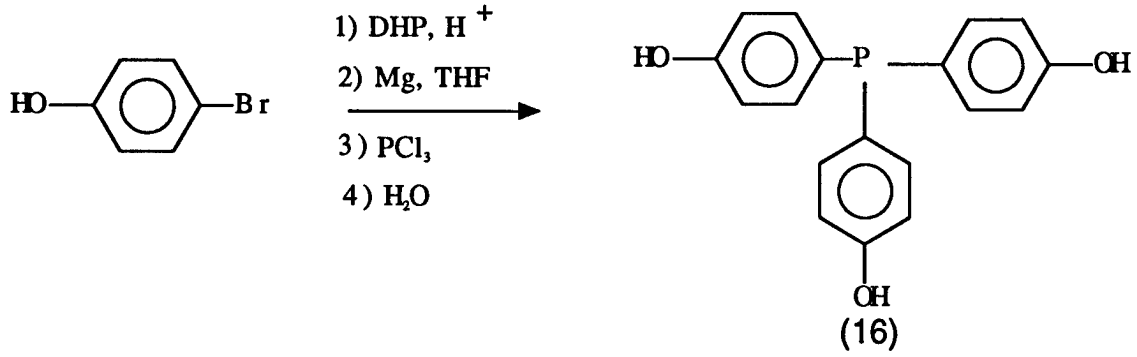

Figure 7. Attempted Route to Tris(phenol)phosphine

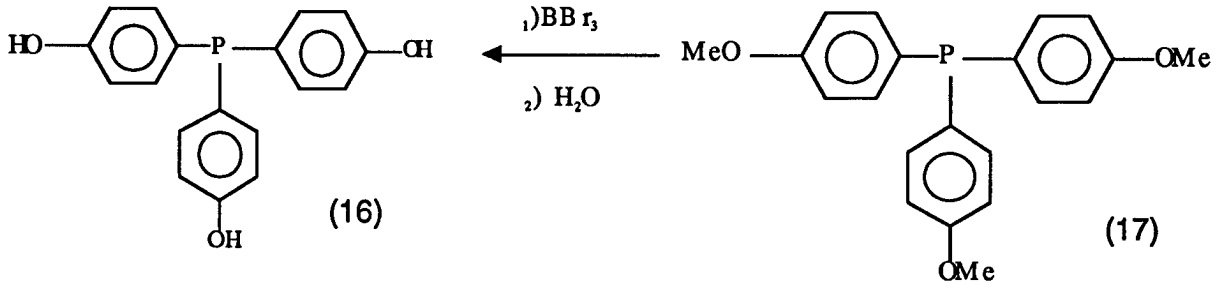

Figure 8. Synthesis of Tris(phenol)phosphine

The transformation of the tris(phenol)phosphine (16) to the tricyanate (18) was attempted under the conditions used in the phenoxide pathway, with promising results (Figure 9). Nevertheless, the amounts of starting material available for experimentation did not allow for accumulation of substantial quantities of the product since the reactions yielded a mixture difficult to purify. Tricyanate (18) is of particular interest because it would give a phosphorous containing backbone polymer of high triazine content. Such a polymer would not have the migration problems associated with additives.

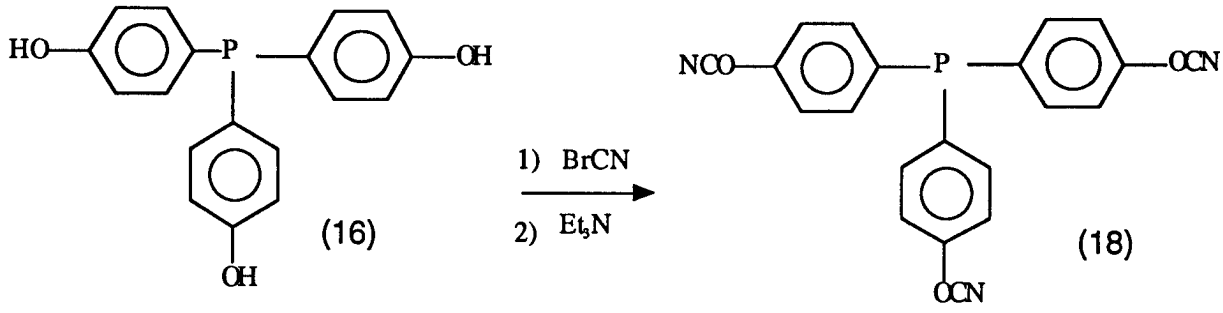

Figure 9. Cyanation of Tris(phenol)phosphine

CONCLUSIONS AND RECOMMENDATIONS

Phenoxide Pathway

a. The first objective of this project was fully accomplished with positive results. The phenoxide pathway to produce aromatic dicyanates with the cyanate groups in different rings needs no further modification.

b. For aromatic dicyanates with the cyanate groups in the same ring and for all tricyanates, we suggest moving from cyanogen bromide to cyanogen chloride as cyanating reagent. It must be noted that this seemingly minimal change involves certification for self-contained respirator use.

c. Nonaromatic cyanates should not be pursued further.

Cyanuric Pathway

In view of the result obtained on the nucleophilic displacement reactions (Figures 4 and 6), it is recommended that the cyanuric pathway be abandoned.

Organophosphorous Pathway

a. It is recommended that the phosphorous compounds be studied further. Once again, moving to cyanogen chloride seems warranted. The preparation of the tricyanate ester monomer (18) should have high priority.

b. Since the tris(methoxyphenyl)phosphine (17) seems to be a good starting material for the preparation of the tricyanate ester monomer (18), an efficient procedure for its preparation needs to be developed.

c. Since contamination by phenol results in exothermic decomposition, we suggest as targets only, completely cyanated products.

ACKNOWLEDGEMENTS

Experimental work on this project was presented by Mr. Christopher Baldwin in partial fulfillment for his B.S. degree from Stockton. The strong support of Dr. Richard Lyon from the FAA is greatly appreciated. Mr. Richard Walters (from Galaxy Scientific Corporation) and Dr. Jonathan Griffiths (from Richard Stockton College) performed the IR analysis on the samples. These contributions are appreciated. Support for partial funding for a Chromatotron by Dr. Barbara Byrne and Stockton's Administration is acknowledged. Grant support from the FAA (Grant # 95-G-028) made not only this work possible but also the acquisition of equipment through this funding to expand Stockton's capabilities for organic synthesis.

REFERENCES

1. A. W. Snow (1994) in "The Chemistry and Technology of Cyanate Ester Resins," edited by I. Hamerton, Blackie Academic and Professional, pg 2-6.
2. Grigat, E. and Putter, R. (1967) Angew, Chem. Int. Ed. 6, 206.
3. Solomons, T. W. Graham (1992) in "Organic Chemistry," 5th Ed. John Wiley & Sons Inc.
4. E. D. Weil in the "Handbook of Organophosphorous Chemistry," R. Engel, Ed., 1992.
5. D. M. Knauss, T Kashiwagi, and J. E. McGrath, Pol. Mat. Sci. and Eng. 71, 229 (1994).
6. I-Yuan Wan, T. Kashiwagi, and J. E. McGrath, Pol. Mat. Sci. and Eng. 71, 233 (1994).
7. John, J. A., and Tour, J. M. *J. Am. Chem. Soc.* **1994**, *116*, 5011.

ENVIRONMENTALLY FRIENDLY INORGANIC ADDITIVES

NANOCOMPOSITES: A REVOLUTIONARY NEW FLAME-RETARDANT APPROACH

Jeffrey W. Gilman and Takashi Kashiwagi
Fire Science Division
National Institute of Standards and Technology
Gaithersburg, MD

Joseph D. Lichtenhan
Phillips Laboratory
Edwards Air Force Base, CA

ABSTRACT

The fire-retardant (FR) properties of a new class of materials, organic-inorganic nanocomposites, are reported. The cone calorimeter data show that the peak heat release rate (HRR), the most important parameter for predicting a fire hazard, is reduced by 63% in a nylon-6 clay-nanocomposite containing a clay mass fraction of only 5%. Not only is this a very efficient FR system, but it does not have the usual drawbacks associated with other FR additives. That is, the physical properties are not degraded by the additive (clay), instead they are greatly improved. Furthermore, this system does not increase the carbon monoxide or soot produced during the combustion as many commercial fire retardants do.

INTRODUCTION

In the pursuit of improved approaches to fire-retarding polymers, a wide variety of concerns must be addressed, in addition to the flammability issues. For commodity polymers the low cost of these materials requires that the fire-retardant (FR) approach also be of low cost. This limits the solutions to the problem primarily to additive type approaches. These additives must be low cost and easily processed with the polymer. In addition, any additive must not excessively degrade the other performance properties, and it must not create environmental problems in terms of recycling or disposal of the final product. However, currently available flame-retardant approaches for nylon tend to reduce the thermal and mechanical properties of the nylon[1,2].

Nylon-6 clay nanocomposites, first developed by researchers at Toyota Central Research and Development Laboratories, are hybrid organic polymer-inorganic materials with unique properties when compared to conventional filled polymers. The nylon-6 clay nanocomposites (clay mass fractions from 2% to 70%) are synthesized by ring-opening polymerization of ε-caprolactam in the presence of cation exchanged montmorillonite clay[3]. The layered silicate structure of the montmorillonite clay is represented in Figure 1. This process creates a polymer

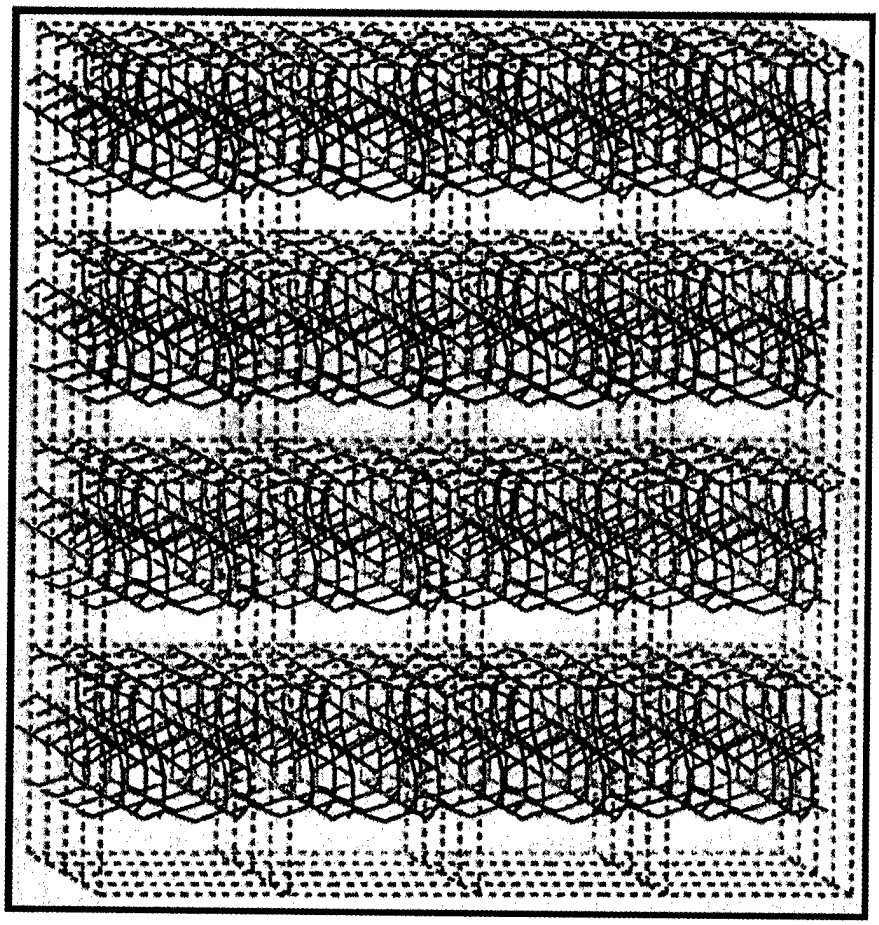

GSC.0034.96-14

Figure 1. Representation of the Montmorillonite Clay Structure Showing the Silicate Layers and the Interlayer Gap or Gallery

layered silicate nanocomposite with either a delaminated hybrid structure or an intercalated hybrid structure (see Figure 2), depending on the clay content. The intercalated structure, which forms when the mass fraction of clay is greater than 20%, is characterized by a well ordered multilayer with spacing between the silicate layers of only a few nanometers. The delaminated hybrid structure, which forms when the mass fraction of clay is less than 20%, contains the silicate layers individually dispersed in the polymer matrix[4]. The mechanical properties for the nylon-6 clay nanocomposite with 5% clay mass fraction show excellent improvement over pure nylon-6. The nanocomposite exhibits a 40% higher tensile strength, 68% greater tensile modulus, 60% higher flexural strength, 126 % increased flexural modulus, and comparable Izod and Charpy impact strengths. The heat distortion temperature (HDT) is increased from 65°C (nylon-6) to 152°C (nylon-6 clay nanocomposites with clay mass fractions $\geq$5%)[5]. To evaluate the feasibility of controlling polymer flammability via a nanocomposite approach, we have examined the flammability properties of nylon-6 clay nanocomposites with clay mass fractions of 2% and 5% and compared them to those for pure nylon-6 and other flame-retarded nylons.

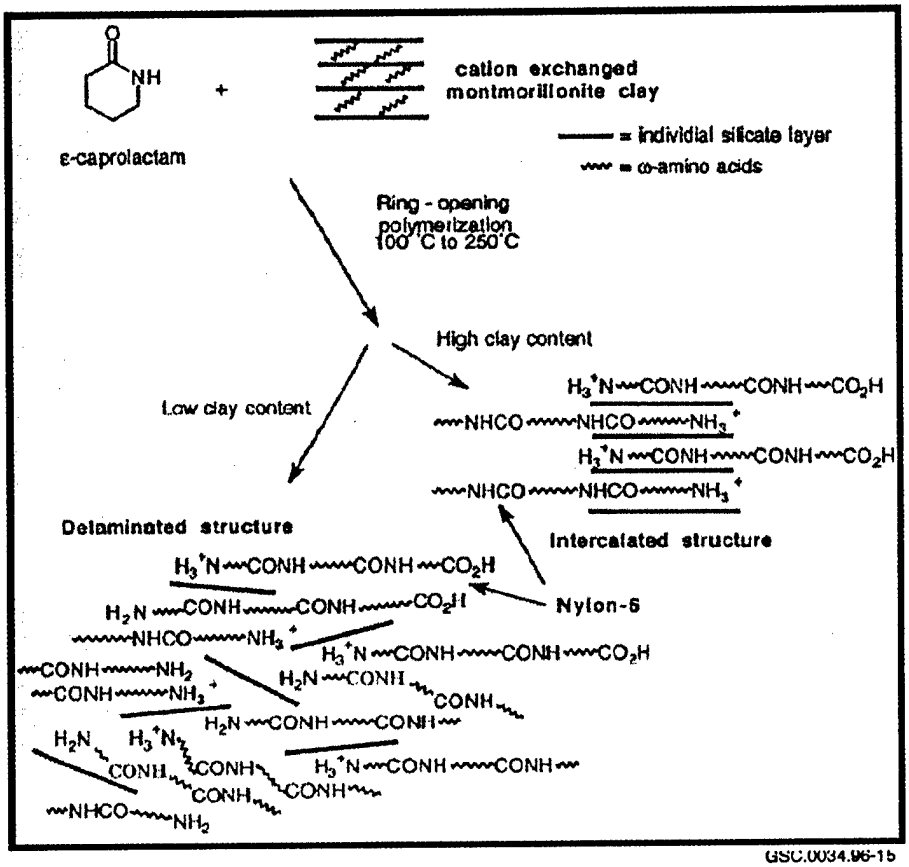

Figure 2. Diagram of the Process Used to Prepare Polymer Layered Silicate Nanocomposites With Either a Delaminated Hybrid Structure or an Intercalated Hybrid Structure

EXPERIMENTAL

All nylon-6 clay nanocomposites (clay mass fraction of 2% and 5%) and nylon-6 were obtained from UBE industries and used as received[6]. The above nanocomposites will be referred to as nylon-6 clay nanocomposite (2%) and nylon-6 clay nanocomposite (5%), respectively. Evaluations of flammability were done using the cone calorimeter[7]. The tests were done at an incident heat flux of 35 kW/m^2 using the cone heater. A heat flux of 35 kW/m^2 represents a typical small-fire scenario[8]. Peak heat release rate, mass loss rate, and specific extinction area (SEA) data, measured at 35 kW/m^2, are reproducible to within ±15%. The carbon monoxide and heat of combustion data are reproducible to within ±10%. The uncertainties for the cone calorimeter are based on the uncertainties observed while evaluating the thousands of samples combusted to date. Cone samples were prepared by compression molding the samples (~55 g) into 75 x 50 mm rectangular plaques 15 mm thick using a press with a heated mold. The thermogravimetric analysis was on a Perkin-Elmer 7 Series TGA. Four runs of each sample type were typically run, the results averaged and the uncertainties calculated using standard methods. For the differential TGA plots (Figure 3) the uncertainty in $d(m/m_0)/dT$ ($°C^{-1}$), of the $d(m/m_0)/dT$ versus temperature plot, was found to be ±20% (i.e., ±1 standard deviation) and the uncertainty in the temperature at the maximum, in the $d(m/m_0)/dT$ versus temperature plot, was found to be ±2% (±1 standard deviation). These uncertainties are shown as error bars on data points at 390 and 460°C in Figure 3.

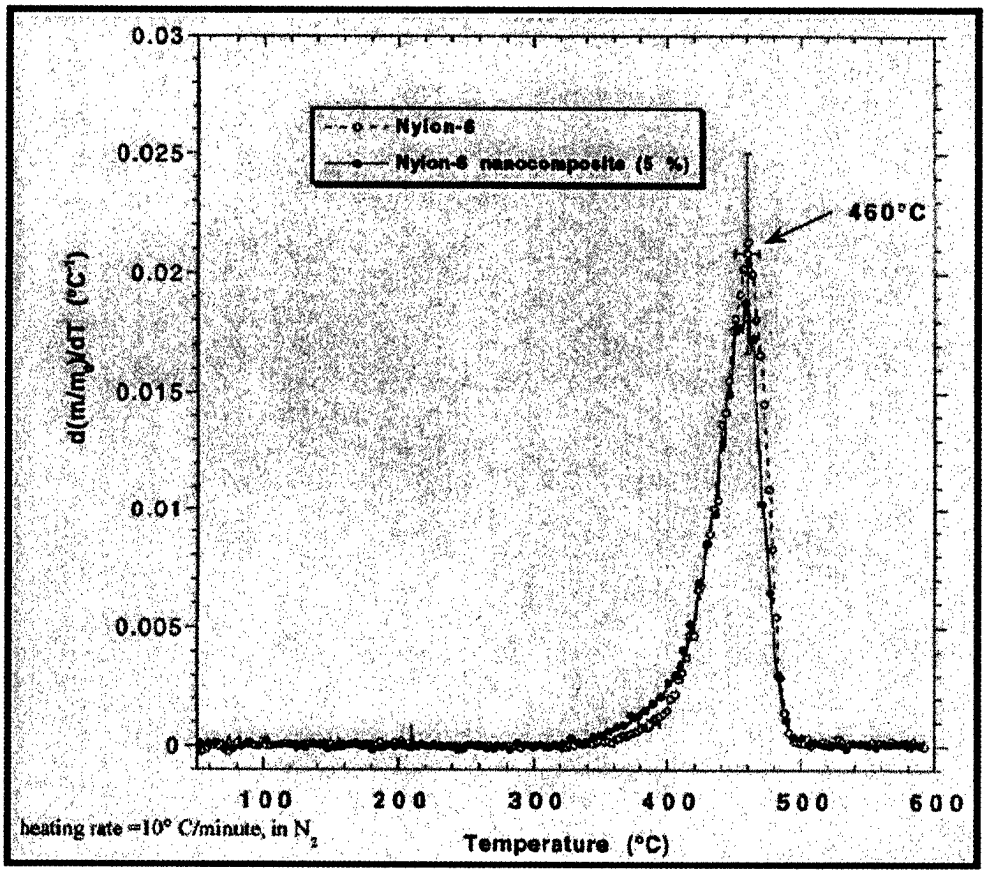

Figure 3. Comparison of the Derivative of the TGA Curves for Nylon-6 and the Nylon-6 Clay-Nanocomposite (5%). There is apparently no significant difference in thermal stability.

RESULTS AND DISCUSSION

Cone Calorimeter

Heat Release Rate

The heat release rate (HRR) data from the cone calorimeter for nylon-6, nylon-6 clay-nanocomposite (2%), and nylon-6 clay-nanocomposite (5%) when exposed to a 35 kW/m² heat flux are shown in Figure 4. The clay-nanocomposites reduce the *peak* HRR of nylon-6 by 32% and 63%, respectively. The fraction of clay present in the nanocomposite, at these levels, is directly proportional to the reduction in HRR. The *peak* heat release rate has been shown to be the most important parameter for predicting fire hazards.

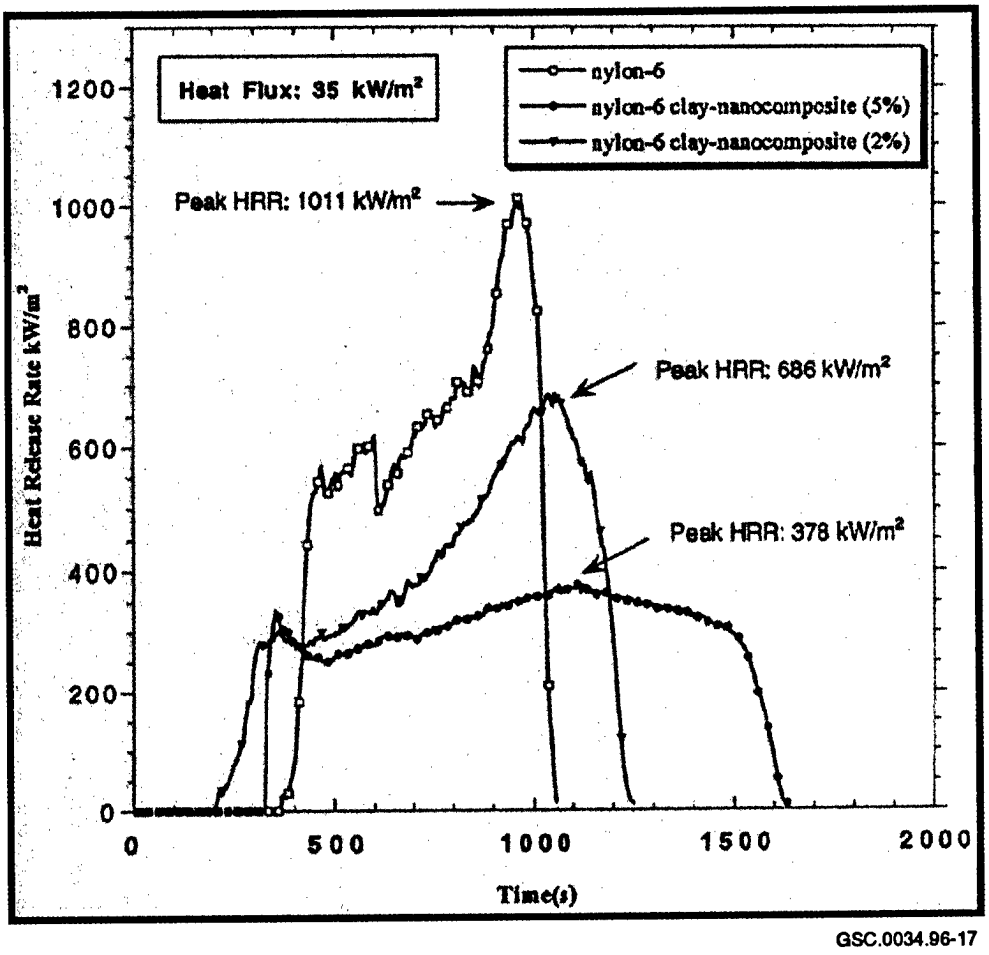

Figure 4. Comparison of the Heat Release Rate (HRR) Plot for Nylon-6, Nylon-6 Clay-Nanocomposite (Mass Fraction 2%) and Nylon-6 Clay-Nanocomposite (Mass Fraction 5%) at 35 kW/m² Heat Flux Showing Respectively the 32% and 63% Reduction in HRR's for the Nanocomposites

Visual observations of the combustion experiments, in the cone calorimeter, reveals different behavior for the nylon-6 clay-nanocomposites compared to the pure nylon-6 from the very beginning of the thermal exposure. A thin char layer forms on the top of all the samples in the first several minutes of exposure prior to ignition. In the case of pure nylon-6, this char layer fractures into small pieces early in the combustion. The char does not fracture with the nylon-6 clay-nanocomposites. This tougher char layer survives and grows throughout the combustion, yielding a rigid multicellular char brick with the same dimensions as the original sample. The HRR curves for the nylon-6 clay-nanocomposites show the double maxima characteristic of material that forms a char layer during combustion[9]. The nanocomposite structure appears to enhance the performance of the char through reinforcement of the char layer. Indeed, transmission electron microscopy (TEM) of a section of the combustion char from the nylon-6 clay-nanocomposite (5%) shows a multilayered silicate structure. This layer may act as a mass transport barrier slowing the escape of the volatile products generated as the nylon-6 decomposes. An additional explanation, proposed by Giannelis et al. after they observed self-extinguishing behavior of a polycaprolactone nanocomposite, attributes the low flammability to the excellent barrier properties of the nanocomposite. The nanocomposite's low permeability for liquids and

gases may slow the transport of volatile fuel through the nanocomposite and into the gas phase[10]. The differential thermogravimetric analysis data, comparing the nylon-6 thermal stability to that for the nylon-6 clay-nanocomposite (5%), are shown in Figure 3. Surprisingly, within the uncertainty of the data, there is little apparent difference in thermal stability. Therefore, it is not likely that the reduced flammability is due to a higher thermal stability of the nanocomposites compared to the pure nylon-6. Furthermore, formation of *new* carbonaceous char is not the primary mechanism responsible for the reduced flammability, since very little additional carbonaceous char is formed and such a small change (reduction) in the carbonaceous fuel available for combustion is not sufficient to explain the observed HRR reduction.

Heat of Combustion, Carbon Monoxide, and Smoke

Most fire retardants function by one of the following mechanisms: (1) by changing the condensed phase chemistry, which usually results in the formation of a char, (2) by altering the gas phase chemistry, (3) by endothermically cooling the material, or (4) through some combination of these. Some of the more effective fire retardants (by mass fraction), such as halogen and some phosphorus based systems, reduce polymer flammability by their ability to form gaseous intermediates which scavenge flame propagating free radicals (e.g., OH and H) thereby inhibiting complete combustion to CO_2. The result is to lower the heat of combustion of the polymer/fire-retardant formulation and lower the HRR. An inherent drawback to the gas phase flame-retardant approach is that an increase in the *yields* of carbon monoxide (CO) and soot are usually observed. In some cases, depending on how effective the system is at reducing the HRR, this can also increase the *rate* of CO and smoke generation[11]. This is undesirable since CO and smoke (the combination of soot and combustion gases) are the primary cause of death in most fires[12].

A comparison of the heats of combustion for nylon-6, nylon-6 clay-nanocomposite (2%), and nylon-6 clay-nanocomposites (5%) is shown in Figure 5. These data show that the nylon-6 clay-nanocomposites (2%) and (5%) have the same heats of combustion as nylon-6. The specific extinction area (SEA) data (a measure of soot) for nylon-6 and nylon-6 clay-nanocomposite (5%) are shown in Figure 6 and Table 1. The nanocomposite has about a 50% greater mean SEA than pure nylon-6. Figure 7 and Table 1 show the CO yield data for nylon-6 and nylon-6 clay-nanocomposite (5%). Here we observe a factor of two increase in the CO yield for the nanocomposite. This type of behavior may be due to a small increase in the concentration of olefinic or aromatic compounds present in the gas phase. Typically, the SEA yield is much more sensitive to the level of olefinic or aromatic compounds than the heat of combustion is. Hamins et al. found an increase in soot levels in methane flames when only 1 mole % of toluene was added to the fuel[13]. Possibly, the silicate is catalyzing the formation of olefinic or aromatic compounds, i.e., through dehydrogenation reactions, during the decomposition in the condensed phase. Furthermore, recent thermal decomposition studies have shown that nylon-6 produces CO during pyrolysis in inert atmospheres[14]. The silicate may also be catalyzing this process. Since there is no change in the heat of combustion and only relatively small changes in the SEA and CO yields, it is reasonable to conclude that the nanocomposites' lower HRR are from changes in the condensed phase decomposition processes and not from a gas phase effect.

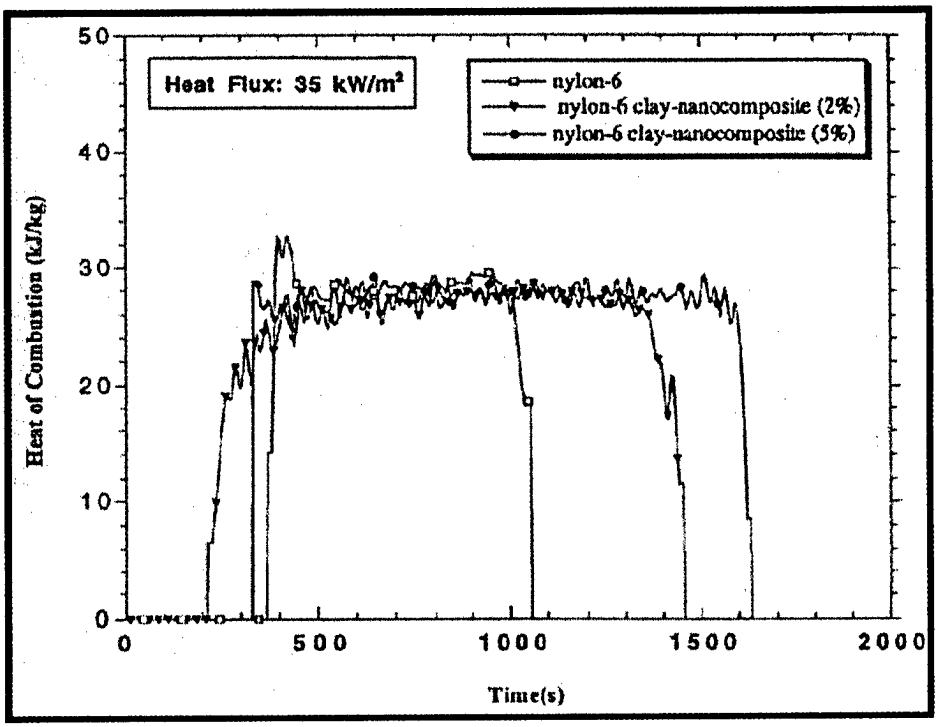

GSC.0034.96-18

Figure 5. Comparison of the Heat of Combustion (H_C) for the Nylon-6 Clay-Nanocomposites and Nylon-6. This data indicates that the clay-nanocomposite is not effecting the gas phase combustion of the nylon-6.

Table 1. Cone Calorimeter Data

Sample	Residue Yield (%) ± 0.3	Peak HRR (% decrease) (kW/m^2) ± 15%	Mean Heat of Combustion (MJ/kg) ± 10%	Total Heat Released (MJ/m^2) ± 10%	Mean Specific Extinction Area (m^2/kg) ± 10%	Mean CO yield (kg/kg) ± 10%
Nylon-6	0.3	1011	27	413	197	0.01
Nylon-6 clay-nano-composite 2%	3.4	686 (32%)	27	406	271	0.01
Nylon-6 clay-nano-composite 5%	5.5	378 (63%)	27	397	296	0.02
Nylon-6,6	0	1190	30	95	200	0.01
Nylon-6,6 -PO 4% Phosphorus	8.5	490 (58%)	18	50	1400	0.16

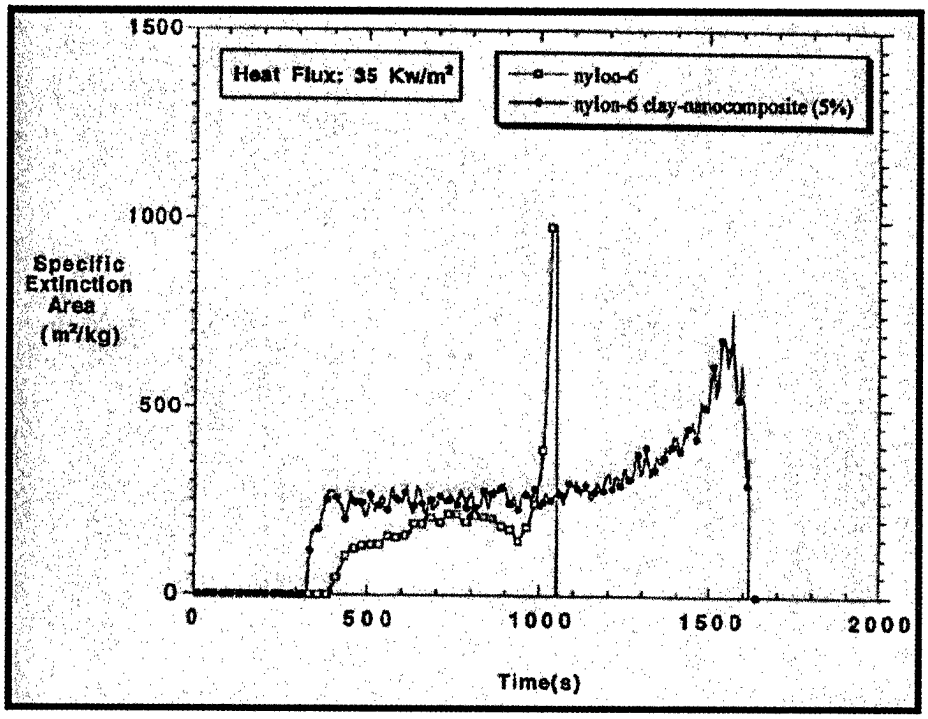

Figure 6. Comparison of the Specific Extinction Area (SEA) Data (a measure of soot) for Nylon-6 and Nylon-6 Clay-Nanocomposite (5%). The nanocomposite has about a 50% greater mean SEA than pure nylon-6 (also see Table 1).

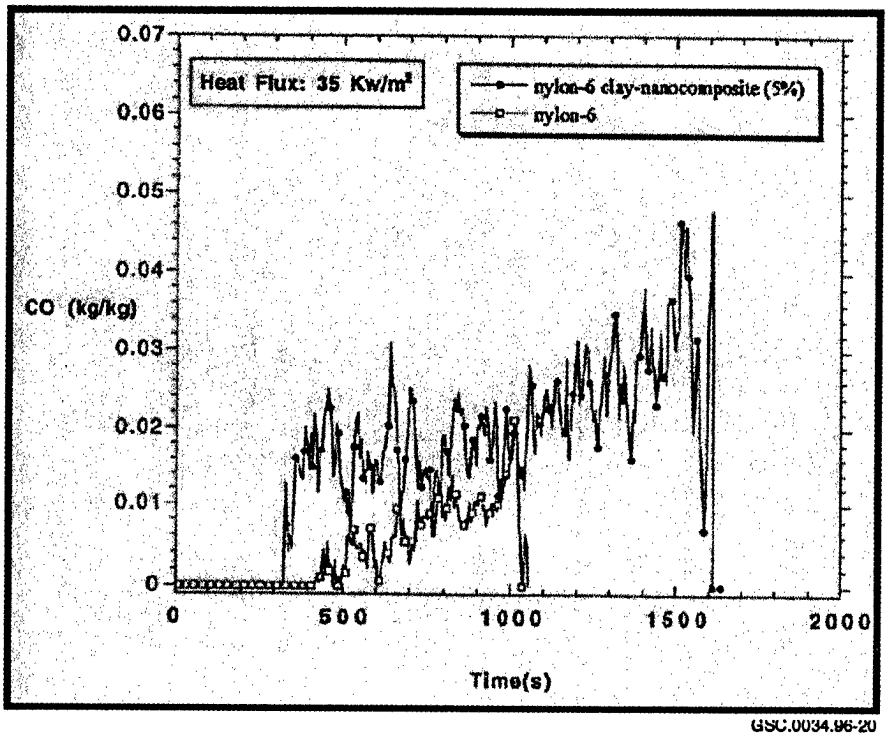

Figure 7. Comparison of the CO Yield Data for Nylon-6 and Nylon-6 Clay-Nanocomposite (5%). A factor of two increase is observed in the CO yield for the nanocomposite (also see Table 1).

Figure 8 shows the mass loss rate data for nylon-6, nylon-6 clay-nanocomposite (2%), and nylon-6 clay-nanocomposites (5%). The three curves closely resemble the HRR curves (Figure 4), indicating that the reduction in HRR for the nanocomposites is primarily due to the reduced mass loss rate and the resulting lower fuel feed rate to the gas phase. To evaluate the fire safety of a flame-retarded material, it is useful to examine the *rate* of soot and CO generation instead of just the soot and CO *yield*. The extinction rate (m^2/s) (Figure-9) is obtained from the product of the SEA (m^2/kg) and the mass loss rate (kg/s). The CO production rate (kg/s) (Figure 10) is obtained from the product of the CO yield (kg/kg) and the mass loss rate (kg/s). The lower mass loss rates give lower *rates* of soot generation, and similar CO production rates, during the combustion of the nanocomposites as compared to the pure nylon-6. The nanocomposites are therefore fire-safe materials in terms of HRR, soot, and CO production.

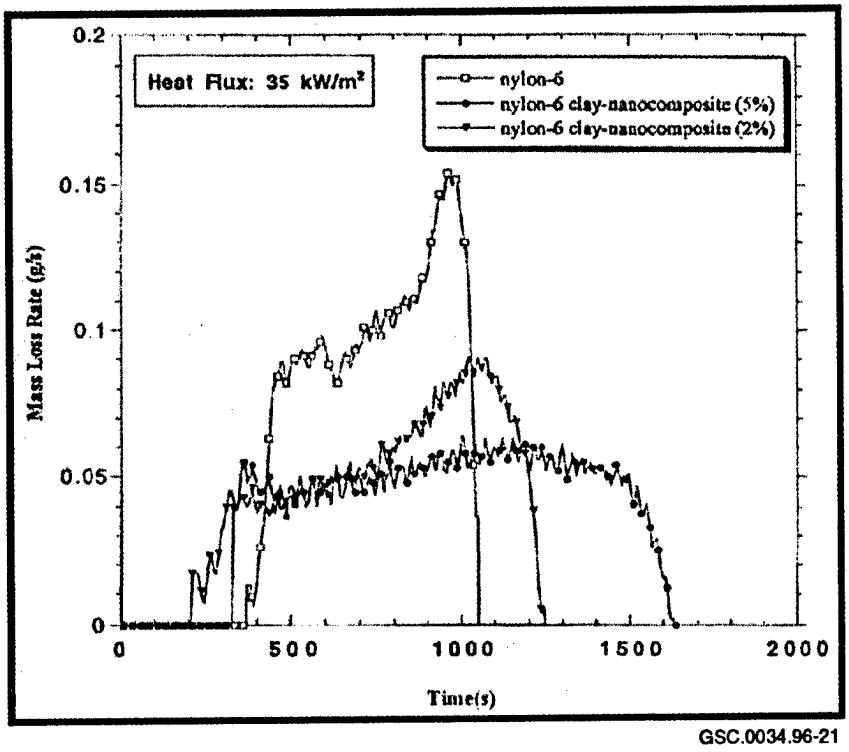

Figure 8. The Mass Loss Rate Data for Nylon-6, Nylon-6 Clay-Nanocomposite (2%), and Nylon-6 Clay-Nanocomposites (5%). The three curves closely resemble the HRR curves (Figure 2), indicating that the reduction in HRR for the nanocomposites is primarily due to the reduced mass loss rate and the resulting lower fuel feed rate to the gas phase.

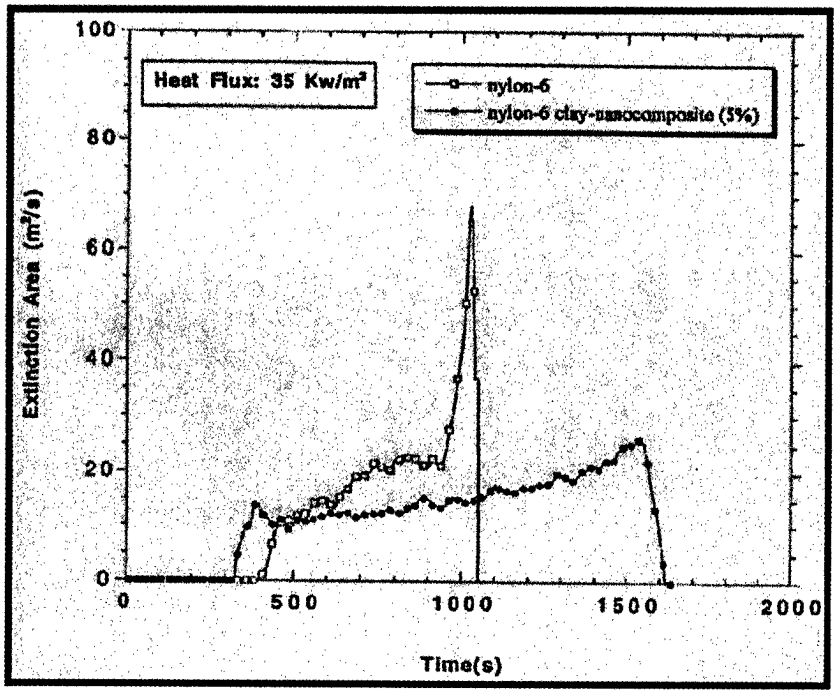

Figure 9. The Extinction Rate (m^2/s) Data, Obtained From the Product of the SEA (m^2/kg) and the Mass Loss Rate (kg/s). The lower mass loss rates give lower rates of soot generation for the nanocomposites.

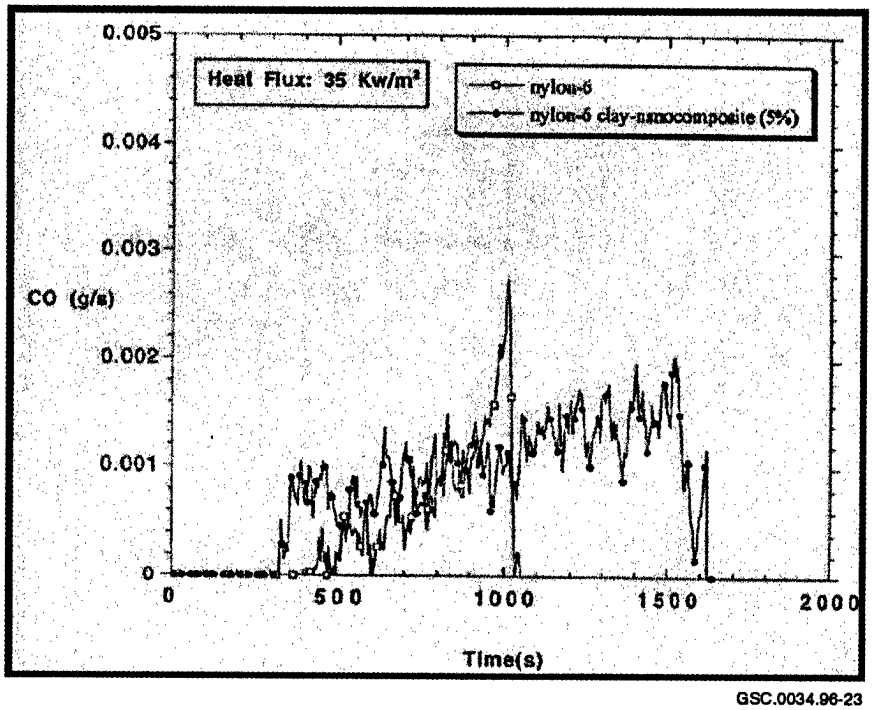

Figure 10. The CO Production Rate (kg/s) Data, Obtained From the Product of the CO Yield (kg/kg) and the Mass Loss Rate (kg/s). The lower mass loss rates give similar rates of CO generation during the combustion of the nanocomposites as compared to the pure nylon.

OTHER FLAME-RETARDANT APPROACHES

Comparison of the nylon-6 clay-nanocomposites to other flame-retarded nylon systems, such as a nylon-6,6 triphenylphosphine oxide copolymer (nylon-6,6-PO), where the flame retardant is also combined with the nylon at the molecular level further illustrates the unique benefits the nanocomposite approach offers. Table 1 shows that the nylon-6,6-PO copolymer gives a similar reduction in HRR (58%) to that for the nanocomposite (63%) at a comparable level of incorporation of flame retardant (4% mass fraction of phosphorus). The phosphine oxide copolymer appears to function by increasing the amount of char formed (8.5%) and by reducing the heat of combustion (by 40%). Unfortunately, for the reasons explained above for flame retardants which act on the gas phase combustion processes, the SEA is *seven* times greater and the CO yield is increased by *sixteenfold*[15]. Even though the mass loss rate for the copolymer is 50% lower than that for pure nylon-6,6, the extinction *rate* is still four times greater and the CO *rate* is still ten times greater than that for pure nylon-6,6. Another additive FR system for nylon, based on ammonium polyphosphate (APP), requires $\geq$35 % mass fraction of additive to significantly effect the flammability (measured by oxygen index) of nylon-6, and as mentioned in the introduction, this results in as much as a 20% loss of mechanical properties. Finally, it should be noted that the nano-dispersed clay composite structure has a very different effect on the flammability of nylon than *macro- or meso-dispersed* clay-polymer mixtures. Bourbigot and Le Bras found, in their extensive study of clays in an intumescent polypropylene system, that montmorillonite clay, similar to the ion exchanged montmorillonite clay used to make the nylon nanocomposite, actually decreased the limiting oxygen index, i.e., *increased* the flammability of the intumescent polypropylene[16].

FUTURE WORK

The ring-opening catalyzed synthesis by which the nylon-6 clay-nanocomposites are prepared yields the delaminated structure shown in Figure 1. In this structure the ammonium end group on the nylon-6 interact ionically with the anionic silicate layer. Characterization of the nylon-6 clay-nanocomposites (2% and 5%) by Usuki et al. revealed that 30% and 50%, respectively, of the nylon-6 polymer chains were bound to the silicate through this interaction. It is possible that it is only this fraction of the nylon that imparts the superior flammability and mechanical properties. Other polymer silicate nanocomposites based on a wide variety of resins, such as polystyrene, epoxy, poly(ethylene oxide), polysiloxane, polyesters, and polyphosphazenes, have recently been prepared via melt intercalation[17]. These materials possess varying degrees of interaction between the polymer and the silicate layer and provide the opportunity to study the effect this variable has on flammability and to determine if the clay-nanocomposite approach is useful in reducing the flammability of other polymers. We are continuing to investigate the mechanism of flame retardancy in clay and other nanocomposite materials.

Polymer Flammability of Polymer-Nanocomposites

To evaluate the feasibility of controlling polymer flammability via a *nanocomposite* approach, we have examined the flammability properties of nylon-6 clay nanocomposites and compared them to those for pure nylon-6 and other FR nylons. The cone calorimeter data show that the peak heat release rate (HRR) is reduced by two-thirds in a nanocomposite containing only 5% clay. Not only is this a very efficient FR system, but it does not have the usual drawbacks

associated with all other FR additives. That is, the physical properties are not degraded by the additive (clay), instead they are greatly improved. Furthermore, this system does not increase the carbon monoxide or soot produced during the combustion, as many commercial fire retardants do.

Recently, a wide variety of other polymer-silicate nanocomposites based on resins such as polystyrene, epoxy, poly(ethylene oxide), polysiloxane, polyesters, and polyphosphazenes have been prepared via an efficient, environmentally friendly "melt intercalation" process developed by Giannelis and coworkers at Cornell University. These materials will provide the opportunity to improve on these initial results and to determine the mechanism by which nanocomposites reduce polymer flammability. This work is part of a collaborative project between NIST, Air Force Phillips Laboratory, and Cornell University to study the structure-flammability relationships of polymer-silicate nanocomposites.

Fire-Retardant Additives Based on Transition Metal Oxides

A new inorganic additive system based on ceramic powders was found to be an excellent flame retardant for both commodity and engineering polymers, e.g., polypropylene, nylon, phenolic-triazines, and Ultem polyimide. This system approaches accomplishment of the program performance goals. The peak HRR, at an incident heat flux of 50 kW/m^2 , for Ultem is reduced from 180 kW/m^2 to 100 kW/m^2. This system even maintains most of the effectiveness at 70 kW/m^2.

An NIST patent disclosure has been filed on the work.

Effect of Preceramic Polymers on the Flammability of Organic Polymers

In collaboration with the Air Force Phillips lab (Dr. Joe Lichtenhan), we have studied the effectiveness of three preceramic polymers as fire retardants when blended with organic polymers. In general, the preceramic polymers are very effective at reducing the flammability of the highly flammable thermoplastic organic polymers we examined so far, such as PP, Kraton, and Pebax, without degrading the mechanical properties.

A joint NIST/Air Force patent disclosure has been filed on these results.

Cross-Link Versus Flammability Study

We have synthesized a variety of cyanate ester functionalized copolymers of styrene combined with poly butadiene and methylmethacrylate. An SPE preprint on this work was written and presented at the ANTEC '96 SPE meeting.

Hoechst Celanese and Lonsa Corp. are in the process of evaluating the cyanate ester copolymers as toughening agents in CE composites.

This FAA funded research parallels similar work at NIST funded by an industrial consortium, The Environmentally Friendly Flame Retardants Consortium.

ACKNOWLEDGMENTS

The authors would like to thank the Federal Aviation Administration for partial funding of this work through Interagency Agreement DTFA0003-92-Z-0018. We would also like to thank Jack Lee for cone calorimeter analysis, Dr. C. Jackson and Dr. H. Chanzy for TEM analysis, Dr. M. Nyden and Dr. E. Manias (Cornell University) for the montmorillonite structure, and Professor E. Giannelis (Cornell University) for helpful discussion.

REFERENCES

1. S. Levchik, G. Camino, L. Costa, and G. Levchik, *Fire and Materials*, 19, 1 (1995).
2. A. Hochberg, *Proceedings of the Fall FRCA Meeting*, Naples, FL., 159 (1996).
3. A. Usuki, Y. Kojima, M. Kawasumi, A. Okada, Y. Fukushima, T. Kurauchi, and O. Kamigaito, *J. Mater. Res.* 8, 1179 (1993).
4. E. Giannelis, *Adv. Mater.* 8, 29 (1996).
5. Y. Kojima, A. Usuki, M. Kawasumi, A. Okada, Y. Fukushima, T. Kurauchi, and O. Kamigaito, *J. Mater. Res.* 8, 1185 (1993).
6. Certain commercial equipment, instruments, materials, services, or companies are identified in this paper in order to specify adequately the experimental procedure. This in no way implies endorsement or recommendation by NIST.
7. V. Babrauskas, R. Peacock, *Fire Safety Journal*, 18, 255 (1992).
8. V. Babrauskas, *Fire and Materials*, 19, 243 (1995).
9. A. Marchal, et al., *Polymer Degradation and Stability*, 44, 263 (1994).
10. E. Giannelis and P. Messersmith, *J. Polym. Sci. A:Polym. Chem.*, 33, 1047 (1995).
11. M. Barnes, P. Briggs, M. Hirschler, A. Matheson, and T. O'Neill, *Fire and Materials*, 20, 1 (1996).
12. B. Harwood and J. Hall, *Fire J.* 83, 29, (1989).
13. A. Hamins, D. Anderson, and H. Miller, *Combust. Sci. and Tech.*, 71, 175 (1990).
14. P. Hornsby, J. Wang, R. Rothon, G. Jackson, G. Wilkinson, and K. Cossick, *Polymer Degradation and Stability*, 51, 235 (1996).
15. I. Wan, J. McGrath, and T. Kashiwagi, in "Fire and Polymers II", G. Nelson, Ed., ACS Symposium Series **599**, American Chemical Society, Washington, DC (1995).
16. M. Le Bras and S. Bourbigot, *Fire and Materials*, 20, 39 (1996).
17. Reference 4 and R. Vaia, K. Jandt, E. Kramer, and E. Giannelis, *Macromolecules*, 28, 8080 (1995).

SURFACE-ACTIVE FLAME RETARDANTS

Wei Chen and Thomas J. McCarthy
Polymer Science and Engineering Department
University of Massachusetts
Amherst, Massachusetts 01003

ABSTRACT

The objective of the research in progress in our laboratories at UMass is to use surface free energy minimization to enhance the efficacy of flame retardants in organic polymers. Our current studies are focused on preparing perfluoroalkyl-substituted fullerenes (C_{60}) and studying their mobility and surface activity in polystyrenes of various molecular weight (Figure 1). Fullerenes have not been tested as flame retardants, but they should function both to starve the surface of hydrogen (they can be considered a molecular char) and to trap radicals to suppress combustion mechanisms.[1] The surface activity of the fluorinated fullerenes should allow for low levels of retardant loading and in a fire, cause a thermodynamically driven replenishing of flame retardant at the surface. This is one class of flame retardants, but this strategy should prove generally effective for a variety of flame-retardant classes.

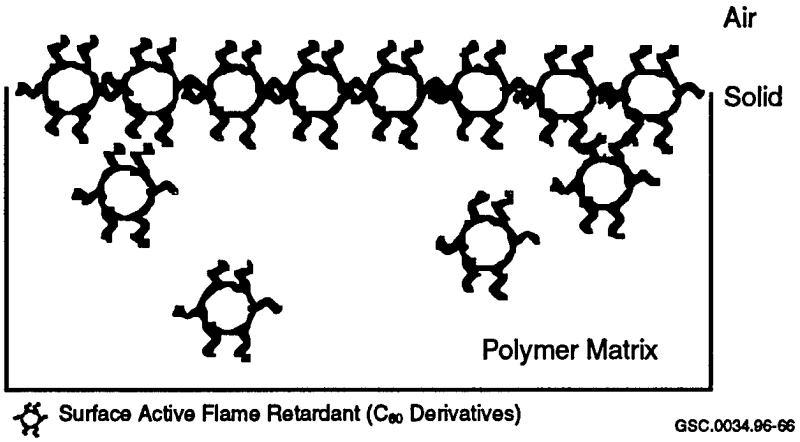

Figure 1. Surface Active Flame Retardants

INTRODUCTION

Most interfacial properties, for example adhesion or wettability, of solid materials depend upon, among other parameters, the chemical composition of the outermost region at the physical boundaries (surfaces) of the solid object. We suspect that ignition of polymers is such a property. Organic polymer surfaces are uniquely complex, in a number of regards, among materials surfaces: Most polymers under many conditions exhibit dynamic surfaces with chains rotating and repeating on time scales and dimension scales which depend on the polymer structure and

the environment. Surface chain mobility varies greatly from polymer to polymer; surface regions can have different degrees of crystallinity, and common polymers exhibit glass transition temperatures (T_g) over a temperature range greater than 400°C.

The mobility of polymer surfaces in materials which can display different surface structures is of practical importance as desired surface properties can be the result of one particular surface orientation. A rather extensive literature has grown in the past 20 years[2] which describes surface reconstruction in a variety of polymer materials of this type. A portion of this literature has been reviewed.[3] Homopolymer surfaces can display different properties by selective orientation of surface functionality which can vary depending on the processing conditions and/or the environment.[4-16] Random, graft, and block co-polymers as well as polymer blends can concentrate one (or another) component at the surface in response to processing or the environment.[17-35] Surface-modified polymers can also display different surface structure and properties.[19,36-45]

Solid organic polymer objects, because of the high molecular weight of their molecules, are inherently non-equilibrium structures[46] and because of relaxation and transition phenomena their structures and properties are time- and temperature-dependent. Polymer surface modifications are often carried out with the objective of increasing the surface free energy of the material to permit or enhance adhesion. Normally polar functional groups are introduced by chemical reaction. These modified structures are inherently unstable with respect to other structures that display lower surface free energies which the material can assume (relax to) given sufficient chain mobility. The spontaneous migration of polar functional groups from the surface toward the bulk has been described for many surface-functionalized polymers.[36-42]

Several groups have recently shown that perfluoroalkyl groups which are incorporated into polystyrene are surface-active.[47-52] X-ray photoelectron spectroscopy, contact angle, and other techniques indicate a surface excess (over the bulk) of fluorine due to the adsorption (surface segregation) of the low surface energy fluorocarbon at the polymer-air interface. Our strategy is to make fullerenes surface-active by attaching perfluoroalkyl groups.

PROGRESS

We have prepared perfluoroalkyl fullerenes in 70% isolated purified yield by reacting C_{60} with perfluorohexyl iodide (equation 1). Elemental analysis indicates that ~5 perfluorohexyl groups are attached on average. The modified fullerenes are soluble in freon-113 and hexafluorobenzene.

$$CF_3CF_2CF_2CF_2CF_2CF_2I + C_{60} \xrightarrow[200°C,\ 24\ h]{1,2,4\text{-trichlorobenzene}} C_{60}(CF_3CF_2CF_2CF_2CF_2CF_3)_{5.2} \quad (1)$$

We have prepared blends of the perfluoroalkyl fullerenes with polystyrene by spincasting films from toluene/freon-113 solutions onto silicon wafers. Polystyrene samples were prepared by anionic polymerization and had narrow molecular weight distribution and Mn values of 6.5 K and 62 K. Some films were dried at reduced pressure at room temperature and others were vacuum dried at 110°C overnight. Surface analysis indicates that the perfluoroalkyl fullerenes are

extremely surface-active. X-ray photoelectron spectroscopy (XPS) and contact angle analysis indicate that the surface is a near close-packed array of perfluoroalkyl fullerenes. Figure 2 shows adsorption kinetics for the migration of perfluoroalkyl fullerenes from the bulk to the surface as assessed by quantitative XPS and contact angle analysis. As can be seen in the XPS data (F:C ratio), the surface region is fullerene-rich after 1 day at room temperature. The contact angle (water and hexadecane) results indicate close-packed perfluoroalkyl groups. The data also indicate that adsorption occurs on casting. Both 15° and 75° takeoff angle XPS data are reported; the former indicates the composition of the outermost ~10 Å of the samples and the latter indicates the outermost ~40 Å.

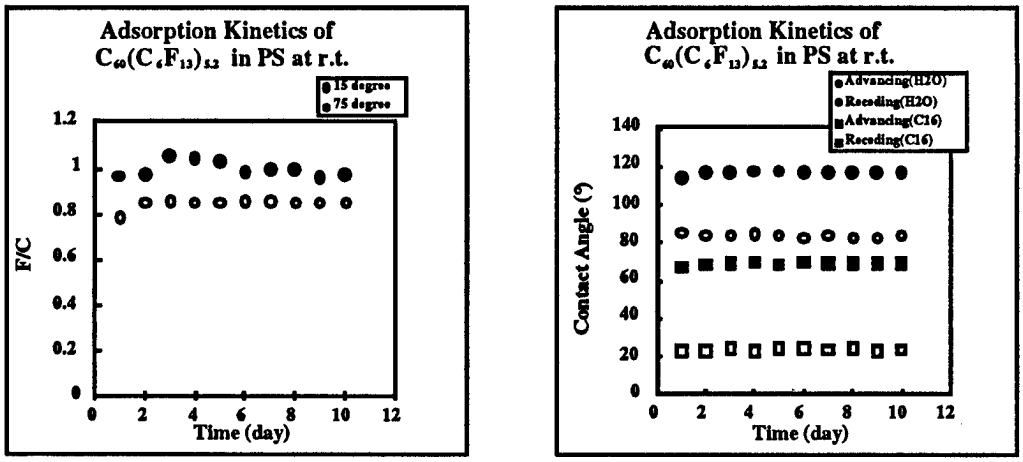

Figure 2. Adsorption of Perfluoroalkylated Fullerenes from the Bulk of Polystyrene (Mn ~ 65 K) to the Polymer-Air Interface at Room Temperature. The data indicate that adsorption occurs on casting.

Concentration isotherms (at room temperature) were determined by XPS and contact angle and it was determined that the perfluoroalkylated fullerenes exhibit isotherms of the high-affinity type; as little as 0.5 weight % saturates the surface. Figure 3 shows these data.

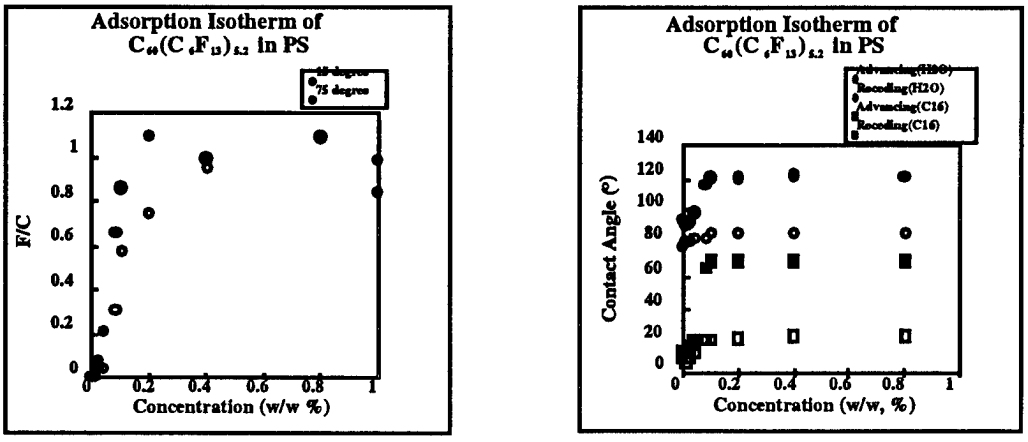

Figure 3. Adsorption Isotherms for Perfluoroalkylated Fullerenes in Polystyrene (Mn ~ 65 K) at Room Temperature

NOTES AND REFERENCES

1. Touval, I., "Antimony and Other Inorganic Flame Retardants" under "Flame Retardants," *Kirk-Othmer Encyclopedia of Chemical Technology*, 4th ed. John Wiley and Sons: New York, 1993, vol. 10, pp 936-954.
2. It should be noted that functional group mobility was proposed in 1938 to explain contact angle hysteresis: Langmuir, I. *Science* **1938**, *87*, 493.
3. Andrade, J.D., Gregonis, D.E., and Smith, L.M., in *Surface and Interfacial Aspects of Biomedical Polymers*; Andrade, J.D., Ed.; Plenum: New York, 1986, Vol. 1, Chapters 2 and 7.
4. Good, R.J.; Kotsidas, E.D., *J. Coll. Interfac. Sci.* **1978**, *66*, 360.
5. Schonhorn, H., *Macromolecules* **1968**, *1*, 145.
6. Schonhorn, H. and Ryan, F.W., *J. Phys. Chem.* **1966**, *70*, 3811.
7. Wang., L.-H. and Porter, R.S., *J. Appl. Polym. Sci.* **1983**, *28*, 1439.
8. Carre, A. and Schreiber, H.P., *J. Coat. Tech.* **1982**, *54*, 31.
9. Good, R.J. and Kvikstad, J.A.; Bailey, W.O., *J. Coll. Interfac. Sci.* **1971**, *35*, 314.
10. Baier, R.E. and Zisman, W.A., *Macromolecules* **1970**, *3*, 70.
11. Baier, R.E. and Zisman, W.A., *Macromolecules* **1970**, *3*, 462.
12. Reardon, J.P. and Zisman, W.A., *Macromolecules* **1974**, *7*, 920.
13. Petke, F.D. and Ray, B.R., *J. Coll. Interfac. Sci.* **1969**, *31*, 216 and references cited therein
14. Holly, F.J. and Refojo, M.F., *J. Biomed. Mat. Res.* **1975**, *9*, 315.
15. Owen, M.J., *Ind. Eng. Chem. Prod. Res. Dev.* **1980**, *19*, 97.
16. Tse, J. and Adamson, A.W., *J. Coll. Interfac. Sci.* **1979**, *72*, 515.
17. O'Malley, J.J. and Thomas, H.R., *Macromolecules* **1979**, *12*, 323.
18. Thomas, H.R., O'Malley, J.J., and Lee, G.M., *Macromolecules* **1979**, *12*, 996.
19. Gagnon, D.R. and McCarthy, T.J., *J. Appl. Polym. Sci.* **1984**, *29*, 4335.
20. Phillips, R.W. and Dettre, R.H., *J. Coll. Interfac. Sci.* **1976**, *56*, 251.
21. Sohn, J. and Ree, T., *J. Appl. Polym. Sci.* **1984**, *29*, 4237.
22. Schmitt, R.L.,Gardella, J.A., Jr., Magill, J.H., Salvatti, L. Jr., and Chin, R.L., *Macromolecules* **1985**, *18*, 2675.
23. Yoon, S.C. and Ratner, B.D., *Macromolecules* **1986**, *19*, 1068.
24. Widmaier, J.M. and Meyer, G.C., *J. Appl. Polym. Sci.* **1983**, *28*, 1429.
25. Takahara, A., Tashita, J., Kajiyama, T., Takayanagi, M., and MacKnight, W.J., *Polymer* **1985**, *26*, 987.
26. Lavielle, L. and Schultz, J., *J. Coll. Interfac. Sci.* **1985**, *106*, 438.

27. Hogt, A.H., Gregonis, D.E., Andrade, J.D., Kim, S.W., Dankert, J., and Feijen, J., *J. Coll. Interfac. Sci.* **1985**, *106*, 289.

28. Andrade, J.D., Ma, S.M., King, R.N., and Gregonis, D.E., *J. Coll. Interfac. Sci.* **1979**, *72*, 488.

29. Pennings, J.F.M. and Bosman, B., *Coll. Polym. Sci.* **1979**, *257*, 720.

30. Pekala, R.W. and Merrill, E.W., *J. Coll. Interfac. Sci.* **1984**, *101*, 120.

31. Ruckenstein, E. and Gowisankar, S.V., *J. Coll. Interfac. Sci.* **1985**, *107*, 488.

32. Ruckenstein, E. and Gowisankar, S.V., *J. Coll. Interfac. Sci.* **1986**, *109*, 557.

33. Pennings, J.F.M., *Coll. Polym. Sci.* **1978**, *256*, 1155.

34. Schwarcz, A., *J. Appl. Polym. Sci. Polym. Phys. Ed.*. **1974**, *12*, 1195.

35. Le Grand, D.G. and Garnes, G.L., Jr., *Polym. Prepr. (Am. Chem. Soc., Div. Polym. Chem.)* **1970**, *11(2)*, 442.

36. Holmes-Farley, S.R., Reamey, R.H., Nuzzo, R., McCarthy, T.J., and Whitesides, G.M., *Langmuir* **1987**, *3*, 799.

37. Baszkin, A. and Ter-Minassian-Saraga, L., *J. Coll. Interfac. Sci.* **1973**, *43*, 190.

38. Yasuda, H., Sharma, A.K., and Yasuda, T., *J. Appl. Polym. Sci. Polym. Phys. Ed.*. **1981**, *19*, 1285.

39. Baszkin, A. and Ter-Minassian-Sarage, L., *Polymer* **1974**, *15*, 759.

40. Dwight, D.W. and Riggs, W.J., *J. Coll. Interfac. Sci.* **1974**, *47*, 650.

41. Rasmussen, J.R., Bergbreiter, D.E., and Whitesides, G.M., *J. Am. Chem. Soc.* **1977**, *99*, 4746.

42. Gerenser, L.J., Elman, J.F., Mason, M.G., and Pochan, J.M., *Polymer* **1985** *26*, 1162.

43. Everhart, D.S. and Reilley, C.N., *Surf. Interfac. Anal.* **1981**, *3*, 126.

44. Everhart, D.S. and Reilley, C.N., *Surf. Interfac. Anal.* **1981**, *3*, 258.

45. Ikada, Y., Matsunaga, T., and Suzuki, M. *Nip. Kag. Kai.* **1985**, *6*, 1079.

46. Chapter 2 of reference 3 contains an excellent discussion of polymer structure, relaxations and transitions in regard to polymer surface dynamics.

47. Iyengar, D.R., Perutz, S.M., Dai, C.-A., Ober, C.K., and Kramer, E.J., *Macromolecules* **1996**, *29*, 1229.

48. Schaub, T.F., Kellogg, G.J., Mayes, A.M., Kulasekere, R., Ankner, J.F., and Kaiser, H. *Macromolecules* **1996**, *29*, 3982.

49. Affrossman, S., Bertrand, P.,Hartshorne, M., Kiff, T., Leonard, D., Pethrick, R.A., and Richards, R.W., *Macromolecules* **1996**, *29*, 5432.

50. Affrossman, S., Hartshorne, M., Kiff, T.,Pethrick, R.A., and Richards, R.W., *Macromolecules* **1994**, *27*, 1588.

51. Elman, J.F., Johs, B.D., Long, T.E., and Koberstein, J.T., *Macromolecules* **1994**, *27*, 5341.

52. Hunt, Jr., M.O., Belu, A.M., Linton, R.W., and DeSimone, J.M., *Macromolecules* **1993**, *26*, 4854.

MUTUALLY INTERPENETRATING ORGANIC-INORGANIC NETWORKS

Bruce Novak
Polymer Science and Engineering Department
University of Massachusetts
Amherst, Massachusetts 01003

BACKGROUND

Unusual properties can be achieved by increasing interfacial interactions through the synthesis of materials which show a high degree of mixture, or interpenetration, between the two dissimilar phases. To this end, we have been interested in using the sol-gel process *(Scheme I)* to develop new routes into hybrid materials which contain both inorganic and organic components commingled into new, intimate morphologies.[1] The degree of phase separation in these materials can vary, but domain sizes are typically on the nanometer scale. In some cases, the domain sizes are reduced to a level such that true molecular composites are formed. As a result of this intimate mixing, these hybrids are often highly transparent, a property which renders them amenable to applications outside the boundaries of traditional composites.

Scheme I

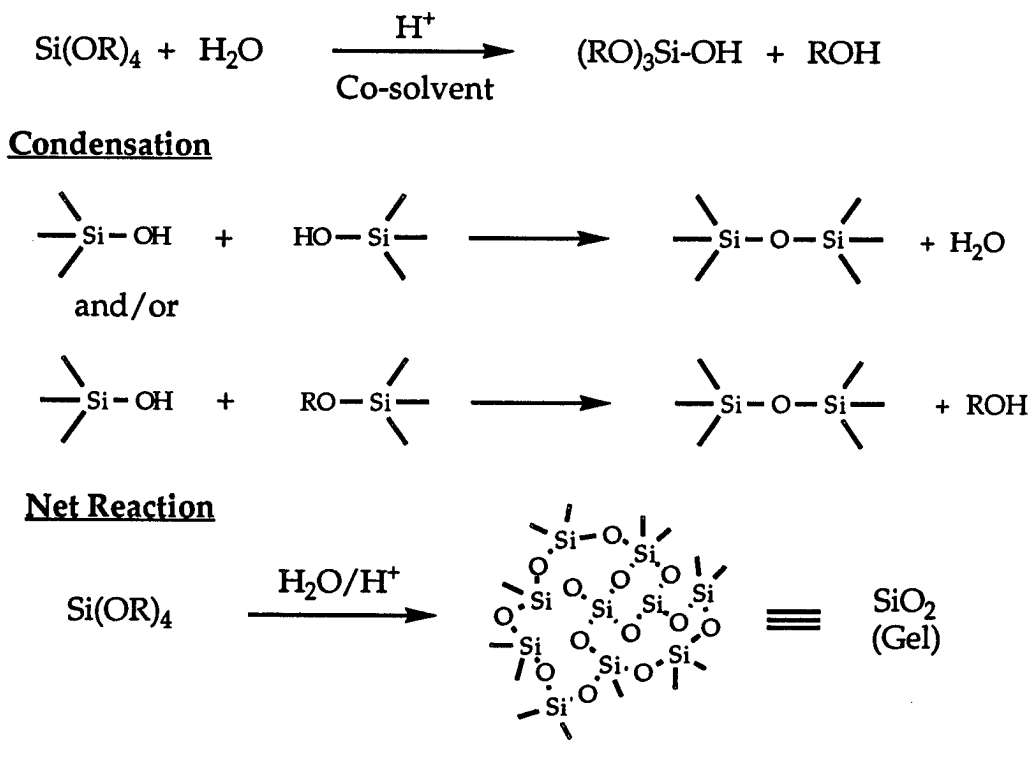

Our past work involved the formation of inorganic networks (SiO_2) through a sol-gel process using tetraalkoxysilane with polymerizable alkoxide moieties.[2] By employing *in situ* organic polymerization catalysts (ROMP or free radical), the alcohol liberated during the formation of the inorganic network is polymerized. By using a stoichiometric quantity of water, and additional polymerizable alcohol as a cosolvent if needed, all components are converted into either the organic polymer or the inorganic network. Because no evaporation is necessary, large-scale shrinkages are eliminated (Scheme II).

Scheme II

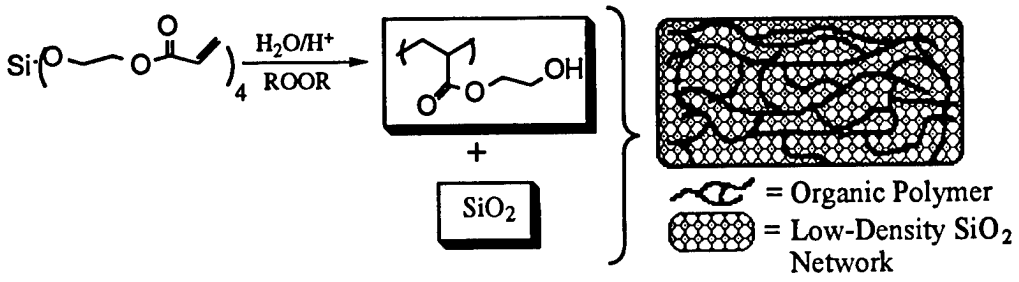

The glass content of these composites is controlled by the stoichiometry of the tetraalkoxysilane precursor and typically ranges from 10%-15%. Current work in this area is directed at increasing the glass content in these composites by synthesizing poly(silicic acid ester) derivatives possessing the same polymerizable alkoxides.[3] By controlling both the silicic acid branching ratio and the degree of alkoxide substitution, nonshrinking composites with glass contents greater than 50% can be fabricated. These semi-interpenetrating polymer network (SIPN) composites display excellent properties in comparison to the pure polymers or to conventional composites of similar composition. These prototype composites remain unoptimized in that the phase separated regions (although on the nanometer scale) are comprised of amorphous silica. Further improvement in properties would be expected if ordered nanophases could be formed. One main advantage that organic-inorganic interpenetrating networks (IPNs) have over conventional composites in aircraft applications is that the same mechanical properties can be obtained at lower loadings of the heavy, inorganic phase. Therefore at a fixed density, IPNs or nanocomposites can be stronger than conventional materials. Their thermal stability should also be noted. Interpenetrating inorganic networks into organic polymers can greatly improve their thermal stability. For example, the decomposition temperature of poly(2-hydroxyethyl-methacrylate), HEMA, can be increased a full 100°C, from 265 to 366°C, by interpenetration with SiO_2 using these simultaneous methods.

We have hypothesized that further improvements in properties could be realized by forming ordered inorganic phases (e.g., high-aspect-ratio fibers, nanotubes, etc.) within the polymer matrix. We are interested in working within the same nonshrinking paradigm, but in contrast to our previous *in situ* systems that yield amorphous SiO_2 domains, we seek to develop new methods that will allow us to form nanostructures *in situ* in the shape of well-defined, high-aspect-ratio glass fibers or networks. Our approach involves the formation of elongated templates (crystallites, aggregates, etc.) or three-dimensional ramified structures that seed the growth of silica at their surfaces. In this way, elaborate three-dimensional structures can be coated with silicate jackets that lock in their reinforcing structures.

Researchers from Japan recently reported the formation of silicate nanotube structures from sol-gel reactions run in the presence of tartaric acid.[4] The mechanism of tube formation is not known although the authors speculated on the formation of tartaric acid dimers, that when stacked together, form a template upon which the SiO_2 condensation could occur. We view this explanation as highly unlikely based on the size scale of the dimer structure (0.1 nm in diameter) versus the interior diameter of the tubes (200-300 nm). Nevertheless, this was an interesting observation that became the starting point of our investigation.

IN SITU TEMPLATING OF HIGH-ASPECT-RATIO FIBERS WITH AMMONIUM TARTRATE CRYSTALS

During mechanical property characterization it was discovered that glass fiber reinforcement of the IPN greatly improves the mechanical behavior compared with 10% fiber reinforcement of the polymer as shown in Figure 1.

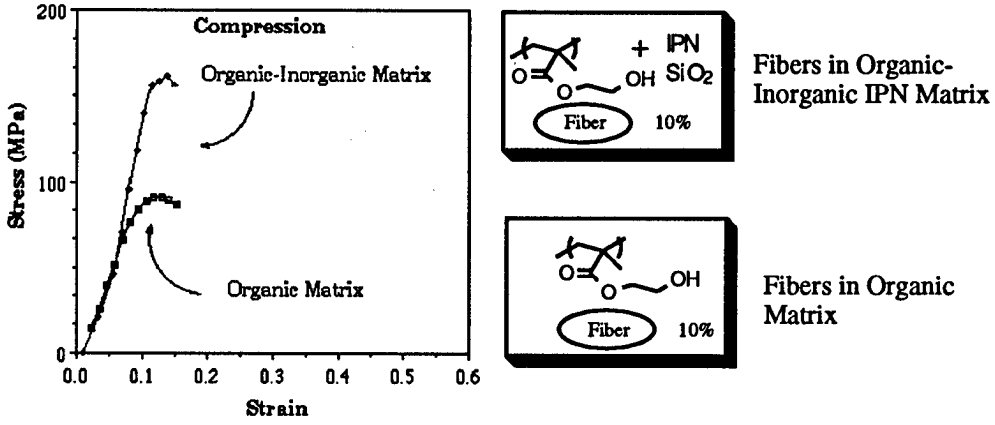

Figure 1. A Comparison of the Mechanical Strength of Two Glass Fiber Composites: One Made From Fibers Embedded into a Pure Organic Matrix (HEMA) and the Other Made From Embedding Glass Fiber into a Matrix Made of an Interpenetrating Network of HEMA and SiO_2

Based on this observation an improved composite could be synthesized *in situ* by the addition of a third component that would act as a sol-gel template. We are working on the development of two such templating processes that are based on a solution of the tetraalkoxysilicate and dissolved template precursor. The precursor is designed to self assemble into templates which would then seed the growth of SiO_2 on their surfaces. The full embodiment of this approach will involve the simultaneous formation of the organic matrix phase thereby insuring intimate mixing of all the components. A schematic of this process is shown in Figure 2.

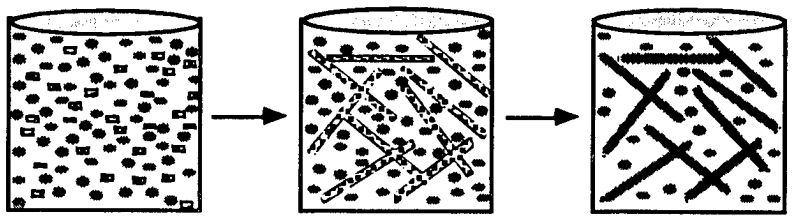

Figure 2. Schematic of Templating Process Using in situ Grown Crystals

The first templating process was adapted from a recent report that hollow, micron-scale SiO_2 tubes can be synthesized by a modified sol-gel reaction. The mechanism of the tube formation was speculated on but was not truly delineated. The reported synthesis is shown in Scheme III.

Upon reinvestigation of this work, we have discovered the mechanism of this templating process to be that ammonium tartrate (ATT) crystals form in the basic alcoholic solution resulting from the addition of ammonium hydroxide and these ATT crystals act as fiber templates. The addition

Scheme III

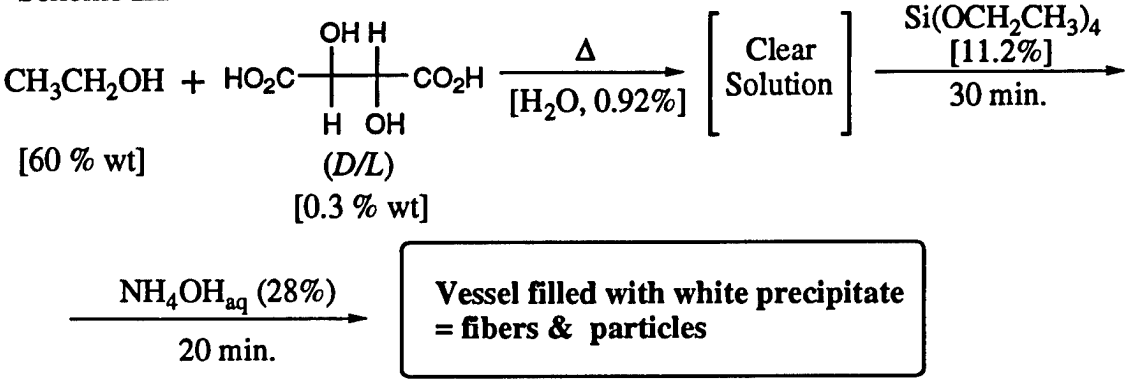

of ammonium hydroxide causes the crystallization of ammonium tartrate and catalyzes the coating of the crystals with SiO_2. Washing of the coated crystals with water dissolves the ammonium tartrate out from within the SiO_2 coating leaving a hollow silicon tube. Figure 3 shows scanning electron microscopy (SEM) photographs of the ammonium tartrate crystals and the SiO_2 fibers obtained from this synthesis. We are currently developing methods of growing these fibers simultaneously with PHEMA/SiO_2 IPN formation.

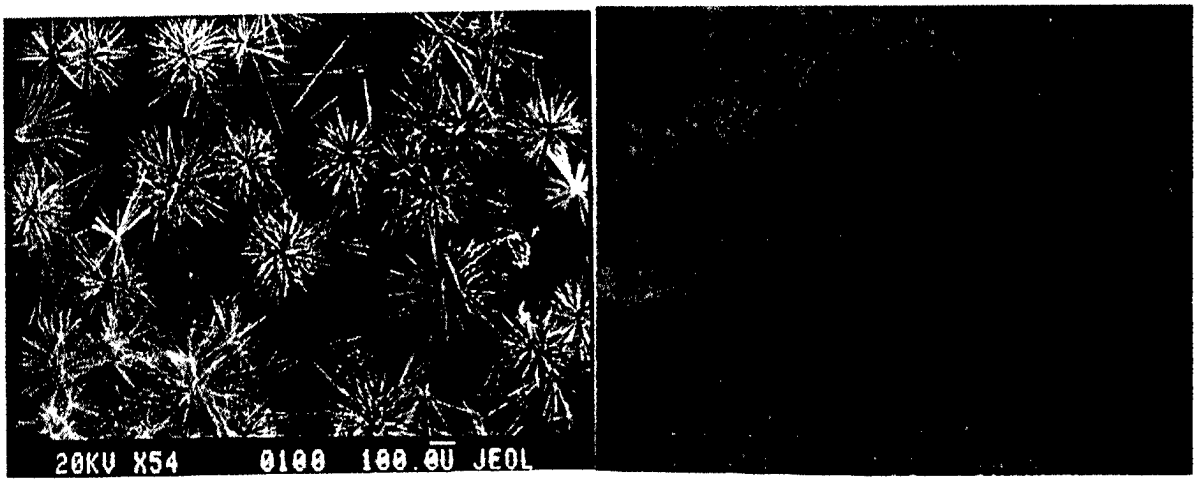

Figure 3. Left: Ammonium Tartrate Crystals One Minute After Crystallization Began. Right: SiO_2 Fibers Obtained From Templating Process.

In our hands, these coating were not uniform in nature so we have investigated the use of a pre-condensed precursor that should coat the crystals at an accelerated rate. Specifically, we have studied the condensation of poly(silicic acid) (PSA) as an alternative method for coating these

superstructures.[3] PSA is synthesized by adding 3M HCl to sodium metasilicate in tetrahydrofuran (THF) at 0°C. The polymer is then extracted with salt saturated THF (equation 1). The inorganic precursor remains soluble in the THF solution.

We are currently studying the reaction conditions that will facilitate successfully coating these templates. The addition of ATT crystals to a PSA-THF solution causes the preferential condensation of PSA at the crystal surface. The coatings achieved are uniform and become thicker with longer exposure times. Figure 4 shows SEM photographs of ATT crystals coated with PSA. Complete in situ processes are currently being studied based on this new approach.

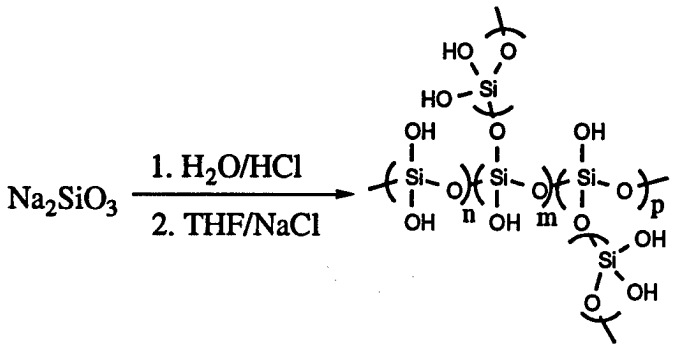

(1)

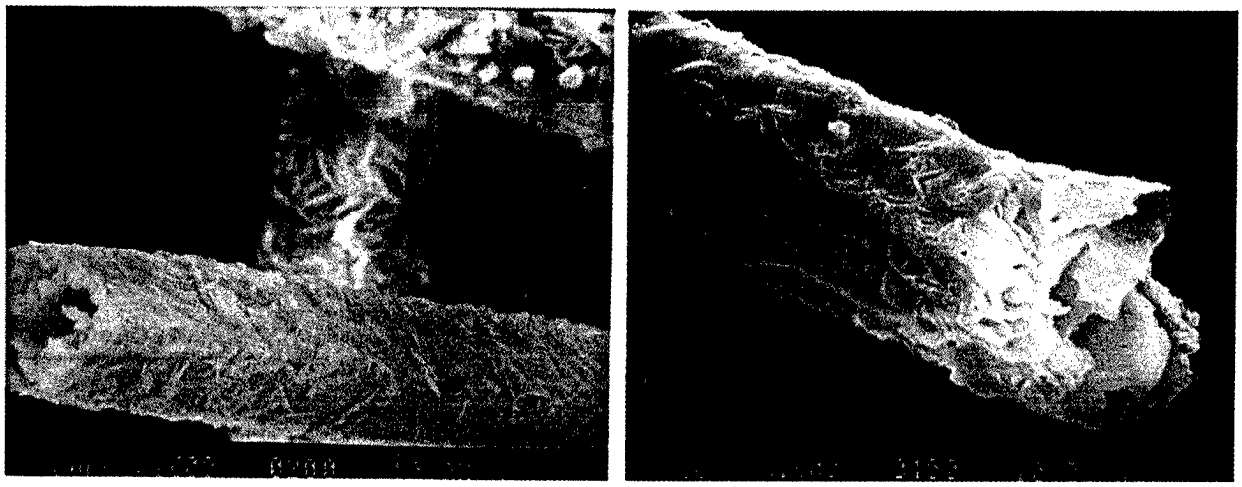

Figure 4. ATT Crystals Coated With SiO_2 Derived From the Precondensed PSA Precursor

The second templating system under investigation makes use of a self-assembling organic gelator. Recently, small molecular weight compounds have been developed that spontaneously form long-range, three-dimensional structures reversibly in organic solvents and oils.[4,5] The structures are pervasive throughout the liquid such that its ability to flow is limited and behaves as a solid. The binding forces present in the ramified gelling structure are hydrogen bonds between adjacent molecules. The chemical structures of the building blocks of these gel networks are based upon a rigid central core surrounded by hydrogen bonding sites with long flexible spacer arms emanating from each site. These molecules self assemble into highly ramified fibrous structures in a variety of organic solvents by forming hydrogen-bonded central cores

from which the hydrocarbon tails extend. The long-range structure, hydrogen bonding induced stacking, and the chemical structure of one of the gelling agents we are studying are shown in Figure 5. The concept being pursued in this phase of the work involves establishing the gelator template within the composite precursor system and then allow the simultaneous polymerization and sol-gel reaction to occur to yield an IPN with the SiO_2 coated superstructures acting as reinforcing component. We have attempted to coat these structures with SiO_2 using the same reactants mentioned above in Scheme III, with the exclusion of tartaric acid, but this approach proved unsuccessful due to phase separation of the ammonium hydroxide from the gelled reactants.

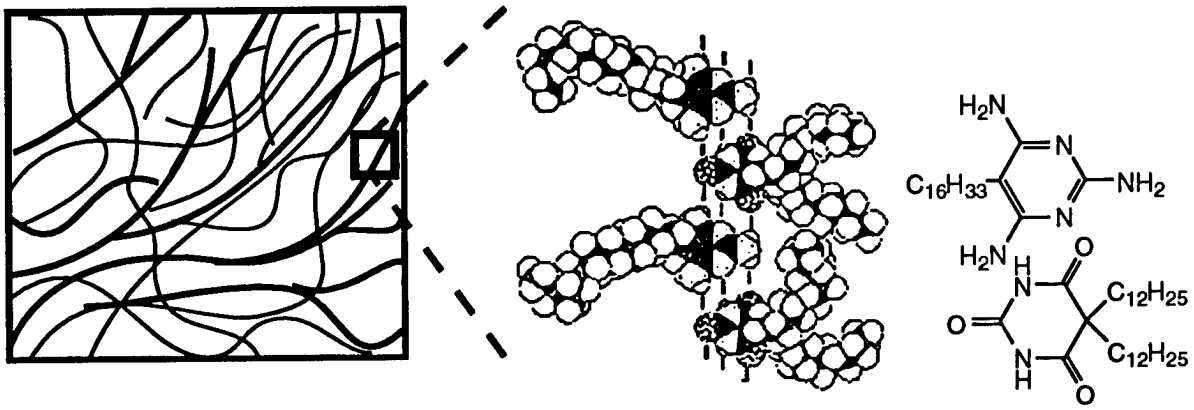

Figure 5. Schematic of Gelator Superstructure, Stacking of Molecules, and Chemical Structure, Respectively

Future work on this project will be the investigation of the fracture properties of the PHEMA IPN composites and how the morphologies of the components affect these properties, synthesis, and characterization of an *in situ* reinforced IPN composite materials and the characterization of these complex composite systems via ultrasonic spectroscopy.

REFERENCES

1. B. M. Novak, *Adv. Mater.*, 5, 422 (1993).
2. M. W. Ellsworth and B. M. Novak, *J. Am. Chem. Soc.* 13, 2756 (1991).
3. M. W. Ellsworth and B. M. Novak, *Chem. Mater.*, 5, 839 (1993).
4. Y. Matsui and H. Nakamura, *J. Am. Chem. Soc.* 117, 2651 (1995).
5. K. Hanabusa, T. Miki, Y. Taguchi, T. Koyama, and H. Shirai, *J. Chem. Soc., Chem. Commun.*, 1382 (1993).

ORGANIC-INORGANIC HYBRID POLYMERS FROM RENEWABLE SOURCES

S. Baliat, S.L. Jouppi, R.M. Laine, R. Tamaki, D.R. Treadwell, C. Zhang, R. Baranwal, and C. Worthen
Contribution from the Depts. of Materials Science and Engineering, Chemistry and the Macromolecular Science and Engineering Center.
University of Michigan, Ann Arbor, MI 48109-2136.

ABSTRACT

Silica can be dissolved in ethylene glycol in the presence of a catalytic amount of strong amine base to form a novel monomer, $Si(OCH_2CH_2OH)_4$, which serves as the starting point for the synthesis of novel silicon containing polymers with a wide variety of properties. For example, curing with 1.3 equivalents of glycerol provides an environmentally benign polymer that can be cast as it cures to give thin films that are hard and stable in air to almost 400°C. TGA ceramic yields for this material are 55 wt. %. Another type of reaction permits the synthesis of cubic silsesquioxanes, $[HSiMe_2OSiO_{1.5}]_8$ or $[vinylSiMe_2OSiO_{1.5}]_8$, which can be cast and co-polymerized to give highly microporous material that should behave like aerogels and provide novel high-temperature (to 300°C) insulating (thermal, electrical, etc.) materials. TGA ceramic yields for this material are 90^+ wt. %.

INTRODUCTION

The synthesis of easily processed polymers with good strength and stability at high temperatures is a subject of continuing and intense interest because such polymers are potential replacements for metal and ceramic components in aerospace structures. Several engineering polymers (typically rigid-rod/liquid crystalline polymers) currently in commercial production meet the high-strength and high-temperature stability criteria. These polymers are slowly finding application in critical aerospace components; however, high synthesis and/or high processing costs continue to limit their utility. Although considerable efforts are being directed towards reducing both synthesis and processing costs, engineering polymers, by their very nature, are always likely to be difficult to process. Thus, finished components likely will also be relatively expensive. There continues to be a need to develop low-cost, easily processed polymers that coincidentally offer good mechanical properties at high service temperatures.

Most engineering polymers consist of aromatic units joined by a minimum number of non-aromatic linkers that provide flexibility and functionalization to enhance processability. In part, the reason these polymer structures are so stable is the absence of saturated moieties, e.g., alkyl groups with relatively low bond dissociation energies (85-95 kcal/mol), that limit use temperatures. Highly flexible $-[Me_2SiO]_n-$ segments, with low T_g (-127°C) and an Si-O bond

dissociation energy >120 kcal/mol, are occasionally used as alternative linkers. Unfortunately, polysiloxanes typically depolymerize at ≈ 210-220°C with n ≥ 3.

Phenylsiloxane -$[Ph_2SiO]_n$- and silsesquioxane ($RSiO_{1.5}$) polymers are stable to relatively high temperatures. For example, methyl- and arylsilsesquioxanes, -$(MeSiO_{1.5})_n$-, are stable to 500-600°C[1-3]. Unfortunately, these silicon based polymers are quite brittle and expensive. Despite this, the very high Si-O bond dissociation energy remains attractive for the development of new polymers with good-to-excellent high-temperature properties.

The presence of silicon species offers the additional advantage that in oxidizing/harsh environments these compounds transform to silica glasses which protectively coat substrates thereby eliminating/significantly diminishing combustion[4].

The above features, when coupled with our recent discovery that SiO_2 can be a direct source of silicon containing compounds[4-6], suggest a novel and inexpensive route to processable fireproof silicon containing polymers. The basis for our approach to new Si containing polymers is described in the following section.

BACKGROUND

High surface area silica reacts with metal hydroxides or oxides in ethylene glycol (EG) to give either anionic pentacoordinated or dianionic hexacoordinated silicon complexes[5-7]:

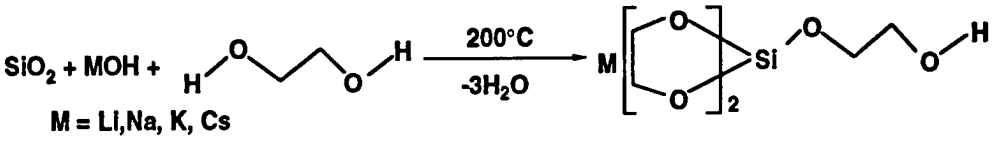

(1)

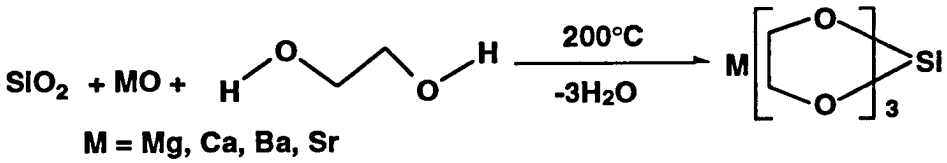

(2)

These ionic compounds are crystalline; however, they easily convert to processable polymers by exchange with longer chain diols, which cannot act as bidentate ligands. Thus, heating the crystalline Li salt with tetraethylene glycol (PEG_4) displaces EG, which distills off to form a processable, ionic polymer[8]:

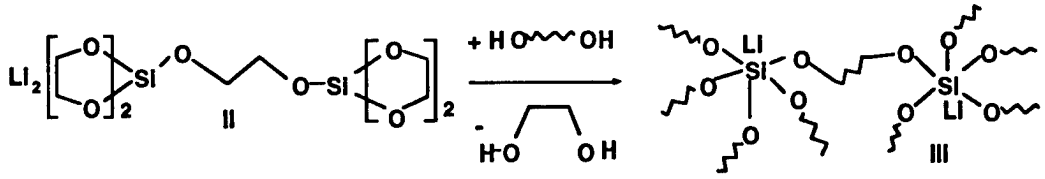

(3)

Surprisingly, all of these compounds and polymers are stable in air to temperatures of 330-390°C, but are moisture sensitive[9]. More recently, in efforts to develop a means to dissolve SiO_2 without using metal oxide or hydroxide bases, we discovered that amine bases can be used instead. Moreover, catalytic amounts of amines can be used to dissolve silica (and alumina). This provides access to a wide variety of silicon containing monomers that offer considerable potential for processing low-cost, environmentally friendly polymers with diverse properties[10-15]. We present here examples of two types of silicon containing materials that (1) can be made directly and inexpensively from silica, (2) offer flame resistance, (3) offer good-to-excellent processability, and (4) offer quite diverse properties.

Organic/Inorganic Hybrid Siloxanes

Frye et al.[16] showed that pentacoordinated silicates with ammonium counterions were not stable above ≈ 100°C. This work suggested that catalytic amounts of strong amine bases, e.g., triethylenetetramine (TETA), will cause SiO_2 to react with 1,2 or 1,3 diols or polyols to form neutral polysiloxanes. Thus heating SiO_2 in excess EG with 2 mol % TETA at 200°C (b.p of EG) eliminates water to form (30 h) the monomer $Si(OCH_2CH_2OH)_4$:

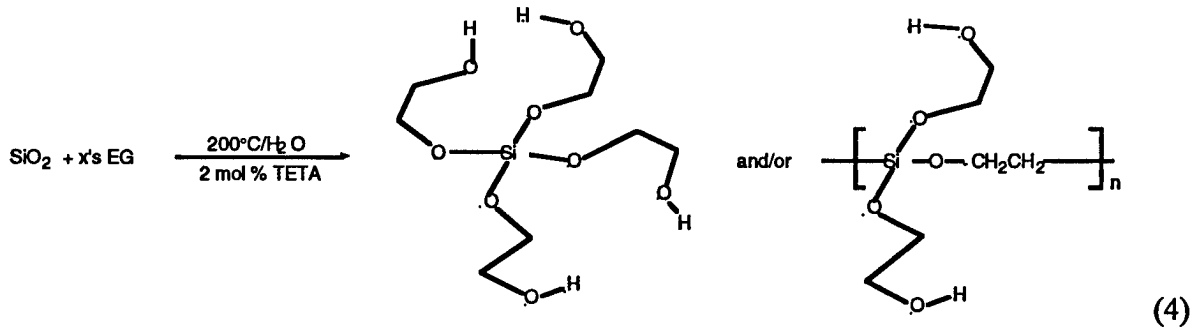

(4)

This liquid has a single ^{29}Si NMR peak at -82 ppm where $Si(OEt)_4$ has a peak at -82.1 ppm. The TGA ceramic yield is 22 wt. % at 1000°C in air as expected for $Si(OCH_2CH_2OH)_4$. On heating in a vacuum, a brittle solid results which has a ceramic yield of 40 wt. %, a chemical analysis, and a solid state NMR(10,14) that support formation of $Si(eg)_2$:

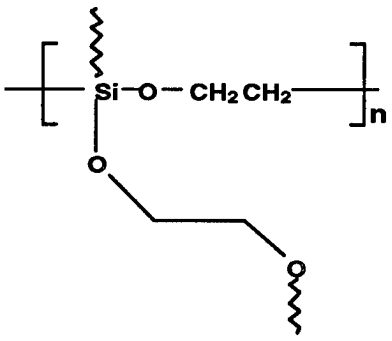

This polymer is stable in air to 390°C as shown in the Figure 1 TGA. Furthermore, despite being totally cross-linked, it redissolves in EG (via pentacoordinated silicon species) and can be further processed. Alternately, heating with other diols leads to exchange to form less brittle materials

[e.g., $Si(PEG_4)_2$]. The $Si(PEG_4)_2$ polymer with longer intracross-link chains appears to be more flexible than the $Si(eg)_2$ polymer. The moisture stability of these cross-linked polymers has not been examined in detail. We plan to develop a detailed understanding of the various types of polymers that can be made directly from $Si(eg)_2$ or $Si(OCH_2CH_2OH)_4$ and their properties. We are currently exploring the synthesis of glycerolato siloxane, reaction[5], an environmentally benign material both in terms of synthesis, processing, and disposal. This polymer is also stable

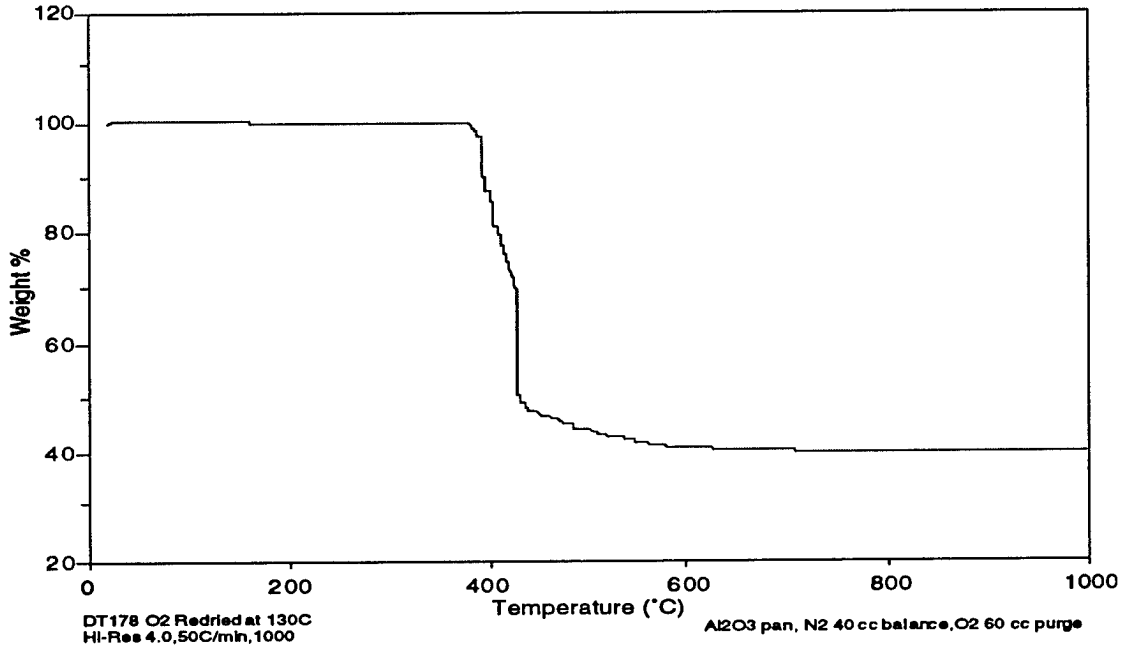

Figure 1. TGA Profile of $Si(eg)_2$ in Air (HiRes™ 4 Ramp Rate)

to relatively high temperatures and exhibits almost the same TGA profile as shown above for $Si(eg)_2$. We can now cast transparent films from $EG/Si(OCH_2CH_2OH)_4/HOCH(OH)CHCHOH$ mixtures simply by heating under a slight vacuum at temperatures of 120-200°C. The resulting films are hard, somewhat brittle, and slightly moisture sensitive if they are not cured to ≥ 250°C. Figure 2 provides a TGA profile of one such film cured at 250°C/1 h. Note that the anticipated char yield is 40 wt. % if all of the organic materials are eliminated. There is a slight mass loss at temperatures below 400°C because of either residual solvent (EG) or some moisture picked up when the sample was crushed for the TGA studies. At > 800°C, even in air, the samples remain black from retained carbon. *Note that even without aromatic groups, this green polymer is stable to almost 400°C.*

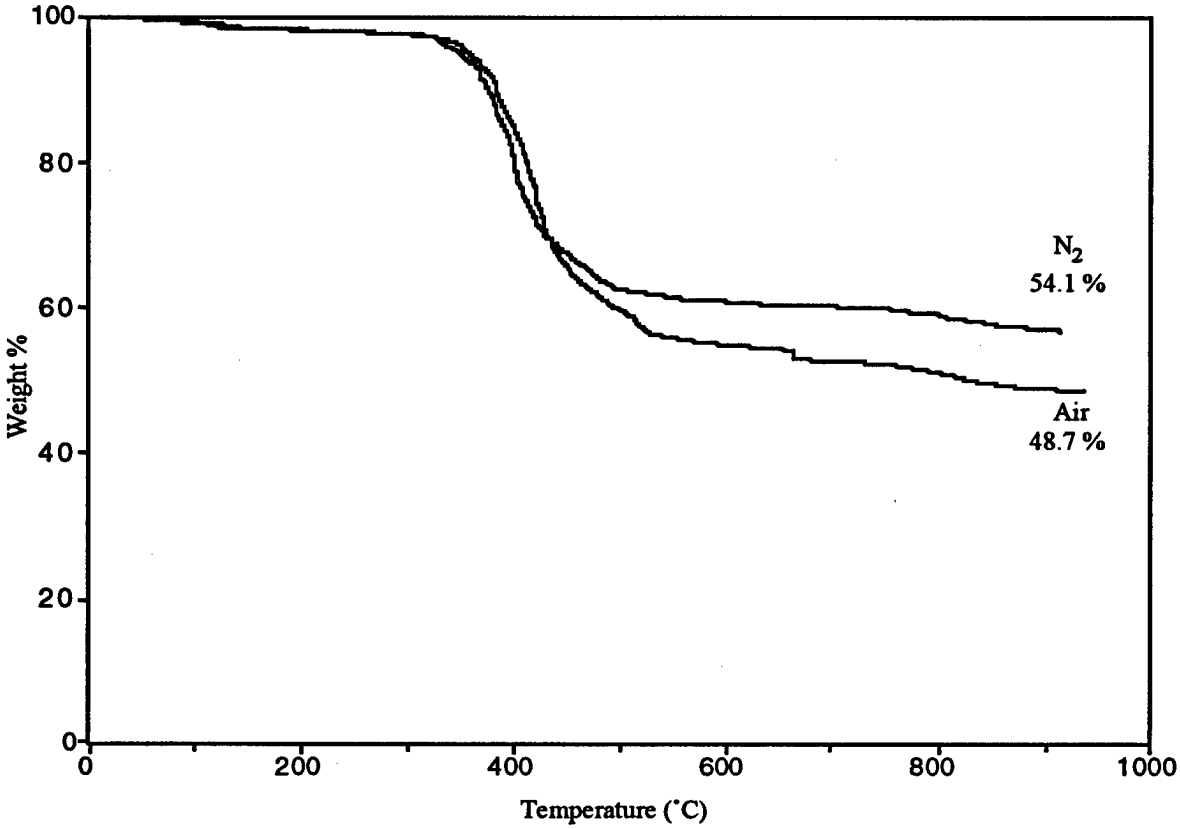

Figure 2. TGA Profiles of $Si[OCH(O)CHCHO]_{1.3}$ Cured at 250°C/N_2

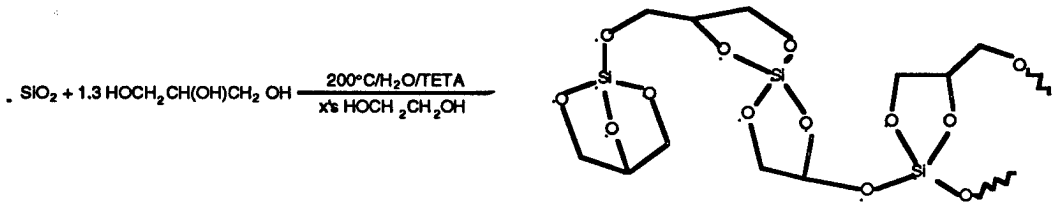

(5)

Our current goal is to increase polymer toughness and eliminate any moisture sensitivity. Preliminary studies suggest that addition of small amounts (2-5 wt. %) of $HO[Me_2SiO]_nOH$ (n = 20) improves toughness and moisture sensitivity. Foamed versions of this polymer (produced by curing at 250°C at 5-10 torr) self-extinguish following ignition with a small flame. In future studies we plan to explore the utility of other polyols including cellulose for the fabrication of novel polymers. At a later date, we plan to improve the char yield by addition of dihydroxy-aromatics which can be used to produce LC siloxanes[17].

$Si(eg)_2$ also provides access to a series of quite unique materials that offer tremendous potential as lightweight thermal and sound insulation and air filtration. One additional and special use may exist as a crushable material for protecting black boxes[18]. These novel materials are prepared in nearly quantitative yield via the following reactions:

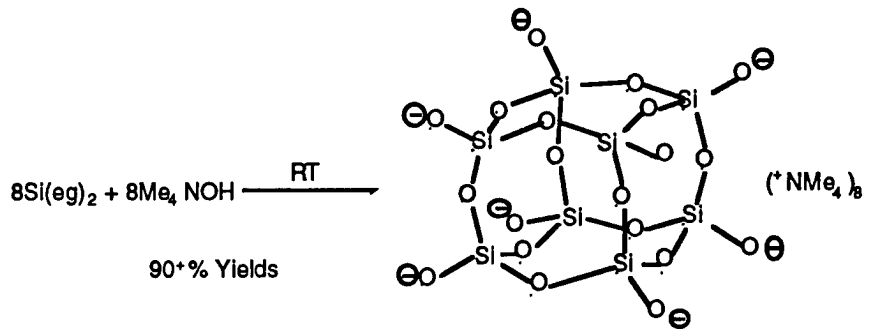

(6)

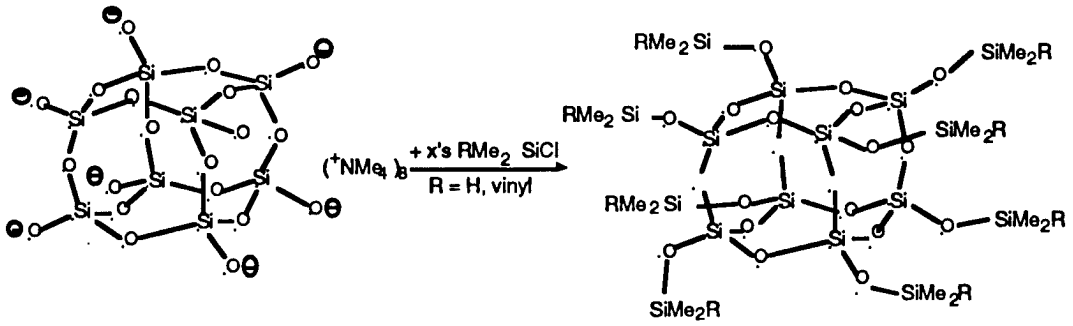

(7)

The vinyl and hydridosilyl cubes can be cross-linked via simple Pt catalyzed hydrosilylation to give very high surface area materials. For example, the polymer formed in reaction 8 below was found by solid state ^{29}Si NMR [19] to be 82%-84 % cross-linked exclusively by ethylene linkages. Specific surface area measurements show that the solvent-free material (prepared at 60°C/1-3 h in toluene) had an average surface area of ≈ 400 m^2/g[12, 13].

Finally, the pore size distribution is rather unique (see Figure 3), ranging from 10 to 40 Å which is extremely narrow and indicates only microporosity. To our knowledge, no other simple, one-step synthesis provides porous materials with such control over pore size distribution. We have also characterized this porosity with positron annihilation spectroscopy (PALS) and small-angle x-ray scattering (SAXS) and find that the BET derived microporosity is very close to that predicted from PALS and SAXS[20]. The potential properties of this microporous material are similar to those of aerogels[18,21]. Consequently, diffusion of gases, sound, and heat through this material is expected to be very slow. In principle this easily prepared and inexpensive but brittle material could offer excellent insulation for aircraft interiors and exteriors as long as it was used in non load bearing applications.

For example, because it is nearly transparent, it might be used to coat window interiors to cut down on heat loss through window panes. In addition, this material is barely susceptible to oxidation. Figure 4 shows the TGAs of the polymer in air and nitrogen. Future studies on this type of material will focus on improving the material's mechanical properties without sacrificing control of porosity. Thus, efforts will be made to change the length of the unit that bridges the cubic silsesquioxane cores to provide additional flexibility.

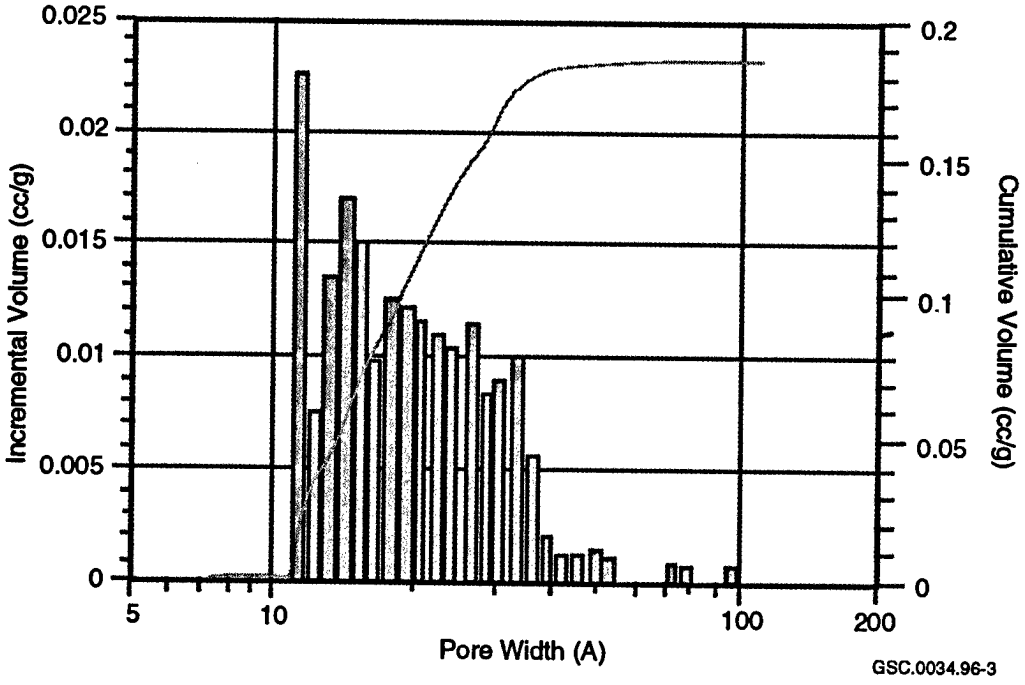

Figure 3. Pore Volume for Spacer Cube Hydrosilylation Product

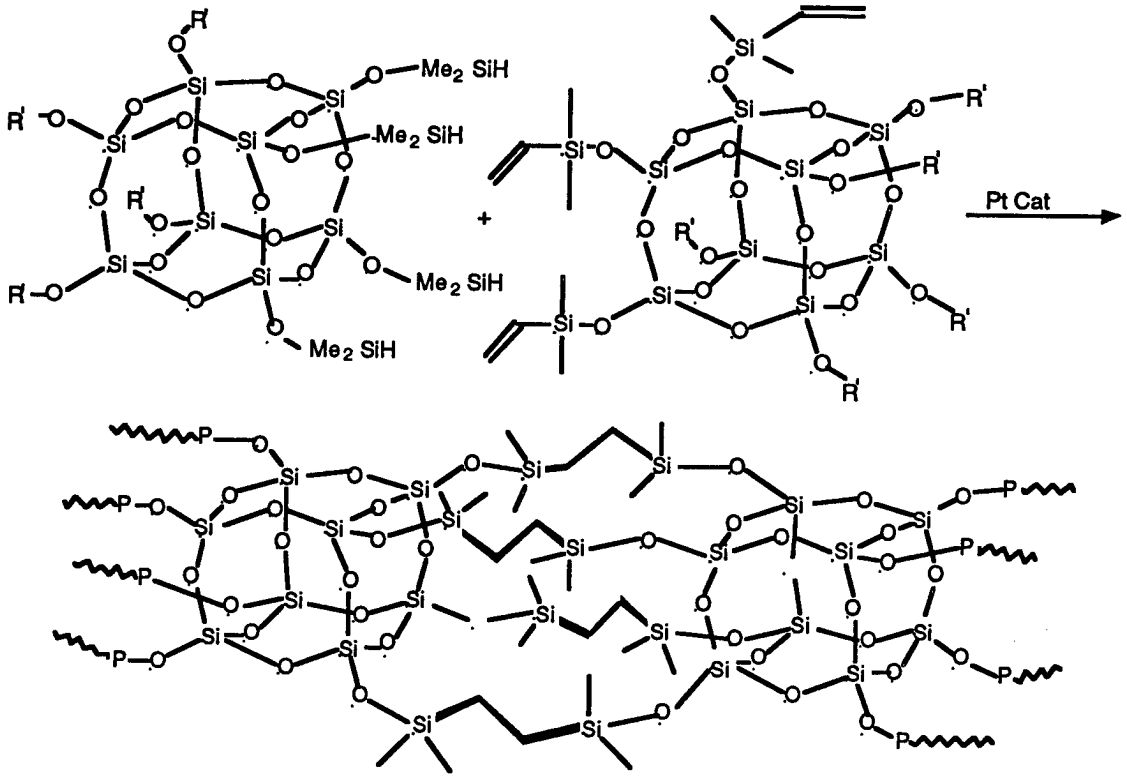

(8)

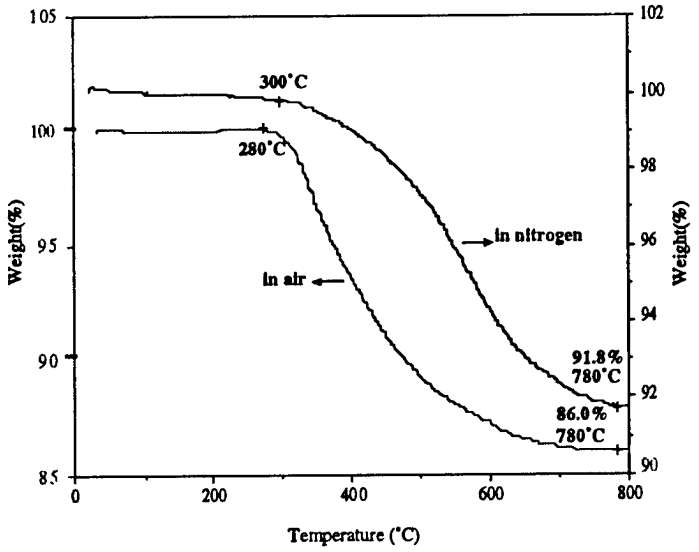

Figure 4. TGA Profiles of Coupled Spacer Hydrido and Vinyl Cubes. No further mass changes are seen beyond 800°C.

SUMMARY

Several novel materials with quite diverse properties can be made directly from the monomer $Si(OCH_2CH_2OH)_4$ prepared by dissolution of silica (including sand) in ethylene glycol using amine bases. This inexpensive monomer will cross-link on heating by itself or with other diols, triols, or polyols to give materials that are stable to temperatures approaching 400°C in air without the addition of aromatics. Films can be cast if the cross-linking reaction is carried out in the cast form. The mechanical properties of these films need to be assessed and modifications to the polymer and/or processing methods made to establish polymer-structure property relationships. At present, the cast films appear to be hard and brittle and somewhat moisture sensitive, thus the goal of future work will be to improve toughness and moisture sensitivity.

A second material made from the same monomer, $Si(OCH_2CH_2OH)_4$, is a brittle, low-mass, highly-microporous poly(vinylenesilsequioxane) that should offer properties similar to aerogels. That is, this transparent, castable material should offer good-to-excellent sound, thermal, and electrical insulation in non load bearing applications. Future efforts will be directed towards reducing brittle behavior without sacrificing the microporous nature of the materials.

ACKNOWLEDGEMENTS

We would like to thank the Federal Aviation Administration for generous support of this work through contract No. 95-G-026.

REFERENCES

1. R.H. Baney, M. Itoh, A. Sakaibara, and T. Suzuki, Chem. Rev. 95, 1409 (1995).
2. R.M. Laine, K.A.Youngdahl, F. Babonneau, J.F. Harrod, M.L. Hoppe, and J.A. Rahn, Chem. Mater. 2, 464 (1990).
3. D.A. Loy and K.J. Shea, Chem. Rev. 95, 1431-42 (1995).
4. J.W. Gilman, D.S. Schlitzer, and J.D. Lichtenhan, J. Appl. Polym. Sci. 60, 591 (1996).
5. R. M. Laine, K. Y. Blohowiak, T. R. Robinson, M. L. Hoppe, P. Nardi, J. Kampf, and J. Uhm, Nature 353, 642 (1991).
6. K.Y. Blohowiak, D.R. Treadwell, B.L. Mueller, M.L. Hoppe, S. Jouppi, P. Kansal, K.W. Chew, C.L.S. Scotto, F. Babonneau, J. Kampf, and R.M. Laine, Chem. Mater. 6, 2177 (1994).
7. M.L. Hoppe, R.M. Laine, J. Kampf, M.S. Gordon, L.W. Burggraf, and Angew, Chem. Int. 32, 287 (1993).
8. K.W. Chew, B. Dunn, T.A. Faltens, M.L. Hoppe, R.M. Laine, L. Nazar, and H.K. Wu, Am. Chem. Soc. Poly. Prprts. 34, 254 (1993).
9. P. Kansal and R.M. Laine, J. Am. Ceram. Soc. 77, 875 (1994) .
10. R.M. Laine, B.L. Mueller, T. Hinklin, D. Treadwell, S. Dumrongvaraporn, and M. Jiraporn, "Neutral Alkoxy and Aryloxy Silanes from SiO_2," submitted for publication.
11. R.M. Laine, D.R. Treadwell, B.L. Mueller, C.R. Bickmore, K.F. Waldner, and T. Hinklin, J. Chem. Mater. 6, 1441 (1996).
12. C. Zhang and R.M. Laine, J. Organomet. Chem. 521, 199 (1996).
13. A. Sellinger and R. M. Laine, J. Mater. Chem. 8, 1592 (1996) and references therein.
14. R.M. Laine, B.L. Mueller, and T. Hinklin, U.S. Patent No.5,418,298 May 23, 1995.
15. R.M. Laine, K. Waldner, C. Bickmore, and D.Treadwell, U.S. Pat. "Double Alkoxide Monomers, Oligomers and Polymers,"--allowed, Sept. 1996.

16a C.L. Frye, J. Am. Chem. Soc. 92, 1205 (1970).

16b C.L. Frye, ibid. 93, 6805 (1971).

17. D.J. Ray, R.M. Laine,T.R. Robinson, and C. Viney, Molec. Crystal and Liquid Crystal Sci. Technol., Sect. A, 225, 153 (1992).
18. Dr. Arlon Hunt, Director, Microporous Materials Laboratory, Lawrence Berkley Laboratories, private communication (1996).
19. F. Babonneau, C. Bonhomme, C. Zhang, R. Baranwal, and R.M. Laine, unpublished work (1996).
20. C. Soles, H. Hristov, A. Yee, C. Zhang, A. Yee, and R.M. Laine, unpublished work.
21. C.J. Brinker and G. Scherer; Sol-Gel science: The Physics and Chemistry of Sol-Gel Processing, Academic Press, Boston (1990).

FIRE-RESISTANT ALUMINOSILICATE COMPOSITES

Richard E. Lyon
Fire Safety Section, AAR-422
Federal Aviation Administration William J. Hughes Technical Center
Atlantic City International Airport, NJ 08405

P.N. Balaguru and Andrew Foden
Department of Civil Engineering
Rutgers the State University of New Jersey

Usman Sorathia
Carderock Division, Naval Surface Warfare Center
Bethesda, MD

Joseph Davidovits and Michel Davidovics
GEOPOLYMERE
F-02100 St.-Quentin, FRANCE

ABSTRACT

The fire response of a potassium aluminosilicate (Geopolymer) matrix carbon fiber composite was measured and the results compared to organic matrix composites being used for transportation, military, and infrastructure applications. At irradiance levels of 50 kW/m^2 typical of the heat flux in a well developed fire, glass- or carbon-reinforced polyester, vinylester, epoxy, bismaleimde, cyanate ester, polyimide, phenolic, and engineering thermoplastic laminates ignited readily and released appreciable heat and smoke, while carbon-fiber reinforced Geopolymer composites did not ignite, burn, or release any smoke even after extended heat flux exposure. The Geopolymer matrix carbon fiber composite retains 67 percent of its original flexural strength after a simulated large fire exposure.

INTRODUCTION

The flammability of organic polymer matrix, fiber-reinforced composites limits the use of these materials in marine platforms and ships[1], ground transportation[2], and commercial aircraft[3] where fire hazards are important design considerations because of restricted egress. Although carbon fiber and glass fibers are inherently fire resistant and significant progress has been made in recent years to develop new, high-temperature, thermo-oxidatively stable fibers from boron, silicon carbide, and ceramics[4], parallel work on high-temperature/fire-resistant matrix materials to bind the fibers has not kept pace. At the present time, affordable, low-temperature processable matrix materials for fire-resistant composites are unavailable since most organic polymers soften and ignite at temperatures of 400-600°C, characteristic of fuel fire exposure conditions.

The Federal Aviation Administration has recently initiated a research program to develop aircraft cabin materials with an order-of-magnitude reduction in fire hazard compared to current interior

materials[5]. The flammability requirement for new materials is that they withstand a 50 kW/m^2 incident heat flux characteristic of a fully developed aviation fuel fire without releasing significant amounts of heat or propagating an external fuel fire into the cabin compartment for several minutes[6]. The goal of the program is to eliminate cabin fire as a cause of death in aircraft accidents. However, voluntary adoption of new fire-resistant materials technology by aircraft and cabin manufacturers requires that it be cost-effective to install and use[7]. To this end, a new, low-cost, inorganic polymer derived from the naturally occurring geological materials is being evaluated.

Materials

Aluminosilicate Resin — The Geopolymer matrix resin being evaluated for fireproof aircraft cabin interior panels, marine structural composites, and infrastructure applications is a potassium aluminosilicate, or poly(sialate-siloxo), with the empirical formula $Si_{32}O_{99}H_{24}K_7Al$. A representative structure deduced from the elemental composition, x-ray diffraction, and ^{29}Si magic angle spinning nuclear magnetic resonance spectroscopy (^{29}Si MAS-NMR) of the cured and dried Geopolymer is a linear poly(metasilicate) with tetracoordinate aluminate cross-links as illustrated in Figure 1[8]. This particular resin hardens to an amorphous or glassy material at moderate temperatures with a density of 2.14 g/cm^3 and is one of a family of inorganic Geopolymer materials described previously[8,9].

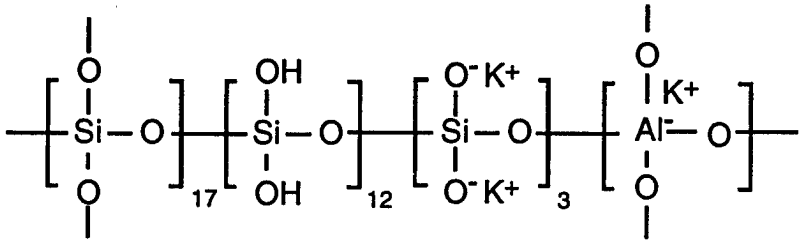

Figure 1. Geopolymer Structure

The Geopolymer potassium aluminosilicate resin was prepared by mixing 100 g of an aqueous silica + potassium oxide solution with 135 g of a silica powder having SiO_2/AlO_2 in a mole ratio of 27/1. The liquid and solid components were mixed for 1 minute at room temperature in a food processor. The as-mixed viscosity of the Geopolymer resin was measured at room temperature (20°C) in a dynamic rheometer (Rheometrics RDA-II) using parallel plate mode with 25-mm-diameter stainless steel plates. Figure 2 is a plot of the room temperature viscosity of the Geopolymer resin *versus* time after mixing. The initial mix viscosity of the Geopolymer resin is about 2 Pa-s (20 Poise) and the resin remains workable for about 4-5 hours at room temperature.

Differential scanning calorimetry studies were conducted to determine the extent of reaction of the Geopolymer resin during the 3-hour, 80°C composite cure cycle. The isothermal conversion of the Geopolymer resin as a function of time at 80°C was determined using a Perkin Elmer DSC-7 Differential Scanning Calorimeter on resin samples of approximately 50 mg which were mixed and immediately placed in sealed stainless steel sample pans. Heat flow *versus* time for the cure exotherm was recorded and the instantaneous extent of reaction was calculated from the cumulative heat evolution divided by the total heat of the reaction. The total heat of the curing reaction was determined to be 16.42 ± 0.49 J/g in separate temperature scanning experiments.

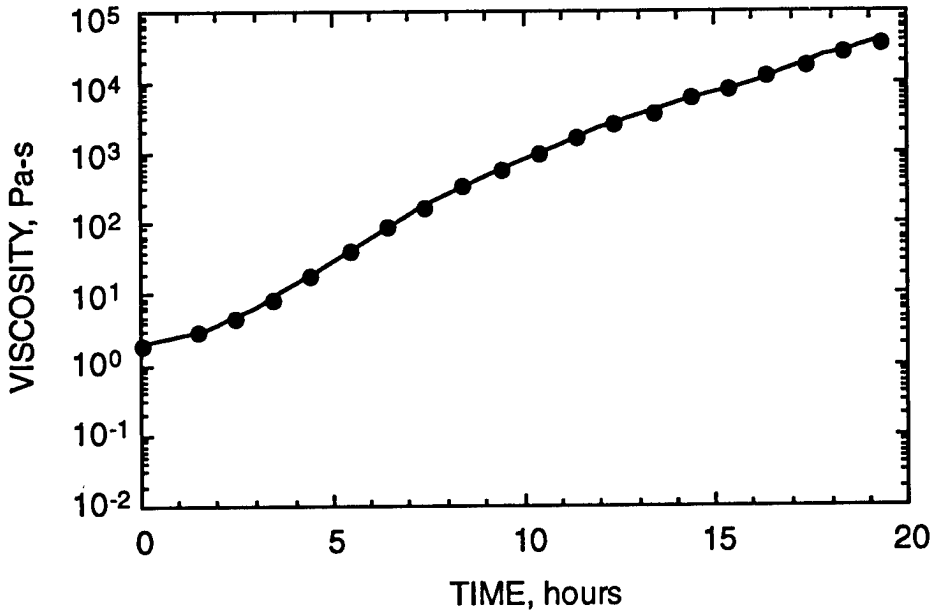

Figure 2. Room Temperature (20°C) Viscosity of Geopolymer Resin Versus Time After Mixing

Figure 3 shows data for the extent of reaction and viscosity of the Geopolymer resin *versus* curing time at 80°C. The onset of rapid viscosity increase corresponds to approximately 50% completion of the Geopolymer reaction. The curing reaction reaches 99% completion after 1 hour at 80°C.

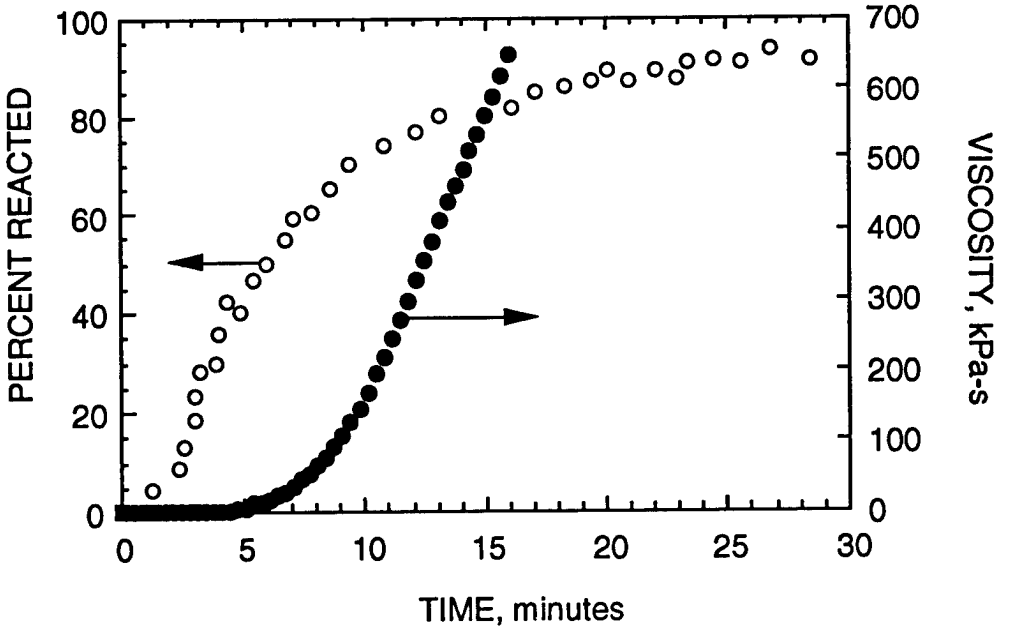

Figure 3. Extent of Cure (o) and Viscosity (●) of Geopolymer ResinVersusTime at 80°C

Thermogravimetric analyses were conducted on a Perkin Elmer TGA-7 Thermogravimetric Analyzer to determine the weight loss history of the cured Geopolymer resin at elevated temperatures. Samples of 10 mg were heated at 10°C per minute in an inert environment (99.99% nitrogen) and the mass of the sample recorded *versus* temperature. Figure 4 shows the residual mass and its first derivative *versus* temperature for the cured Geopolymer resin in the TGA experiments. It is observed that the resin is thermally stable up to about 250°C, at which temperature a 7 percent weight loss occurs over the range 250-625°C. The mass loss at temperatures >250°C is assumed to occur through a dehydration reaction which yields gaseous H_2O according to

$$2\,(SiO_3^{-2} \bullet 2M^+) - OH \xrightarrow{\Delta} (SiO_3^{-2} \bullet 2M^+)_2\ O + H_2O\ (\uparrow) \qquad (1)$$

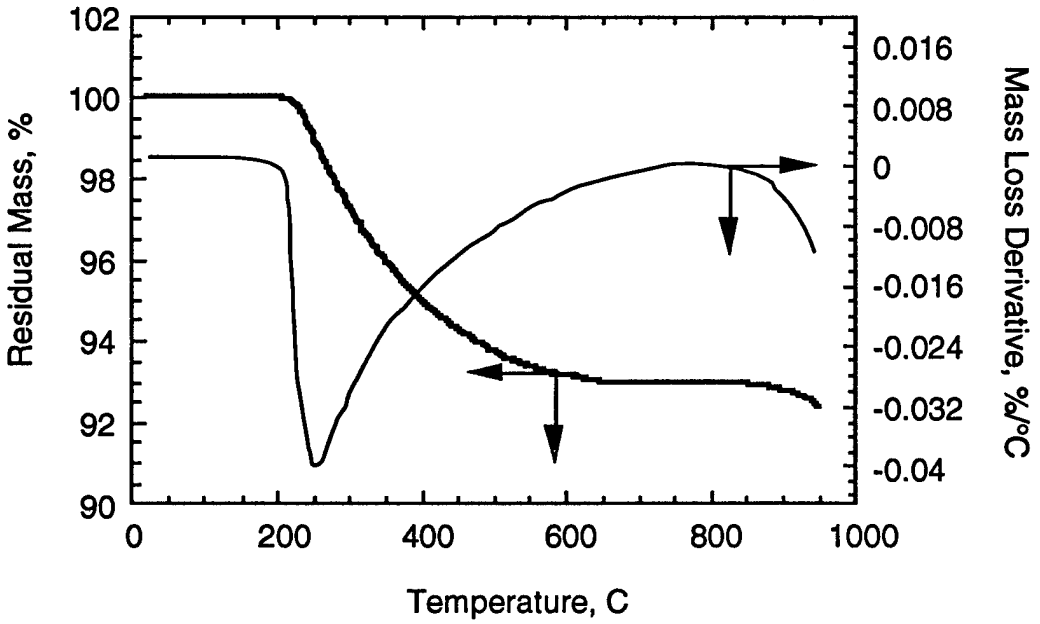

Figure 4. Thermogravimetric Data for Geopolymer Resin Heated at 10°C/min. Heavy line is residual mass and thin line is the mass loss derivative.

The dehydration reaction produces steam at many times its liquid volume and pressure resulting in an unconstrained volume expansion of the resin of 488 ± 48% at 850°C. The resulting morphology is a microcellular amorphous material at room temperature. At temperatures above 850°C a small secondary weight loss occurs producing a strong, fused, glassy resin. The secondary weight loss temperature is near the melting point (976°C) of potassium metasilicate (K_2SiO_3 in Figure 1) and may be final dehydration of the molten resin.

Composite Fabrication — Cross-ply fabric laminates were made by hand rolling the deaerated Geopolymer liquid resin into a 0.193 kg/m² (5.7 oz/yd²), 3K plain weave, Amoco T-300, carbon fabric and air drying 30 seconds at 80°C to remove residual moisture and develop tack. Unidirectional tape was used to fabricate cross-ply laminates for off-axis tensile testing of inplane shear properties. In all cases, hand-impregnated plies were cut, stacked, and cured in a vacuum bag at 80°C in a heated press with 0.3 MPa pressure for 3 hours. The panels were then removed

from the vacuum bag and dried for an additional 24 hours at 100°C or until constant weight was achieved. Approximately 22% of the as-mixed liquid resin is water, about half of which is removed during the curing and drying process.

Final thickness of the 25-layer fabric laminates was a uniform 5.6 mm and the density was 1.85 g/cm^3. Warp direction tensile specimens were cut from 4-layer fabric laminates. Visual inspection of cut edges revealed that the laminates were substantially free of large voids. Hand impregnation and layup resulted in a fiber volume fraction of approximately 50%-55% and void fraction of less than 5% in the Geopolymer laminates.

Organic matrix cross-ply laminates of polyester (PE), vinylester (VE), epoxy (EP), cyanate ester (CE), bismaleimide (BMI), PMR-15 polyimide (PI), and phenolic (PH) thermoset resins as well as thermoplastic polyphenylene sulfide (PPS), polyetheretherketone (PEEK), polyetherketoneketone (PEKK), polyarylsulfone (PAS), and polyethersulfone (PES) resin matrices were prepared from commercial S-glass, E-glass, or carbon fabric prepregs. The details of material composition and fabrication have been described elsewhere[10-12]. Some of the phenolic laminates were hand impregnated[13] and contained only about 34 volume percent fiber compared to a nominal 60 volume percent fiber for all of the commercial prepreg materials. The density of these cured laminates ranged from about 1.55 to about 1.98 g/cm^3 at the nominal 60 volume percent carbon and glass fiber loading, respectively.

Methods

Ignitability, Heat Release, and Smoke (ASTM E-1354) — Peak heat release rate, 300-second average heat release rate, total heat release, mass loss during burning, ignitability (time to ignition), and the specific extinction area of smoke produced were measured in an oxygen consumption calorimeter employing a conical radiant heater to provide 50 kW/m^2 of radiant energy to the surface of a 10- by 10-cm sample having a nominal thickness of 6 mm. The sample is positioned horizontally on a weighing device with a spark igniter 2.54 cm above the surface to ignite combustible vapors (piloted ignition). The mass flowrate of air past the burning sample is measured as well as the amount of oxygen consumed from the air stream by the combustion process, and these measurements are used to calculate the heat release rate (HRR) of the burning material using a factor of 13.1 kJ of heat produced per gram of oxygen consumed[14].

Flame Spread Index (ASTM E-162-83) — Flame spread across a surface is one measure of the propensity of a material to propagate a fire. Downward flame spread was measured after ignition of a 15- by 46-cm sample by a radiant heat source. Only the combustible organic matrix composites were tested in this procedure as the Geopolymer sample would not support flaming combustion.

Residual Flexural Strength (ASTM D-790) — Specimens were tested for flexural strength before and after the fire test to determine the residual strength of the composite panels after fire exposure. Specimens having dimensions 7.6 by 7.6 cm were exposed to a 25 kW/m^2 radiant heat source for a duration of 20 minutes according to ASTM E-662 protocol for smoke generation in a flaming mode. The panels were reclaimed and five coupons, 1.27 cm wide by 7.6 cm long were cut from each for flexural testing on a universal testing machine. The Geopolymer composites were not subjected to the ASTM E-662 protocol because they would not burn.

Instead panels were tested at room temperature (22°C) or subjected to temperatures of 200°C, 400°C, 600°C, and 800°C for 60 minutes in a forced air oven. The oven exposure at 400°C is comparable to the equilibrium surface temperature of a vertically oriented, unit-emissivity surface exposed to 25 kW/m^2 of radiant energy in quiescent air for the same time period[15]. The original sample thickness was used to calculate a nominal flexural strength after the fire (organic resins) or thermal exposure (Geopolymer) test.

Tensile Properties (ASTM D3039-76) — Tensile strength and modulus of cross-ply fabric laminates were measured in the warp fiber direction using 4-ply specimens.

Inplane Shear Properties (ASTM D3518-76) — The inplane shear strength and stiffness of a unidirectional Geopolymer laminate was determined by measuring the tensile stress–strain response of ±45-degree laminates fabricated from unidirectional carbon fiber tape.

Interlaminar Shear Properties (ASTM D3846) — Interlaminar shear tests were conducted on Geopolymer-carbon fabric laminates by applying direct shear over an area of approximately 80 mm^2 on an 80- x 12-mm double-notched compression specimen which was 6 mm thick. Failure occurred between the notches in all cases and the failure plane was interlaminar. Tests were conducted at ambient temperature (22°C) on samples which were subjected to a one-hour exposure at 200, 400, 600, 800, and 1000°C in a forced air oven. The interlaminar shear strength of a phenolic resin/T-300 carbon fabric laminate was determined using a short beam shear specimen according to ASTM D2344 and the specimen was a [0/±45/90] quasi-isotropic layup of phenolic resin impregnated Hercules IM-7 carbon fabric.

RESULTS AND DISCUSSION

Table 1 lists the inplane shear, interlaminar shear, warp tensile, and flexural properties of the Geopolymer-carbon fiber/fabric cross-ply laminates. The room temperature strengths of the Geopolymer-carbon fiber/fabric laminates are 343, 245, and, 14 MPa for warp tensile, flexure, and interlaminar shear, respectively. The corresponding values for a phenolic resin–T-300 carbon fabric cross-ply laminate are 436 and 290 MPa for warp tensile and flexural strength, respectively, and 24 MPa for interlaminar (short beam) shear strength[13]. Moduli for the Geopolymer resin cross-ply fabric laminate in the warp tensile and flexure tests are 79 GPa and 45 GPa, respectively, compared to 49 GPa and 29 GPa for the corresponding moduli of a phenolic resin composite[13].

Table 1. Mechanical Properties of Geopolymer Carbon Fiber Composites

Property	Max. Temp. (°C)	Number of Samples Tested	Modulus (GPa)	Strength (MPa)
Inplane Shear	22	3	4.0 ± 0.1	30.5 ± 1.2
Interlaminar Shear	22	5		14.1 ± 0.6
	200	5		12.5 ± 0.3
	400	5		6.8 ± 0.4
	600	5		4.6 ± 0.1
	800	5		4.6 ± 0.2
	1000	5		5.6 ± 0.5
Warp Tensile	22	5	79 ± 2.0	343 ± 31
Flexure	22	5	45.3 ± 0.9	245 ± 8
	200	5	36.5 ± 4.0	234 ± 10
	400	5	27.5 ± 2.5	163 ± 6
	600	5	18.3 ± 1.4	154 ± 24
	800	5	12.3 ± 0.5	154 ± 9

Table 2 summarizes all of the cone calorimeter data for the composite specimens. Individual values for percent weight loss during the fire test, time to ignition, peak heat release rate, 300-second average heat release rate, total heat released per unit area, and specific extinction area of smoke are reported for each material. Average values of these fire parameters were calculated for families of the organic materials grouped together according to chemistry (condensation/ phenolics, addition/thermosets), physical properties (engineering thermoplastics), or end-use applications (high-temperature/advanced thermosets). It is seen that this somewhat arbitrary grouping leads to variations within groups which can be greater than the variation between groups. However, the averages are fairly representative of each type of material, and it is clear that the Geopolymer composite is noncombustible while all of the organic polymer matrix composites support flaming combustion. It was noted that the Geopolymer resin became white after fire exposure but did not ignite or smoke even after 10 minutes in the cone calorimeter.

It is important to try to understand how or if the fire parameters in Table 2, measured in a small-scale bench test, relate to the actual fire hazard of a composite material in the use environment. This is a very difficult task and it is necessary to realize that no single parameter will provide the best estimation of the fire hazard of a material in all situations because the hazard depends to a large extent on where and how the material is used (e.g., enclosed space, open space, structural, nonstructural, etc.).

Table 2. Fire Calorimetry Data for Cross-Ply Laminates at 50 kW/m² Irradiance[10-12]

RESIN	FIBER	Weight Loss	Time to Ignition	Peak HRR	300 s Average HRR	Total Heat Release	Smoke
		%	Seconds	kW/m²	kW/m²	MJ/m²	m²/kg
Isophthalic polyester	Glass	–	77	198	120	–	378
Vinyl Ester	Glass	–	78	222	158	–	861
Vinyl Ester	Glass	26	74	119	78	25	1721
Epoxy	Glass	–	105	178	98	30	580
Epoxy	Glass	19	18	40	2	29	566
Epoxy	Glass	28	49	181	108	39	1753
Epoxy	Glass	22	50	294	135	43	1683
Epoxy	Carbon	24	94	171	93	—	—
THERMOSETS		24	68	175	99	33	1077
Cyanate Ester	Glass	22	58	130	71	49	898
PMR-15 polyimide	Glass	11	175	40	27	21	170
Bismaleimide	Glass	25	141	176	161	60	546
ADVANCED THERMOSETS		19	124	115	86	43	538
Phenolic	Glass	–	210	47	38	14	176
Phenolic	Glass	12	214	81	40	17	83
Phenolic	Glass	6	238	82	73	15	75
Phenolic	Glass	10	180	190	139	43	71
Phenolic	Glass	3	313	132	22	12	143
Phenolic	Carbon	28	104	177	112	50	253
Phenolic	Carbon	9	187	71	41	14	194
PHENOLICS		11	206	111	66	23	142
Polyphenylenesulfide	Glass	13	244	48	28	39	690
Polyphenylenesulfide	Carbon	16	173	94	70	26	604
Polyarlylsulfone	Carbon	3	122	24	8	1	79
Polyethersulfone	Carbon	–	172	11	6	3	145
Polyetheretherketone	Carbon	2	307	14	8	3	69
Polyetherketoneketone	Carbon	6	223	21	10	15	274
ENGINEERING PLASTICS		8	207	35	22	15	310
Geopolymer	Carbon	0	∞	0	0	0	0

It has been suggested that heat release rate of a material measured in small-scale tests under simulated radiant exposure conditions is the single most important parameter in characterizing

the hazard of a material in a fire[16]. Recently, it was shown that a combined parameter which is the ratio of the peak heat release rate to the time to ignition, also known as the flame propagation index (FPI) or flashover parameter, is a more accurate predictor of time to flashover in both room and aircraft compartment fires because it more accurately accounts for thickness effects of the material[17]:

$$\text{Flame Propagation Index (FPI)} = \frac{\text{Peak Heat Release Rate (kW/m}^2\text{)}}{\text{Time to ignition (seconds)}} \qquad (2)$$

Flashover is a phenomenon unique to compartment fires where incomplete combustion products accumulate at the ceiling and ignite causing total involvement of the compartment materials and signaling the end to human survivability. Consequently, in a compartment fire the *time to flashover* is the time available for escape and this is the single most important factor in determining the fire hazard of a material or set of materials in a compartment fire. The Federal Aviation Administration has used the time to flashover of materials in aircraft cabin tests as the basis for a heat release and heat release rate acceptance criteria for cabin materials for commercial aircraft[6]. Figure 5 shows the calculated time to flashover of the 6-mm-thick composite material groups from Table 2 if they were used as wall linings in an 8- x 12-ft room which is 8 feet high. The equation used to estimate the time to flashover from the peak heat release rate/time to ignition ratio (FPI) from Table 2 is[17]

$$\text{Time to flashover (sec)} = 991 - 629 \log_{10} \text{FPI} \qquad (3)$$

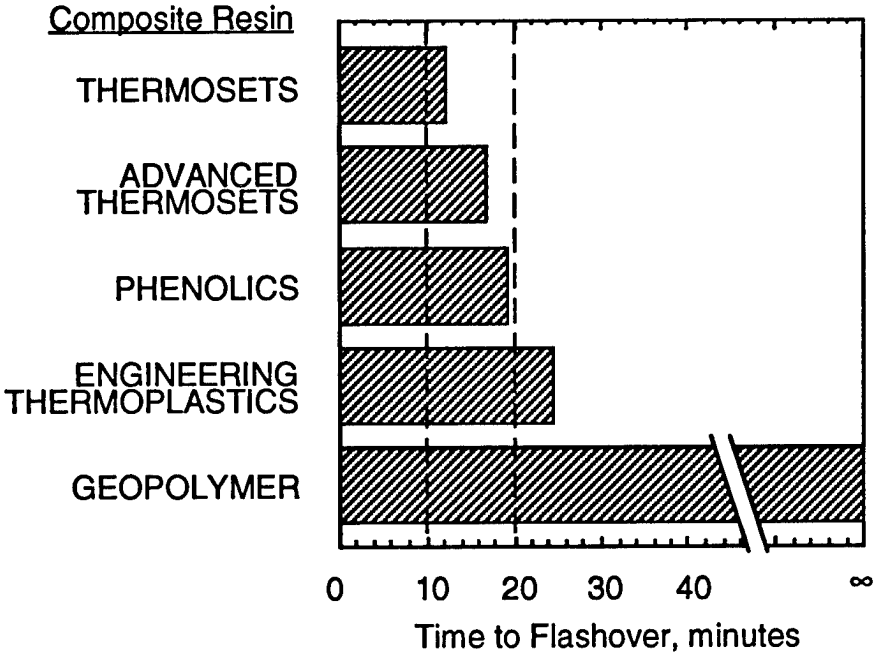

Figure 5. Predicted Time to Flashover in ISO 9705 Corner/Room Fire Test with Various Structural Composites as Wall Materials

Equation 3 is an empirical equation which correlates EURIFIC full-scale fire test data[18] for 13 different lining materials ($r^2 = 0.94$) obtained according to ISO 9705 corner wall/room fire test

using the 100/300 ignition option (100 kW fire for 10 minutes + 300 kW fire for additional 10 minutes) in the corner of a room 3.6 m long x 2.4 m wide x 2.4 m high. For comparison to the predicted behavior of the composite materials in Figure 5, materials in the ISO 9705 test with 10- to 12-minute flashover times include a melamine high-pressure laminate on noncombustible board, steel faced polymeric foam with mineral wool backing, fire-retardant PVC on gypsum wallboard, fire-retardant particle board, and a fire-retardant textile on gypsum wallboard.

The calculated values for time to flashover of organic and Geopolymer composites in a full-scale room test shown in Figure 5 provide a qualitative ranking of the fire hazard of these materials in a compartment. The engineering thermoplastics are predicted not to reach flashover during the 20-minute ignition period but could generate appreciable smoke, while the Geopolymer composite will never ignite, reach flashover, or generate any smoke in a compartment fire. It is possible that the actual time to flashover of the continuous fiber-reinforced composite laminates listed in Table 2 would be significantly different from the calculated values displayed in Figure 5 and full-scale validation tests of these materials are required to design for fire protection.

The flame spread index provides a relative measure of the speed at which the flame front of a burning composite travels. Consequently the flame spread index provides a qualitative ranking of the rate of fire growth in an open environment. Figure 6 shows a plot of the ratio of the peak heat release rate/time to ignition (FPI) from Table 2 for selected materials which were also tested for flame spread index. The correlation is seen to be very good between the flame propagation index determined in the bench-scale cone calorimeter test and the measured ASTM E-162 flame spread index for these cross-ply composite laminates. According to this plot, the Geopolymer composite would have a flame spread index of zero, indicating that the Geopolymer composite would be an excellent fire barrier.

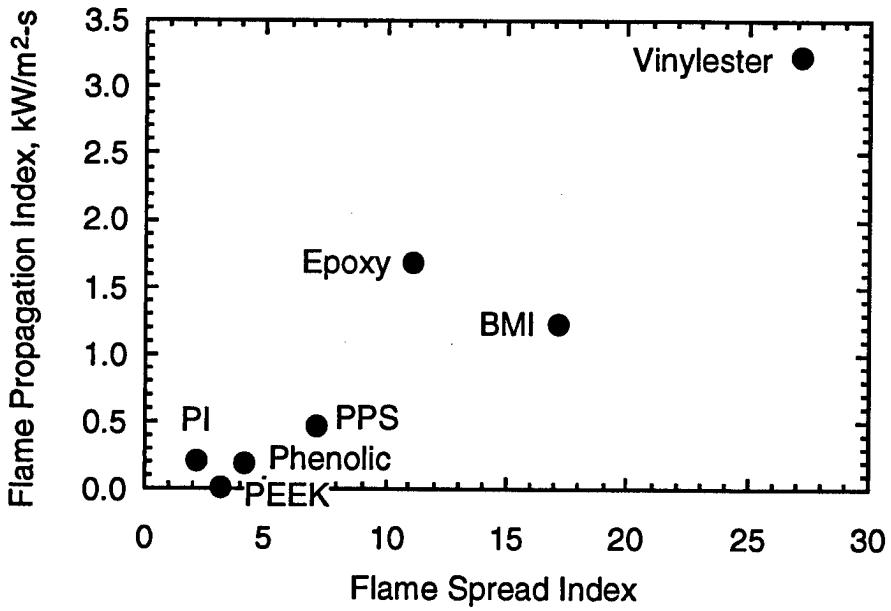

Figure 6. Flame Propagation Index at 50 kW/m² Incident Heat Flux Versus Flame Spread Index for a Number of Glass-Reinforced Organic Polymer Composites

In general, the initial matrix dominated strengths (i.e., inplane shear, interlaminar shear, transverse tension, and compression) of additional cured thermoset or thermoplastic organic matrix composites are significantly higher than for the Geopolymer resin composites because of better fiber-to-matrix adhesion and potentially fewer voids. Fiber dominated strengths (i.e., tension, flexure) of organic matrix composites are generally somewhat higher than for the Geopolymer resin composites because of the higher fiber-to-matrix adhesion which results in better load transfer between broken and unbroken fibers during testing to failure. However, thermoset resins, such as the phenolic which cross-link via a condensation reaction to form volatile products which can be trapped in the composite as voids, have comparable resin dominated failure strengths.

Differences in the initial strength of organic matrix and Geopolymer resin composites can be compensated in the design phase of a component or structure by simply modifying the dimensions of the structural element. However, the residual strength of a fire-exposed composite structure is determined not only by its physical dimensions but also by thermal transport properties, material chemistry, and thermal stability of the composite. Comparison of the composite resin categories on the basis of percent residual flexural strength retained after the fire exposure is shown in Figure 7. The values represent a combined average for the thermoset (vinylester, epoxy), advanced thermoset (BMI, PI), phenolic, and engineering thermoplastic (PPS, PEEK). The Geopolymer-carbon fabric cross-ply laminate which was subjected to a 400°C oxidizing (air) environment for 1 hour instead of the 25 kW/m² radiant exposure retains 67% of its original 245 MPa flexural strength. The failure mode in the 400°C exposed Geopolymer composite flexural test was a shear delamination near the neutral axis corresponding to a maximum shear stress at failure of about 6.5 MPa, in close agreement with the value of 6.8 MPa obtained for the interlaminar shear strength of the notched compression specimen after 400°C aging in air.

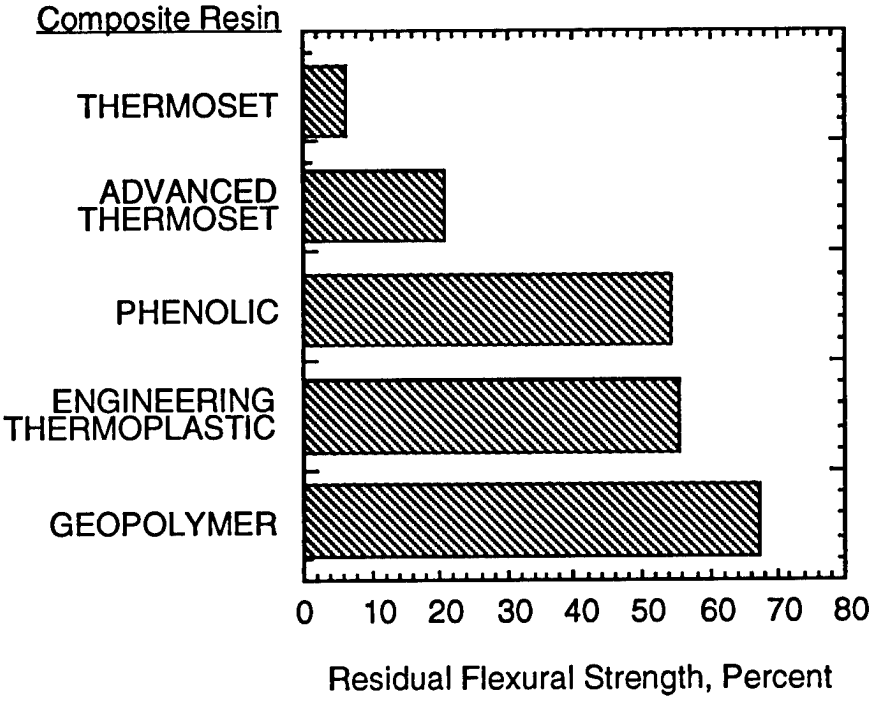

Figure 7. Residual Warp-Direction Flexural Strength of Cross-Ply Laminates After Fire/Thermal Exposure

Table 3 compares some thermomechanical properties of fiber-reinforced concrete[19,20], structural steel[20,21], a 7000-series aluminum[22] used in aircraft structures, a phenolic-E-glass fabric cross-ply laminate[13], a phenolic-carbon fabric cross-ply laminate[13], and the Geopolymer-carbon fabric cross-ply laminate[8]. Maximum temperature capability is defined as the temperature in air at which the nominal tensile or flexural strength falls to one-half of its room temperature value. The Geopolymer-carbon fiber composite, even in the prototype configuration tested, significantly outperforms fiber-reinforced concrete with regard to flexural strength and surpasses concrete and structural steel in temperature capability.

Specific flexural strength is the flexural strength of the material divided by the bulk density and is the figure of merit for weight-sensitive applications such as aerospace and surface transportation vehicles. Similarly, specific modulus is defined here as the tensile (Young's) modulus of the material divided by its bulk density. In the case of the anisotropic cross-ply laminates the warp tensile modulus is used for the calculation. The Geopolymer composite is superior to all of the materials listed with regard to specific modulus and is second only to the phenolic-carbon cross-ply laminate in specific strength. However, the Geopolymer-carbon fabric laminate is unique in its high-temperature structural capability and fire resistance.

Table 3. Typical Properties of Structural Materials

MATERIAL	Density	Tensile Modulus	Specific Modulus	Flexural Strength	Specific Flexural Strength	Maximum Temperature Capability
	kg/m^3	GPa	$MPa\text{-}m^3/kg$	MPa	$MPa\text{-}m^3/kg$	°C
Fiber-Reinforced Concrete	2300	30	13.0	14	0.006	400
Structural Steel	7860	200	25.4	400	0.053	500
7000 Series Aluminum	2700	70	25.9	275	0.102	300
Phenolic-Carbon Fabric Laminate[13]	1550	49	31.6	290	0.187	200
Phenolic-E-Glass Fabric Laminate[13]	1900	21	11.0	150	0.074	200
Geopolymer-Carbon Fabric Laminate	1850	76	41.0	245	0.132	≥ 800

Figure 8 shows the relationship between as-fabricated specific strength and approximate materials cost for the materials listed in Table 3. It is clear that cost increases exponentially with specific strength. However, the higher cost of materials used in air and ground transportation vehicles is offset by fuel savings over the operating life of the vehicle. The materials cost of a Geopolymer composite is presently on the order of $12 per pound — 95 percent of which is the cost of the intermediate-modulus carbon fiber fabric which comprises a nominal sixty percent of the composite volume. The Geopolymer resin itself costs about one dollar per kilogram. The cost of resin preimpregnated fabric (prepreg) is approximately twice the material cost for the composites shown in Figure 8.

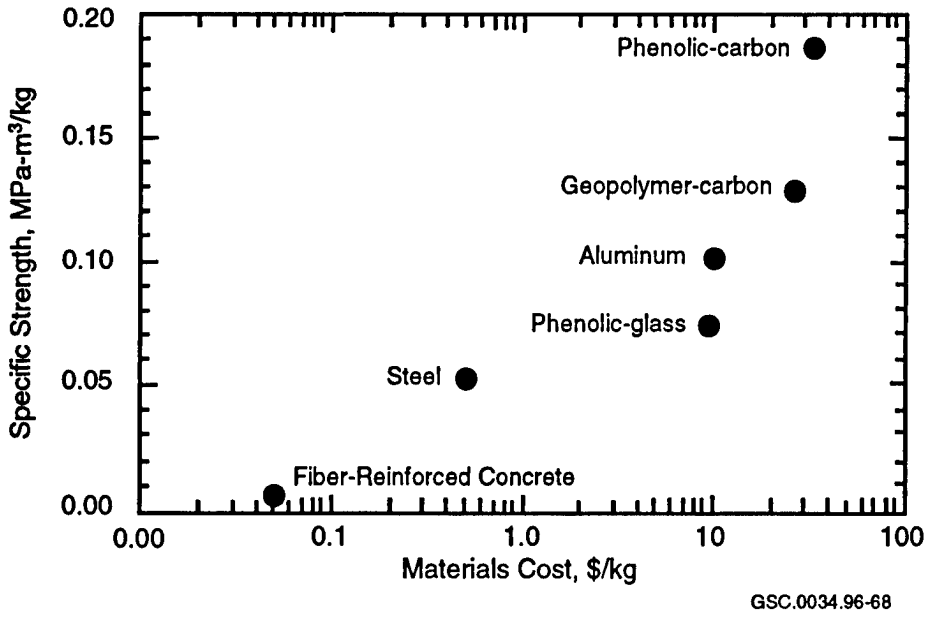

Figure 8. Specific Flexural Strength Versus Materials Cost

CONCLUSIONS

Carbon fiber-reinforced potassium aluminosilicate resin (Geopolymer) composites are non-combustible materials which are ideally suited for construction, transportation, and infrastructure applications where a combination of fire endurance, noncombustibility, and specific flexural strength is needed. Carbon fabric-reinforced Geopolymer cross-ply laminates have comparable initial strength to fabric reinforced phenolic resin composites but have higher use temperatures and better strength retention after fire exposure. In comparison to structural steel, the Geopolymer composite falls short in flexural strength, modulus, and cost but the temperature capability is superior. Consequently, in applications requiring fire endurance, replacement cost, or the added cost of a fire barrier must be figured into the material cost for metallic structures.

Aircraft manufacturers and operators are sensitive to fuel costs so that the figure of merit for this application remains specific strength (strength/density). The high specific flexural strength, flexural modulus, temperature capability, and noncombustibility of the Geopolymer composite make it ideally suited for fire-resistant aircraft components. The capability for hand lay up or filament winding and low-temperature curing suggests applications in seismic retrofit of bridge and building interior columns where upgraded fire resistance and good adhesion to concrete is required. Load bearing capability during severe fire exposure, where temperatures reach several hundred degrees Centigrade, will be significantly higher than organic resin composites, steel, and aluminum which soften and lose nearly all of their compressive strength well below these temperatures. Consequently, applications in the chemical industry for fireproof pipe, tanks, and decking are also being considered.

REFERENCES

1. Demarco, R.A. (1991)."Composite Applications at Sea: Fire Related Issues," *Proc. 36th Int'l. SAMPE Symposium*, April 15-18, pp. 1928-1938.
2. Hathaway, W.T. (1991). "Fire Safety in Mass Transit Vehicle Materials," *Proc. 36th Int'l. SAMPE Symposium*, April 15-18, pp. 1900-1915.
3. R.G. Hill, T.I. Eklund, and C.P.Sarkos (1985). "Aircraft Interior Panel Test Criteria Derived from Full-Scale Fire Tests," DOT/FAA/CT-85/23.
4. Engineered Materials Handbook, Vol. 1. , COMPOSITES, ASM International, Metals Park, OH, 1987.
5. Lyon, R.E. (1995). "Fire Safe Aircraft Cabin Materials," in Fire and Polymers, ACS Symposium Series Number 599, G.L. Nelson, ed., American Chemical Society, Washington, D.C., p. 618.
6. Lyon, R.E. (1994). "Advanced Fire-Safe Aircraft Materials Research Program," Technical Report DOT/FAA/CT-94/60.
7. R.E. Elliot, "Aircraft Interior Integration," Aerospace Engineering, May 1995.
8. Davidovits, J. (1991)."Geopolymers: Inorganic Polymeric New Materials," *J.Thermal Analysis*, 37, pp.1633-1756.
9. Davidovits, J. and Davidovics, M. (1991). "Geopolymer: Ultra-High Temperature Tooling Material for the Manufacture of Advanced Composites," *Proc. 36th Int'l SAMPE Symposium*, pp. 1939-1949.
10. Scudamore, M.J. , Briggs, P.J., and Prager, F.H. (1991). "Cone Calorimetry–A Review of Tests Carried Out on Plastics for the Association of Plastics Manufacturers in Europe,"*Fire and Materials*, 15, pp. 65-84.
11. Sorathia, U., Dapp, T., and Kerr, J. (1991). "Flammability Characteristics of Composites for Shipboard and Submarine Internal Applications," *Proc. 36th Int'l SAMPE Symposium*, pp. 1868.
12. Sorathia, U., Rollhauser, C.M., and Hughes, W.A. (1992)."Improved Fire Safety of Composites for Naval Applications," *Fire and Materials*, 16, pp. 119-125.
13. Sorathia, U., Telegadas, H., and Beck, C. (1994). "Mechanical and Flammability Characteristics of Phenolic Composites for Naval Applications," *Proc. 39th Int'l SAMPE Symposium*, pp. 1940.
14. Babrauskas, V. (1992). "Heat of Combustion and Potential Heat," in Heat Release in Fires, Chapter 8, Elsevier Applied Science, New York, pp. 207-223.
15. Foden, A. J., Lyon, R.E., and Balaguru, P.N. (1996). "High-Temperature Inorganic Resin for Use in Fiber Reinforced Composites," *Proceedings of the First International Conference on Composites in Infrastructure (ICCI 96)*, Jan. 15-17, Tucson, Arizona.
16. Babrauskas, V. and Peacock, R.D. (1992)."Heat Release Rate: Single Most Important Variable in Fire Hazard," *Fire Safety Journal*, 18, pp. 255-272.

17. Hirschler, M. M. (1995) in Fire and Polymers, ACS Symposium Series Number 599, G.L. Nelson, ed., American Chemical Society, Washington, D.C.

18. Sundstrom, B. (1991). "Classification of Wall and Ceiling Linings," *Proceedings of the EURIFIC Seminar*, Copenhagen, Denmark, September 11-12.

19. Balaguru, P. N. and Surendra, P. S. (1992). Fiber Reinforced Cement Composites, McGraw-Hill, Inc., New York.

20. Harmathy, T.Z. (1988). "Properties of Building Materials," in SFPE Handbook of Fire Protection Engineering, Chapter I-27, pp.378-391, Society of Fire Protection Engineers, Boston, MA.

21. CRC Handbook of Tables for Applied Engineering Science (1979). "Engineering Materials and Their Properties," Section 1, pp. 3-137, CRC Press, Inc. Boca Raton, FL.

22. MIL-HDBK-5F (1990). Military Handbook, Chapter 3, pp. 348, Department of Defense, Washington, D.C.

DEVELOPMENT OF SILICONE RESINS FOR USE IN FABRICATING LOW-FLAMMABILITY COMPOSITE MATERIALS

Timothy C. Chao, Gary T. Burns, Dimitris E. Katsoulis, and William C. Page
Dow Corning Corporation
Midland, Michigan 48686

ABSTRACT

Silicones exist as fluids, elastomers, and resins. In general, silicones have high thermal stability and resistance to oxidation and chemical attack. In fire scenarios, silicones exhibit low rates of burning and combustion, and this results in low heat release rates. In this study, a series of vinyl functional silicone resins were prepared and cured through hydrosilylation and free radical reactions. By incorporating fillers and reinforcements, a variety of compositions were formulated which were burned in the cone calorimeter to obtain heat release rate data. The results showed that the peak heat release rate varied with the composition of the silicone resin and the type of filler used. With certain filler and resin combinations, peak heat release rates down to 98 kW/m^2 were obtained. One cured resin formulation exhibited a peak heat release rate less than 10 kW/m^2 at an incident heat flux of 50 kW/m^2. This is the lowest peak heat release rate value ever observed for silicone materials. In addition, some burned chars retained their shape and integrity with no cracking. Char yields up to 97% were achieved. A good correlation was observed between the peak heat release rate measured in the cone calorimeter and the 3% weight loss temperature measured by thermogravimetric analysis (TGA) in helium.

Furthermore, the TGA char yields measured in helium can be used to predict those measured in the cone calorimeter. This research shows that silicone resins are good candidates for fabricating low-flammability composite materials.

INTRODUCTION

Silicones are a class of commercially important inorganic polymers with an alternating backbone of silicon and oxygen. In general, silicones can be formulated as $(R_nSiO_{(4-n)/2})_m$ where n = 1-3, $m \geq 2$. The most common R groups are methyl or phenyl although other R groups such as hydrogen, silanol, alkoxy, vinyl, fluoroalkyl, and longer alkyl chains are used[1].

Silicone structures can be described by using the letters M, D, T, and Q to represent monofunctional, difunctional , trifunctional, and quadrifunctional monomer units (Table 1).

Silicones have many unusual properties. Important among these are their thermal stability and resistance to oxidation and chemical attack. The higher bond energy of the silicon-oxygen linkage compared to a carbon-carbon bond makes silicones more thermally stable than most organic materials.

Table 1. Formulas, Functionality, and Symbols for Silicones

Formula	Functionality	Symbol
$R_3SiO_{1/2}$	mono	M
$R_2SiO_{2/2}$	di	D
$RSiO_{3/2}$	tri	T
$SiO_{4/2}$	quadri	Q

Fire-resistant materials have been studied extensively during the past decades[2]. The Federal Aviation Administration has initiated a research program to develop low-flammability materials for use in aircraft cabin interiors. The polymers which are currently being investigated include polybenzoxazines, polyimides, phosphine oxide copolymers, polyphosphazine, siloxane polymers, etc. Higher molecular silicone fluids and silicone elastomers and resins have good fire resistance properties. They have generated a lot of interest in the past and a continuing growth is expected. In this research, silicone resins were chosen for fabricating low-flammability composite materials.

Silicone resins are rigid materials with three-dimensional, highly cross-linked structures[3]. Most of them contain $RSiO_{3/2}$ (T) or $SiO_{4/2}$ (Q) units as basic building blocks and are either solvent-soluble solids or liquids prior to cross-linking. By varying the R group and the reaction conditions, resins with a range of functional groups can be made. Cross-linking generally occurs through these functionalities. Commonly, the resins are cross-linked through condensation reactions of silanol groups although hydrosilylation or free radical addition reactions are used when unsaturated R groups have been incoporated into the resin. A comparison of silanol-silanol condensation and hydrosilylation is tabulated in Table 2.

Table 2. Comparison of Silanol-Silanol Condensation and Hydrosilylation

Cure Method	Advantage	Disadvantage
Silanol-silanol condensation $\equiv SiOH + HOSi\equiv \rightarrow \equiv SiOSi\equiv + H_2O$	More fire resistant* Lower carbon containing chars	H_2O formed during cure Higher curing temperatures required
Hydrosilylation $\equiv SiCH{=}CH_2 + HSi\equiv \rightarrow \int SiCH_2CH_2Si\equiv$	No H_2O formed during cure Lower curing temperatures Required less shrinkage	Less fire resistant** Carbon-carbon bond formed

* The peak heat release rates are ~ 50-100 kW/m² under 50 kW/m² heat flux.
** The peak heat release rates on early samples are ~ 150-200 kW/m² under 50 kW/m² heat flux. Optimization efforts continue.

In this study, a series of vinyl functional silicone resins were synthesized and cured through hydrosilylation. By incorporating fillers such as amorphous particles, layered silicates, and commercial fibers, a variety of compositions were formulated. The effect of the filler structure and composition on fire performance, char formation, and char integrity was studied. In addition, the relationship between peak heat release rates and char yields as measured by a cone calorimeter and TGA data was investigated.

EXPERIMENTAL

Synthesis

Silicone resins were prepared from the corresponding alkoxysilanes using the following procedure. To a mixture of alkoxysilane, vinyl containing disiloxane, and 10^{-5} equivalents of trifluoroacetic acid was added 4 equivalents of H_2O dropwise. After heating (~ 70°C) for 3 hours, the reaction was neutralized with $CaCO_3$ and the alcohol removed under vacuum. To the resulting suspension was added 10^{-3} equivalents of KOH and 2 equivalents of toluene. The reaction was refluxed and the water removed through a Dean-Stark trap. After the water was removed, the suspension was refluxed for an additional 10 hours under N_2, cooled, and 0.02 equivalents of vinyl containing chlorosilane was added. After refluxing for 3 hours, water was added to the reaction to hydrolyze any residual chlorosilane followed by the addition of $NaHCO_3$. The mixture was dried over $MgSO_4$, filtered, and the solvent removed by evaporation until a 60 wt% solution of the resin in toluene was obtained. The yield of the resin was approximately 90%.

Analysis

Solution ^{29}Si NMR spectra were recorded on a Varian VXR-200 MHz spectrometer operating at 79.46 MHz. A 30 wt % solution in $CDCl_3$ and $Cr(acac)_3$ (0.02 M) was used. Gel permeation chromatography (GPC) data were obtained on a Waters GPC equipped with a 410 differential refractometer detector and all values are relative to polystyrene standards. Carbon and hydrogen analyses were done on a Perkin Elmer CHN2400 elemental analyzer. Thermal gravimetric analysis data were recorded on a DuPont 951 TGA analyzer using a heating rate of 10°C/min and a flow rate of 100 cm^3/min in air or helium. Heat release rates were measured on a cone calorimeter (Custom Scientific Instrument) using 4- x 4- x 1/4-inch samples under an incident heat flux of 50kW/m^2.

Hydrosilylation Cure of Silicone Resins

Slabs 4- x 4- x 1/4-inch were prepared for fire testing as follows. A mixture of the silicone resin and the cross-linker were prepared and an appropriate amount of filler was added. After mixing, an inhibitor and catalyst were added. The molar ratio of SiH to SiVi was ~ 3.5:1, the Pt concentration was 50-100 ppm and the weight ratio of inhibitor to Pt was 100:1. The catalyzed resin was compression molded into a 4- x 4- x 1/4-inch slab at 180°C for 30 min.

RESULTS AND DISCUSSION

Curing

Both free radical (peroxide cure) and hydrosilylation cures were evaluated. However, the samples cross-linked with peroxides foamed during the fire test, suggesting that the resins were incompletely cured. Therefore, hydrosilylation cure was used in this study using trifunctional or tetrafunctional SiH containing cross-linkers.

Char Analysis

The silicon resins with different organic groups attached were cured, burned in the cone calorimeter, and the charred samples analyzed as a function of depth from the top surface. The data are summarized in Table 3 and Figure 1. Under the test conditions, all of the silicone resins gave what appear to be carbonaceous chars covered by a thin layer of silica ash. From this study a good correlation was seen between the carbon content in the resin and the carbon content in the char. In addition, the carbon content increased as the distance from the top surface or heat source increased. The data is consistent with the presence of a slightly oxidizing atmosphere at the surface of the burning resin but with a reducing atmosphere within the resin matrix.

Table 3. Elemental Analysis of Carbon and Hydrogen of Charred Samples

	Calculated[a] (%)		Found (%)		Difference (D)		Relative Decrease vs Polymer (%)	
Resin	C	H	C	H	C	H	C	H
I	55.0	5.0	39.4[b]	2.1[b]	15.6	2.9	28.2	59.0
			42.8[c]	2.5[c]	12.2	2.5	22.0	50.0
			44.3[d]	2.8[d]	10.7	2.2	19.5	44.2
II	47.9	5.3	38.1	2.9	9.8	2.4	20.5	45.1
			40.4	3.5	7.5	1.8	15.7	33.6
			41.2	4.3	6.7	1.0	13.8	19.8
III	40.0	5.6	31.0	2.9	9.0	2.7	22.6	48.2
			32.4	3.6	7.6	2.0	19.0	35.9
			33.7	4.3	6.3	1.3	15.7	23.2
IV	28.4	7.5	23.1	3.3	5.3	4.2	18.8	55.6
			26.2	4.2	2.2	3.3	7.8	44.1
			26.6	4.8	1.8	2.7	6.4	36.4

a Based on the formula determined by ^{29}Si NMR.
b Upper layer, silica ash not included.
c Middle layer. ≥
d Bottom layer.

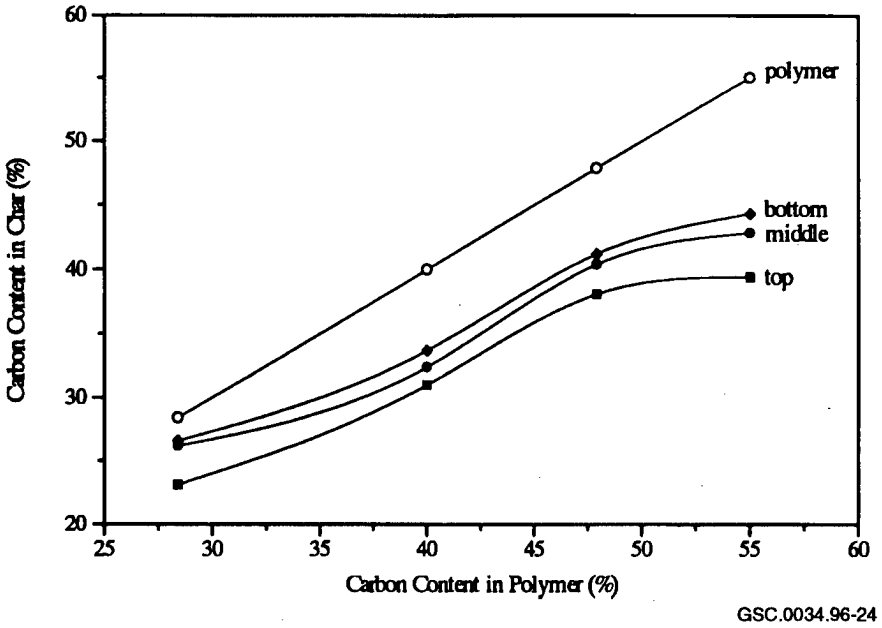

Figure 1. Relationship Between Carbon Content in Polymers and Those in Chars as a Function of Depth Profile

Filler Effect on Char Integrity and Fire Performance of Silicone Resins

The fillers used in this study included amorphous particles, layered silicates, and fibers. In general, during the fire test the particulate fillers caused cracking while several of the layered silicates gave good char integrity. However the best char integrity was obtained with fibrous fillers. These results suggest that fillers with high aspect ratios are ideal candidates for future use. An example of the excellent char integrity is shown in Figure 2. The mechanical properties of charred samples are currently being investigated.

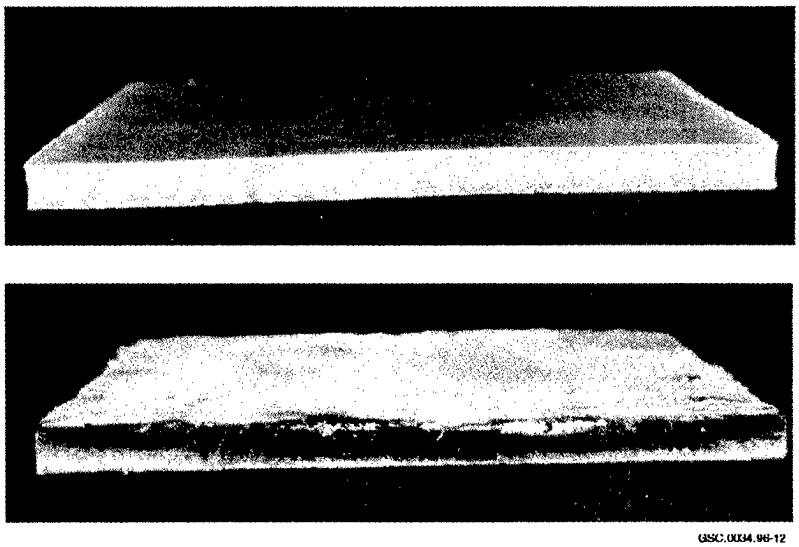

Figure 2. A Fiber-Reinforced Silicone Resin Composite Before (Top) and After (Bottom) Burning in a Cone Calorimeter at an Incident Heat Flux of 50 kW/m^2

As for fire performance (Table 4), most resins have peak heat release rates of 150-200 kW/m^2 at an incident heat flux of 50 kW/m^2 when fillers were not used. When fillers were incorporated, the peak heat release rate reduced to 100-150 kW/m^2. It is expected that by using fire-retardant additives, increasing the filler loading, and modifying the structure of the resin and cure system, materials with peak heat release rates below 50 kW/m^2 can be achieved without sacrificing the processability of the resins.

Table 4. Cone Calorimeter Data for Silicone Resins with Fibrous Fillers. Cross-linkers used were trifunctional* or tetrafunctional. Heat flux was 50 kW/m^2. A 4″ x 4″ x 1/4″ slab was used.

Resin/Filler	Filler Volume (%)	Density (g/cm^3)	Ignition Time (s)	Peak Heat Release Rate (kW/m^2)	Char Yield (%)
Resin 1					
No filler*		1.10	61	221	74
No filler		1.07	51	188	76
Fiber A	33	1.60	97	162	93
Fiber A	40	1.74	121	137	95
Fiber B	12	1.20	52	137	88
Fiber B	12	1.22	72	144	90
Fiber B	11	1.20	75	133	88
Fiber C	3	1.20	48	175	88
Fiber D	23	1.54	141	139	93
Fiber D	40	1.75	136	150	93
Fiber D	6	1.24	51	171	88
Fiber E	20	1.23	69	200	81
Fiber E	7	1.16	60	152	84
Fiber F	9	1.20	113	158	90
Resin 2					
No filler*		1.10	90	165	76
Fiber A*	58	1.80	208	135	94
Fiber A	40	1.60	141	98	97

Correlation Between Peak Heat Release Rates, Char Yields, and TGA Data

Although thermogravimetric analysis (TGA) has been used to determine the thermal properties of polymers, the relationship between TGA data and fire test results have only been established in a few cases[4,5]. In this study, a good relationship between the peak heat release rate and the 3% weight loss temperature measured in helium was found. The 3% weight loss temperatures were chosen because in one case char yield reached 96%. As shown in Figure 3, most materials had 3% weight loss temperatures of ~ 500°C and heat release rates ~ 150 kW/m^2. As the 3% weight loss temperatures increased to 700-750°C, the peak heat release rates decreased to 50 kW/m^2 or below. One cured resin had a peak heat release rate less than 10 kW/m^2.

Relationships between char yields of burned samples and those measured by TGA are shown in Figure 4. The data showed that the char yields of burned samples were close to those measured

in helium instead of air. As char yields increased, the differences between those measured in helium or air decreased. Explanations for these results are currently being investigated.

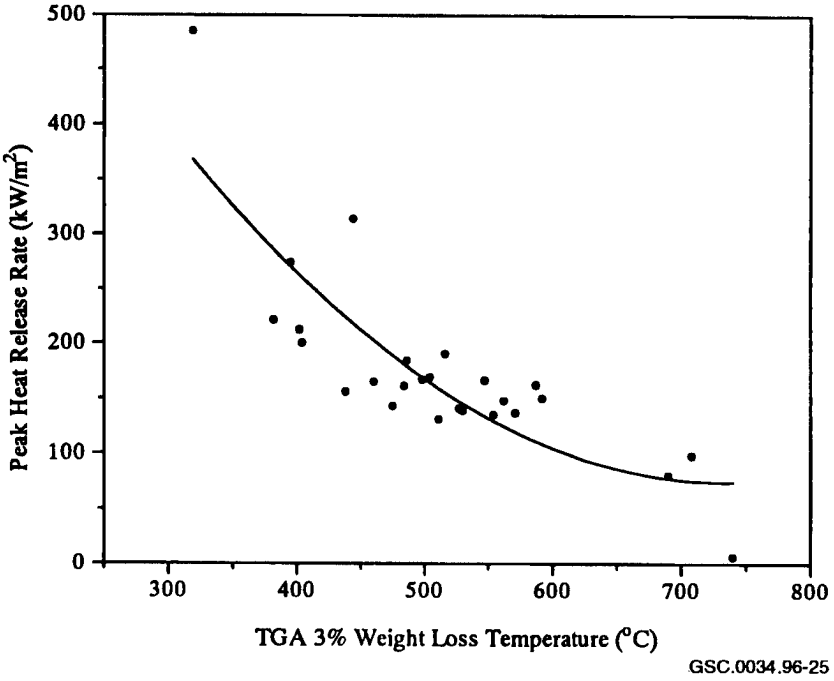

Figure 3. Relationship Between TGA 3% Weight Loss Temperature and Peak Heat Release Rate

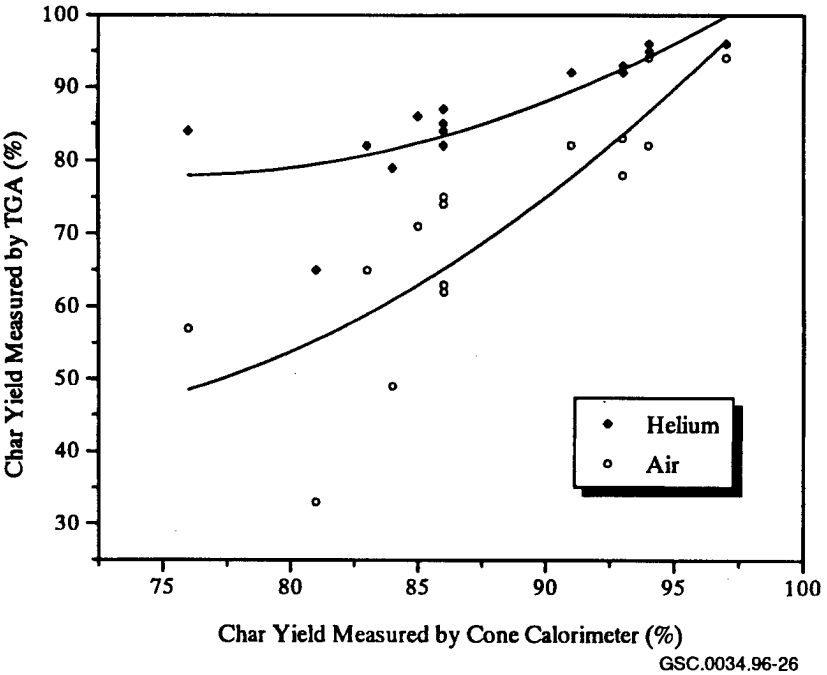

Figure 4. Relationship Between Char Yields Measured by Cone Calorimeter and by TGA in Helium or Air

CONCLUSIONS

The silicone resin composites used in this study had peak heat release rates between 100-150 kW/m^2 under 50 kW/m^2 incident heat flux. Layered silicates and fibrous fillers gave good char integrity and high char yields. In addition, good correlation exist between TGA and cone calorimeter data. These results demonstrate that silicone resin composites with low flammability can be made and TGA can be used as a tool for predicting flammability of silicone resins.

ACKNOWLEDGMENTS

This research has been supported by Federal Aviation Administration under Grant No. 95-G-05. We gratefully acknowledge Dr. Richard E. Lyon for his support. Also, we are thankful to Dr. Forrest O. Stark for his suggestions.

REFERENCES

1. B. Hardman and A. Torkelson, "Silicones," *Encyclopedia of Chemical Technology*, 3rd ed. Vol. 20, John Wiley & Sons, New York (1988).
2. G. L. Nelson, ed., "Fire and Polymers," ACS Symposium Series Number 599, American Chemical Society, Washington, D. C. (1995).
3. R. H. Baney, M. Itoh, A. Sakakibara, and T. Suzuki, *Chem. Rev.*, 55, 1409 (1995).
4. T. D. Gracik and G. L. Long, *Thermochemica Acta*, 212, 163 (1992).
5. T. D. Gracik, G. L. Long, U. Sorathia, and H. E. Douglas, *Thermochemica Acta*, 212, 209 (1992).

FIRE-RETARDENT POLYETHERIMIDE NANOCOMPOSITES

Jongdoo Lee, Tohru Takekoshi, and Emmanuel P. Giannelis
Department of Materials Science and Engineering
Cornell University, Ithaca, NY 14853

ABSTRACT

Polyetherimide-layered silicates nanocomposites with increased char yield and fire retardancy are described. The use of nanocomposites is a new, environmentally benign approach to improve fire resistance of polymers.

INTRODUCTION

As use of synthetic polymers has grown dramatically over the last three decades so have efforts to control polymer flammability. Developments to that end have included intrinsically thermally stable polymers, fire-retardant fillers, and intumescent fire-retardant systems[1]. An effective way to improve fire resistance has relied on the introduction of highly aromatic rings into the polymer structure. An increase in the aromaticity yields high char residues that normally correlate with higher oxygen index and lower flammability. The often high cost of these materials and the specialized processing techniques required, however, have limited the use of these polymers to certain specialized applications. The effectiveness of fire-retardant fillers is also limited since the large amounts required make processing difficult and might inadvertently affect mechanical properties.

Polymer nanocomposites, especially polymer-layered silicate (PLS) nanocomposites, represent a radical alternative to conventionally filled polymers[2]. Because of their nanometer-size dispersion the nanocomposites exhibit markedly improved properties when compared to their pure polymer constituents or their macrocomposite counterparts. These include increased modulus and strength, decreased gas permeability, increased solvent resistance, and increased thermal stability. For example, a doubling of the tensile modulus and strength is achieved for nylon-layered silicate nanocomposites containing as little as 2 vol. percent inorganic. In addition, the heat distortion temperature of the nanocomposites increases by up to 100°C extending the use of the composite to higher temperature environments, such as automotive under-the-hood parts. Furthermore, the relative permeability and solvent uptake of the nanocomposites decreases by almost an order of magnitude.

Polymer-layered silicate nanocomposites exhibit many advantages: (a) they are lighter in weight compared to conventionally filled polymers because high degrees of stiffness and strength are realized with far less high density inorganic material; (b) they exhibit outstanding diffusional barrier properties without requiring a multipolymer layered design, allowing for recycling; and (c) their mechanical properties are potentially superior to unidirectional fiber-reinforced polymers because reinforcement from the inorganic layers will occur in two rather than in one dimension.

Melt intercalation of high polymers is a powerful new approach to synthesize polymer-layered silicate nanocomposites. This method is quite general and is broadly applicable to a range of commodity polymers from essentially nonpolar polystyrene, to weakly polar poly(ethylene terephthalate) to strongly polar nylon. PLS nanocomposites are, thus, processable using current technologies and easily scaled to manufacturing quantities. In general, two types of hybrids are possible: *intercalated,* in which a single, extended polymer chain is intercalated between the host layers resulting in a well ordered multilayer with alternating polymer/inorganic layers and *delaminated,* in which the silicate layers (1 nm thick) are exfoliated and dispersed in a continuous polymer matrix.

In this paper we report the synthesis, thermal properties, and flame resistance of polyether imide nanocomposites. Both the decomposition temperature and the char yield of the nanocomposites is much higher than that of the polymer or a conventionally filled system at similar loadings to the nanocomposites.

EXPERIMENTAL

Polyetherimides were synthesized according to the published methods[3,4] from 4,4'-(3,4-dicarboxyphenoxy)diphenylsulfide dianhydride and a series of aliphatic diamines using m-cresol as solvent. Organically modified layered silicates were prepared as previously outlined by a cation-exchange reaction between Li fluorohectorite (cation exchange capacity, CEC, of 1.5 meq/g, particle size 10 μ) or Na montmorillonite (CEC = 0.9 meq/g, particle size 1 μ) and the corresponding protonated primary amine. Nanocomposites were synthesized either statically or in a microextruder. In the former, the silicate and the polymer were mechanically mixed and formed into a pellet (25 mm^2 x 5 mm) using a hydraulic press and a pressure of 70 MPa. The pellets were subsequently annealed in vacuum at 170°C for several hours. The microextruded samples were processed at 195°C for 30 min. and at a rate of 30 rpm.

X-ray diffraction analysis was performed using a Scintag θ-θ diffractometer and Cu Kα radiation. Thermal analysis was performed on a DuPont Instruments 9900 thermal analyzer at a heating rate of 10°C/min under flowing air or nitrogen.

RESULTS AND DISCUSSION

The family of aliphatic polyether imides used and their characteristics are summarized in Table 1. In contrast to their aromatic counterparts, the aliphatic PEI are amorphous with no evidence for any melting transitions. As the length of the aliphatic chain, m, increases the glass transition of the polymer decreases. The narrow MW range was accomplished by carefully controlling the reactant stoichiometry during polymerization.

Pristine mica-type layered silicates usually contain hydrated Na^+ or K^+ ions. Ion exchange reactions with cationic surfactants including primary, tertiary, and quaternary ammonium ions render the normally hydrophilic silicate surface organophilic, which makes intercalation of many engineering polymers possible. The role of the alkyl ammonium cations in the organosilicates is

to lower the surface energy of the inorganic host and improve the wetting characteristics and, therefore, miscibility with the polymer.

Table 1. Properties of Synthesized Polyetherimides (PEI)

Polymer	Length of Aliphatic Amine, m	T_g /°C	M_w	M_n	M_w/M_n
PEI-6	6	123	45,000	38,000	1.18
PEI-7	7	114	36,000	31,000	1.16
PEI-8	8	110	43,000	35,000	1.23
PEI-9	9	85	43,000	35,500	1.21
PEI-10	10	83	42,000	33,000	1.27

X-ray diffraction measurements provide a quick measure for nanocomposite formation. Generally intense reflections in the range $2\theta = 3\text{-}9°$ indicate either an ordered intercalated hybrid or an immiscible system. The former, however, shows an increase in the d-spacing corresponding to the intercalation of the polymer chains in the host galleries while in the latter the d-spacing remains unchanged. In delaminated hybrids, on the other hand, XRD patterns with no distinct features in the low 2θ range are anticipated due to the introduced disorder and the loss of structural registry in the silicate layers.

Table 2 summarizes the x-ray diffraction analysis of montmorillonite and fluorohectorite nanocomposites with PEI-10. Na-montmorillonite, being hydrophilic, leads to an immiscible system. In contrast, nanocomposites are formed with the organically modified silicates. As the length of the organic cation (from C12 to C18) or the charge density of the host increases a transition from exfoliated to intercalated nanocomposites is observed. This behavior is in accord with the predictions of the mean-field thermodynamic model for hybrids developed in our group[5].

Table 2. X-Ray Diffraction Analysis of PEI-10 Nanocomposites

Organosilicate	Nanostructure
Dodecylammonium montmorillonite, MC12	Delaminated
Tetradecylammonium montmorillonite, MC14	Delaminated
Hexadecylammonium montmorillonite, MC16	Delaminated
Octadecylammonium montmorillonite, MC18	Intercalated
Dioctadecyldimethylammonium montmorillonite, M2C18	Intercalated
Na montmorillonite	Immiscible
Dodecylammonium fluorohectorite, FC12	Intercalated
Tetradecylammonium fluorohectorite, FC14	Intercalated
Hexadecylammonium fluorohectorite, FC16	Intercalated
Octadecylammonium fluorohectorite, FC18	Intercalated

Figure 1 shows the TGA in air of pristine PEI and three hybrids containing 10 wt.% silicate. The corresponding TGA in nitrogen is shown in Figure 2. Both the intercalated and delaminated nanocomposites show a delayed decomposition temperature compared to the unfilled polymer. Interestingly, the immiscible hybrid containing the same amount of silicate shows no improvement, suggesting that formation of the nanostructure is responsible for the increases in thermal stability.

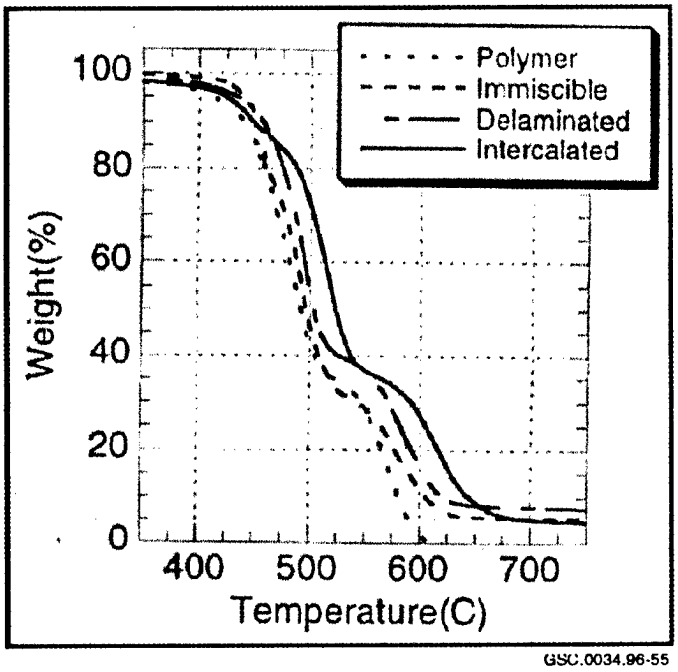

Figure 1. TGA of PEI-10 and PEI-10 Hybrids in Air

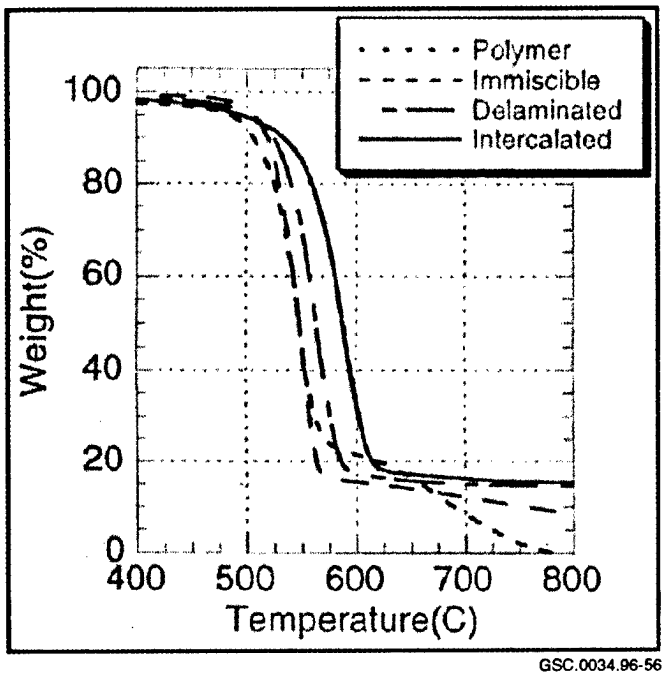

Figure 2. TGA of PEI-10 and PEI-10 Hybrids in Nitrogen

Figures 3 and 4 show the isothermal TGAs for the above systems in air at 450 and 500°C, respectively. The intercalated nanocomposites show a much higher char yield than any of the other systems. For example, for the 450°C isothermal the intercalated nanocomposite retains about 90% and 45% of its weight after 20 and 120 min., respectively. The corresponding numbers for the pure polymer are 45% and 15%. In the 500°C isothermal, the polymer is completely lost after 40 min. while the char yield of the intercalated nanocomposite is ~55%.

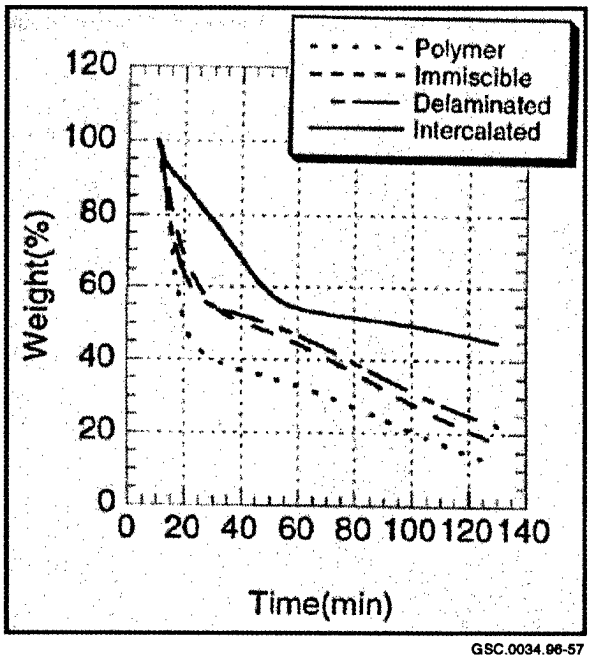

Figure 3. Isothermal at 450°C in Air

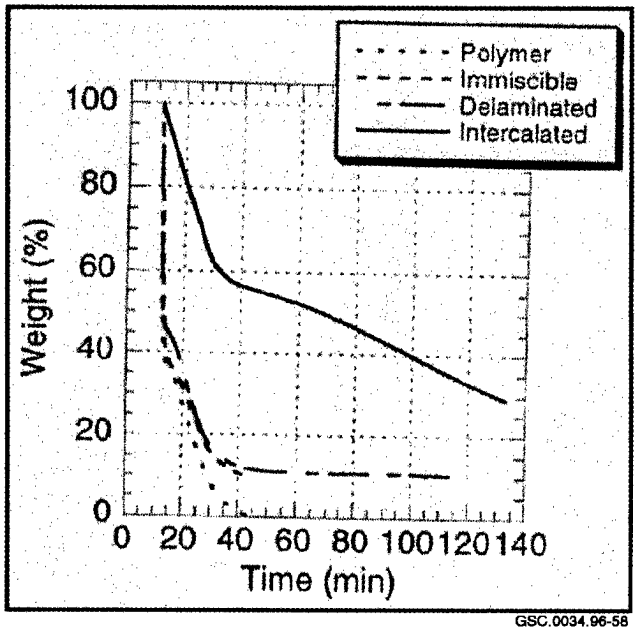

Figure 4. Isothermal at 500°C in Air

While there appears to be a difference between the intercalated and delaminated nanocomposites we have found no difference between the fluorohectorite- and montmorillonite-based nanocomposites as long as they exhibit the same nanostructure suggesting that the particle size of the silicates is not an important factor. Additionally, the thermal stability was independent of the cation in the organosilicate with the nanostructure again being the predominant variable.

Even though the mechanism is unknown at present the nanocomposites show significant fire retardancy when compared to the pure polymer (Figure 5). In both cases the specimens were exposed to open flame for about 10 sec. The pure polymer persisted burning after the flame was removed until it was externally extinguished. In contrast, the nanocomposite became highly charred but maintained its original dimensions and ceased burning after the flame was removed.

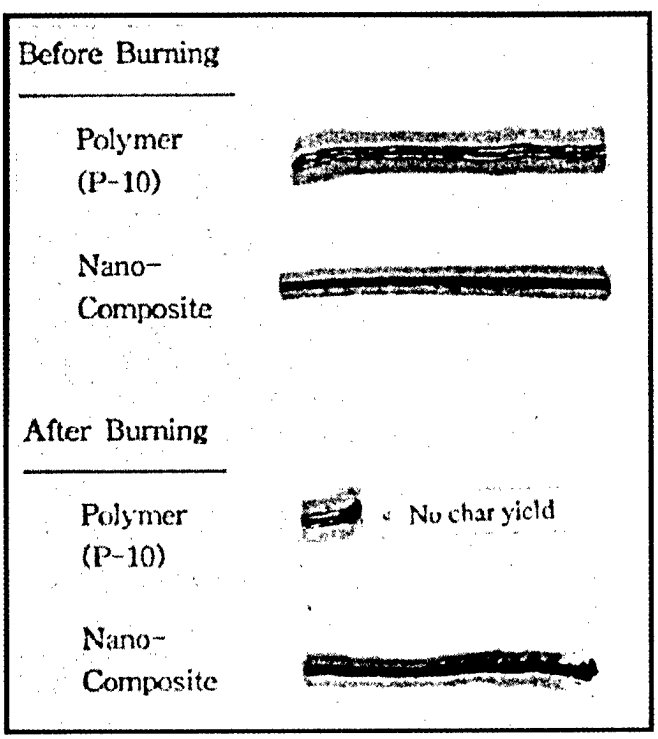

Figure 5. Fire Test of PEI and PEI Nanocomposite

ACKNOWLEDGEMENTS

This work was supported by a grant from the Department of Transportation (FAA, Dr. R. Lyon).

REFERENCES

1. G.L. Nelson, Ed., Fire and Polymers, ACS Symposium Series 599, 1995.
2. E.P. Giannelis, Advanced Materials, 8, 29 (1996).
3. T. Takekoshi, J.E. Kochanowski, J.S. Manello, and M.J. Webber, J. Polym. Sci., Polym. Chem. Ed. 23, 1759 (1985).
4. T. Takekoshi, J.E. Kochanowski, J.S. Manello, and M.J. Webber, J. Polym. Sci., Polym. Symp. 74, 93 (1986).
5. R.A. Vaia and E.P. Giannelis, submitted for publication.

POLYPHOSPHAZENE BLENDS

Michael M. Coleman and Paul C. Painter
Department of Materials Science and Engineering
The Pennsylvania State University
University Park, PA 16802

ABSTRACT

In addition to outstanding fire-retardant properties, plastic materials that are envisaged for use in aircraft cabins of the future must have a wide variety of physical and mechanical properties, ranging from a soft foam that is typically used for a cushion, to a tough wear-resistant fiber used in carpeting, to engineering materials that are employed for structural purposes. Our goal is to use the inherent flame-retardant properties of polyphosphazenes in combination with the desirable physical properties of other polymers through the formation of miscible blends and interpenetrating networks. Here we report on our initial experimental and theoretical studies.

INTRODUCTION

In addition to outstanding fire-resistant properties, plastic materials that are envisaged for use in aircraft cabins of the future must have a wide variety of physical and mechanical properties, ranging from a soft foam that is typically used for a cushion, to a tough wear-resistant fiber used in carpeting, to engineering type materials that are employed for structural purposes. Furthermore, these materials must be readily processed into desired end products and be economically viable. This is indeed a challenge and one that will surely test the ingenuity of polymer scientists.

Polyphosphazenes, with their inorganic nitrogen/phosphorous backbone, are inherently fire resistant[1]. Furthermore, within this broad class of (co)polymers it is possible to optimize fire resistance by the careful selection of pendant side groups, a task being actively pursued by Professor Allcock and his coworkers. However, given the ever-present economic considerations and the wide range of physical and mechanical properties required for the polymeric materials used in aircraft cabins, fire-resistant polyphosphazenes are most likely to find application in some form of blend, mixture, or composite.

The phase behavior of such polymer-polymer mixtures is crucial, because it strongly influences the chemical, physical, and mechanical properties of the resultant material. Intimate mixing of the chosen polyphosphazene with other polymers is desired if we are to optimize fire resistance of the polymer mixture. However, conditions governing the mixing of polymers are stringent and, in general, the probability that a mixture of two polymers chosen at random will form a

single-phase (miscible) polymer blend is exceedingly low[1]. In fact, in the vast majority of cases, random mixing of two polymers results in grossly phase-separated materials. Macromolecular compatibilizers (usually block or graft copolymers) can and are employed to decrease the domain size of the dispersed phase and produce a more homogeneous dispersion, but ideally, intimate mixing, exemplified by a single-phase (miscible) mixture, is optimum. Miscible polymer mixtures are the exception not the rule, but over the past decade the utilization of relatively strong intermolecular interactions, especially hydrogen bonds, as a driving force for polymer-polymer mixing has made it possible to design such systems[2]. Fortunately, polyphosphazenes are particularly amenable to the incorporation of specific functional groups. We are not limited to this approach, however, and another way to achieve the intimate mixing of polymers is to perform *in situ* chemical reactions between the two polymers. By designing the appropriate chemistry, a myriad of grafting or transreactions can be contemplated that will result in intimate mixing through the formation of different types of copolymers and interpenetrating networks. Again, the unique chemistry of polyphosphazenes makes this approach facile.

In the forthcoming section we report on the progress made during the first year of this award and we will focus our attention on preliminary studies involving the two major methods for intimate polymer mixing mentioned above. First, we will describe the results obtained from a polyurethane/polyphosphazene foamed blend in which we grafted a polyphosphazene into the polyurethane network. We will then describe miscible polyphosphazene blends that have been made with vinyl phenol copolymers.

RESULTS AND DISCUSSION

Polyphosphazene/Polyurethane Mixtures

Polyurethane foams, ranging from the soft foams used in cushions to the relatively hard foams used for structural and insulation purposes, are remarkably versatile and find numerous applications in aircraft cabins. In their pure state, however, these materials are highly flammable[3]. The production of polyurethane foams involves the formation of a "blown" three-dimensional polymeric network from relatively low molecular weight (and low viscosity) polyol and diisocyanate precursors, which makes it a fine system to test whether or not it is feasible to graft polyphosphazenes onto a network and thereby impart fire resistance.

Appropriate functional groups that react rapidly with isocyanates include primary amines, hydroxyls, and carboxylic acids[4]. Accordingly, in order to graft a polyphosphazene onto the polyurethane network *in situ* it is necessary to have such groups present in side groups of the polyphosphazene. A polyphosphazene containing carboxylic acid groups, poly[bis(carboxylatophenoxy)phosphazene] (PBCPP), which have been shown to have excellent thermal stability[2j], was synthesized in Professor Allcock's laboratory. The grafting reaction envisaged is depicted in Scheme 1. The polyol and isocyanate terminated prepolymers were kindly supplied by the Bayer Corporation, Pittsburgh, PA, and formulated by mixing in equal amounts to yield a hard foam (typical of that employed for structural insulation).

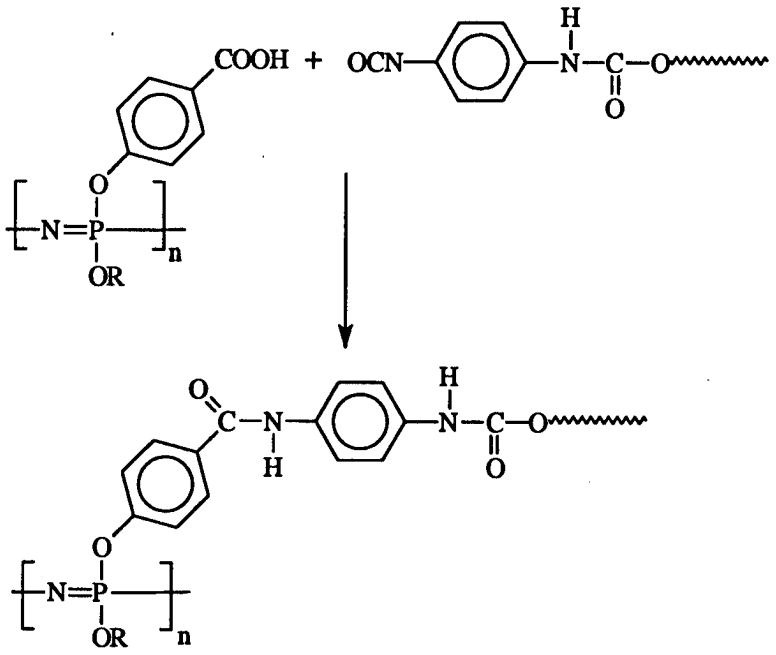

Scheme 1

Various amounts of PBCPP and the polyol were premixed in a polyethylene beaker. An equal weight (based on the total weight of PBCPP plus polyol) of the isocyanate terminated prepolymer was added and stirred rapidly. The mixture was quickly poured between two large Teflon® coated steel sheets separated by approximately 0.5 cm. The resultant foam formed a circular disc which was allowed to cool for 2 hours before it was removed from the steel plates. The density of the foams is a function of the temperature of the initial ingredients (before reaction of the isocyanate groups). By trial and error it was determined that reproducible dense foams could be prepared at a temperature of 0°C and used for preliminary flame testing.

Preliminary tests of relative flammability using a simple Bunsen burner method (ASTM 4804) and thermal gravimetric analyses (TGA) (both employed primarily for scouting purposes) were performed on foam samples containing 0, 5, 10, 15, 20, and 30 weight percent PBCPP. All flame tests were carried out inside a fume hood with its fan turned off and sash down to minimize external air currents. Bars of dimension 1.27 cm (0.5 in) x 12.7 cm (5.0 in) were cut from the foam disc and marked at 1.91 cm (0.75 in) from each end. The sample bar was placed horizontally in a clamp at a 45° angle with respect to the perpendicular of the table at a height of 38.1 cm (15 in). A Bunsen burner using natural gas was placed in a clamp and tilted at an angle of 30° towards the tip of the sample bar at a height of 1.27 cm (0.5 in) below the sample. The burner was ignited away from the sample and adjusted so the flame was 1.91 cm (0.75 in) long, with the tip of the flame being slightly yellow. The burner was then moved into position directly below the sample and held there for 30 sec. or until the sample burned to the first mark and then removed. The average time taken to burn from the first and last mark was recorded for the foamed blends of different composition.

Figure 1 illustrates pictorially the exceptional combustibility of the pure polyurethane foam (i.e., that in the absence of flame retardants). The sample ignited upon exposure to the flame, rapidly burned and was totally consumed within 40 sec. leaving a black char. Foam samples containing 5%-15% PBCPP had little overall effect on combustibility. However, at a 20% loading of PBCPP the samples self-extinguished, as shown in Figure 2. Once the flame was removed, after the full 30-sec. limit had elapsed, the sample continued to burn slowly for a further 20 sec. and then self-extinguished at 55 sec. This charred region of the sample was then visually examined. Only the outer skin (approximately one-third of the material), which resembled a black glassy char, appeared to have been affected by the flame. Moreover, this char appears to form a protective coating over the internal bulk of the material, which appeared unaffected by the burning process. The above results are encouraging, but they do suggest that a minimum of ≈ 20% of the polyphosphazene will be necessary to impart fire resistance to polyurethane foams.

The TGA data are shown graphically in Figure 3. While these data are not expected to correlate very well with flammability per se, TGA is a facile method useful for scouting degradation studies. The trends observed in weight loss as a function of temperature for the different foams are consistent with the major conclusion gained from the flame tests described above, i.e., that a minimum loading of 20% PBCPP in the polyurethane foam is necessary to impart fire resistance (note that the TGA curves for the 20% and 30% PBCPP are essentially identical).

There appears to be three important temperature regimes in the TGA of these polyurethane foams. The onset of significant degradation occurs at ≈ 200°C for the virgin polyurethane foam and the material gradually looses ≈ 45% of its mass as the temperature is raised to 350°C. A more gentle plateau region from ≈ 350-500°C is then observed over which the material looses another 15% of its mass. From 500-600°C the virgin polyurethane foam essentially decomposes and there is little of the material remaining. The general overall shape of the TGA curves for the polyurethane/ PBCPP foams between 200 and 500°C are similar, but displaced vertically on the weight loss axis. The TGA data collapses to single curve above ≈ 20% PBCPP loading in the 200-500°C range, with a maximum weight loss of ≈ 40% at 500°C. This weight loss is only marginally less than that of pure PBCPP at the same temperature and this result suggests the polyurethane foams containing >20% PBCPP (see above) are self-extinguishing after exposure to the flame because of the formation of a PBCPP protective char.

Approximately 3, 14, 16, 20, and 28 percent of the original mass remains at 600°C as observed for the foams containing 0, 10, 15, 20, and 30 weight percent PBCPP, respectively. The correlation between the initial amount of PBCPP in the mixture and the char remaining at 600°C is striking, but we should be careful in drawing the conclusion that the char is simply PBCPP, because pure PBCPP yields a char equivalent to ≈ 55% of the original mass at the same temperature[2j].

The Phase Behavior of Polyphosphazene Blends

A myriad of different functional groups can be substituted onto the phosphazene backbone and it should be possible to design miscible fire-retardant polyphosphazene blends[1]. However, little is known about the phase behavior of polyphosphazene blends and group molar attraction and molar volume constants for the -N=P- group have not been previously determined. These

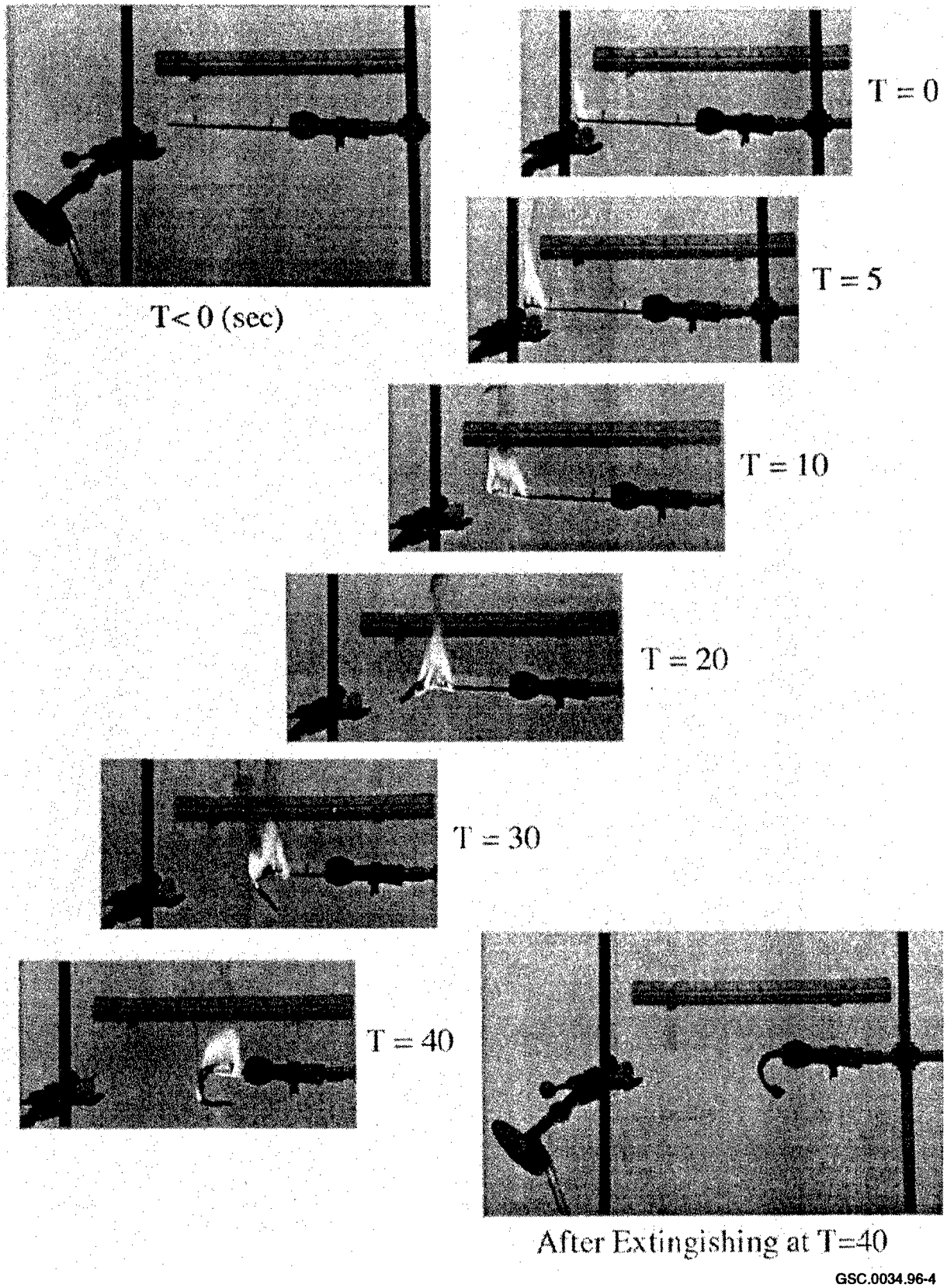

Figure 1. Simple Flame Test for the Virgin Polyurethane Foam

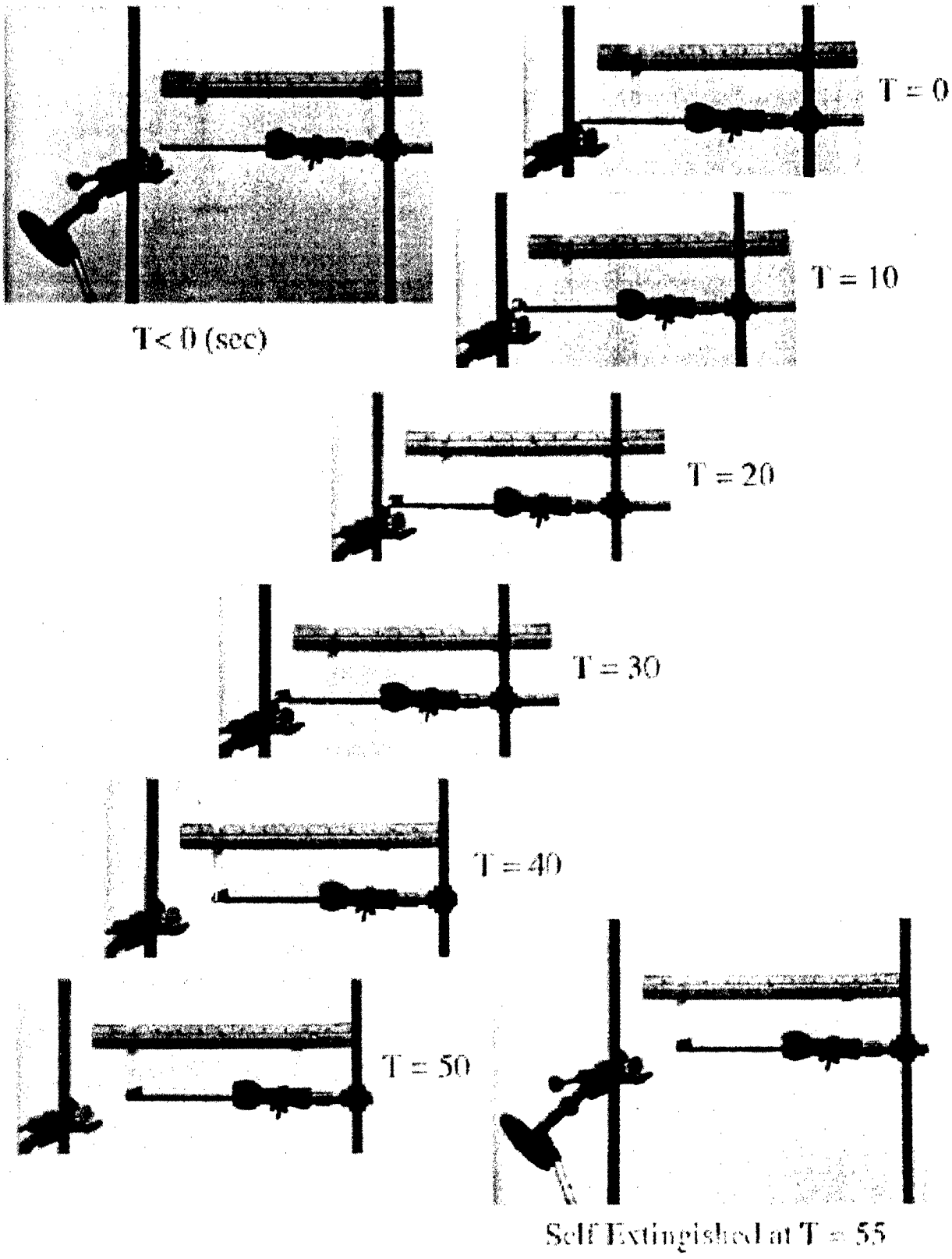

Figure 2. Simple Flame Test for the Polyurethane Foam Containing 20 Weight Percent PBCPP

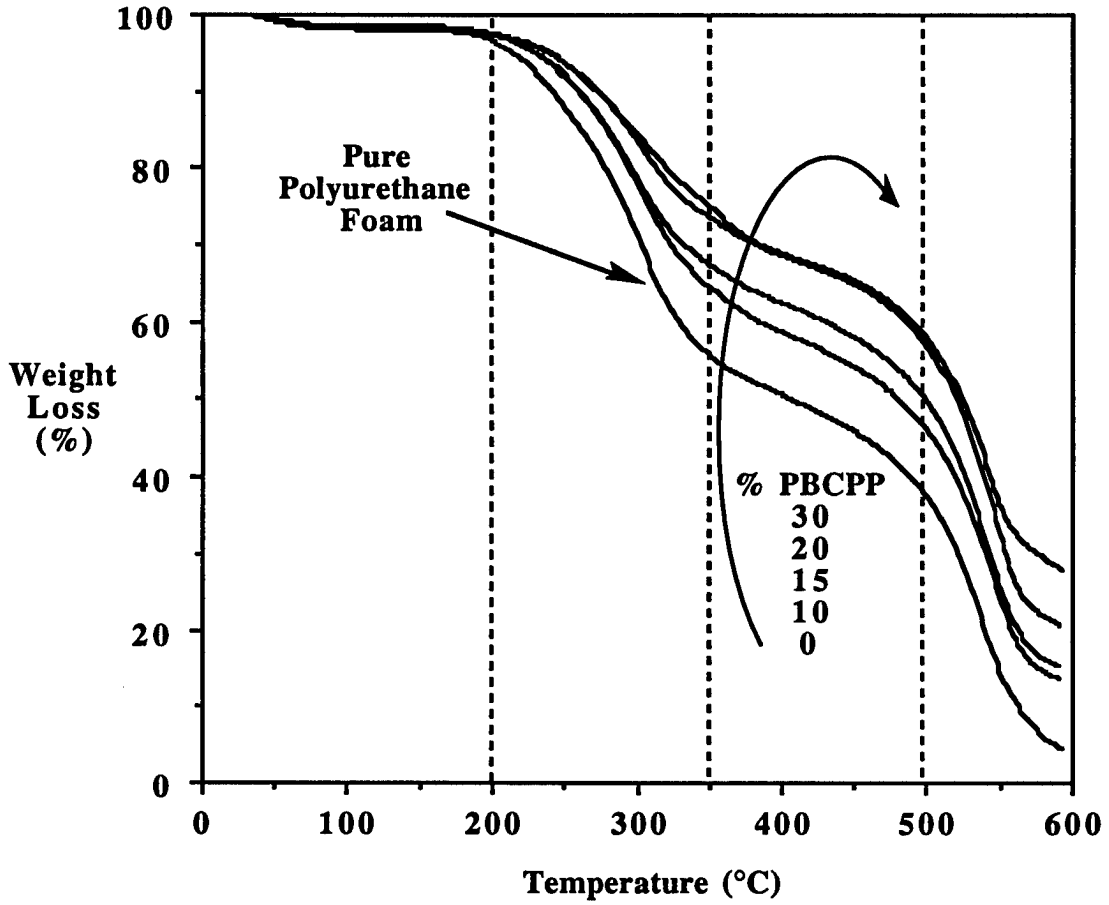

Figure 3. TGA Curves for the Virgin Polyurethane Foam and Foamed Blends Containing 10, 15, 20, and 30 Weight Percent PBCPP

parameters are required for the calculation of the solubility parameters of phosphazene polymers, which, in turn, are needed to predict the phase behavior of polyphosphazene blends[1]. Obtaining these parameters from physical chemical measurements on low molecular weight analogues is not practicable, however. Thus our strategy is to determine these group contributions from systematic experimental studies of a series of miscible polyphosphazene blends. This will involve the characterization of a number of polyphosphazene blend systems by FTIR, thermal analysis, and light scattering and extracting the desired physical chemistry data from experimental miscibility windows and maps. Having obtained the -N=P- group contributions we will be in a position to predict the phase behavior of polyphosphazene blends that are potentially being considered as flame-resistant materials.

Systematic experimental studies of a series of relatively simple poly[bis(n-alkyl ether)phosphazene] (PBAEP) blends with (co)polymers containing the 4-vinyl phenol segment have been initiated[1,5]. Studies of the miscibility window of the not too dissimilar poly(4-vinyl phenol) (PVPh) blend system with the analogous series of poly(vinyl alkyl ethers) were performed in our laboratories previously[6].

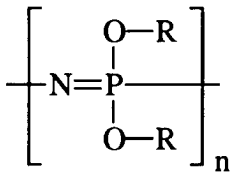

(PBAEP)

PBAEP samples, where R = methyl (PBMEP), ethyl (PBEEP), n-propyl (PBPEP), n-butyl, n-pentyl (PBPeEP), and n-hexyl through to n-decyl were synthesized in Professor Allcock's laboratory.

Typical scale expanded FTIR spectra in the hydroxyl stretching region of pure PVPh and the 20:80 blends with PBEEP and PBPEP are shown on the left-hand side of Figure 4. The infrared spectrum of PVPh is characterized by two major bands at ≈ 3320 and ≈ 3550 cm^{-1}. PVPh strongly self-associates and the former broad band reflects the wide distribution of chain-like hydrogen bonded OH - - - OH multimers present, while the latter is attributed to hydroxyl dimer formation.

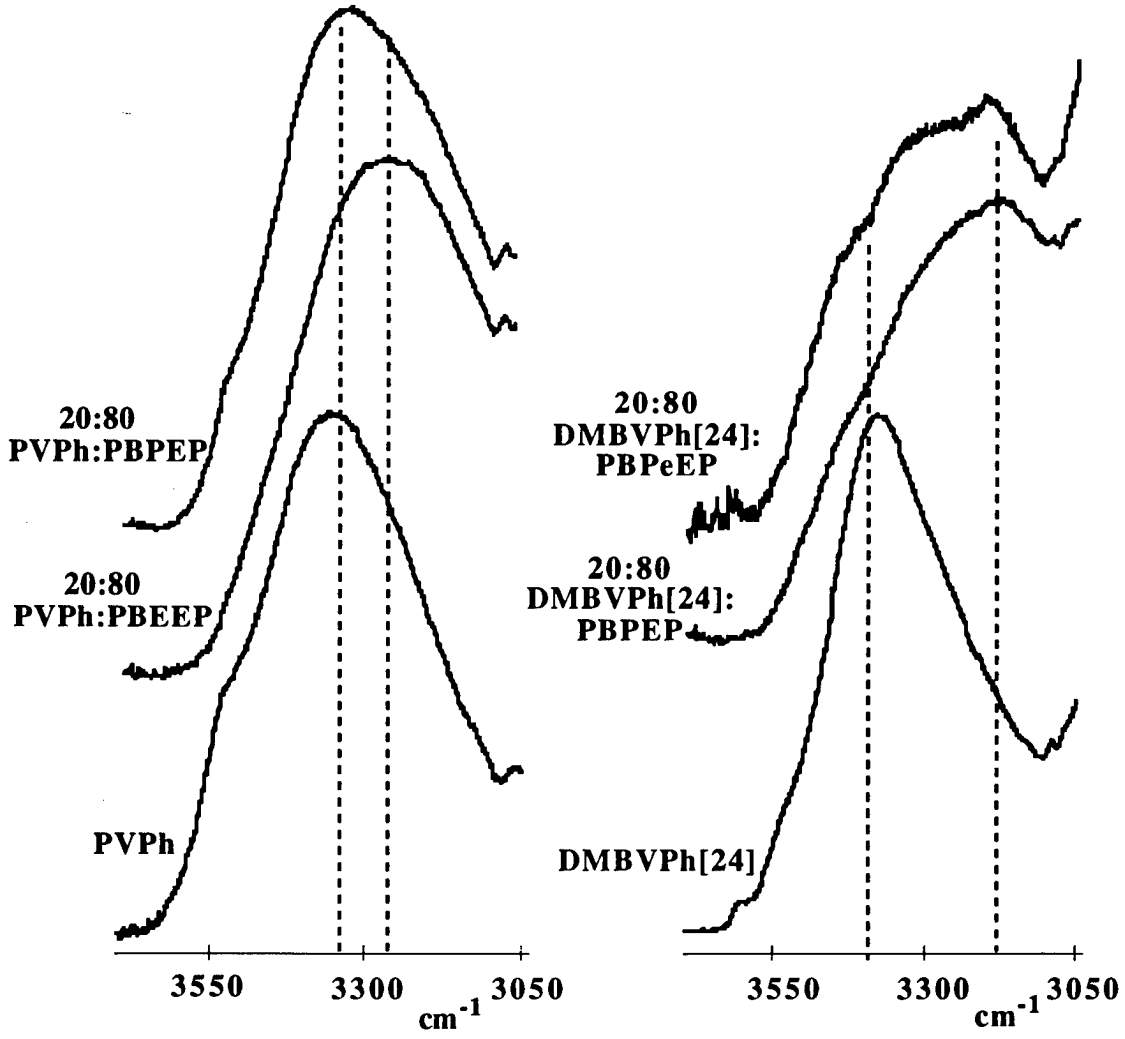

Figure 4. FTIR Spectra Recorded in the Hydroxyl Stretching Region

If upon mixing PVPh with a large excess of a particular PBAEP a single-phase blend is formed, then one would expect to see evidence of an infrared band that can be attributed to hydrogen bonded hydroxyl/ether oxygen interactions (i.e., OH - - - O<). Such a band is observed in the spectrum of the PBEEP blend at ≈ 3250 cm^{-1}. In contrast, if the blend formed is grossly phase separated, the spectrum in the hydroxyl stretching region will resemble that of pure PVPh as it exists in its own phase and is not in intimate contact with the PBAEP. This is observed in the spectrum of the PBPEP blend. These results suggest that the miscibility window for PVPh blends only extends to PBEEP, which is similar to that of the analogous poly(vinyl alkyl ether) blends[6].

In recent studies[1,5] we have demonstrated that much wider miscibility gaps can be obtained by manipulating solubility parameters through copolymerization. For example, PVPh is miscible with ethylene-co-vinyl acetate (EVA) copolymers containing from 0 to ≈ 50 wt % ethylene, but a 2,3-dimethylbutadiene-co-vinyl phenol copolymer with only 24 wt % vinyl phenol (DMBVPh-[24]) is miscible with an EVA containing 86 wt % ethylene[1]. A similar effect was anticipated for the PBAEP blends. On the right-hand side of Figure 4 are shown FTIR spectra of DMBVPh[24] and 20:80 blends with the n-propyl and n-pentyl ether phosphazenes (PBPEP and PBPeEP, respectively). Both appear to be highly mixed and these preliminary data suggest that the miscibility gap is indeed much wider.

Frankly, the hydroxyl stretching region of the spectrum is very difficult to interpret and almost impossible to use for quantitative analysis. Accordingly, we have also initiated studies of PBAEP blends with butyl methacrylate-co-vinyl phenol copolymers (BMAVPh) that contain relatively small amounts of butyl methacrylate. Increasing the complexity by introducing another competing functional group into the polymer chain containing the phenolic hydroxyl group may seem illogical, but in fact we can now employ the carbonyl group of the BMA segment to quantitatively measure the fraction of hydroxyl/ether oxygen interactions present in a PBAEP blend at equilibrium[7]. Representative examples are shown in Figure 5. Here we see dramatic differences in the relative areas of the free (nonhydrogen bonded) and hydrogen bonded carbonyl bands at ≈ 1730 and 1700 cm^{-1} in PBEEP blends with BMAVPh[90].

These results are encouraging and it is from FTIR studies such as these that we hope to determine the physical parameters necessary to predict the phase behavior of fire-resistant polyphosphazene blends.

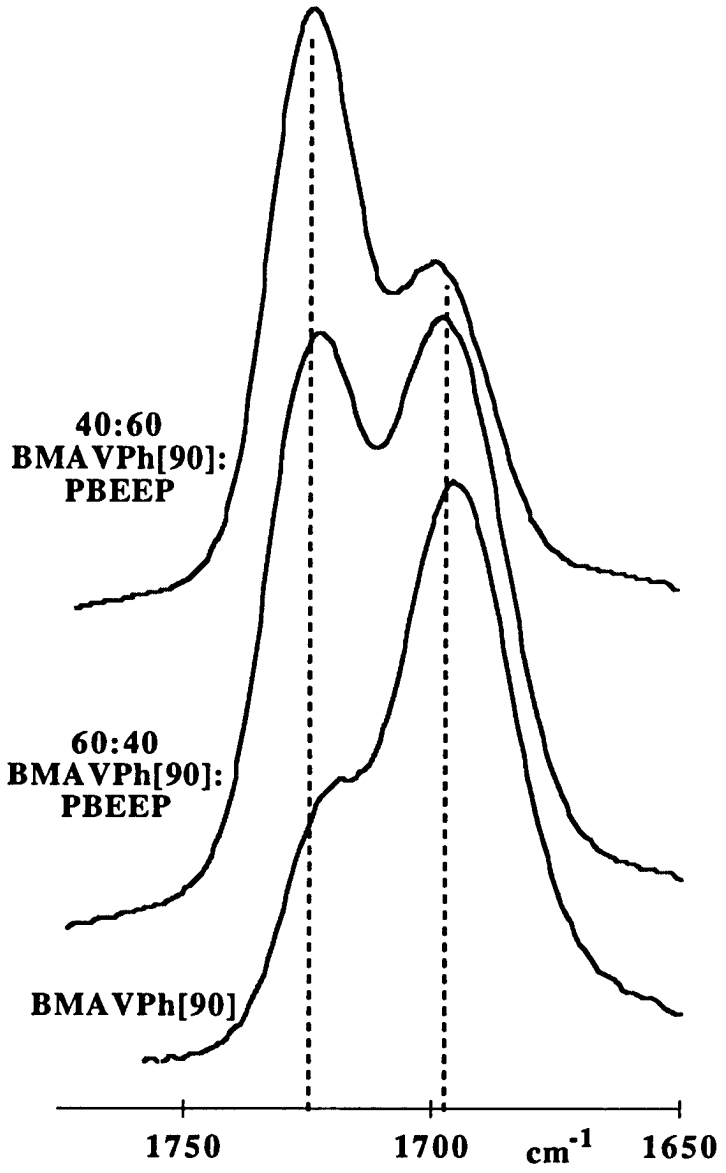

Figure 5. FTIR Spectra Recorded in the Carbonyl Stretching Region

REFERENCES

1. (a) M. M. Coleman, J. F. Graf, and P. C. Painter, "Specific Interactions and the Miscibility of Polymer Blends," Technomics, Lancaster, PA (1991). (b) M. M. Coleman and P. C. Painter, *Prog. Polym. Sci.*, 20, 1 (1995).

2. (a) H. R. Allcock, G. Y. Moore, and W. J. Cook, *Macromolecules*, 7, 571 (1974). (b) K. Sebata, J. H. Magill, and Y. C. Alarie, *J. Fire Flam.*, 9, 50 (1978). (c) L. Goldfarb, N. D. Hann, R. L. Dieck, and D. C. Messersmith, *J. Polym. Sci. Polym. Chem.*, 16, 1505 (1978). (d) S. V. Peddada and J. H. Magill, *J. Fire Flam.*, 11, 63 (1980). (e) P. J. Lieu, J. H. Magill, and Y. C. Alarie, *J. Fire Flam.*, 11, 167 (1980). (f) S. V. Peddada and J. H. Magill, *Macromolecules.*, 16, 1258 (1983). (g) T. N. Bowmer, R. C. Haddon, S. Chester-Hicks, M. A. Gomez, C. Morco, and J. G. Fatou, *Macromolecules*, 24, 4827 (1991). (h) S. J. Maynard, T. R. Sharp, and J. F. Haw, *Macromolecules*, 24, 2794 (1991). (i) H. R. Allcock, G. S. McDonnell, G. H. Riding, and I. Manners, *Chem. Mater.*, 2, 425 (1990). (j) C. S. Reed, K. S. TenHuisen, P. W. Brown, and H. R. Allcock, *Chem. Mater.*, 8, 440 (1996).

3. (a) N. Grassie, in "Polymer Handbook," 3rd edn., J. Brandrup and E. H. Immergut, Eds., Interscience, New York (1989). (b) F. Gaboriaud and J. P. Vantelon, *J. Polym. Sci. Polym. Chem.*, 20, 2063 (1982). (c) A. Ballistreri, S. Foti, P. Maravigna, G. Montaudo, and E. Scamperrino, *J. Polym. Sci. Polym. Chem.*, 18, 1923 (1980). (d) R. B. Barendregt and P. J. Van Den Berg, *Thermochem. Acta*, 38, 181 (1980).

4. H. R. Allcock and F. W. Lampe, "Contemporary Polymer Chemistry," Prentice Hall, Englewood Cliffs, NJ (1981).

5. (a) M. M. Coleman, G. J. Pehlert, and P. C. Painter, *Macromolecules*, 29, 6820 (1996). (b) P. C. Painter, B. Veytsman, S. Kumar, S. Shenoy, J. F. Graf, Y. Xu, and M. M. Coleman, *Macromolecules*, accepted. (c) M. M. Coleman, G. J. Pehlert, X. Yang, J. B.Stallman, and P. C. Painter, *Polymer*, 37, 4753 (1996). (d) G. J. Pehlert, X. Yang, P. C. Painter, and M. M. Coleman, *Polymer*, 37, 4763 (1996).

6. (a) E. J. Moskala, D. F. Varnell, and M. M. Coleman, *Polymer*, 26, 228 (1985). (b) C. J. Serman, Y. Xu, P. C. Painter, and M. Coleman, *Polymer*, 32, 516, (1991).

7. (a) C. Le Menestrel, D. E. Bhagwagar, P. C. Painter, M. M. Coleman, and J. F. Graf, *Macromolecules*, 25, 7101 (1992). (b) Y. Xu, P. C. Painter, and M. M. Coleman, *Polymer* 34, 3010 (1993). (c) Y. Xu, D. E. Bhagwagar, P. C. Painter, and M. M. Coleman, *Makromol. Chem. Macromol. Symp*, 84, 307 (1994).

MODELING

MOLECULAR DYNAMICS MODELING OF THERMAL DEGRADATION IN POLYMERS

Marc R. Nyden
Building and Fire Research Laboratory
National Institute of Standards and Technology
Gaithersburg, MD 20899

ABSTRACT

This report presents the progress we have made in the development of a generic molecular dynamics model which accounts for the major chemical reactions involved in the thermal degradation of polymeric materials. The strategy employed in the design of the most recent version of this model was to interface our code for performing reactive dynamics on simple vinyl polymers with a commercial molecular dynamics package (Discover 95). The expanded range of applicability of the integrated model is illustrated by applying it to the study of thermal degradation in polypropylene and polystyrene.

INTRODUCTION

Synthetic polymers comprise a significant fraction of the fire load borne by commercial aircraft interiors. The flammability, smoke, and toxicity characteristics of these materials may impact passenger survivability in the event of an in-flight or postcrash fire. This realization has provided an impetus for the development of new methods to improve the fire resistance of polymers.

Unfortunately, the traditional trial and error approach to the design of fire-resistant materials is not cost effective. One of the achievements of the Materials Fire Research Group at BFRL/NIST has been the development of a unique molecular dynamics model, hereafter referred to as MD_REACT, which accounts for the major reaction channels involved in the thermal degradation of polymers[1-3]. The range of applicability of the original versions of this model, however, was limited to the study of simple vinyl polymers such as polyethylene. Many commercially available molecular dynamics software packages have the capability to build a much wider range of molecular structures and have access to extensive compilations of the parameters which are needed to describe the atomic level forces which govern the thermal motion of polymers. Unfortunately, these commercial molecular dynamics codes do not allow for the formation of new bonds from the free radical fragments generated when bonds in the polymer break and, therefore, cannot account for the chemical reactions which play a major role in the thermal degradation process.

The strategy employed in the development of a generic molecular dynamics code capable of modeling thermal degradation in a wide range of polymers was to make use of an interprocess

communications protocol (IPC) to pass coordinates, forces, and connectivity information between MD_REACT, which computes the reactive force field, and Discover 95[4], a commercially available molecular dynamics code offered by Molecular Simulations[5], which updates the molecular structure on the basis of the solution to the equations of motion.

The purpose of this report is to provide an overview of the progress we have made in the development of this integrated model which possesses the capability to model thermal degradation in a wide range of polymers. The capabilities of the present version of this model are illustrated by applying it to the study of thermal degradation in polystyrene and polypropylene.

BACKGROUND

The burning of most polymers may be viewed from the perspective of a simple model whereby volatile hydrocarbons, which are formed during the thermal degradation of the condensed phase, are combusted in the gas phase. The basis of this model is the hypothesis that all of the available oxygen is depleted in the flames above the surface of the solid. The cycle must be initiated by heat supplied from an external source, but it is self-sustaining as long as sufficient energy is generated and transferred to the surface of the polymer to further degrade it into fuel. The size of the fire is measured by the net rate-of-heat release (rhr) during this process.

Research conducted in this laboratory has focused on using molecular dynamics modeling to identify factors which alter the condensed phase thermal degradation chemistries of polymers in ways which effect a reduction in their flammability. The objective of this work has been to provide insights into the mechanism of char formation during thermal degradation. Charring increases the fraction of the fuel retained in the condensed phase so that less combustible gases are evolved. The presence of a surface char also insulates the unburnt polymer from the external heat source and obstructs the outward flow of combustible products from the degradation of the interior. Computer movies obtained from our simulations of the thermal degradation of polyethylene (Figure 1) indicated that cross-linked polymers tended to undergo further cross-linking when burned, eventually forming a high molecular weight, thermally stable char (Figure 2). This prediction was confirmed by char yield measurements made on γ and e^- -irradiated polyethylene (2,3) and chemically cross-linked poly(methyl methacrylate).

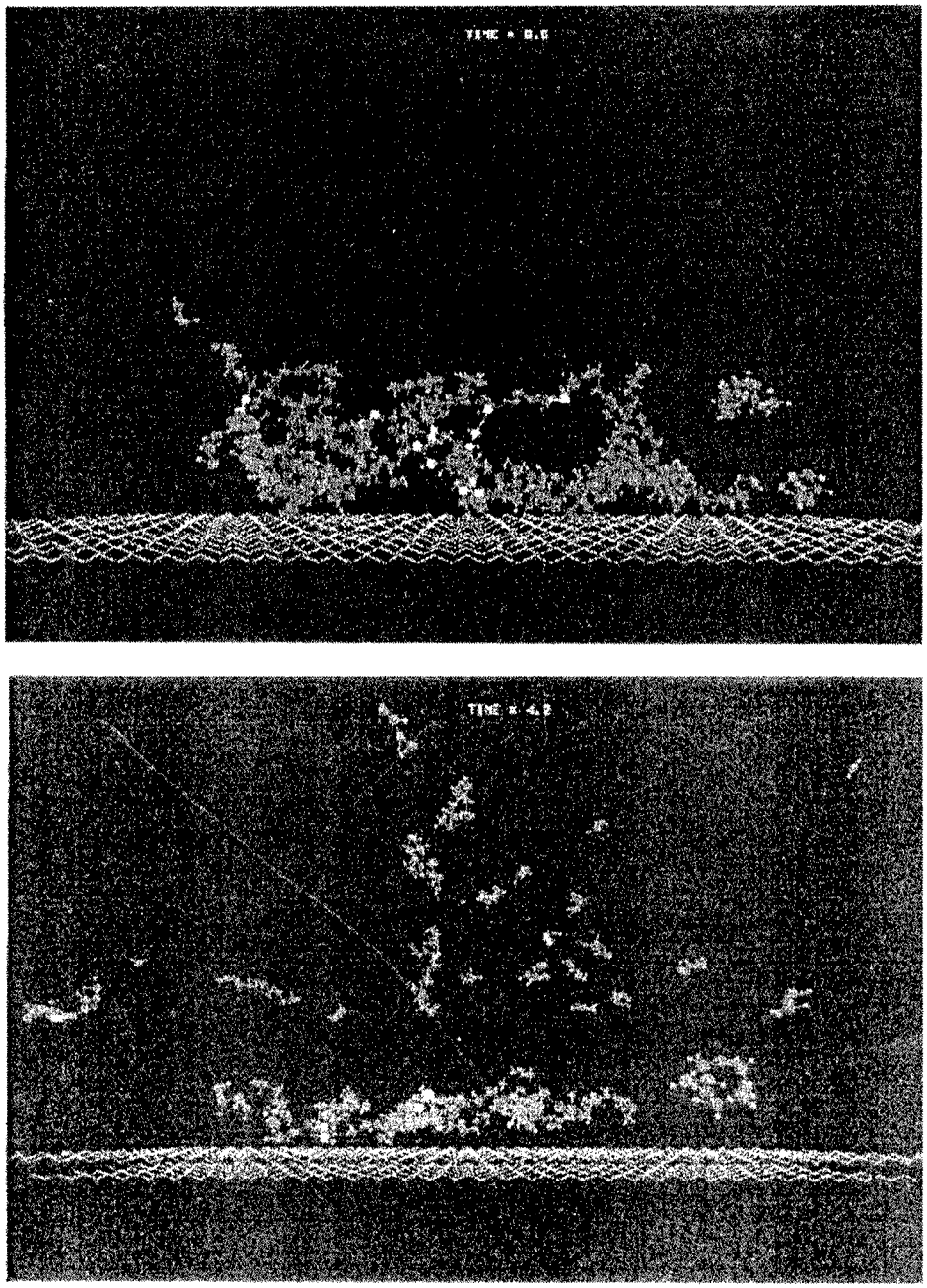

Figure 1. Still Frames From the Thermal Degradation of Polyethylene Illustrating how the Chains Break Before They Have a Chance to Cross-Link

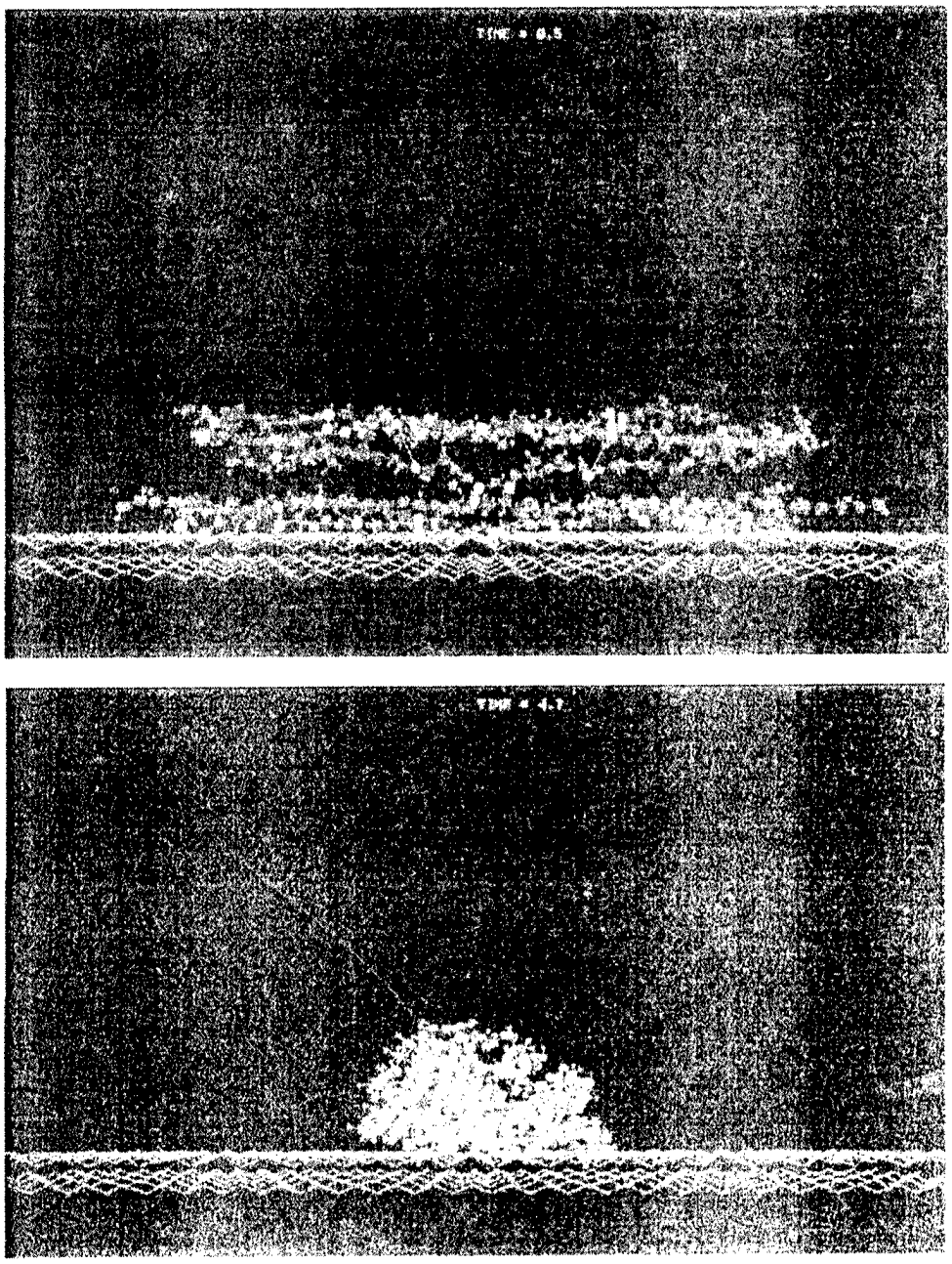

Figure 2. Still Frames From the Thermal Degradation of Cross-Linked Polyethylene Showing the Formation of a Thermally Stable, Char-Like Residue

THEORY

Molecular Dynamics

Molecular dynamics consists of solving Hamilton's equations of motion for each of the 3N molecular degrees of freedom. In this equation p_i and q_i denote the Cartesian components of momentum and position, respectively.

$$\frac{\partial H}{\partial p_i} = \frac{dq_i}{dt}, \qquad \frac{\partial H}{\partial q_i} = -\frac{dp_i}{dt}, \tag{1}$$

The Hamiltonian of the model polymers considered in the present investigation, which is based on the CVFF forcefield[6] (one of several force fields which are distributed with Discover 95), is summarized in equation 2. The first term on the right-hand side of this equation represents the kinetic energy of the N atoms in the model polymers. The next terms are the potential energies for bond stretching (V_b) and bending (V_a) and a torsional potential (V_t) which restricts internal rotation around the covalent bonds. The last term represents the nonbond potential energy (V_{nb}) resulting from the interactions between all pairs of atoms which are not part of the same covalent bond angle (i.e., between atoms which are separated by at least two atoms).

$$H = \sum_{i}^{3N} \frac{p_i^2}{2m_i} + \sum_{ij}^{nbonds} V_b(r_{ij}) + \sum_{ijk}^{nangles} V_a(\theta_{ijk}) + \sum_{ijkl}^{ntorsions} V_t(\phi_{ijkl}) + \sum_{ij}^{npairs} V_{nb}(r_{ij}) \tag{2}$$

The potential energy for stretching the covalent bonds is described by a Morse function where r_{ij} is the distance between covalently bonded atoms, r_e is the equilibrium bond length, D is the amount of energy required to dissociate the bond, and $\alpha = [k_b/(2D)]^{1/2}$, where k_b is the force constant.

$$V_b = D[1 - \exp(-\alpha(r - r_e))]^2, \tag{3}$$

The potential energy for bond bending is represented by the quadratic function where θ denotes the angle defined by the dot product of the normalized bond vectors between three adjacent atoms (denoted i, j, and k) and k_θ is the corresponding force constant.

$$V_a = S(ij)S(jk)k_\theta(\theta - \theta_e)^2, \tag{4}$$

Rotations about covalent bonds are restricted by the torsional potential where the dihedral angle, ϕ, is defined by the three bond vectors between four adjacent atoms (i, j, k, and l). The parameters, K_Φ, n, and ϕ_0 determine the height, multiplicity, and position of the barrier to internal rotation.

$$V_t = S(ij)S(jk)S(kl)K_\phi[1 + \cos(n\phi - \phi_e)], \tag{5}$$

The switching functions, which are used to turnoff the forces due to bending and twisting as the relevant bonds approach dissociation, are determined from equation 6 with a = 40 nm^{-1}. The dissociation distances, r_d, depend on the nature of the bond and are determined from an energy-based criterion which is discussed in the following subsection. It is the presence of the switching functions in equations 4 and 5 which distinguishes the reactive force field used in our model from the CVFF force field which is included with Discover 95.

$$S(ij) = \frac{1}{2}(1-\tanh(a(r_{ij}-r_d))), \tag{6}$$

The nonbond potential energy is represented by the Lennard Jones function where r is the distance between nonbonded atoms. No explicit accounting is made for electrostatic interactions or hydrogen bonds in the present version of the model.

$$V_{nb} = \varepsilon[(\frac{r^*}{r})^{12} - 2(\frac{r^*}{r})^6], \tag{7}$$

Reactions

Bond dissociation and formation are simulated in MD_REACT by the following algorithm. A list of the free radical sites, which are generated when bonds in the polymer break, is updated at every time step. These free radicals are eligible to react with each other to form new bonds. The specific criterion used in MD_REACT is that two free radical sites are formed whenever the energy stored in the bond between them approaches the average thermal energy, kT. The program generates a new set of bonds consisting of all possible covalent interactions between the available free radicals and retains those corresponding to the lowest energy subject to the constraints implicit in the valency of the atoms. That is, a section of code is implemented which ensures that there are never more than four bonds to any carbon atom, more than one bond to any hydrogen atom, and so on. Of course, the number of bonds to an atom can, and frequently does, decrease from its maximum value as a result of bond scission reactions. The bond table in Discover 95 is modified and the trajectory of the polymer is updated accordingly.

In this way, the model accounts for many of the reaction pathways which are involved in the thermal degradation of polymers[7]. Some of these reactions are illustrated, using polystyrene as the prototype, in Figure 3. Listed from top to bottom, these include bond scission, depolymerization, intramolecular hydrogen transfer, chain stripping, intramolecular cyclization, intermolecular cross-linking and radical recombination reactions.

Interface

The interface to Discover 95 is established using the IPC protocol developed by MSI. The input file for the Discover 95 run contains a BTCL[8] command string which initializes an IPC connection in server mode and launches MD_REACT as an external process. A series of database operations which identify and replace the high energy bonds are executed at every time step. The energy and forces calculated in Discover 95 do not include the contributions due to the

presence of the switching functions in equations 4 and 5. These corrections are computed in MD_REACT and passed to Discover 95 in the form of a BTCL restraint.

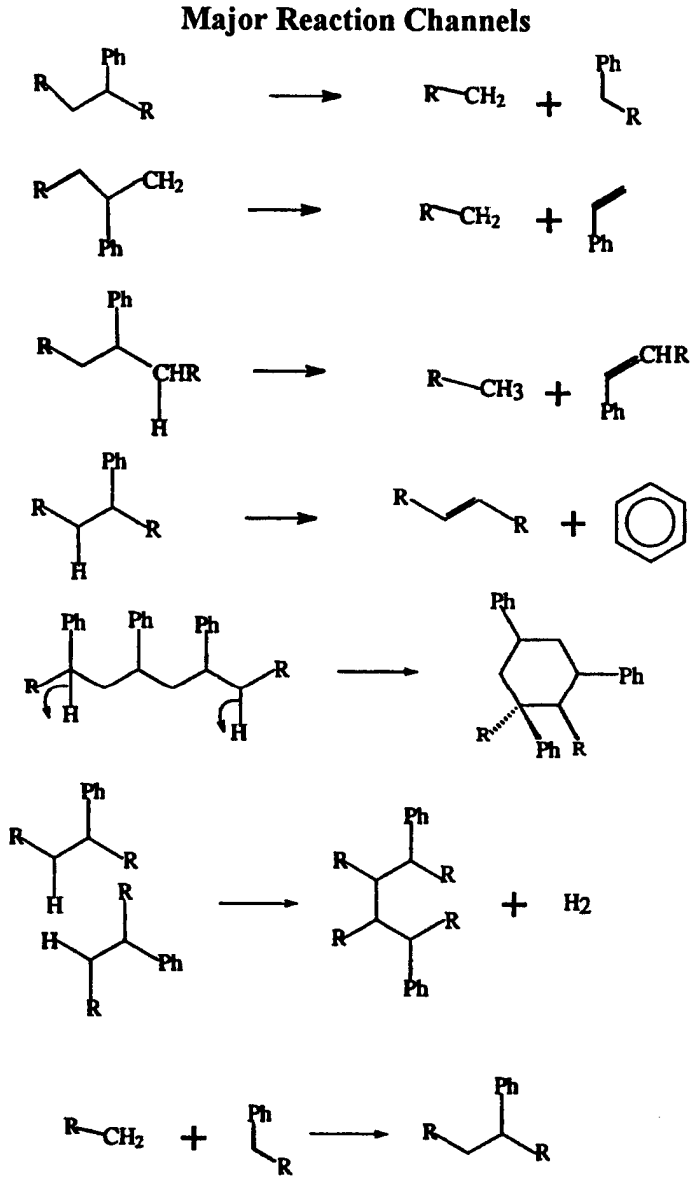

Figure 3. Reaction Channels Used in the Simulations of Thermal Degradation

Periodic Boundary Conditions

MD_REACT was recently upgraded to provide the capability to use periodic boundary conditions. This was implemented by replicating the degrading polymer chains in space (Figure 4), thereby creating ghost atoms, and keeping track of all of the new bonds which form from reactions involving actual free radical fragments and their ghosts. The use of periodic boundary conditions increases the utility of the model by making it possible to maintain realistic densities in simulations of the thermal degradation of isolated chains within the bulk polymer. A new

subroutine which calculates the mass of the residual polymer, which is defined in the code as the mass of the model polymer contained in the mother cell, was also introduced which provides the capability to make quantitative comparisons of thermal stability.

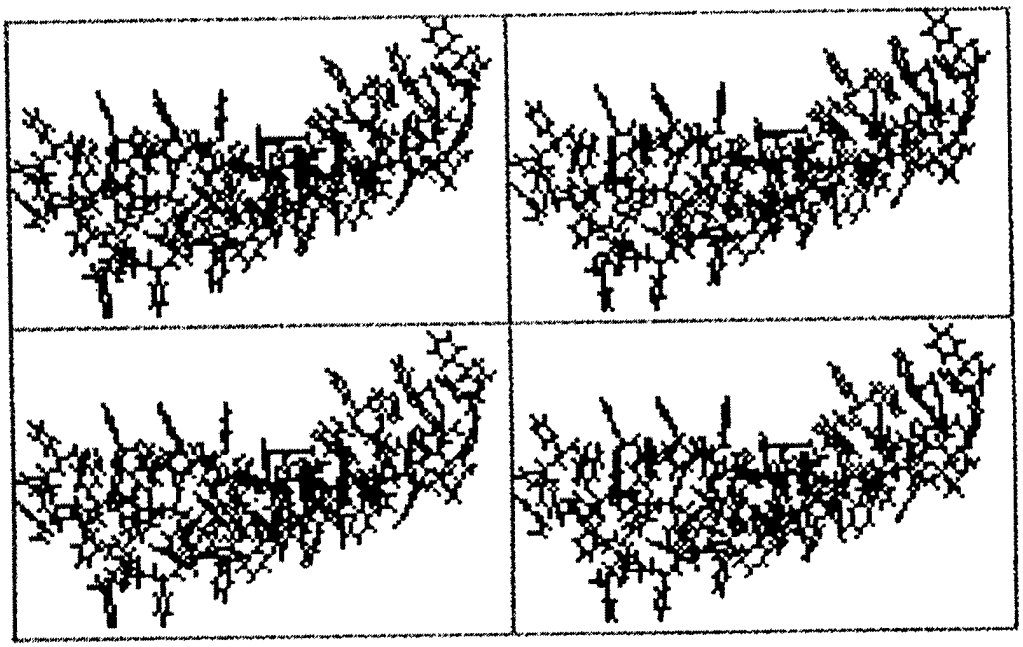

Figure 4. Periodic Display of Polystyrene

COMPUTER EXPERIMENTS

Procedure

The CVFF force field was augmented with new atom types, denoted as ccf for a carbon atom bonded to a free radical site (cf) and ccp corresponding to an aliphatic carbon bonded to an aromatic carbon (cp), to account for the formation of monomers via β-scission and the special stability of benzyl radicals. These atom types were equivalenced to the generic aliphatic carbon atom type (c) for all potential energy terms except bond stretching. The dissociation energies (D) of bonds to ccp atoms were lowered by the resonance stabilization energy of 50 kJ/mol (12 kcal/mol) for each benzyl radical formed[9]. On this basis, the parameters used to represent the dissociation energies of the ccp-ccp and ccp-c bonds were reduced from the CVFF value of 368 kJ/mol for c-c bonds to 268 kJ/mol and 318 kJ/mol, respectively, and the value for ccp-h bonds was reduced from 454 kJ/mol to 404 kJ/mol. The formation of pi bonds during β-scission were modeled by reducing the dissociation energies of c-ccf and h-ccf bonds by 317 kJ/mol (to 51 kJ/mol and 137 kJ/mol, respectively) which corresponds to the difference between a carbon-carbon single and double bond.

Polystyrene

Simulations of thermal degradation were performed on two models of isotactic polystyrene. The models consisted of three chains with 20 styrene monomers in each chain which were

predominately bonded in a head-to-tail fashion (i.e., the phenyl rings were bonded to alternating backbone carbons). The effect of head-to-head bond defects (i.e., phenyl rings bonded to adjacent carbons) was investigated by introducing a total of nine head-to-head bonds (three per chain) in one of the model polymers. The initial geometries were obtained for both models by minimizing the CVFF energies until the maximum derivative was less than 0.001 using the conjugate gradient algorithm in Discover 95.

The simulations of thermal degradation were performed in two steps. First, the model polymers were equilibrated by integrating the equations of motion over a constant temperature path at 1500 K for 0.1 picosecond (100 time steps) using the full CVFF force field with cross terms. The purpose of including cross terms in the equilibration was to facilitate an efficient transfer of thermal energy into the stretching modes which are responsible for bond dissociation. The reactive dynamics were then carried out at constant temperatures of 2000 K, 1000 K, and 500 K for 5.0 picoseconds (5000 time steps) using the reactive force field summarized in equations 2-7.

Polypropylene

The polypropylene model consisted of four chains with 25 monomers in each chain. The initial geometries were obtained, as described above in the case of polystyrene, by minimizing the CVFF energies until the maximum derivative was less than 0.001 using the conjugate gradient algorithm in Discover 95. In this case, the model polymers were equilibrated for 0.045 picosecond at 2500 K, and the reactive dynamics were carried out at 1000 K for 5 picoseconds. A surface, which was constructed by fusing cyclohexanol rings, was introduced in some simulations in order to assess the effect of electrostatic interactions between the polymer and the surface on the thermal degradation of the polymer.

RESULTS

Polystyrene

Displayed in Figure 5 is a still frame from the computer animation of a representative trajectory which indicates the formation of styrene monomers via β-scission and benzyl radicals by dissociation of c-ccp bonds. These and other reactions producing styrene oligomers, toluene, benzene, ethene, and acetylene were observed to occur with regularity in all of the simulations performed in this study. These results are in reasonable accord with experimentally determined product distributions[10].

The presence of the head-to-head bond defects in one of the models was only apparent in the simulations where the reactive dynamics was carried out at 500 K. In this case, the predominant reaction paths involved dissociation of the head-to-head bonds which are by far the weakest bonds in these polymers. This behavior, however, was not observed in the higher temperature simulations.

Polypropylene

These simulations were performed to gain insights into the mechanism of the thermal degradation of polypropylene and of polypropylene in the presence of an interacting surface. On the basis of these simulations, it appears that the initiation reaction is random scission of $CH\text{-}CH_3$ bonds creating secondary free radical fragments (i.e., the free radical site is in the middle of the chain).

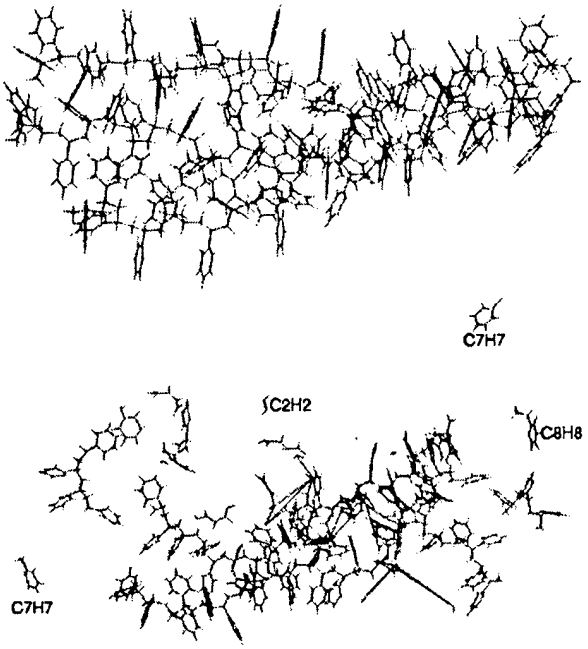

Figure 5. Still Frames From a Computer Animation of a Representative Trajectory Depicting the Structures of Polystyrene at the Onset of the Simulation (top) and After 1200 Time Steps of Reactive Dynamics at 2000 K (bottom)

This is followed either by cross-linking or beta-scission of the chains. The latter process results in the formation of unsaturated molecules and secondary free radical fragments which can either unzip to monomer or transfer hydrogens in the process of forming double bonds. This mechanism is summarized in Figure 6. Suprisingly, our simulations consistently indicate that the presence of surface increases, rather than decreases, the rate of the initiation reaction. However, the surface also appears to facilitate cross-linking, which presumably leads to char, by interfering with the translational movement of some of the larger free radical fragments. In contrast, computer simulations of polyethylene in the presence of the same surface indicate that the initiation reaction in this case is random scission of $CH_2\text{-}CH_2$ bonds which comprise the polymer backbone. This process results in the formation of primary radicals (i.e., the radical sites are on the ends of the chains) which do not cross-link.

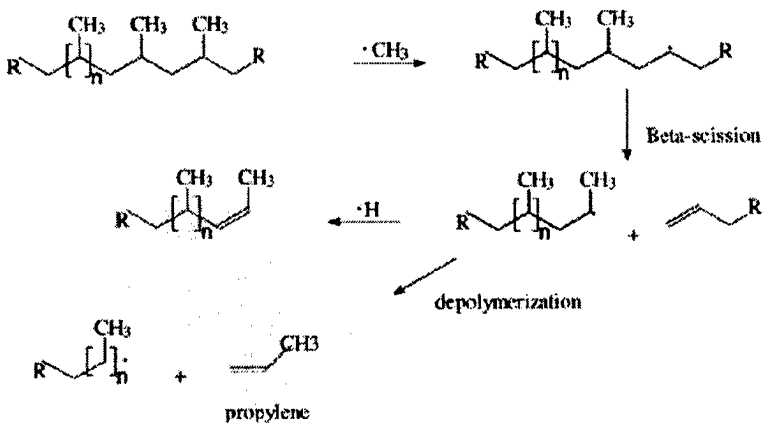

Figure 6. Mechanism of the Thermal Degradation of Polypropylene

SUMMARY AND CONCLUSIONS

A series of computer simulations of the thermal degradation of polystyrene and polypropylene were performed. The major reaction paths observed in the simulated thermal degradation of polystyrene were β-scission producing styrene monomer; random scission resulting in the formation of oligomers; and dissociation of c-ccp bonds yielding benzyl radicals and toluene. The formation of benzene, ethene, and acetylene were also frequently observed. The effect of head-to-head bond defects on the thermal degradation of the model polymers was only apparent in the low-temperature simulations. In the case of polypropylene, the major reaction products were methyl radical, methane, propylene monomer, and unsaturated polymer fragments. The presence of an interacting surface catalyzed initiation, but at the same time, promoted intermolecular cross-linking.

ACKNOWLEDGEMENTS

This paper was based, in part, on work done under a Cooperative Research and Development Agreement between NIST and MSI (CRADA: CN-1241). Partial support for this work was provided by the Federal Aviation Administration under Interagency Agreement DTFA003-92-Z-0018 monitored by Dr. Richard E. Lyon. MRN would like to acknowledge the contribution of David U. Martin who was willing and able to answer all of my questions about BTCL, Discover 95, and the San Diego area while I was a visiting scientist at MSI.

REFERENCES

1. M.R. Nyden and D.W. Noid, Phys. Chem. **95**, 940 (1991).
2. M.R. Nyden, G.P. Forney, and J.E. Brown, Macromolecules **25**, 1658 (1992).
3. M.R. Nyden, J.E. Brown, and S.M. Lomakin, Mat. Res. Soc. Symp. Proc. **278**, 47 (1992).
4. Discover 95, Biosym Solutions, 6 (1995).

5. Certain commercial equipment, instruments, materials, or companies are identified in this paper in order to specify adequately the experimental procedure. This in no way implies endorsement or recommendation by NIST.

6. P. Dauber-Osguthorpe, V.A. Roberts, D.J. Osguthorpe, J. Wolff, M. Genest, and A.T. Hagler, Proteins: Structure, Function and Genetics **4**, 31 (1988).

7. C.F. Cullis and M.M Hirschler, The Combustion of Organic Polymers, Clarendon Press, Oxford, England (1981).

8. Discover User Guide, Part 3, Biosym/MSI, (1995), San Diego.

9. J.B. Pedley, R.D. Naylor, and S.P. Kirby, Thermochemical Data of Organic Compounds, Chapman and Hall, London (1986).

10. S.L. Madorsky, Thermal Degradation of Organic Polymers, John Wiley, New York (1964).

MOLECULAR MODELING AND MICROCALORIMETRY FOR POLYMER PYROLYSIS AND FLAMMABILITY

Phillip R. Westmoreland, Karin Rotem, and Taline Inguilizian
University of Massachusetts Amherst

INTRODUCTION

Computational quantum chemistry is used as a tool to predict thermochemistry and kinetics for new polymers proposed to aid fire resistance of aircraft interiors. The results will be applied in modeling by us and others of the overall process of polymer pyrolysis, ignition, and combustion. *Ab initio* (BAC-MP4 corrections to HF/6-31G*//MP4/6-31G**) and semiempirical (PM3) electronic-structure methods are used. Initial work has focused on effects of chain size and stereoregularity on bond dissociation energies (BDE) in polycarbodiimides. For the base case of $(\text{-CNH -NH-})_n$, the BDE of the C-N bond in the chain was shown to be 85 kcal/mol either for steroregular C=NH side groups or polymer with a back-to-back regularity defect, while a head-to-head defect reduced the BDE by about 6 kcal/mol. Parallel work is beginning on experimental characterization of milligram-sized samples using simultaneous TGA, DSC, and GC/MS analyses, which will be the basis for testing mechanistic models of polymer pyrolysis, flammability, and soot formation.

BACKGROUND

Recent developments in computational chemistry make it possible to determine thermodynamic and kinetic information accurately for a molecule or reaction mechanism. A common practice used to generate rate constants is by analogy for reactions that are too difficult to test experimentally. This project uses available computational tools to determine thermochemistry and kinetics directly, such as heat of formation, absolute entropy, free energy, rate constants, and bond dissociation energies.

When a polymer burns, initially the surface melts and the polymer's weakest bond breaks. This fission can occur in the chain, in fragments bonded to the chain, or between them. If decomposition is instead by concerted reaction yielding only molecular species, it does not cause subsequent free radical reactions. The resulting polymer radical can then beta-scission, abstract, or cross-link[1]. Beta-scissioning is breaking the bond beta to the radical, forming a pi bond in the alpha bond. If it is fast, the polymer chain will unzip into monomer or break off fragments which may burn and form soot in the gas phase. Beta-scission steps with higher activation energies will slow or arrest the polymer degradation. Alternatively, the radical may abstract an atom from elsewhere on the polymer or from another polymer, moving the radical site. Another possibility is combination with another radical or addition to a pi bond, forming a cross-link. Cross-linking gives a higher melt viscosity, which leads to bubbles and a more insulating char.

A polymer's flammability is thus strongly influenced by the ease of the first bond fission. A good measure of this is the bond dissociation energy or enthalpy (BDE), the heat of reaction for bond fission from the molecule into free radicals, AB -> A+B. The activation energy for kinetics of this fission will be approximately the BDE, so a molecule containing only strong bonds requires higher temperatures to break down the structure.

The products of the beta scission are determined largely by relative activation energies, which usually parallel the BDE's but are much lower. Activation energy is normally measured by correlating rate constants with temperature, but it may be calculated from energy of the transition state relative to the decomposing radical. In some cases, the transition-state energy can be estimated by analogy, but theoretical quantum chemistry can increasingly be used to identify the transition state's structure and to compute its energy.

THEORETICAL METHODS USED

The present calculations apply *ab initio* electronic-structure methods to predict thermochemistry and transition-state properties for small model compounds. These results are directly useful, and they also add quantitative accuracy to semiempirical methods used for larger polymer chains.

For *ab initio* calculations, energy is calculated from the Schrödinger equation assuming linear combination of atomic orbitals and the Born-Oppenheimer approximation, geometries are optimized, and frequencies are calculated. The level of theory for these calculations is unrestricted Hartree-Fock with 6-31G(d,p) atomic-orbital basis sets, described in shorthand as a UHF/6-31G* level. Hartree-Fock theory neglects any interaction between electrons in different molecular orbitals. To improve the energy, it is recalculated for the above structure at a higher level of theory that does include electron correlation, unrestricted Møller-Plesset second- or fourth-order perturbation theory, using a larger, more complete basis set (UMP2/6-31G** or UMP4/6-31G** level). The computer code used for these calculations is Gaussian 94[2].

Even at the highest levels of *ab initio* methods, corrections are necessary to obtain suitably accurate thermochemistry. The BAC-MP4 method of Melius is especially effective[3, 5] and is used here. It applies empirical corrections to the electronic energies obtained as described above (UHF/6-31G*//UMP4/6-31G**) based only on the bond length and bonded atoms. Frequencies are corrected by multiplying by 0.89 (a widely accepted amount for HF frequencies), S^{o}_{298} and $C^{o}_{p,298}$ are calculated by statistical mechanics, and high-pressure-limit rate constants are calculated by transition-state theory.

Molecules with more than eight heavy atoms (heavier than H) cannot be analyzed by this method as the MP4 calculation time and storage scales as N_{heavy} to the seventh power. We have tested the polymer calculations on the Cornell Supercomputer Center's SP-2 computer, and a nine-heavy-atom problem (the polycarbodiimide trimer) was estimated to require 2 weeks.

One alternative that is being tested is a new BAC-MP2 method due to Melius[4], based on a UHF/6-31G*//UMP2/6-31G** calculation. Although MP2 is not a high level of theory and thus not as accurate, first indications are that the method yields accurate predictions in far faster times, for example 2 hours instead of 2 weeks.

Our usual alternative for molecules of large sizes is semiempirical molecular-orbital theory at a PM3 level. Good accuracy can be achieved for closed-shell molecules of conventional bonding types. While BDE's necessarily require calculations for free radicals, performing both *ab initio* and semiempirical MO calculations on a few small-model compounds permits calibration of the more approximate semiempirical method.

Quantum-chemical calculations are performed on UNIX workstations (Indigo[2] and Power Indigo[2], Silicon Graphics Inc.). Molecular visualization is by several programs, most notably Cerius[2] (Molecular Simulations Inc.) on the workstations and Ball & Stick[(6)] on the Macintosh.

INITIAL THEORETICAL RESULTS

Initial calculations have focused on the polycarbodiimides being synthesized in the group of Bruce Novak (see Thermally Labile Polymers that Release Radical Traps: Polycarbodiimides). The overall goal is to predict decomposition and flammability behavior, but the three tactical goals are to establish (1) how long the model compound must be to give a satisfactory bond dissociation energy, (2) how does stereoregularity along the polymer chain affect stability of the C-N bonds in the chain as measured by BDE, and (3) how do the groups substituted along the chain affect stability. The first two issues are addressed here.

Polycarbodiimides are made up of -(C=NR)-NR'- repeating groups synthesized from RN=C=NR' monomers. The -(C=NR)- group is flat, and the R's are cis or trans to the -NR'- group. These R's may be pointed all in the same direction along the chain, have a back-to-back symmetry break or defect (two R's trans to the -NR'- between them), have a head-to-head symmetry break (two R's cis to the -NR'- between them), or have a mixture of symmetry breaks, the extreme being a perfectly alternating pattern.

PM3-optimized structures for isolated chains of the 8-mer are shown in Figure 1, where both R and R' are set as H and the polymer ends are capped with H's. While it is not yet clear whether the located structures are the globally optimum structures, some structural predictions are clear. The amine group in the chain is pyramidal at zero K. In small molecules, such a group is dynamically flat, but its inherent nonflatness can be expected to influence the structure of the polymer. Second, the =NH groups tend to be offset as a helix in long steroregular chain segments, but symmetry breaks lead to coiling of steroregular segments. These changes in structure prove to have a small effect on stability of the bond at the symmetry break.

Extensive study of these symmetry effects and chain length is summarized by Figure 1. The BDE of the C-N bond in the chain was shown to be 85 kcal/mol either for steroregular C=NH side groups or for polymer with a back-to-back regularity defect, while a head-to-head defect reduced the BDE by about 6 kcal/mol. There is some variation, but for 4 to 8 mers, the simple bond dissociation energy is free of small-size or large-size interferences from the polymer or the radical; the radical fragments were not constrained to be of the same configuration as in the original polymer, which causes large computational uncertainties here for 10 mers and higher.

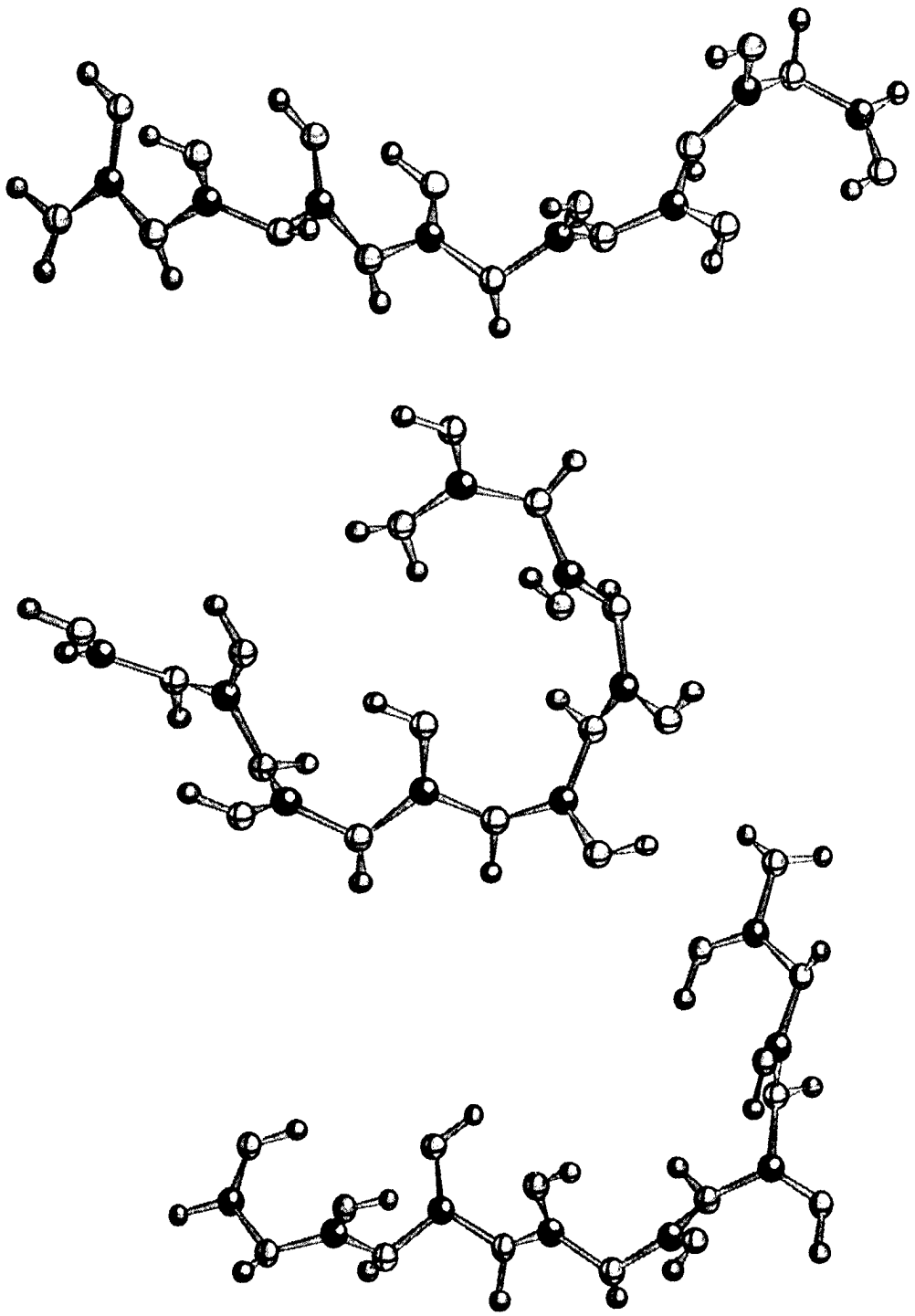

Figure 1. Eight mer of Simple Polycarbodiimide in Stereoregular Configuration (Top), With Back-to-Back Symmetry break (Middle), and With Head-to-Head Symmetry Break (Bottom)

This value compares very well to the *ab initio* result using the dimer. This calculation, which optimized to a back-to-back structure, gave $\Delta H^{\circ}_{f,298}$ of 85.77 kcal/mol. At the same time, it must be noted that the semiempirical $\Delta H^{\circ}_{f,298}$ for the dimer is 71.7 kcal/mol.

Continuing work is examining the effects of changing R and R' from H and extends the work to new polymers. The work will also begin to integrate with new experimental work on pyrolysis of standard and new polymers (described next).

PLANNED MICROCALORIMETRY EXPERIMENTS ON PYROLYSIS AND COMBUSTION

It is increasingly important to link our synthesis, chemical characterization, mechanical characterization, and thermochemical modeling to data on pyrolysis and flammability. The key is to make small-scale measurements of properties that fit directly into flammability models and correlations.

Toward this end, we have identified as especially suitable the data capabilities of creating a combined TGA/DSC/GCMS apparatus. A Rheometrics STA1500 TGA/DSC unit was purchased with non-FAA funds, has been delivered, and soon will be linked to a Hewlett-Packard GC/MS.

The proposed plan of work is as follows:

- Sweep gas flow will be set up and calibrated after Rheometrics and Hewlett-Packard installers set up the TGA/DSC and its GCMS interface.
- Simple flammable reference materials will be characterized experimentally: Low-density polyethylene, high-density polyethylene, and polystyrene.

These polymers will be pyrolyzed in inert gas, yielding simultaneous TGA mass-loss data and DSC heat consumption/generation data. At a predetermined temperature, a gas sample will be injected from the exhaust into the GC sampling valve for GC-MS analysis. By repeating the experiment with sampling at different temperatures, composition of evolved gases will be measured as a function of temperature and heating rate.

- Decomposition onset temperature, total mass loss, and maximum rate of heat consumption will be used to test initial flammability correlations.
- Kinetics correlations will be developed based on statistical models. From the pre-reaction data, we will obtain heat-capacity data for use in flammability models. From the product identities, we will predict soot loadings.

The DSC data mostly reflect kinetics of the initial chain breaking, while the TGA data depend on the depolymerization rate with products being measured by GC/MS. Phase-change effects will be compared using LDPE versus HDPE. A useful method of modeling the respective processes is the classical method of Anthony and Howard (*AIChE J.*, 1976), which analyzed weight-loss data as due to one or more first-order reactions with a Gaussian distribution of activation energies. We would apply this approach to both TGA and DSC data, collected simultaneously, to extract the coupled kinetics. From our molecular modeling, we also propose to estimate kinetics to plug into such a model and be compared.

- New fire-resistant polymers will be characterized in the same way. This technique allows evaluation of small samples such as are generated in the synthesis labs. Application of the data to data-analysis.
- Properties from reference materials will be used to test empirical correlations and develop mechanistic correlations with available flammability tests like cone calorimetry, which require large amounts of sample.

Richard Lyon of the FAA has described a simple but practical new microcalorimeter that will also be useful based on a TGA with continuous analysis of a gas component. We expect that our apparatus with its DSC capability will offer complementary results. By adding an oxygen or CO_2 analyzer for continuous analysis (versus the discrete samples analyzed by GC-MS), we will try to compare the results of the two apparata.

REFERENCES

1. Kashiwagi, T. (1994). *Twenty-Fifth Symp. (Intl.) on Combustion,* 1423.
2. Fritsch, M., *et al.* (1995). "Gaussian 1994," Gaussian, Inc.
3. Melius, C.F. (1990). *Chemistry and Physics of Energetic Materials* (S.U. Bulusu, ed.), Kluwer Academic Publishers: Dorderecht, 21.
4. Melius, C. F. (1996). *Twenty-Sixth Symp. (Intl.) on Combustion,* in press.
5. Melius, C.F. and Binkley, J. S. (1984). *Twentieth Symposium (International) on Combustion,* 575.
6. Müller, N. (1995). "Ball & Stick, Version 3.7," Cherwell Scientific Publishing.

ATOMISTIC MOLECULAR MODELS OF AMORPHOUS POLYBENZOXAZINE AT BULK DENSITY AND AS A THIN FILM

Won-kook Kim and Wayne L. Mattice
Department of Polymer Science
The University of Akron
Akron, OH 44325-3909

ABSTRACT

Polybenzoxazines are attractive materials for applications that require resistance to flame. Fully atomistic molecular models have been constructed and relaxed for amorphous polybenzoxazine at its bulk density of 1.1 g/cm^3. The Hildebrand solubility parameter for the amorphous material is calculated to be 8.3 ± 0.7 (cal/cm^3)$^{1/2}$. About 70% of the phenolic hydroxyl groups act as hydrogen bond donors in the amorphous material. Most of the hydrogen bond acceptors are nitrogen atoms. Intramolecular hydrogen bonds are more prevalent than intermolecular hydrogen bonds. The number of hydrogen bonds is slightly lower in the bulk than in the isolated chain. Fully atomistic models have also been constructed for very thin films, where the surfaces are exposed to a vacuum. The surface layer of the thin films has a thickness that is slightly less than 10 Å. The thin films have surface energies that are calculated to be in the range of 46 ± 6 erg/cm^2.

INTRODUCTION

Polybenzoxazines are potentially useful materials in an environment where resistance to flame is required. In order to understand the molecular basis for their response at temperatures where the potential for thermal degradation exists, we have created and analyzed fully atomistic models for amorphous polybenzoxazine under three conditions:

1. An isolated chain under Θ conditions.
2. An amorphous material at a density of 1.1 g/cm^3.
3. A thin film which presents its surfaces to a vacuum.

The polymer used in this work has a repeating sequence of

$$—C_6H_3(CH_3)(OH)—CH_2—N(CH_3)—CH_2—$$

where the main chain passes through the aromatic unit at positions that are *ortho* to the phenolic hydroxyl group, and the methyl substituent is *para* to this hydroxyl group.

The methodology for the construction of the model for the amorphous polymer at its bulk density of 1.1 g/cm^3 is derived from the procedure introduced by Theodorou and Suter[1] for the

construction of atomistic models of atactic polypropylene at bulk density. Using poly(1,4-cis-butadiene) as their material, Misra et al.[2] showed how similar models can be used as a starting point for the construction of fully atomistic models for the surface presented to a vacuum. Variants of these two methods are employed here.

METHODS

Rotational Isomeric State Model for Polybenzoxazine

The relatively large rigid unit provided by the aromatic ring system and the strong directional interactions provided by hydrogen bonds pose special challenges to the development of well relaxed fully atomistic models of amorphous polybenzoxazine at bulk density. For this reason, special care must be used in the design of the initial conformation of the chain, because subsequent relaxation after the imposition of periodic boundaries cannot be expected to produce large changes in the coordinates of the atoms. We have surmounted this challenge by first developing a rotational isomeric state model for the polybenzoxazine, and then using the rotational isomeric state model for the creation of the initial conformations of the chains that are subjected to relaxation under periodic boundary conditions.

The rotational isomeric state model was designed by calculation and analysis of the conformational energy surface for

$$CH_3—C_6H_3(CH_3)(OH)—CH_2—N(CH_3)—CH_2— C_6H_3(CH_3)(OH)—CH_3$$

using the usual approach[3,4] and including the conformational effects on the main chain that arise from rotation about the C—O bonds, the formation of intramolecular hydrogen bonds, and the instantaneous stereochemistry that arises from the nonplanar arrangement of the three C—N bonds to each nitrogen atom. As expected, the chain has lower unperturbed dimensions when the chirality at the nitrogen atoms is random than when there is an excess of one chirality over the other. The dimensionless characteristic ratio, C_n, defined as

$$C_n \equiv \langle r^2 \rangle_0 / n \langle l^2 \rangle \tag{1}$$

is found to be quite small, due in part to the attractive short-range interaction between the phenolic hydroxyl group and the nitrogen atom. As $n \rightarrow \infty$, the value of C_n approaches a limit of 2.0 when the chain has the most likely distribution of states for the C—O bonds, with random chirality at the nitrogen atoms. Here $\langle r^2 \rangle_0$ denotes the mean square unperturbed end-to-end distance, and $n\langle l^2 \rangle$ is the product of the number of bonds in the main chain and their mean square lengths. This result is important because the small value of C_∞ justifies the use of relatively small periodic cubic amorphous cells, with sides of about 20 Å, for the construction of the fully atomistic models.

The bond probabilities conventionally[3,4] denoted as $q_{\xi\eta;i}$, the pair probabilities denoted as $p_{\xi\eta;i}$, and the conditional probabilities denoted by $q_{\xi\eta;i}$ were constructed and employed in the usual

way[3,4] to generate a few thousand representative unperturbed chains, each with a degree of polymerization of 32 and methyl terminated. Representative chains with end-to-end distances near the average value defined by C_n were selected for the construction of the amorphous cells. One of the chains selected is depicted in Figure 1, along with the periodic box employed in the next section for the construction of the models of the material at bulk density.

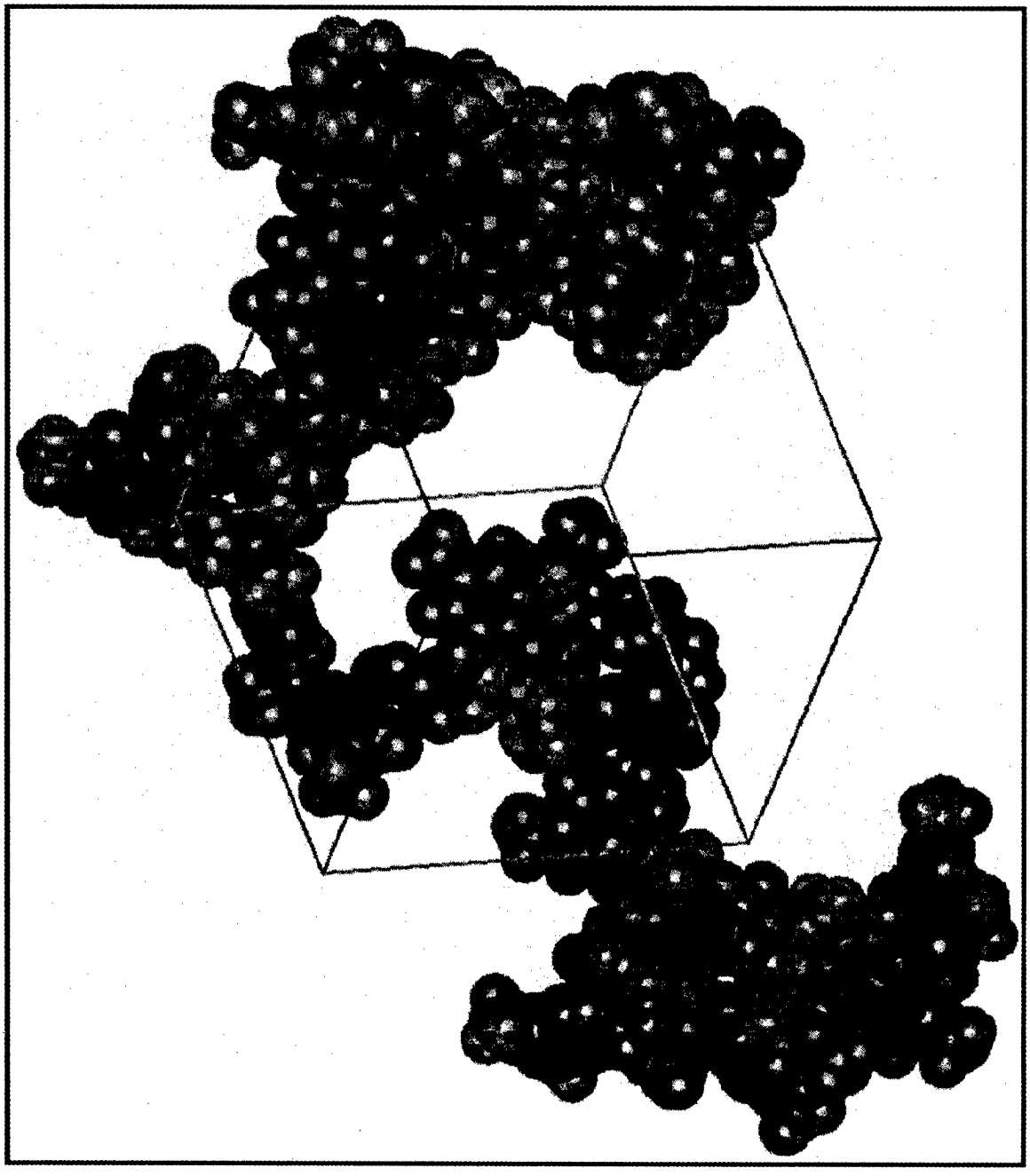

GSC.0034.96-27

Figure 1. A Representative Unperturbed Chain of Polybenzoxazine and the Cubic Box Used for Construction of the Model for the Material at Bulk Density

RESULTS

Amorphous Cells

The amorphous cells are generated using periodic boundary conditions in three dimensions, with a cubic period box selected to produce the target density of 1.1 g/cm^3. Using a method that includes energy minimization and short molecular dynamics runs at 500 K, five independently generated amorphous cells were relaxed to reasonable final energies. Several other starting structures could not be relaxed sufficiently with the computational power available, and these structures were abandoned. One of the fully relaxed amorphous cells is depicted in Figure 2.

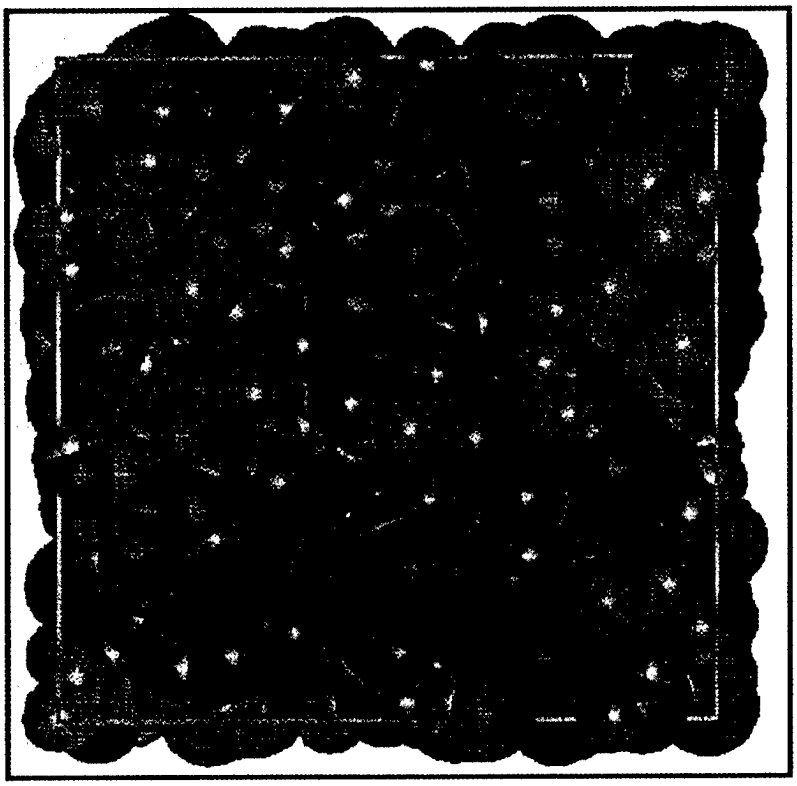

GSC.0034.96-28

Figure 2. A Relaxed Amorphous Cell of Polybenzoxazine at a Density of 1.1 g/cm^3. All atoms are depicted as spheres with full van der Waals radii.

The following properties were deduced from the analysis of the five independently generated amorphous cells.

- The Hildebrand solubility parameter is 8.3 ± 0.7 (cal/cm^3)$^{1/2}$.
- There is a tendency for parallel alignment of two rings if their centers are separated by less than about 5.6 Å, but no preferred orientations are observed if their separation exceeds this value.
- Radial distribution functions and orientational order parameters are those expected for an amorphous system.

- About 70% of the phenolic hydroxyl groups participate in hydrogen bonds as hydrogen bond donors.
- About 70% of the hydrogen bond acceptors are nitrogen atoms, with the remainder of the acceptors being oxygen atoms.
- The number of hydrogen bonds in the relaxed amorphous structure at bulk density is only about 2/3 as large as the number that was present in the initial structure of the isolated parent chain under Θ conditions.
- Most of the hydrogen bonds in the bulk amorphous state are intrachain, rather than interchain.

Thin Film

The thin film with both sides exposed to a vacuum was generated from the amorphous cells by expanding the size of the period box along the z axis and then repeating the relaxation procedure.[2] The surface of one of these thin films is depicted in Figure 3. The density profile shows that most of the decline in the density from a value of about 1.05 g/cm^3 at the midplane to a value near zero takes place over a distance that is about 7 Å, which is similar to the results obtained in prior work on poly(1,4-cis-butadiene)[2] and atactic polypropylene.[5] This distance, over which the density is a strong function of z, defines a width for the surface layer. The surface tension, γ, was evaluated from the difference in energy of the thin films and the amorphous cells and the total surface area of the film using the method of Misra et al.[2]

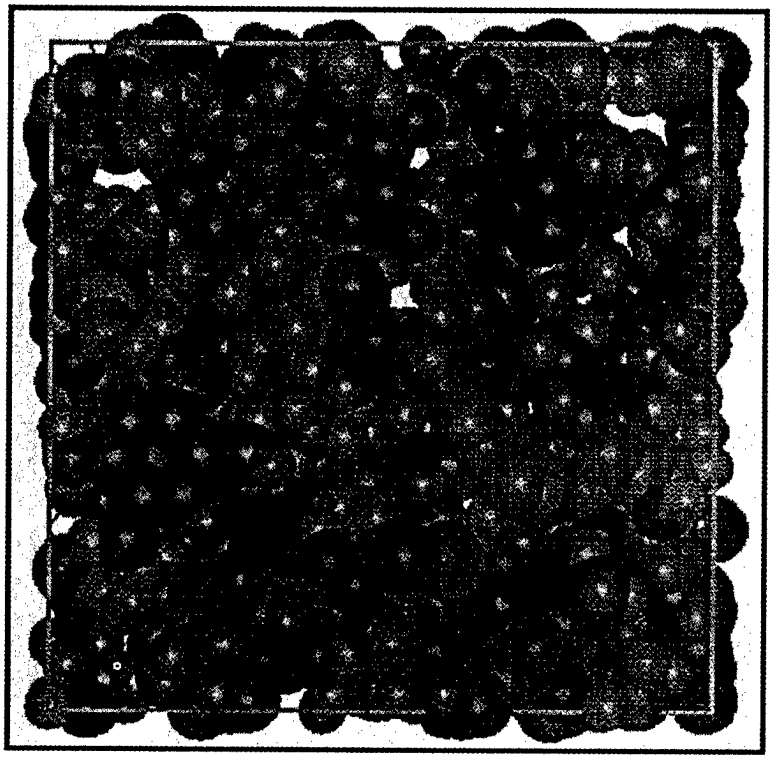

GSC.0034.96-29

Figure 3. The Surface of a Very Thin Film of Polybenzoxazine

$$\gamma = (\langle E_{2D} \rangle - \langle E_{3D} \rangle)/2A \quad (2)$$

Here $\langle E_{2D} \rangle$ and $\langle E_{3D} \rangle$ are the average energies of the thin films and amorphous cells, respectively, and $2A$ is the total surface area of the model for a thin film. (The value of A is the area of the xy surface of the periodic cell.) This method yielded a surface energy of 46 ± 6 erg/cm^2 for polybenzoxazine. As expected, this surface energy is significantly higher than the result of about 26 erg/cm^2 that was obtained for poly(1,4-cis-butadiene) by the same approach[2].

REFERENCES

1. D. N. Theodorou and U. W. Suter, *Macromolecules*, 18, 1467 (1985).
2. S. Misra, P. D. Fleming, III, and W. L. Mattice, *J. Comput.-Aided Mat. Des.*, 2, 101 (1995).
3. P. J. Flory, *Statistical Mechanics of Chain Molecules*, Wiley, New York (1969).
4. W. L. Mattice and U. W. Suter, *Computational Theory of Large Molecules. The Rotational Isomeric State Model in Macromolecular Systems*, Wiley, New York (1994).
5. K. F. Mansfield and D. N. Theodorou, *Macromolecules*, 22, 3143 (1989).

A PYROLYSIS MODEL FOR CHAR-FORMING POLYMERS

Richard E. Lyon
Fire Safety Section, AAR-422
Federal Aviation Administration
William J. Hughes Technical Center
Atlantic City International Airport, N.J. 08405 USA

ABSTRACT

A mass loss model for char-forming polymers is developed from mechanistic pyrolysis kinetics. Under conditions of flaming combustion the coupled rate equations for thermal degradation products and reactants reduce to a single rate law for the residual mass. Exact results are obtained for the mass loss history which include an equilibrium char yield whose value depends only on the relative rates of gas and char formation at a particular temperature. Reaction rate constants for thermolysis of chemical bonds, gas production, and char formation are determinable from parametric fits of the mechanistic charring model to thermogravimetric data. Predictions of the nonisothermal mass loss during constant heating rate experiments are in agreement with experimental data over the expected range of validity.

INTRODUCTION

Full-scale fire tests have demonstrated that the heat release rate of a burning material is the single most important parameter determining its fire hazard in an enclosed environment such as a room[1], submarine[2], rail car[3], or passenger aircraft cabin[4]. Bench-scale fire tests have shown that polymers which form a carbonaceous char during burning have lower ignitability[5] and lower heat release rate than nonchar-forming polymers[6]. Char formation in a fire limits the amount of volatile fuel that can be produced by the burning polymer, provides a thermally insulating layer at the surface to reduce heat transmission into the material, and acts as a diffusion barrier to combustible gases. Despite the empirical relationship between char formation and reduced flammability, mechanistic models for the pyrolysis of char-forming polymers in fires are essentially absent from the literature. The present work addresses the need for a generalized material model which accounts for thermally induced gasification and char formation and which can be evaluated on standard laboratory thermogravimetric equipment. It is hoped that these preliminary results will provide insight into the solid-state thermochemical processes involved in polymer combustion and help guide the search for fire-resistant materials for next generation aircraft interiors.

BACKGROUND

The steps involved in the flaming combustion of solid polymers are described schematically in Figure 1 after Troitzsch[7]. Flaming combustion is initiated by three coupled processes: heating of the polymer, thermal decomposition/pyrolysis, and ignition of the gaseous decomposition products. An ignition source or thermal feedback of radiant energy from the flame supplies heat to the polymer surface which causes thermolytic cleavage of primary chemical bonds in the polymer molecules. Combustible and noncombustible gaseous pyrolysis products mix and react with air in the combustion zone above the surface releasing heat during the production of carbon dioxide, water, and incomplete combustion products such as carbon monoxide and soot.

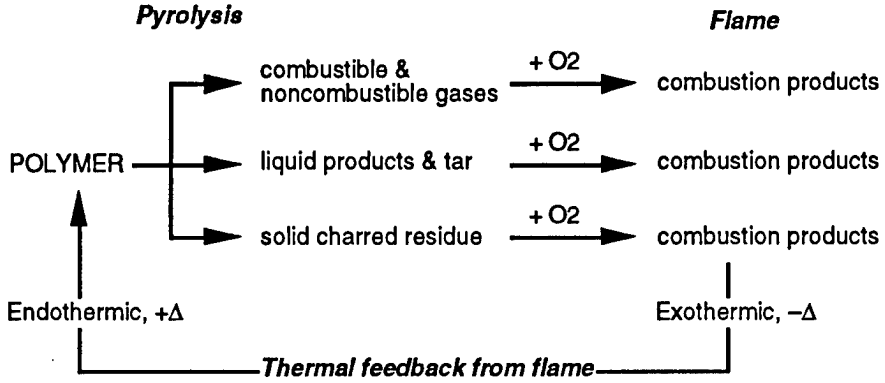

Figure 1. Schematic of the Combustion Process of Solid Polymers, After Reference 1

Figure 1 provides a phenomenological scheme of the combustion process from which a mechanistic kinetic model for polymer combustion can be developed if a pyrolysis mechanism is available which includes all of the relevant species, i.e., gas, tar, and char. The basic thermal degradation mechanism of char-forming polymers has been described as a generalized chemical bond scission process consisting of primary and secondary decomposition events[8-10] as shown schematically in Figure 2. The primary decomposition step occurs by main-, end-, or side-chain scission to form free radical intermediates with subsequent intramolecular and intermolecular hydrogen transfer leading to a primary gas and tar and a hydrogen-deficient primary char residue. The primary char decomposes by dehydrogenation to form the secondary gas and a

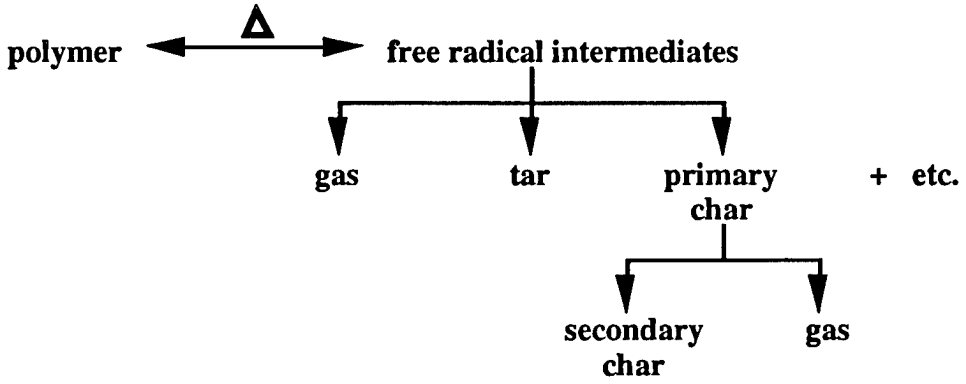

Figure 2. Schematic Representation of Primary and Secondary Decomposition Process in Polymer Pyrolysis

thermally stable secondary char. This pyrolysis scheme accounts qualitatively for the low char yield of hydrogen-rich polymers where hydrogen abstraction occurs readily leading to a preponderance of hydrogenated, low molecular weight volatile species. In the absence of hydrogen atoms, polyaromatic free radical nuclei can recombine to form cross-links or stable, nonvolatile species which resist further decomposition.

PYROLYSIS MODEL

The reactions in the thermal degradation model of Figure 2 are given by equations 1-5. Equations 6-8 extend the anaerobic model to include generalized bulk and surface oxidation reactions in the presence of oxygen which are important to long-term thermoxidative stability and smoldering combustion. In this set of reactions, P is the polymer, I* is the reactive intermediate, G1 and C1 are the primary gas/tar and char, and G2 and C2 are the secondary gas and char. Solid-state bulk and surface oxidation reaction products for the intermediate, primary char, and secondary char are denoted, I^*O_2, $C1O_2$, and $C2O_2$, respectively.

$$P \underset{k_{-p}}{\overset{k_p}{\rightleftharpoons}} I^* \tag{1}$$

$$I^* \xrightarrow{k_{g1}} G1 \tag{2}$$

$$I^* \xrightarrow{k_{c1}} C1 \tag{3}$$

$$C1 \xrightarrow{k_{g2}} G2 \tag{4}$$

$$C1 \xrightarrow{k_{c2}} C2 \tag{5}$$

$$I^* + O_2 \xrightarrow{k_{I^*O}} I^*O_2 \tag{6}$$

$$C1 + O_2 \xrightarrow{k_{c1O}} C1O_2 \tag{7}$$

$$C2 + O_2 \xrightarrow{k_{c2O}} C2O_2 \tag{8}$$

In equations 1-8, k_p and k_{-p} are the rate constants for the forward and reverse polymer dissociation steps, respectively; k_{g1} and k_{c1} are rate constants for primary gas/tar and char

formation; k_{g2} and k_{c2} are the rate constants for secondary gas and char formation; and k_{I^*O}, k_{c1O}, and k_{c2O} are the rate constants for the oxidation reactions of the intermediate species, primary, and secondary chars in the solid state. Although equations 1-8 represent a highly simplified set of reactions and products, the resulting system of rate equations is highly coupled and an analytic solution in terms of the overall sample mass is impossible.

The objective of the present work is to develop a kinetic model of polymer combustion in terms of mechanisms that are important in the burning process, i.e., generation of combustible gases and char formation, but which can be solved for the overall mass loss history of the specimen for verification using laboratory thermogravimetric techniques. Consequently, assumptions will be made about the process of polymer thermal degradation which are relevant to flaming combustion and which will reduce equations 1-8 to a tractable set. The following are proposed:

Assumption A: Thermal dissociation of the polymer is the rate limiting step in polymer combustion, i.e., $P \rightarrow I^*$ is slow compared to the $I^* \rightarrow G1$ and $I^* \rightarrow C1$ reactions to form primary gas and char[11].

Assumption B: The intermediate I* generated in the polymer dissociation step is in dynamic equilibrium with the parent polymer but is consumed in the process of gas and char formation such that its concentration never becomes appreciable and decreases slowly over time as the polymer is consumed. Consequently, the rate of change of I* with time is insignificant compared to the rate of polymer consumption, gas production, and char formation so that for computational purposes $dI^*/dt = 0$. This is the stationary-state hypothesis.

Assumption C: Thermal decomposition of primary char to secondary char and gas, i.e., $C1 \rightarrow C2$ and $C1 \rightarrow G2$ is slow compared to the formation of the primary char $I^* \rightarrow C1$ at typical flaming surface temperatures of 350-600°C. Consequently, only the primary char is considered in formulating the reaction set for the mass loss model.

Assumption D: The thermo-oxidative environment in the pyrolysis zone of a burning solid polymer is anaerobic. Dissolved molecular oxygen and oxygen diffusion into the pyrolysis zone of the solid are considered negligible with respect to their effects on gas and char formation so that equations 6-8 can be neglected in the kinetic model of polymer combustion. This assumption does not preclude the possibility of surface mass loss due thermo-oxidative reactions at the polymer-air interface, e.g., thermogravimetric (TGA) experiments conducted in air or smoldering fires.

In combination with the generalized combustion and pyrolysis schemes of Figures 1 and 2, assumptions A-D lead to a simplified mass loss model for polymer combustion which is shown in Figure 3. This simplified scheme reduces gas and char formation to a single step involving parallel reactions of the active intermediate, I*.

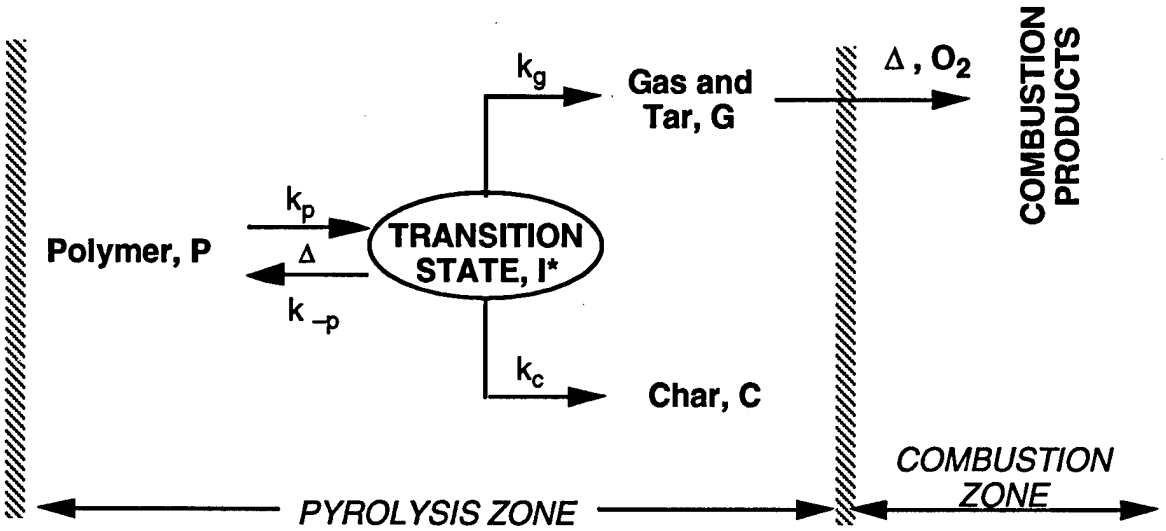

Figure 3. Kinetic Model for Polymer Combustion

The reduced reaction set becomes:

$$P \underset{k_{-p}}{\overset{k_p}{\rightleftharpoons}} I^* \tag{1}$$

$$I^* \xrightarrow{k_g} G \tag{9}$$

$$I^* \xrightarrow{k_c} C \tag{10}$$

and the system of rate equations for the species is

$$\frac{dP}{dt} = -k_p P + k_{-p} I^* \tag{11}$$

$$\frac{dI^*}{dt} = k_p P - \left(k_{-p} + k_g + k_c\right) I^* \tag{12}$$

$$\frac{dG}{dt} = k_g I^* \tag{13}$$

$$\frac{dC}{dt} = k_c I^* \tag{14}$$

According to the stationary-state hypothesis (Assumption B), $dI^*/dt = 0$ so that equation 12 provides the useful result

$$I^* = \left[\frac{k_p}{k_{-p} + k_g + k_c}\right] P = k^* P \tag{15}$$

Substituting $I^* = k^*P$ from equation 15 into equations 11, 13, and 14

$$\frac{dP}{dt} = -\left[k_p - k^*k_{-p}\right]P \tag{16}$$

$$\frac{dG}{dt} = k_g k^* P \tag{17}$$

$$\frac{dC}{dt} = k_c k^* P \tag{18}$$

With $I^* << P$, G, and C, the total mass balance in terms of the initial mass, m_o, is

$$m_o = P + G + C + I^* \approx P + G + C \tag{19}$$

from which with equation 16

$$\frac{dP}{dt} = -\frac{dC}{dt} - \frac{dG}{dt} = -\left[k_p - k^*k_{-p}\right]P \tag{20}$$

The sensible mass of the sample as measured, for example, in a TGA experiment or fire calorimeter test is

$$m = P + C + I^* \approx P + C \tag{21}$$

from which with equations 17 and 20

$$\frac{dm}{dt} = \frac{dP}{dt} + \frac{dC}{dt} = -\frac{dG}{dt} = -k^*k_g P \tag{22}$$

Equation 16 can be solved immediately for P for the initial condition $P = P_o = m_o$ @ $t = 0$ with the result

$$P = m_o \exp\left(-\left[k_p - k^*k_{-p}\right]t\right) \tag{23}$$

Substituting this result for P into equation 22 and separating variables

$$\int_{m_o}^{m} dm' = -\int_0^t k^*k_g m_o \exp\left(-\left[k_p - k^*k_{-p}\right]\tau\right) d\tau \tag{24}$$

the result is

$$\frac{m}{m_o} = 1 - \left[\frac{k_g}{k_g + k_c}\right]\left\{1 - \exp\left(-\left[k_p - k^*k_{-p}\right]t\right)\right\} \tag{25}$$

Equation 25 shows that at infinite time the residual mass approaches an equilibrium value at constant temperature given by

$$\frac{m(\infty)}{m_o} = \left[\frac{k_c}{k_g + k_c}\right] \equiv Y_c \tag{26}$$

where Y_c is the temperature-dependent, equilibrium char yield. Equation 25 can be further simplified by substituting the result

$$k_p - k^* k_{-p} = k_p \left[\frac{k_g + k_c}{k_{-p} + k_g + k_c}\right] \approx k_p \tag{27}$$

for the time coefficient in the exponential term since by Assumption A, $k_{-p} << k_g, k_c$. Substituting equations 26 and 27 into equation 25 yields the final result for the isothermal mass loss history

$$\frac{m}{m_o} = Y_c + (1 - Y_c)\exp(-k_p t) \tag{28}$$

Equation 28 predicts a finite char yield at infinite time if $k_c > 0$ and zero char if $k_c = 0$. The prediction of an equilibrium anaerobic char yield using mechanistic kinetics is consistent with the use of group contributions for the char-forming tendency of polymers to calculate polymer char yield at a particular temperature[8]. Equation 28 also describes the mass loss history of filled polymer systems having an inert filler loading fraction Y_c.

COMPARISON OF PYROLYSIS MODEL TO EXPERIMENT

Equation 28 was used to fit thermogravimetric data for anaerobic, isothermal, mass loss histories at temperatures ranging from 350-450°C for a cross-linked phenolic triazine thermoset resin[12,13]. Experimental data for the isothermal mass loss histories are shown as solid symbols in Figure 4. Solid lines are the best fit of equation 28 to the experimental data using k_p and Y_c as adjustable parameters. Table 1 lists values for k_p and Y_c obtained from the fit of equation 28 to experimental data in Figure 4.

Figure 5 is an Arrhenius plot: $\ln(k_p) = \ln(A) - E_a/RT$ of the T and k_p values in Table-1. The slope is E_a/R from which the activation energy is found to be E_a = 165 kJ/mol. The intercept is the natural logarithm of the frequency factor $A = 10^9$ sec^{-1} for pyrolysis of the phenolic triazine.

It is important to recognize that both the activation energy and the frequency factor for pyrolysis obtained from the loss model for char-forming polymers (equation 28) are significantly lower than values for these parameters obtained using generalized methods for analysis of thermogravimetric data which do not recognize an inert mass component such as char or fillers[14]. In particular, the rate constant at any temperature for the charring model is on the order of the square root of the rate constant for a noncharring model. Consequently, the activation energy for pyrolysis of phenolic triazine resin obtained in the present work (E_a = 165 kJ/mol) is approximately one-half of the value obtained from the same data using generalized (n-th order) models[13] while the char model frequency factor ($A = 10^9$ sec^{-1}) is smaller by a factor of 10^9 sec^{-1}.

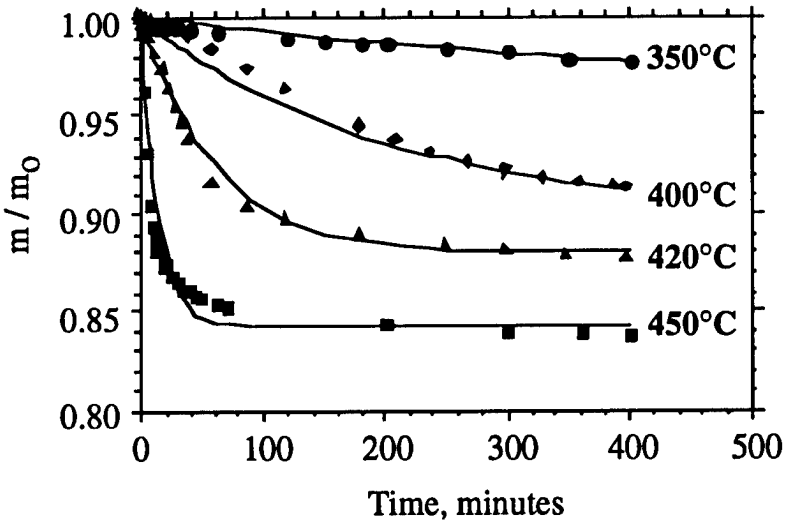

Figure 4. Measured and Calculated Isothermal Mass Loss Histories at Indicated Temperatures for Phenolic Triazine Resin (Solid lines are fit of equation 28.)

Table 1. Best Fit k_p and Y_c Values for Phenolic Triazine Thermoset Resin

T (°C)	k_p (sec^{-1})	Y_c
350	1.4×10^{-5}	0.92
400	8.5×10^{-5}	0.90
420	2.7×10^{-4}	0.88
450	1.2×10^{-3}	0.84

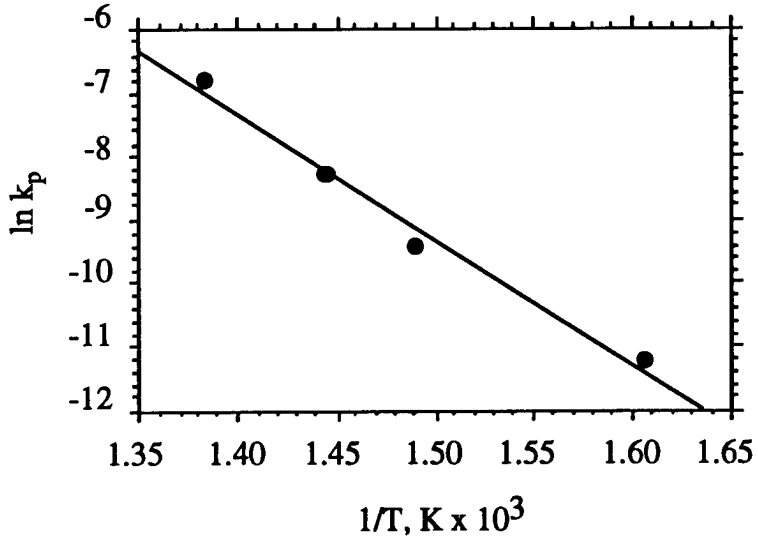

Figure 5. Plot of the Natural Logarithm of k_p Versus Reciprocal Temperature for Phenolic Triazine Resin

Assuming an Arrhenius form for k_g and k_c, equation 26 can be rearranged to give

$$\ln\left[\frac{1-Y_c}{Y_c}\right] = \ln\left[\frac{A_g}{A_c}\right] - \left[\frac{E_g - E_c}{R}\right]\frac{1}{T} \tag{29}$$

so that a plot of $\ln[(1-Y_c)/Y_c]$ versus 1/T has a slope proportional to the difference in activation energies for gas and char formation. Figure 6 shows such a plot constructed from the isothermal char yields in Table 1. The slope gives $(E_g - E_c) = +30$ kJ/mol and the intercept $A_g/A_c = 17$. This result indicates that even though the molecular collision frequency leading to gas production is seventeen times greater than for char formation, char formation has a lower activation energy by 30 kJ/mol. These results substituted into equation 26 allow calculation of the equilibrium char yield as function of temperature.

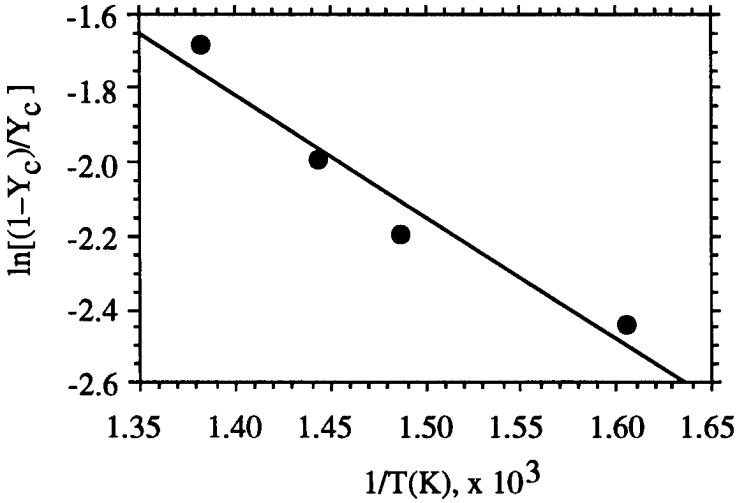

Figure 6. Plot of the Natural Logarithm of $(1-Y_c)/Y_cV$ versus Reciprocal Temperature for the Phenolic Triazine Resin

While estimation of the material parameters governing polymer pyrolysis is best accomplished under isothermal conditions as above, many processes of interest such as the production of combustible gases in a fire occur at finite heating rates. Consequently it is important to be able to predict mass loss under dynamic heating conditions. A constant rate, $\beta = dT/dt$, transforms the independent variable in equation 28 from time to temperature but only a series solution is possible for the integral (14), which for the present case is approximated by

$$\frac{m(T)}{m_o} = Y_c + (1 - Y_c)\exp\left[\frac{-A}{\beta}(T - T_o)e^{-E_a/RT}\right] \tag{30}$$

The predicted mass loss of the phenolic triazine resin at constant heating rates of $\beta = 1$, 5, and 20 K/min calculated from equation 30 is compared to thermogravimetric data in Figure 7. The parametrically determined $A = 10^9$ sec^{-1}, $E_a = 165$ kJ/mol, and the calculated $Y_c(T_{max})$ were used in the calculations. Solid symbols are the thermogravimetric data at the indicated heating rates.

Solid lines are the predictions of equation 30 for those same heating rates, and the dotted line is the calculated equilibrium char yield ($\beta = 0$).

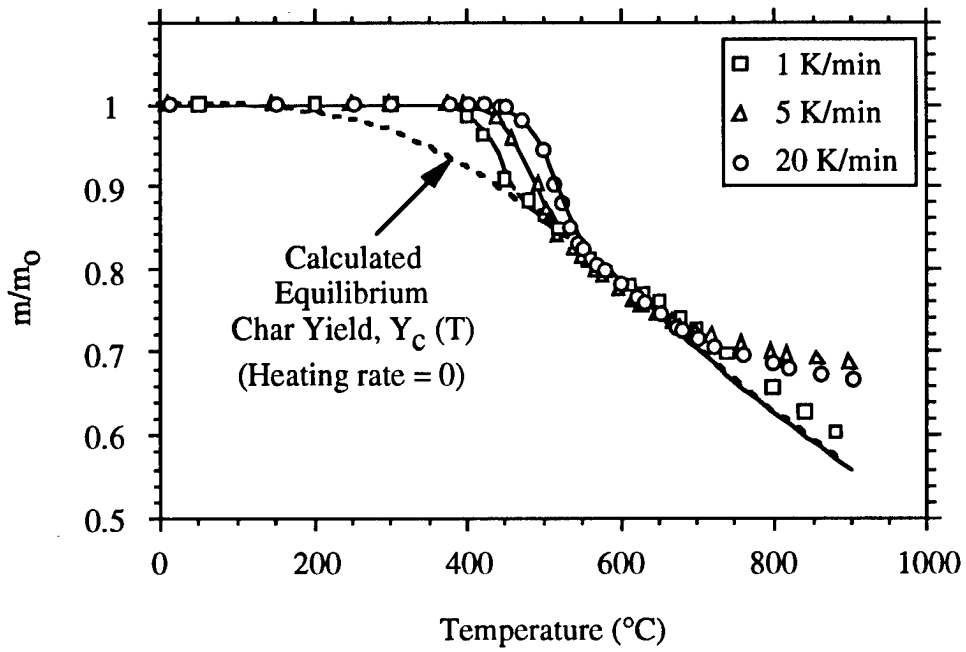

Figure 7. Comparison of Measured and Calculated Mass Loss of Phenolic Triazine Resin in Thermogravimetric Analyses at Constant Heating Rates of β =1, 5, and 20 K/min. Solid lines are fit of equation 30 to experimental data for indicated heating rates. Dotted line is equilibrium char yield versus temperature.

Agreement between the measured and calculated residual mass of the phenolic triazine resin in the scanning TGA experiments is generally good for temperatures below about 600°C as shown in Figure 7. It is seen that the residual mass exceeds the equilibrium char yield at temperatures below about 400°C and that the magnitude of this effect is heating rate dependent. At high temperatures the calculated residual mass and char yield are coincident but underpredict the experimental data. Lack of agreement between the model and the experimental data at high temperatures is a result of neglecting secondary char formation in the simplified mass loss model which considered only the primary processes of char and gas formation.

Mass loss calculations for five decades of heating rate are shown in Figure 8. Heating rates of $\beta \approx 10 - 100$ K/s are characteristic of a burning polymer in a fire[15]. Figure 8 shows that both the peak decomposition temperature and the volatile mass fraction at the decomposition temperature increase significantly for a charring polymer with increasing heating rate as the material becomes essentially superheated. From equation 30 the mass loss rate for $Y_c(T) = \mu$ $Y_c(T_p) = \mu$

$$\frac{-1}{m_o}\frac{dm}{dt} = (1-\mu)\,k_p(T)\left(1+\frac{(T-T_o)}{RT^2}E_a\right)\exp\left[\frac{-(T-T_o)}{\beta}k_p\right] \qquad (31)$$

where $\Delta E = E_g - E_c$ is the energy barrier to gas formation. The maximum mass loss rate during a linear temperature ramp, $\beta = dT/dt$, is obtained by setting the derivative of equation 31 to zero. The approximate result for the maximum mass loss rate of char-forming polymers is

$$\left.\frac{-1}{m_o}\frac{dm}{dt}\right|_{T_{max}} \approx (1 - Y_c)\frac{\beta E_a}{eRT_{max}^2} \tag{32}$$

where Y_c is the equilibrium char yield at the peak mass loss rate (pyrolysis) temperature, T_{max}. According to the char model the peak mass loss rate increases in proportion to the instantaneous volatile fraction, $1-Y_c$, at the decomposition temperature of the polymer. Comparison of equation 32 to the peak mass loss rate for the first-order decomposition of a nonchar-forming polymer

$$\left.\frac{-1}{m_o}\frac{dm}{dt}\right|_{T_{max}} \approx \frac{\beta E_a}{eRT_{max}^2} \tag{33}$$

shows that peak mass loss rate for the char model reduces to the first-order kinetic result when $Y_c = 0$.

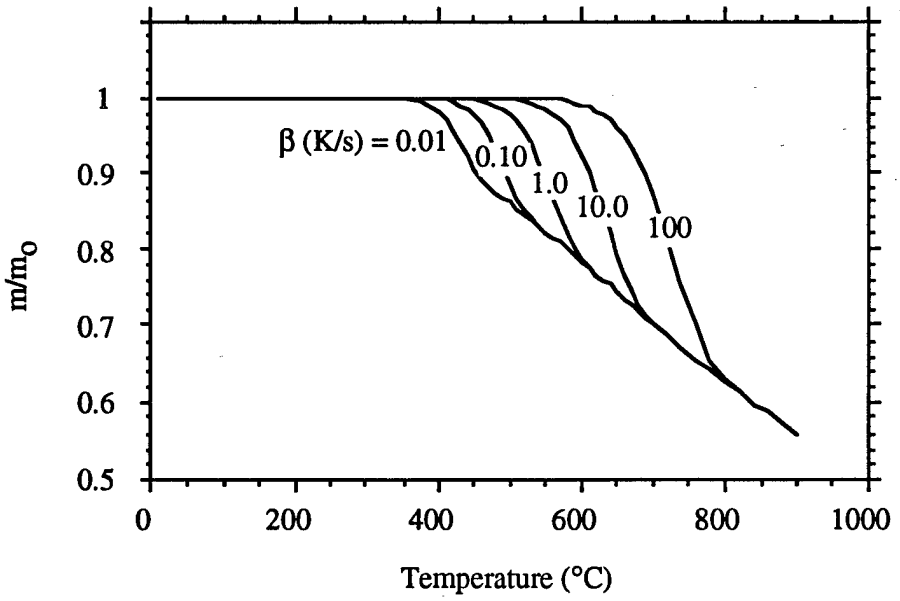

Figure 8. Mass Loss Calculations for Phenolic Triazine Resin for Five Decades of Heating Rate

CONCLUSIONS

The objective of this work was to develop a mass loss model for pyrolysis of char-forming polymers which was amenable to laboratory evaluation on conventional thermogravimetric equipment and mechanistically based to provide insight into the fuel generation processes of these materials in fires. The coupled rate equations for thermal degradation products and reactants

reduced to a single first-order rate law for the isothermal mass by assuming (1) thermolysis of primary chemical bonds in the polymer is the rate-limiting step, (2) mass loss proceeds through an active intermediate which is a stationary state, (3) primary gas production and char formation are competing processes whose magnitude and rate constants are large compared to successive products and rate processes, and (4) conditions are anaerobic. Exact results were obtained for the isothermal mass loss history of a char-forming polymer which included an equilibrium char yield whose value depends only on the relative rates of gas and char formation at a particular temperature. Comparison of the model prediction with the measured mass loss history of a phenolic triazine thermosetting resin in temperature scanning thermogravimetric experiments showed excellent agreement for the primary thermal decomposition step. Of particular significance was the large discrepancy between kinetic parameters determined by fitting experimental mass loss data to the mechanistic charring model and those obtained by fitting the same data with generalized n-th order kinetic models which do not recognize char formation explicitly. It is concluded that activation energies and frequency factors which have been determined for char-forming or filled polymers using generalized n-th order kinetics may be in serious error.

REFERENCES

1. V. Babrauskas and R.D. Peacock, "Heat Release Rate: The Single Most Important Variable in Fire Hazard," Fire Safety Journal, 18, 255-272 (1992).
2. Demarco, R.A. (1991), "Composite Applications at Sea: Fire Related Issues," *Proc. 36th Int'l. SAMPE Symposium*, April 15-18, pp. 1928-1938.
3. Hathaway, W.T. (1991), "Fire Safety in Mass Transit Vehicle Materials," *Proc. 36th Int'l. SAMPE Symposium*, April 15-18, pp. 1900-1915.
4. R.G. Hill, T.I. Eklund, and C.P.Sarkos (1985), "Aircraft Interior Panel Test Criteria Derived from Full-Scale Fire Tests," DOT/FAA/CT-85/23.
5. D.W. Van Krevelen, Properties of Polymers, Elsevier Scientific, NY, 1976, Ch. 26B, "Polymer Flammability."
6. W. Bassett, "Flame-Retardant Thermoplastic Materials for Aircraft Interiors," Proc. Fire-Retardant Chemicals Association Meeting, San Antonio, TX, March 12-15, 1989.
7. J. Troitzsch, International Plastics Flammability Handbook, 2nd Edition, Hanser Publishers, Munich Germany, 1990, Chapter 4.
8. D.W. Van Krevelen, op. cit., Ch. 21, "Thermal Decomposition."
9. P.M.J. Wolfs, D.W. Van Krevelen, and H.I. Waterman, *Brennstoff Chemie*, 40, p. 155 (1959).
10. P. Carty and S. White, "Char Formation in Polymer Blends," *Polymer*, 35(2), 343 (1994).
11. L.A. Wall, "Pyrolysis of Polymers," Flammability of Solid Plastics, Fire and Flammability Series, Vol. 7, Technomic Publ., Westport, CT, 1974, pp. 323-352.

12. R.E. Lyon, F.E. Arnold, J. Rodriguez-Arnold, A. Granville, and S. Das, "Additive Approaches to Improved Fire-Resistance of Cyanate Ester Resins," Fire-Retardant Chemicals Association Meeting, Williamsburg, VA, October 9-12, 1994.

13. J. Rodriguez-Arnold, F.E. Arnold, Jr., and R.E. Lyon, "Thermal Degradation Kinetics of Cyanate Ester Resins," *Thermochimica Acta* (in press).

14. J.H. Flynn and L.A. Wall, "General Treatment of the Thermogravimetry of Polymers," Journal of Research of the National Bureau of Standards–A, Physics and Chemistry, 70A(6) (1966).

15. C.L. Beyler and M.M. Hirschler, "Thermal Decomposition of Polymers," SFPE Handbook of Fire Protection Engineering, 2nd Edition, National Fire Protection Association, Boston, MA, Section 1.1.7, 1995.

COMPUTATIONAL MODEL OF INTUMESCENT CHAR FORMATION*

Kathryn M. Butler
Building and Fire Research Laboratory
National Institute of Standards and Technology
Gaithersburg, MD 20899

ABSTRACT

An intumescent layer protects the underlying surface from fire through the development of a thick char barrier in the presence of excessive heat. The effectiveness of these materials relies on the timing of certain critical chemical events. A three-dimensional numerical model that takes into account bubble hydrodynamics, heat transfer, and chemical reactions is being developed to aid in the design of these materials. The approach and implementation of this model are described and demonstrated.

INTRODUCTION

Intumescent materials provide a thermal and physical barrier to block the high temperatures and rapid flame spread of fires. During exposure to a fire, the temperature within these materials rises, causing melting of the thermoplastic binder. When the temperature corresponds to an appropriate value for the viscosity of the melt, an endothermic gas-producing chemical reaction is triggered. The gas collects in small bubbles, causing the material to swell. Solidification into a thick multicellular char provides an insulating layer that slows the transport of heat and reduces the amount of material that becomes involved in the fire[1]. Intumescent fire retardants have a significant environmental advantage over widely used halogen-based materials, which are effective but tend to produce corrosive and toxic gases upon burning.

Careful design is required to ensure that the events described above occur in the proper order and with the proper timing, since these factors are critical to the protective qualities of the final char. If the blowing agent decomposes before the thermoplastic binder has reached the proper melt viscosity, the resistance to bubble formation will prevent the swelling action. If the blowing agent decomposes too late, large bubbles will be produced, resulting in a fragile char.

Development of intumescent materials has progressed through an empirical approach. A number of successful chemical formulations for protective coatings have been designed over the last 5

* *This material was presented under the title Three-Dimensional Modeling of Intumescent Materials at the ANTEC '96 conference sponsored by the Society of Plastics Engineers, Indianapolis, Indiana, 5-10 May 1996.*

decades, and recent development work has concentrated on intumescent systems as additives to polymeric material[2] and on intumescent properties of certain copolymers. However, our understanding of the physical and chemical mechanisms of intumescence is still quite limited.

Previous models have dealt with intumescent behavior as a problem in one-dimensional heat transfer, with the physical properties of the intumescent layer changing as a function of time to reflect swelling and outgassing[3-6]. In these models, as in a recent three-dimensional model of intumescent seals[7], the rate of expansion is entered as an input quantity. Although these models have assisted in understanding the mechanisms providing thermal protection, they are unable to provide insight into either the complicated sequence of physical, chemical, and thermal events that characterize intumescent behavior or the effect of material properties on performance.

This paper reports on the current stage of development of a three-dimensional model that incorporates bubble and melt hydrodynamics, heat transfer, and chemical reactions to improve our understanding of intumescent mechanisms. The system is modeled as a highly viscous fluid containing a large number of expanding bubbles. The bubbles obey equations of mass, momentum, and energy on an individual basis according to the values of local parameters, and their collective behavior is responsible for the swelling and fire-retardant properties of the material on a global scale. Approximate analytical solutions are sought to enable calculations for approximately 10,000 bubbles on an engineering workstation.

RESULTS AND DISCUSSION

Hydrodynamics Submodel

The intumescent sample is described as an incompressible fluid whose viscosity is a function of temperature. Initially, the sample is a rectangular solid containing a large number (up to 10,000) of infinitesimally small bubble nucleation sites randomly distributed throughout the volume. At time t=0, a specified heat flux is applied to the upper surface of the sample. The energy equation is solved to determine the temperature field in the sample. When the temperature at a given nucleation site exceeds the degradation temperature of the blowing agent, gas is produced, and the bubble begins to grow.

The geometry of a bubble expanding in a local temperature gradient is illustrated in Figure 1. Each expanding bubble experiences forces due to gravity, to gradients of viscosity and surface tension over its surface due to the temperature gradient, and to the motions of other bubbles.

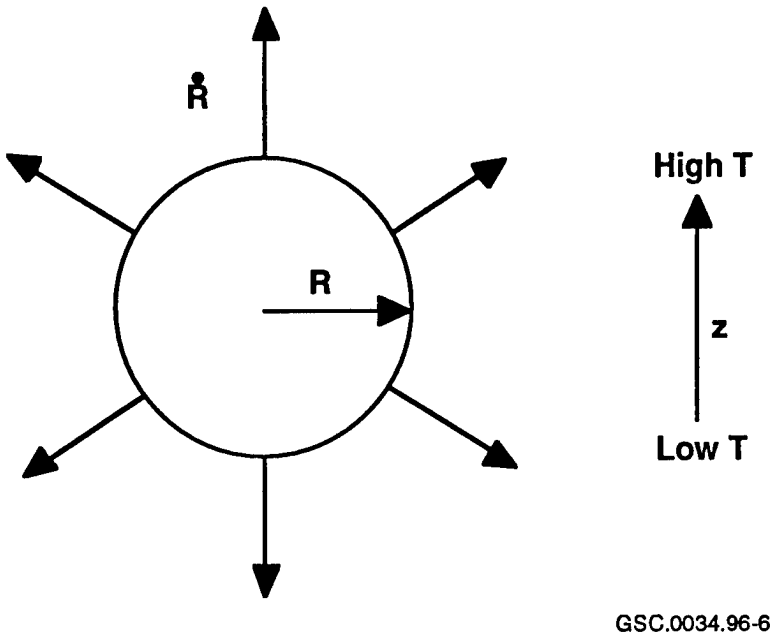

Figure 1. Geometry of the Expanding Bubble

The Reynolds number for this translating motion, $Re = \rho U(2R)/\mu$, is very small due to the small bubble radius R, the low speed U, and the high kinematic viscosity of the melt μ/ρ. Assuming that the bubble remains spherical, which is consistent with low Reynolds number flow, and that the expansion velocity is much greater than the translation, the flow field around a solitary bubble is described by a simple Stokes equation driven by a force due to the gradient of viscosity μ:

$$\frac{\nabla p}{\mu} = \nabla^2 u + 2R^2 \frac{dR}{dt} \nabla \ln\mu \bullet \Delta\left(\frac{r}{r^3}\right), \tag{1}$$

where p is the pressure. The velocity of the bubble through the melt is determined by calculating the terminal velocity resulting from a balance of forces on the bubble. If circulation within the bubble is assumed to be zero due to contamination of the melt from surface-acting products of the chemical reaction and if the thermal conductivity of the bubble is much smaller than that of the melt, the velocity will be

$$u = -\frac{2R}{3}\frac{dR}{dt}\frac{\partial \ln\mu}{\partial T} G e_z - \frac{2}{9\mu}(\rho - \rho_b) R^2 g, \tag{2}$$

where $G = dT/dz$ is the background temperature gradient, ρ the melt density, and ρ_b the bubble density. Viscosity typically decreases with increasing temperature, so the motion induced by the temperature gradient will be in the direction of higher temperature. The variation of viscosity with temperature is currently estimated by the WLF equation for polymer melts[8]:

$$\ln\mu = 13 - \frac{17.44(T - T_g)}{51.6 + T - T_g}, \tag{3}$$

where T_g is the glass temperature. This relationship can be readily modified within the model to include other important factors such as molecular weight.

To tackle the intumescent problem, we need to determine the motion of a large number of bubbles. A simple summation of individual flow fields provides a reasonable approximation for the total flow field if the assumption can be made that the spacing between bubbles is large compared with their size. In order to maintain a boundary condition of no normal flux across the lower surface of the sample, the field from each bubble is balanced by an identical image bubble located beneath the surface. As an example, the flow fields from four expanding bubbles are shown in Figure 2.

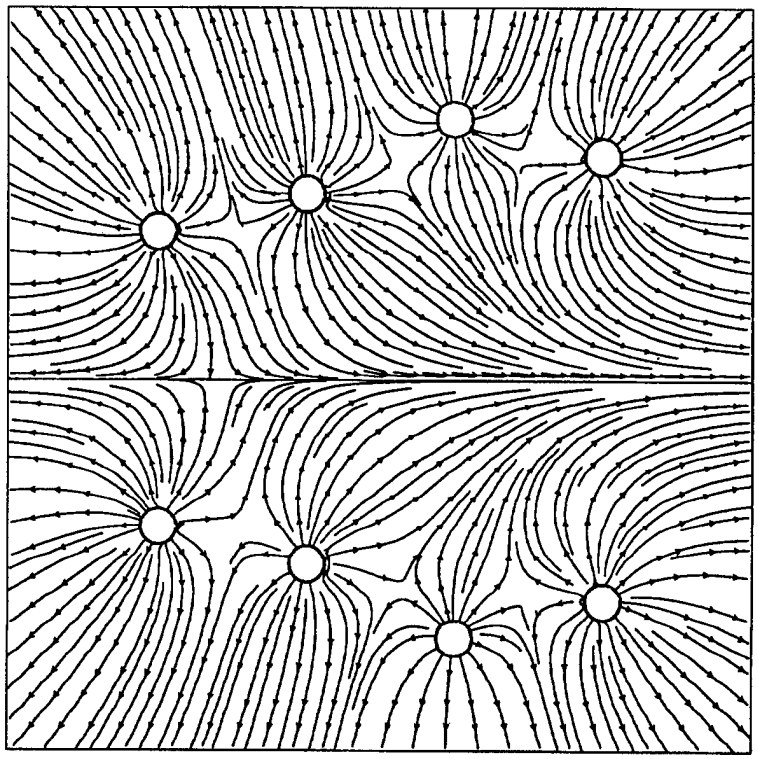

Figure 2. Streamlines Along the Plane of Symmetry for Four Expanding Bubbles and Their Images

The outer surface of the intumescent sample is forced upward by the sum of forces from the bubbles expanding within the melt. As a first approximation for the surface properties of the intumescent material, the bubbles are assumed to be retained by the sample. The upper surface therefore stretches to prevent bubbles from bursting and releasing gases to the exterior.

Heat Transfer Submodel

Upon exposure to the heat flux from a fire, the temperature within the intumescent sample rises, triggering gasification reactions at locations progressively farther from the outer surface. Figure 3 illustrates the behavior of the model over time for a sample in which the central region

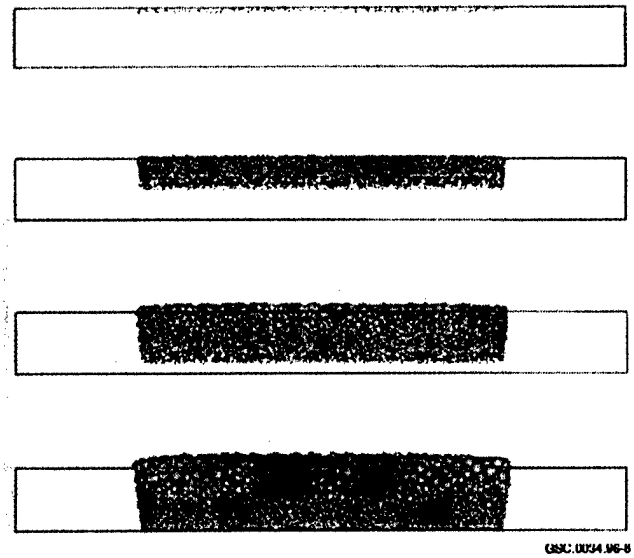

Figure 3. Development of 10,000 Bubbles With Time as a Heat Flux is Applied to the Upper Surface. As the internal temperature increases, nucleation occurs progressively deeper in the melt.

is seeded with 10,000 bubble nucleation sites. In this time sequence, the effects of the porous nature of the intumescent material have been neglected, and the temperature field is determined by solution of a simple one-dimensional diffusion equation with a steady applied heat flux above and an adiabatic boundary condition below.

Modeling the protective qualities of intumescent fire retardants requires consideration of the effects of gas bubbles on heat transfer. Two separate mechanisms are responsible for thermal protection. The degradation of the blowing agent occurs through an endothermic chemical reaction, absorbing heat during the intumescent process, and the thermal conductivity of the bubbles is much lower than that of the surrounding material, resulting in a final char that acts as an insulating layer. A plot of temperature vs. time for a protected substrate displays a plateau from the time intumescence begins until the intumescent front reaches the substrate surface[9].

To observe the effects of a large number of bubbles on heat transfer, we again seek a simple solution for a single bubble. Under similar assumptions as those made for the hydrodynamics model, we expect that the summation of these solutions over all bubbles will provide a reasonable approximation to the total temperature field. The problem to be solved is an expanding and migrating sphere in a temperature gradient. The thermal conductivity of the sphere differs from that of the surrounding fluid, and endothermic chemical reactions take place in the fluid adjacent to the sphere. As a simplifying approximation, we assume that the reactions produce a heat flux q at the surface of the sphere.

In the intumescent melt, where the Reynolds number is very small, the time scales for expansion and translation are much longer than the time scale for thermal diffusion. Under these conditions the temperature solution to the transient energy equation is well-approximated by the analytical solution to a simple Laplace equation with boundary conditions that account for the background temperature gradient and a heat source on the surface

$$T = Gz\left(1+\frac{1-\alpha}{2+\alpha}\right)\frac{R^3}{r^3} + \frac{qR^2}{kr}, \qquad (4)$$

where $\alpha = k_b/k$ is the ratio of the thermal conductivity of the bubble to that of the melt. In the fluid exterior to the bubble, this solution is equivalent to a combination of sink and dipole singularities [10]. The analytical solution for the temperature field around a single bubble in a constant temperature gradient field is shown in Figure 4 for an endothermic reaction alone and in Figure 5 for a bubble with small thermal conductivity relative to the surrounding fluid. Note that in both cases the temperature below the sphere is reduced.

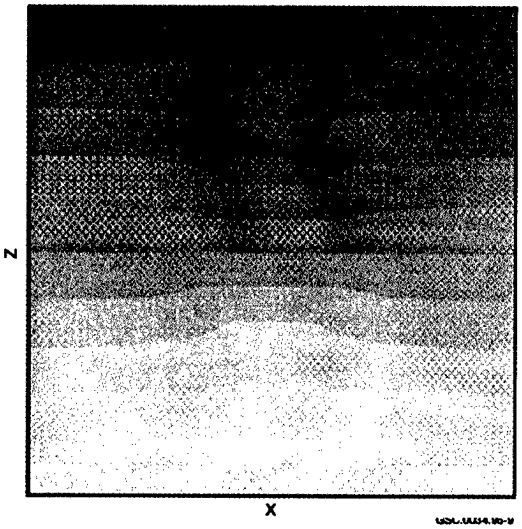

Figure 4. Temperature Contours for a Sphere in a Uniform Positive Background Temperature Gradient With an Endothermic Reaction Taking Place on its Surface. Higher temperatures are indicated by darker shades.

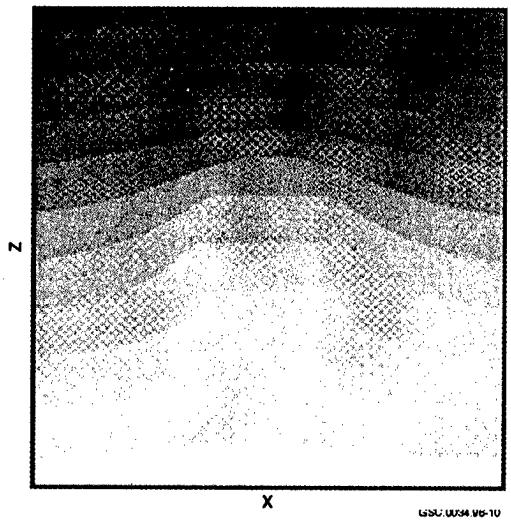

Figure 5. Temperature Contours for a Bubble in a Uniform Positive Background Temperature Gradient. Thermal conductivity of the bubble is one-tenth that of its surroundings.

For multiple bubbles whose separation is much larger than their radius, the total temperature field can be obtained by summing the fields from individual bubbles responding to local conditions. We are interested only in the solution in the melt, whose geometry is rapidly distorted by the growing bubbles. One approach to this complicated geometry is to introduce a Lagrangian coordinate system, which allows us to solve the heat transfer problem in the original rectangular geometry using finite differences. The evolution in time of a set of expanding bubbles arranged in three planes within the sample is shown in Figure 6. Notice that the region beneath the bubbles is cooler than the surrounding substrate due to both thermal conductivity differences and to endothermic reactions at the bubbles.

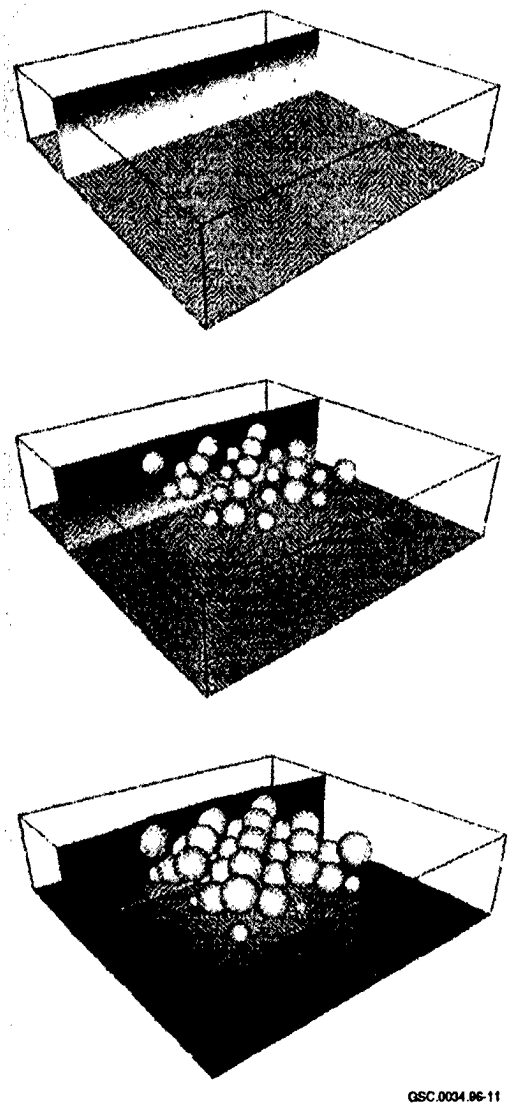

Figure 6. Time Development of a Sample Heated From Above Containing 38 Bubbles Arranged in Three Horizontal Planes, Showing the Effect of Bubbles on Heat Transfer to the Lower Surface. Temperature, displayed on vertical and horizontal cross sections, increases in shades from white to black. Bubble thermal conductivity is one-tenth that of the melt, and each bubble acts as a heat sink due to endothermic chemical reactions. Note the light gray (cooler) region beneath the bubbles.

Bubble Growth Submodel

The growth rate of bubbles in the intumescent material depends on the chemistry of the decomposition of the blowing agent and on the physical properties of the gas and surrounding melt. As the local temperature reaches the point at which decomposition starts, the concentration of gas in the polymeric melt begins to rise. At nearby nucleation points, bubbles begin to expand through diffusion of gas from the melt to the bubble. Initially, bubble growth is opposed by the surface tension of the melt. In a typical viscous liquid, the growth rate during later stages is controlled by liquid inertia and viscosity, by a combination of inertial and thermal effects, and finally, by the transport of heat and mass alone. In the melted intumescent material, however, viscosity is expected to remain a dominant factor until the char solidifies through cross-linking reactions.

In the intumescent model, the locations of bubble nucleation sites are provided as inputs to the model. When the temperature at a site exceeds the temperature at which the blowing agent begins to degrade, the bubble begins to grow. Because surface tension is a factor only for bubble sizes much smaller than those attained during later stages of growth, the earliest stage of bubble growth is neglected. A simple analytic expression for the bubble growth rate can be obtained for a radially symmetric geometry in which diffusion dominates and the translation of the bubble is neglected[11]:

$$\frac{dR}{dt} = DS\left(\frac{P_0}{P_c} - 1\right)\left[\frac{1}{R} + \frac{1}{(\pi Dt)^{1/2}}\right]. \tag{5}$$

In this equation, D is the diffusion coefficient, S the gas solubility, P_0 the initial supersaturation pressure, and P_c the minimum critical pressure for bubble inflation.

A more realistic bubble growth submodel must include viscous resistance to bubble expansion, reaction chemistry, depletion of the blowing agent, and the proximity of other bubbles. A promising approach to this problem is the cell model pioneered by Street et al.[12] in which a solitary bubble expands in a sphere containing a finite amount of melt material.

CONCLUDING REMARKS

The complex nature of intumescent behavior requires a modeling approach that combines physical and chemical behavior for a more complete understanding of the mechanisms involved. The density of expanding bubbles during intumescence is too high to solve the equations of mass, momentum, and energy exactly but not high enough for one-dimensional bulk models to capture the details of the process. In the three-dimensional model presented here, reasonable approximations at the scale of an individual bubble lead to the determination of bulk swelling and thermal properties from fundamental principals. The goal of this model is to provide a tool for design through improved understanding of the sensitivity of intumescent characteristics to various physical and chemical parameters.

Further details of the intumescent processes such as char solidification and non-Newtonian fluid effects can be added to this model as they are understood. The model is designed to run efficiently on an engineering workstation.

ACKNOWLEDGMENTS

The author is grateful to Dr. Howard R. Baum for many helpful suggestions on the modeling and to Dr. Takashi Kashiwagi for insights into the behavior of intumescent materials. This work is supported in part by the Federal Aviation Administration under Interagency Agreement DTFA003-92-Z-0018.

REFERENCES

1. Vandersall, H. L., *J. Fire & Flamm.* **2**:97-140 (1971).
2. Camino, G., Costa, L., and Martinasso, G., *Polymer Deg. & Stab.* **23**:359-376 (1989).
3. Cagliostro, D. E., Riccitiello, S. R., Clark, K. J., and Shimizu, A. B., *J. Fire & Flamm.* **6**:205-220 (1975).
4. Anderson, C. E. and Wauters, D. K., *Int. J. Engrg. Sci.* **22**:881-889 (1984).
5. Buckmaster, J., Anderson, C., and Nachman, A., *Int. J. Engrg. Sci.* **24**:263-276 (1986).
6. Anderson, C., Ketchum, D. E., and Mountain, W. P., *J. Fire Sciences* **6**:390-410 (1988).
7. Pehrson, R. and Barnett, J. R., *J. Fire Prot Engr.* **8**:13-30 (1996).
8. Williams, M. L., Landel, R. F., and Ferry, J. D., *J. Am. Chem. Soc.* **77**:3701 (1955).
9. Anderson, C. E., Dziuk, J., Mallow, W. A., and Buckmaster, J., *J. Fire Sci.* **3**:161-194 (1985).
10. Butler, K. M., Baum, H. R., and Kashiwagi, T., *Proceedings of the International Conference on Fire Research and Engineering*, 261-266, Orlando, FL, 10-15 September 1995.
11. Epstein, P. S. and Plesset, M. S., *J. Chem. Phys.* **18**:1505-1509 (1950).
12. Street, J. R., Fricke, A. L., and Reiss, L. P., *Ind. Eng. Chem. Fundam.* **10**:54-64 (1971).

CHARACTERIZATION

POLYIMIDES

Stephen Z. D. Cheng
Maurice Morton Institute and Department of Polymer Science,
The University of Akron, Akron, Ohio 44325-3909

BACKGROUND

The choice of polyimide materials is based on the fact that this family of polymers not only possesses high thermal and thermo-oxidative stability, but also has a higher oxygen index and char yield than other polymeric materials such as phenolics, epoxies, polyesters, and polyamides. A plot of oxygen index and char residue is shown in Figure 1. Our research focuses on the fire-resistant properties of aromatic polyimide fibers, coatings, and thermoplastics which have a specific molecular design and controlled architecture in order to achieve desired properties for applications in structural and interior components for aircraft.

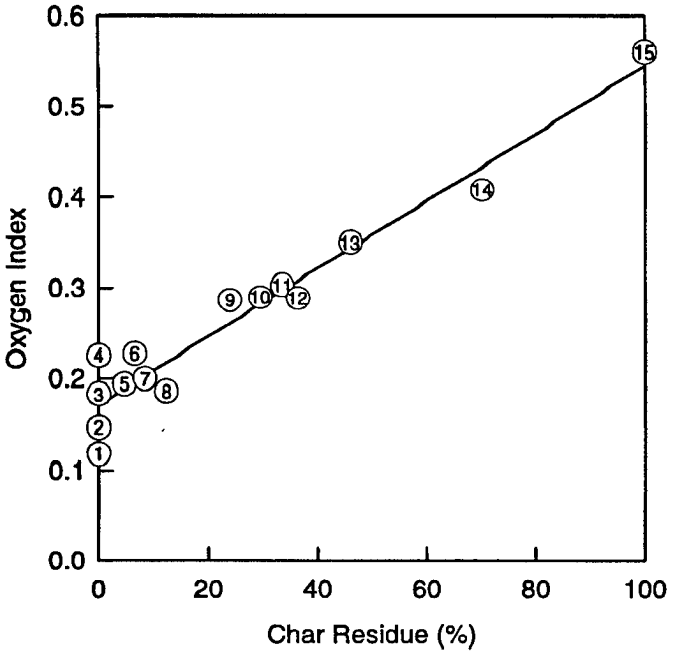

Legend

1. Polyformaldehyde
2. Polyethylene, polypropylene
3. Polystyrene, polyisoprene
4. Nylon
5. Cellulose
6. Poly(vinyl alcohol)
7. PETP
8. Polyacrylonitrile
9. PPO
10. Polycarboneat
11. Nomex
12. Polysulfone
13. Kynol
14. Polyimide
15. Carbon

Figure 1. Correlation Between Oxygen Index and Char Residue

Thermal Degradation Mechanisms in Aromatic Polyimides

Two polyimides were chosen in our study, both of which are based on the synthesis of 3,3',4,4'-biphenyl-tetracarboxylic dianhydride (BPDA) and 2,2'-disubstituted-4,4'-diaminobiphenyl (PFMB and DMB) using a one-step route[1,2]. These materials show excellent potential as fiber forming materials since their tensile properties are equivalent to or better than Kevlar fibers. In addition, these polyimides have two times higher compressive strengths than Kevlar, but more importantly, their thermal stabilities are at least 50°C to 100°C higher[3-6]. The chemical structure of BPDA-PFMB is

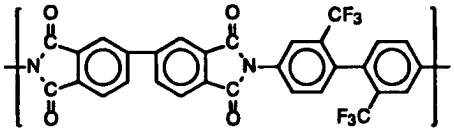

and BPDA-DMB is

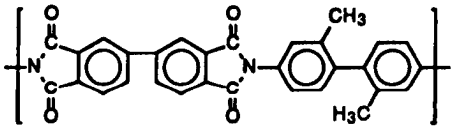

Thermal degradation can be roughly examined via nonisothermal thermogravimetric (TG) experiments under dry nitrogen and air. Both polyimides exhibit excellent thermal and thermo-oxidative stability as shown in Figures 2 and 3. The 5% weight loss temperature of these materials are above 500°C for BPDA-DMB and close to 600°C for BPDA-PFMB. However, these type of experiments do not reflect their true thermal degradation routes. A more precise measurement requires study of the thermal degradation kinetics, which are carried out under isothermal conditions. Figures 4 and 5 show changes in percentage weight loss with time at different isothermal temperatures for BPDA-PFMB in dry nitrogen and air, respectively. From Figure 3, only 1% weight loss is detected at 460°C after 5 hours, indicating the excellent thermal stability of BPDA-PFMB in nitrogen. However, in air, the 1% weight loss is observed at 400°C after 5 hours. This difference of 60°C reveals an effect of thermo-oxidation. Based on the kinetics model proposed by Flynn[7], activation energies of BPDA-PFMB can be calculated using the following equation:

$$\ln(t) = \ln g(\alpha) - \ln A + E_a/(RT) \qquad (1)$$

where t is the isothermal time, $g(\alpha)$ is the integral of the rate of weight loss, A is the pre-exponential factor, R is the gas constant, and E_a is the thermal degradation activation energy. The slope of a plot between $ln(t)$ and $1/T$ at constant weight fraction loss (α) yields this activation energy. This experimental procedure can also applied to BPDA-DMB and other materials such as PBO, PBZT, and Kevlar. Their thermal degradation activation energies in both dry nitrogen and air are listed in Table 1.

Table 1. Thermal Degradation Activation Energies for Different Polymeric Materials

Materials	E_a in dry nitrogen (kJ/mol)	E_a in air (kJ/mol)
BPDA-PFMB	300	200
BPDA-DMB	200	135
PBO	---	130
PBZT	---	115
Kevlar	---	100

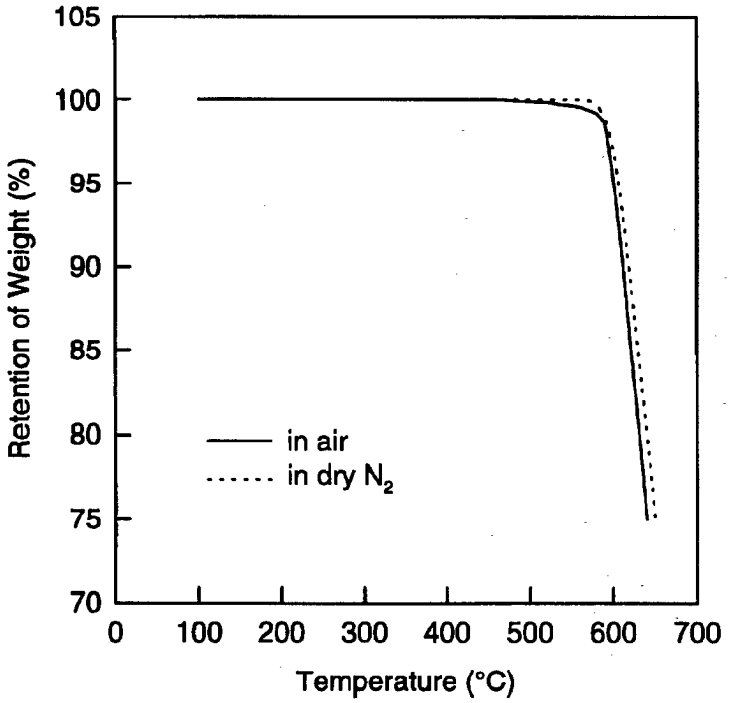

Figure 2. TG Curves for BPDA-PFMB Fibers at a Heating Rate of 10°C/min. Under a Nitrogen and Air Atmosphere

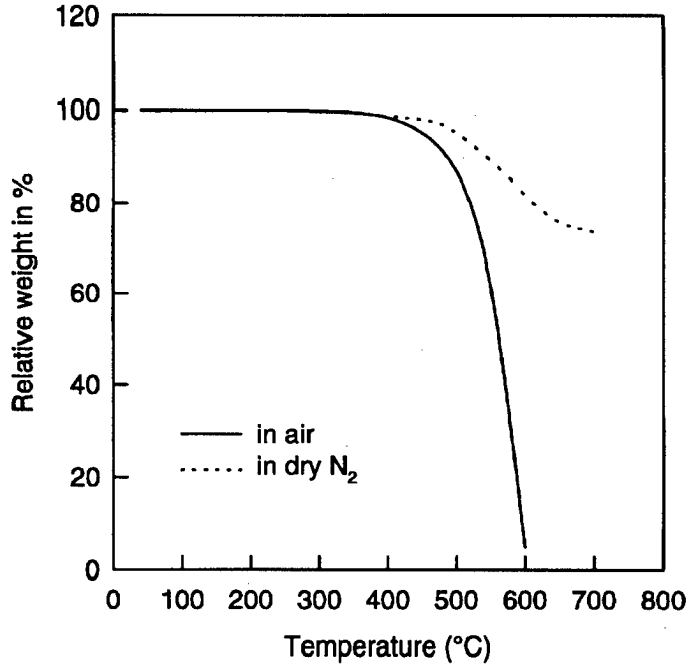

Figure 3. TG Curves for BPDA-DMB Fibers at a Heating Rate of 10°C/min. Under a Nitrogen and Air Atmosphere

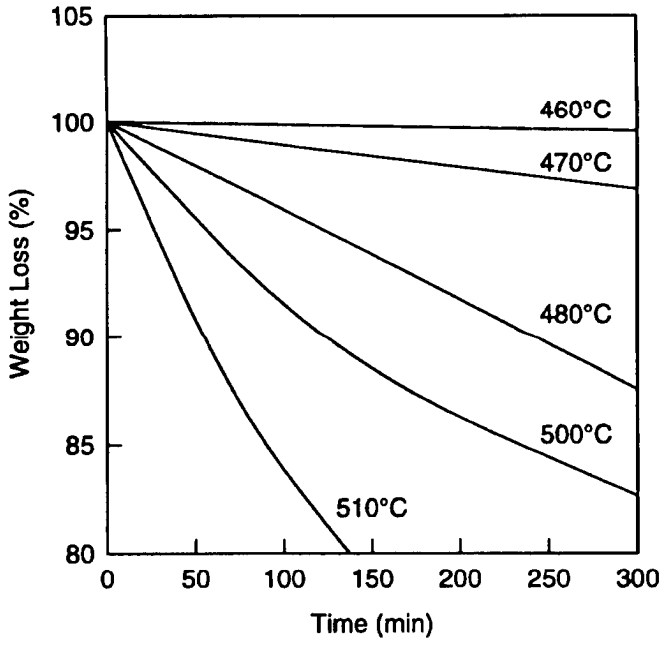

Figure 4. Isothermal Degradation Relationships Between the Percentage Weight Loss Changes and Time for BPDA-PFMB at Different Temperatures in Nitrogen

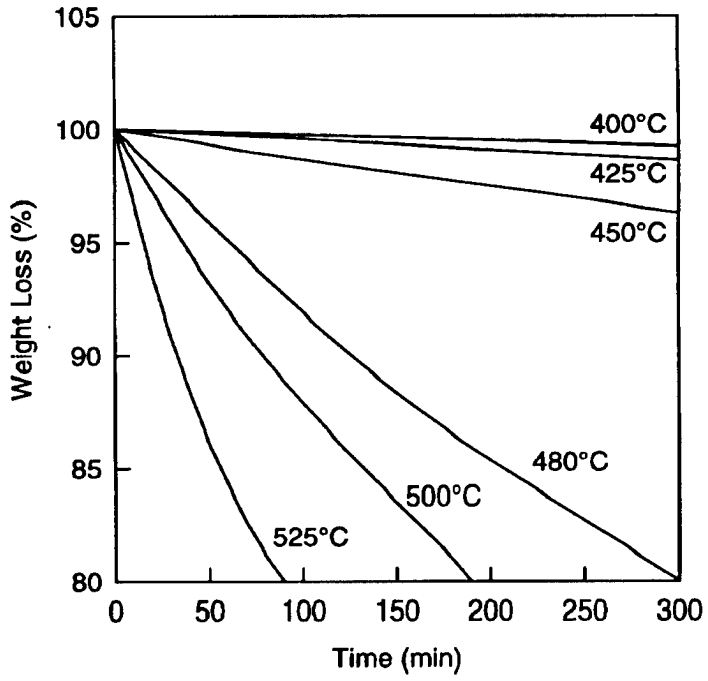

Figure 5. Isothermal Degradation Relationships Between the Percentage Weight Loss Changes and Time for BPDA-PFMB at Different Temperatures in Air

In order to learn about the detailed thermal degradation mechanism, TG-mass spectroscopy (TG-MS) was used at a heating rate of 3°C/min. The temperature dependence of the total ionization current is shown in Figures 6 and 7. The maxima arise from the release of six major fragments: CO, HCN, NH_3, HF, COF_2, and HCF_3 arising from thermal cracking of the diimide and pendant loss. The overall profile indicates that the maximum rate of thermal degradation under vacuum occurs at around 595°C. The results illustrate that the degradation of the pendant groups has maximum intensity at 580°C, as indicated by the HCF_3 ion (Figure 6). The thermal stability of the pendant trifluoromethyl groups is of paramount importance. The electron

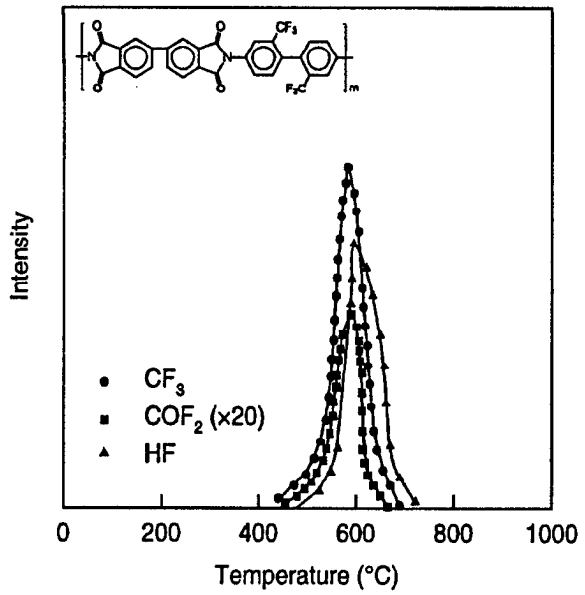

Figure 6. TG-MS Results for the Pendant Group Degradation Under Vacuum

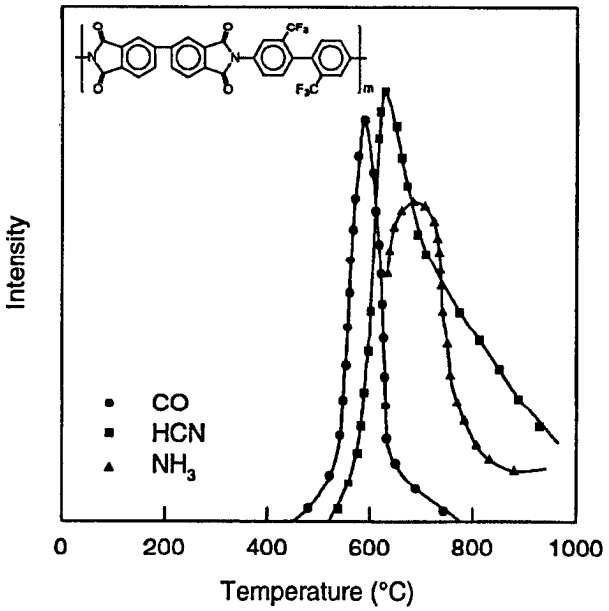

Figure 7. TG-MS Results for the Main Backbone Chain Degradation Under Vacuum

withdrawing nature of the pendant groups in the 2,2'-position of the diamines is responsible for stabilizing the polymer. At higher temperatures, as indicated in Figure 5, we observe the main chain degradation products through the HCN and NH_3 ions. We are currently carrying out the TG-MS experiments on other polyimides and polymers in order to compare the degradation mechanisms.

Thermal Stability Examination of High-Performance Fibers

Mechanical property measurements on BPDA-PFMB and BPDA-DMB fibers show a tensile strength of 3.2 GPa and a modulus of 130 GPa[3-6]. These two newly developed polyimide fibers have been selected for evaluation and comparison of their thermo-oxidative stabilities with PBO, PBZT, and Kevlar 49 fibers.

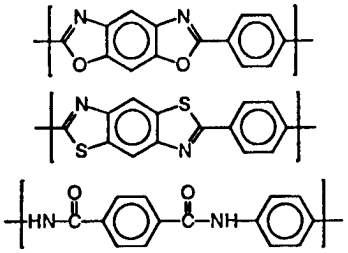

PBO

PBZT

Kevlar

These five fibers have been isothermally aged under circulating air at 205°C. The tensile strength, elongation, and modulus have been monitored at different aging times of 100, 250, 500, 750, 1000, 1500, 2000, and 2500 hours, respectively.

The most reliable information on the real thermo-oxidative stability of a fiber can be obtained from the study of changes in its physical, and in particular, mechanical properties upon prolonged isothermal aging times at elevated temperatures. Figure 8 illustrates the tensile strengths of BPDA-PFMB, BPDA-DMB, PBO, PBZT, and Kevlar 49 fibers after aging for different times in circulating air at 205°C. Figure 9 shows the relationships between the tensile strains of five fibers and aging times under the same isothermal conditions. Figure 10 is a plot of percent strength retention versus isothermal aging time. From this figure, the tensile strength of the BPDA-PFMB fiber remained constant during the first 100-hour exposure and the strain of the fiber decreased about 12%. Thus, the modulus remained unchanged. This phenomenon is similar to the case of annealing a fiber at constant length. In this annealing process, the tensile strength and modulus of the fibers increase and elongation decreases, indicating that further development of crystallinity and orientation in BPDA-PFMB fibers is achieved. Similarly, Figure 6 also shows that the tensile strength of BPDA-DMB fibers was unchanged in the first 100-hour exposure. In contrast, it is evident that the strength retention of PBO, PBZT, and Kevlar 49 fibers drop by 5%, 6%, and 10%, respectively for the same aging time, as shown in Figure 8.

During the isothermal aging process, the strength retention versus aging time can be divided into three stages as shown in Figure 8, i.e., 0-250 hours, 250-1000 hours, and 1000-2500 hours. Table 2 lists the rates of changing strength retention with respect to time. For PBO, PBZT, and Kevlar 49 fibers, their strength retention decreases rapidly in the first stage. The rate of decline slows in the second stage and decreases further in the third stage. Quantitatively, the rates of strength retention change in the first stage are almost twice as fast as those in the second stage;

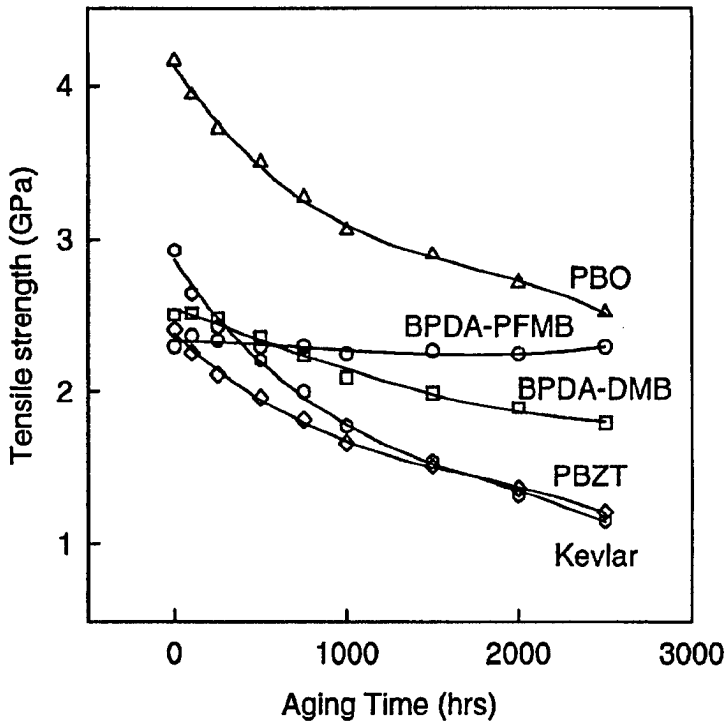

Figure 8. Relationships Between the Tensile Strength and Isothermal Aging Times for BPDA-PFMB, BPDA-DMB, PBO, PBZT, and Kevlar 49 Fibers

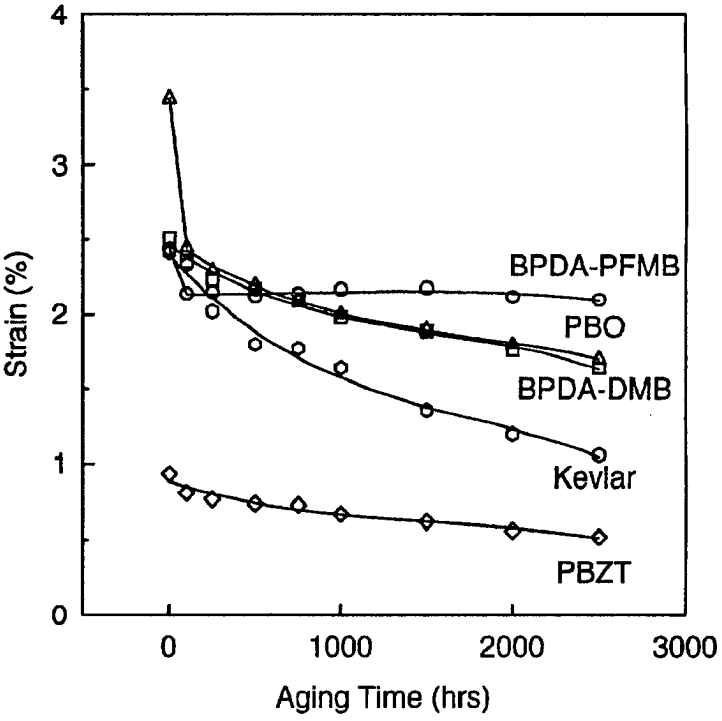

Figure 9. Relationships Between the Tensile Strain and Isothermal Aging Times for BPDA-PFMB, BPDA-DMB, PBO, PBZT, and Kevlar 49 Fibers

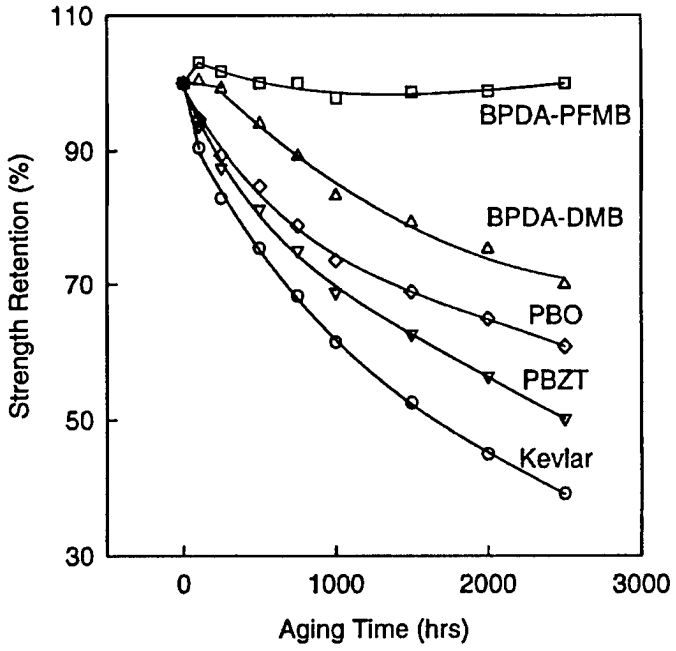

Figure 10. Relationships Between the Percentage of Strength Retention Changes of the Fibers and Isothermal Aging Times for BPDA-PFMB, BPDA-DMB, PBO, PBZT, and Kevlar 49 Fibers

Table 2. Reduction in Fiber Strength with Different Isothermal Stages of Aging Time in Air at 205°C

Sample	First Stage 0-250 hr (%)	Decreasing Rate (%/hr)	Second Stage 250-1000 hr (%)	Decreasing Rate (%/hr)	Third Stage 1000-2500 hr (%)	Decreasing Rate (%/hr)
BPDA-PFMB	0	0	0	0	0	0
BPDA-DMB	1	0.004	17	0.022	17	0.011
PBO	11	0.044	15	0.020	13	0.009
PBZT	12	0.048	19	0.025	19	0.013
Kevlar 49	17	0.068	23	0.031	21	0.014

similarly, in the second stage, the changes are also twice as fast as those in the third stage. Surprisingly, for BPDA-DMB fibers, it was found that the smallest strength retention change is in the first stage. However, the changes in the second and third stages are similar to the cases of PBO, PBZT, and Kevlar fibers. Finally, for BPDA-PFMB fibers, no decrease of strength was found in any of the three stages.

After 2500 hours of aging at 205°C, the strength retention changes of BPDA-PFMB, BPDA-DMB, PBO, PBZT, and Kevlar fibers are 100%, 66%, 61%, 50%, and 39%, respectively. This fits well with the thermal degradation activation energies calculated from TG experiments (Table 1*)*. It is important to note that the difference between the two CF_3 groups in the diamine in BPDA-PFMB as compared to the two CH_3 groups in the BPDA-DMB, diamine contributes to the difference in the thermo-oxidative stabilities of these materials. This may again be attributed

to the electron withdrawing nature of the CF_3 versus the electron donating tendency of the CH_3 group.

Figure 11 shows the strain retention changes of five fibers with respect to the isothermal aging time in circulating air. It is obvious that the strain retention tendency is the same as that of the strength retention for these fibers (Figure 10). It is surprising that the strain retention of PBO fibers shows a drastic decrease in the first 100 hours of aging. Further research is necessary to investigate the cause of this phenomenon. For BPDA-PFMB fibers, the strain on the fiber decreases in the first 100 hours of aging, while the strength increases slightly, and as a result, the modulus increases. In general, the change of modulus during the isothermal aging is critically dependent upon the relative changes between the strength and strain.

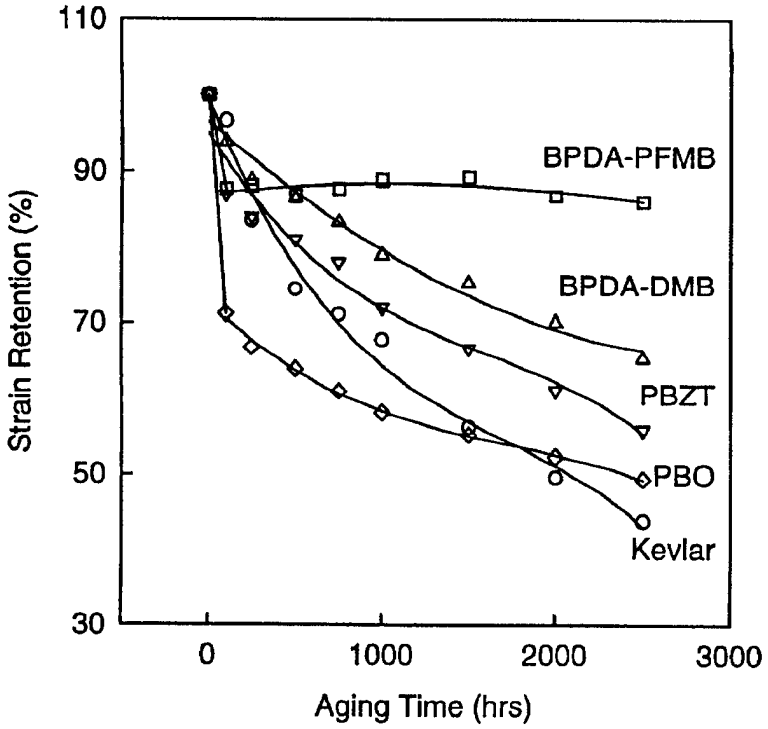

Figure 11. Relationships Between the Percentage of Strain Retention Changes of the Fibers and Isothermal Aging Times for BPDA-PFMB, BPDA-DMB, PBO, PBZT, and Kevlar 49 Fibers

During isothermal aging in air, it is speculated that molecular mechanisms may yield macroscopic changes in mechanical properties of the fibers, in particular, the tensile properties. These mechanisms may include scission of polymer chains, completion of cyclization, and cross-linking in chemical reactions, as well as crystallization, crystal perfection, and orientation changes in physical reactions. The main effect may be the scission of the macromolecules as a result of thermal degradation. With increasing isothermal aging time, the color of the fibers are drastically changed (except for the polyimide fibers), which is believed to be caused by oxidation. Finally, although PBO fibers do not show the best thermo-oxidatitive stability, they still retain the best tensile strength even after long-term isothermal aging.

Fire-Resistant Films and Coatings

It is well known that aromatic polyimides are usually difficult to process since they do not exhibit melt flow before decomposition and are insoluble in conventional solvents. The traditional approach to make processing possible is to use a two-step polymerization route through the soluble poly(amic acid) precursors[1]. For example, polyimide films are generally produced by solution-casting or spin-coating followed by either thermal or chemical imidization. The imidization history affects the ultimate structure, morphology, and properties of the films.

Over the past 8 years a family of organo-soluble, aromatic polyimides have been designed and synthesized in our laboratory. These polyimides were synthesized in refluxing *m*-cresol at high temperatures through a one-step route in which the intermediate poly(amic acid)s were not isolated. Most of the aromatic polyimides which we have synthesized can be easily dissolved in common organic solvents such as acetone, chloroform, 2-pentanone, cyclopentanone, methyl ethyl ketone, tetrahydrofuran, dimethylformamide, N-methylpyrrolidinone, and dimethyl sulfoxide, etc., and can be directly processed to form films or coatings. A major advantage of these aromatic polyimides is that they are extremely thermally and thermo-oxidatively stable. Due to their solubility, these polyimides possess excellent processibility and it is expected that they can be used as thin films or coatings on polymeric substrate surfaces as protective layers[8-10].

The dianhydrides and diamines used to synthesize polyimides are shown in Figure 12. We have initiated thermal degradation studies on these polyimides via TG experiments. The thermal and thermo-oxidation stabilities of all the samples studied are excellent. Their 5% weight losses are above 500°C. We are planning to do isothermal TG and TG-MS experiments as well as flammability measurements in order to establish relationships between the structure and the combustion kinetics and mechanism.

Different molecular weight samples are available in these aromatic polyimides. It is known that chain degradation is associated with the density of end groups in polyimides. Following isothermal experiments carried out in TG and MS, we will investigate the effect of end groups on the degradation and combustion processes. Char yields will be followed by the weight changes of the polyimides during heating. Elemental analysis will also carried out to determine the chemical composition of the char residues.

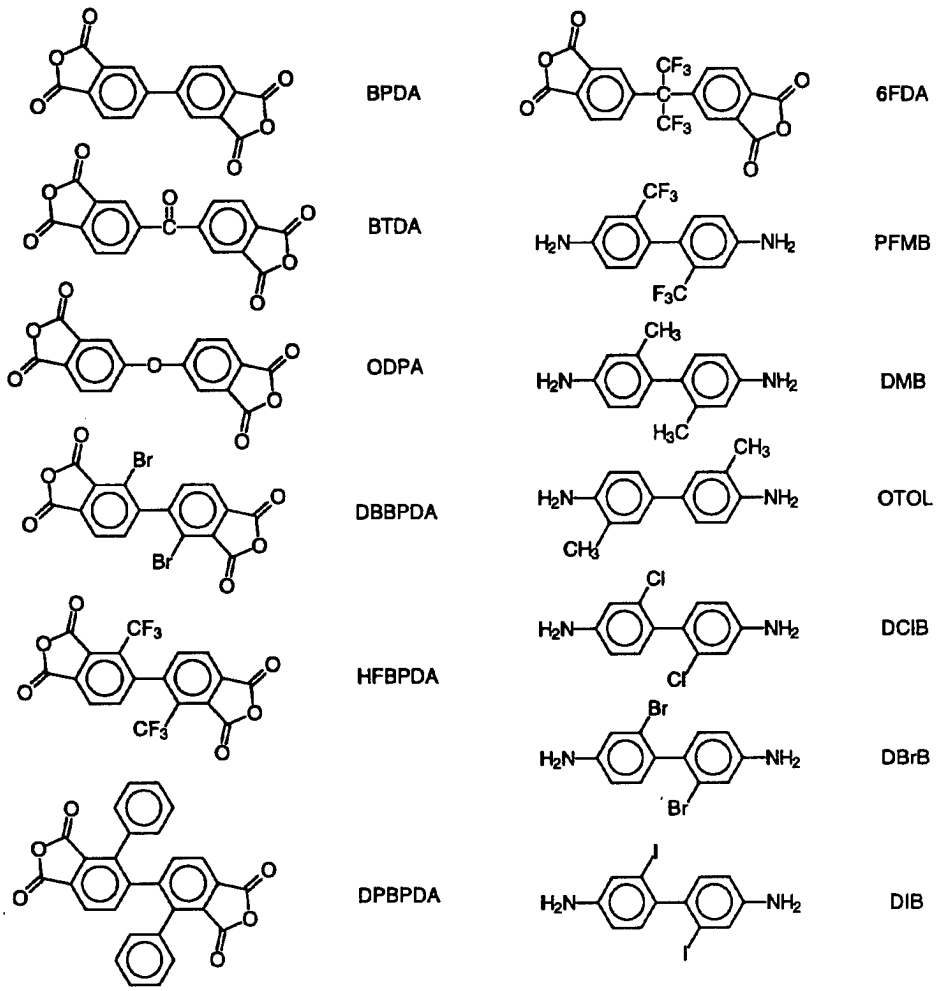

BPDA --- 3,3',4,4'-biphenyltetracarboxylic dianhydride
BTDA --- 3,3,'4,4'-benzophenonetetracarboxylic dianhydride
ODPA --- 4,4'-oxydiphthalic anhydride
DBBPDA --- 2,2'-dibromo-4,4',5,5'-biphenyltetracarboxylic dianhydride
HFBPDA --- 2,2'-bis(trifluoromethyl)-4,4',5,5'-biphenyltetracarboxylic dianhydride
DPBPDA --- 2,2'-diphenyl-4,4',5,5'-biphenyltetracarboxylic dianhydride
6FDA --- 2,2'-bis(3,4-dicarboxyphenyl)-hexafluoropropane dianhydride
PFMB --- 2,2'-bis(trifluoromethyl)-4,4'-diaminobiphenyl
DMB --- 2,2'-dimethyl-4,4'-diaminobiphenyl
OTOL --- 3,3'-dimethyl-4,4'-diaminobiphenyl
DCIB --- 2,2'-dichloro-4,4'-diaminobiphenyl
DBrB --- 2,2'-dibromo-4,4'-diaminobiphenyl
DIB --- 2,2'-diiodo-4,4'-diaminobiphenyl

Figure 12. Chemical Structures of Dianhydrides and Diamines Used in the One-Step Polymerization Route

REFERENCES

1. Harris, F. W. in "Polyimides", Wilson, D., Stenzenberger, H. D., and Hergenrother, P. M. Eds.; Chapman and Hall, New York, Chap. 1, pp. 1-37 (1989).
2. F. W. Harris and S. L.-C. Hsu, High Perform. Polym. 1, 1 (1989).
3. S. Z. D. Cheng, Z.-Q. Wu, M. Eashoo, S. L.-C. Hsu, and F. W. Harris, Polymer 32, 1803 (1991).
4. M. Eashoo, D.-X. Shen, Z.-Q. Wu, C. J. Lee, F. W. Harris, and S. Z. D. Cheng, Polymer 34, 3209 (1993).
5. M. Eashoo, D.-X. Shen, Z.-Q. Wu, F. W. Harris, S. Z. D. Cheng, K. H. Gardner, and B. S. Hsiao, Macromol. Chem. 195, 2207 (1994).
6. D.-X. Shen, Z.-Q. Wu, J. Liu, L. Wang, S. Lee, F. W. Harris, S. Z. D. Cheng, J. Blackwell, T. Wu, and S. Chvalun, Polymers & Polym. Composites 2, 149 (1994).
7. J. H. Fynn, in "Laboratory Preparation for Macromolecular Chemistry", E. McCuffrey Ed., McGraw Hill, New York, 1970, p. 255.
8. F.-M. Li, F. W. Harris, and S. Z. D. Cheng, Polymer 37 (23), pp. 5321-5325 (1996).
9. F.-M. Li, E. P. Savitski, J. Chen, F. W. Harris, and S. Z. D. Cheng, in "Polymers for Advanced Optical Applications," Jenekhe, S. A. and K. Wayne Eds., ACS series, (1997) (in press).
10. F.-M. Li, E. P. Savitski, J. Chen, F. W. Harris, and Cheng, S. Z. D. Polymer 38 (13), pp. 3223-3227 (1997).

THERMOMECHANICAL STABILITY OF RESINS AND COMPOSITES

A. J. Lesser, G. Schueneman, and C. Comeaux
Polymer Science & Engineering, University of Massachusetts
Amherst, Ma. 01003

INTRODUCTION

The primary objective of this effort is to characterize the mechanical behavior and stability of polymer resins and polymer based composites designed for fire situations. The research to date has been focused in two primary thrusts; characterization of mechanical degradation mechanisms of resins exposed to fire situations and the development of a new methods to characterize the mechanical properties and mechanical heterogeneity of small amounts of resins. Results from the first thrust illustrate how key mechanical properties of the resin change as the backbone of a model resin undergoes systematic side-chain reactions and chain scission (i.e., common decomposition reactions in fire situations). These changes in the network structure of the resin can lead to significant changes in the elastic modulus, yield strength, fracture strain (ductility), and fracture toughness of the resin. This, in turn, can dramatically affect the mechanical stability and the structural integrity of a structural component fabricated from these materials. Moreover, due to the low thermal conductivity intrinsic in polymer glasses, it is expected that in high heat flux situations that the decomposition will be heterogeneous with the production of, in general, a char layer, a molten layer, and an embrittled layer between the bulk polymer and the fire. The embrittled layer in particular can initiate microcracks and lead to premature failure and/or fragmentation which, in turn, increases the polymer surface area exposed to the fire. The first part of this progress report summarizes our activities to date in addressing this issue.

The second thrust of our activity has focused on developing a technique which can be used to characterize the mechanical properties and mechanical heterogeneity of small amounts of resin using a noncontact method. The technique we are investigating utilizes ultrasonic spectroscopy to measure density and modulus changes in resins in addition to changes in the structural heterogeneity and viscoelastic behavior of materials. The effort to date has focused on developing a test cell which can monitor in situ changes in the mechanical moduli of Dr. Novak's resins during the polymerization process. Ultimately this technique can be used on any material including those which have been exposed to high heat flux situations to characterize their retention of specific mechanical properties.

RESULTS AND DISCUSSION

The thermo-oxidative decomposition of glassy polymers in fire situations starts by a broad range of reactions which can lead to chain scission of the polymer backbone and additional cross-linking due to side chain reactions. Due to the relatively low thermal conductivities inherent in polymers, these reactions can produce an embrittled surface layer in high heat flux situations.

The surface layer embrittlement, in turn, can cause dramatic reductions in the effective ductility of the resin by localizing the fracture process as shown schematically in Figure 1.

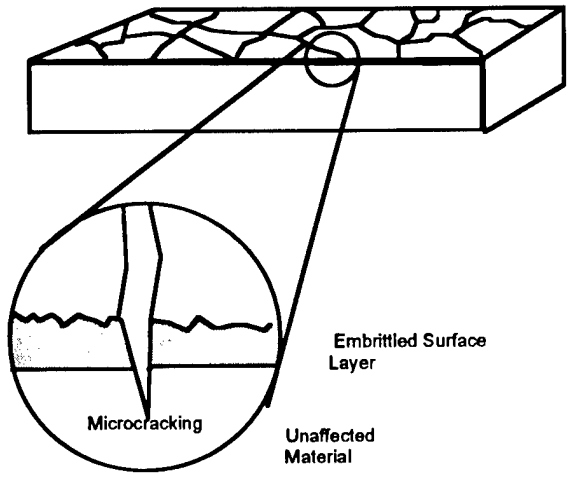

Figure 1. Strain Localization Effects Due to an Embrittled Surface Layer

This section summarizes results from our ongoing study to characterize the deformation and fracture behavior of glassy polymers which contain a embrittled surface layer. Test specimens are fabricated from layered model resin laminates and subjected to uniaxial stress states. Their fracture response is characterized in terms of the molecular structure of the bulk polymer, the molecular structure of the embrittled surface layer, geometrical considerations (e.g., surface layer thickness, etc.), and loading conditions.

Effects of Degradation on Mechanical Properties

The materials used in this investigation include a Diglycidal Ether Bisphenol A (DGEBA) di-Epoxy resin (EPON 825) cured with stoichiometric combinations of Ethylene Diamine (EDA), Methyl Ethylene Diamine (MEDA), and N, N' Dimethyl Ethylene Diamine (DMEDA). The EPON 825 was selected for its narrow molecular weight distribution and has a polydispersity index (M_w/M_n) of 1.01. The curatives EDA, MEDA, and DMEDA are chosen for their molecular similarity and functionality. The EDA and MEDA (with functionalities of 4 and 3, respectively) provide cross-linking to the network while the DMEDA (with a functionality of 2) provides chain extension. The structure of the DGEBA and curing agents are shown in Figure 2. The molecular weight between cross-links, M_c, is controlled by stoichiometrically increasing the amount of DMEDA relative to the EDA and MEDA. M_c is given by

$$M_c = 2\left(\frac{\sum_{f=3}^{\infty}\frac{\Phi_f}{f}}{\sum_{f=3}^{\infty}\Phi_f}\right)\left(\frac{M_e+\sum_{f=2}^{\infty}\frac{M_f}{f}\Phi_f}{\sum_{f=3}^{\infty}\frac{M_f}{f}\Phi_f}\right) \quad (1)$$

where the parameters have the following definitions:

f	functionality of the amine molecule
M_f	molecular weight of the f^{th} functional amine molecule
M_e	epoxide equivalent weight (g resin/mole epoxide, EPON 825 M_e = 175 gms/mol)
Φ_f	mole fraction of amine H's provided by the f^{th} functional amine molecule

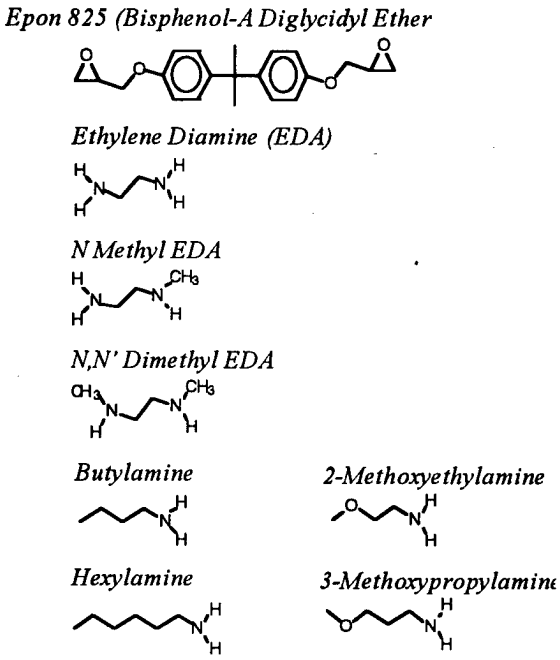

Figure 2. Resin and Curing Agent Structures

Resin embrittlement is systematically modeled by incorporating additional cross-links (figure 3). That is, by changing the amount of difunctional and tetrafunctional curing agents in model resins, we are able to systematically alter the cross-link density of these resins. This enables us to systematically study the effects of the side chain reactions and chain scission without altering the backbone stiffness of the resin. Hence, we can accurately describe the effects that each of these mechanisms have on the mechanical behavior of the resin and relate these changes to changes in the network structure.

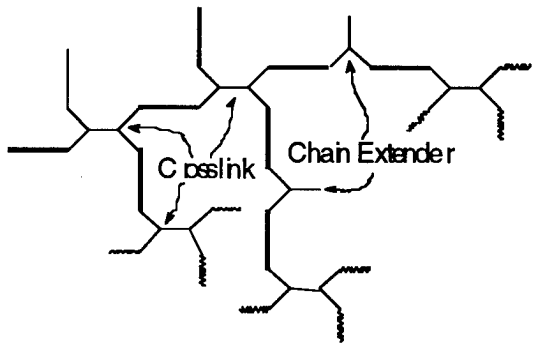

Figure 3. Schematic of Network Structure

The glass transition of these networks increases in accordance with a Fox-Flory type relationship. A plot of T_g of the resin versus cross-link density ($1/M_c$) is shown in Figure 4.

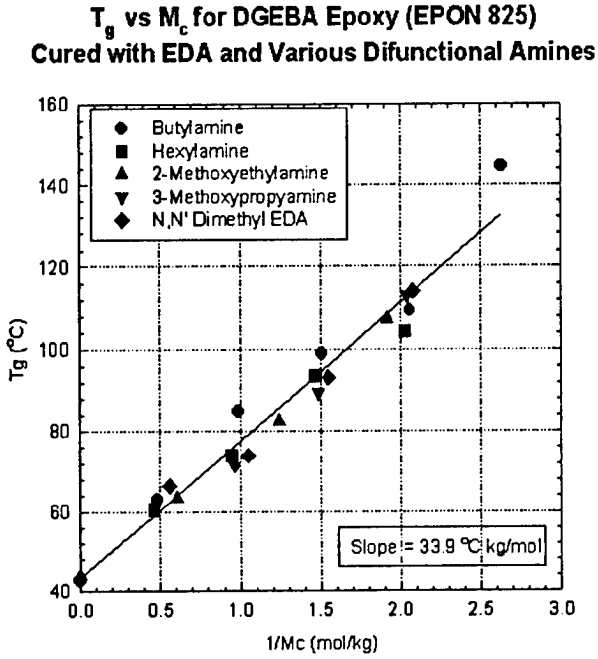

Figure 4. Glass Transition vs. Cross-Link Density for Model Resin Systems

Uniaxial tension and compression tests were also conducted on these network structures to illustrate how the mechanical properties will evolve with side chain cross-linking. These results are shown typically in Figure 5. Careful inspection of the data in Figure 5 shows that, as cross-linking occurs, the fracture strain reduces, the yield stress increases, and the modulus is initially unaffected. At high cross-link densities, the mode of failure in tension changes from yielding to brittle fracture. Consequently, the mechanical properties first affected by additional cross-linking are the fracture strain and the yield response. This combination of properties produces a dramatic reduction in the fracture toughness of the resin. The reduction in fracture strain reduces the resin's capability to dissipate energy in the process zone which accompanies a crack.

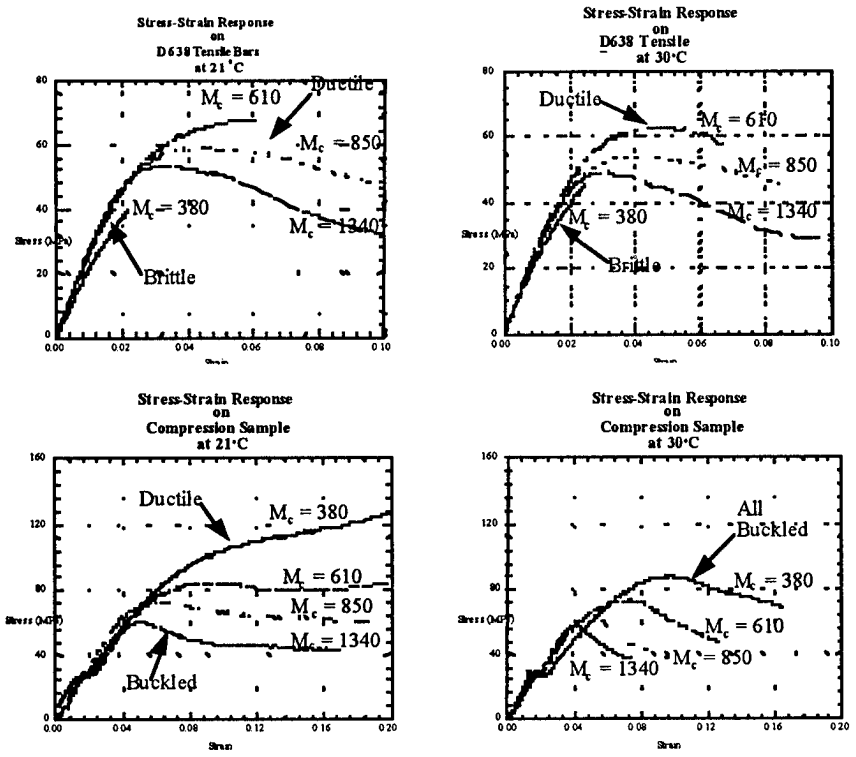

Figure 5. Uniaxial Tension and Compression on Resin Systems with Different Cross-Link Densities

Effects of Embrittled Surface Layers

Layered resin plaques were cast using a multistage process to produce a ductile interlayer coated with an embrittled surface layer. ASTM D638 tensile bars were machined from the plaques and tested on an Instron 1123 uniaxial test machine. As seen in Figure 6, the plaques laminated with a brittle layer failed at lower strains than would be expected for a plaque made up of a homogenous combination of the two different cross-link densities.

The strength of a part which contains an embrittled layer as the result of exposure to a fire situation is governed by geometric considerations (thickness of embrittled layer) and the mechanical properties of both layers. Further studies are underway to ascertain the critical thickness as it relates to the bulk polymer and the embrittled surface layer.

Additional studies will include other potential modes of failure and fragmentation which can occur in a fire situation. During a fire, the embrittled surface layer of a stressed polymer may spall off, thereby dramatically increasing the exposed surface area of the bulk material, which would result in more embrittled surface. To investigate this mode of failure, we used a 4-point bend test geometry to study the interfacial adhesion of the layers as shown in Figure 7. This geometry was selected to assess the interfacial strength of the layers and relate these properties to the properties of the bilayer system.

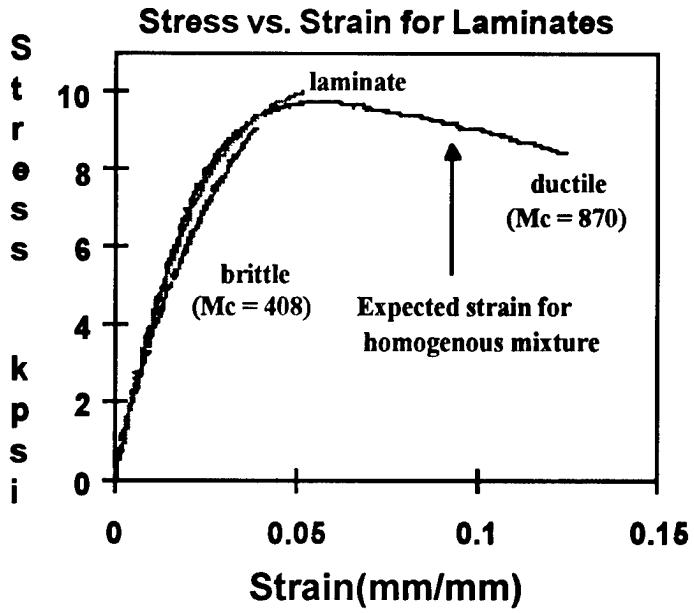

Figure 6. Tensile Test Results for Homogenous and Laminated Brittle/Ductile Samples

4-Point Bend Test for Determining the Strain Energy Release Rate (G) of Polymer-Polymer Interfaces

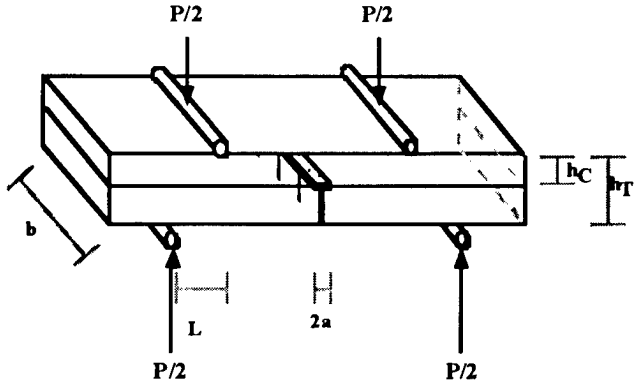

Figure 7. Four-Point Bend Test Method

This method allows a value for the energy release rate for crack propagation, G, to be calculated based on the load (P), the modulus of the layers (E), and geometric parameters (A.G. Evans 1989 J. App. Mech. 56, pp. 77-82).

$$G = \frac{P^2 L^2}{8bE}\left[\frac{1}{I_C} - \frac{1}{I_T}\right] \qquad (2)$$

$$I_c = \frac{bh_c^3}{12} \qquad I_c = \frac{bh_T^3}{12} \tag{3, 4}$$

Results from these tests will allow us to gain insight into the mechanics involved in whether the embrittled layer will remain attached to the bulk material under different stress situations.

Ultrasonic Spectroscopy for Polymers and Composites

Recent advances in digital electronics has enabled the potential of using ultrasonic spectroscopy as a means of characterizing polymers and composites. The intrinsic molecular characteristics of polymers in solution, melt, and in the solid phase have a dramatic effect on the longitudinal wave velocity and attenuation. Moreover, the wave velocity and attenuation in polymers have been shown to be very frequency dependent and related to the viscoelastic characteristics of the material. The objective in this effort is to evaluate the potential of using ultrasonic spectroscopy as a complementary method for characterizing thermomechanical degradation in polymers and composites subjected to high heat flux environments. The primary differences between ultrasonic spectroscopy and other conventional forms of spectroscopy is that sound waves are reflected whenever a change in the elastic moduli and/or density (e.g., acoustic impedance) are encountered. Hence, acoustic spectroscopy may provide information regarding the mechanical heterogeneity of a material necessary to describe the structural stability of a load carrying member in an aircraft.

Single-Pulse Excitation Method

The general approach to ultrasonic spectroscopy involves digitally recording and subsequently analyzing an ultrasonic pulse transmitted through a polymeric media. The recent developments of wide-band transducers, receivers, electronic equipment, and supportive computer equipment have enabled the consideration for this method of characterization. Figure 8 shows the basic diagram for the single-pulse excitation method[1]. In the figure, small letters represent the transfer functions in time domain and the capital letters represent the frequency transfer functions. As shown in the figure, the observed response can be described by the following convolution chain.

$$x(t) = \int g_2(t_3)dt_3 \cdot \int h(t_2)dt_2 \cdot \int g_1(t_1)p(t - t_1 - t_2 - t_3)dt_1$$

Here, p(t) is the electric signal supplied to the transducer at time t, g_1 (t) is the electro-acoustic conversion function of the transducer, g_2 is the electro-acoustic conversion function of the receiver, and h(t) is the response of the polymer sample. The Fourier transforms of the above equation yields

$$X(\omega) = P(\omega)G_1(\omega)H(\omega)G_2(\omega)$$

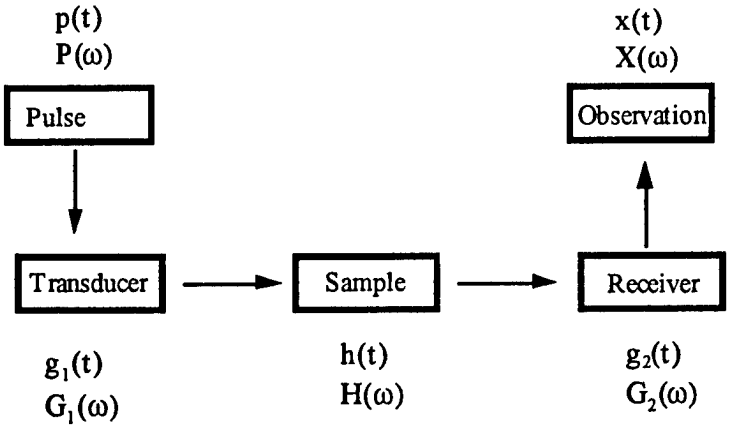

Figure 8. Concept of Ultrasonic Spectroscopy

Therefore, if we have the frequency transfer function for the transducer and receiver, we can evaluate the frequency response of the material. In general, the above approach can be generalized to include the effects of the test cell and other relevant parameters convoluting the measured response. The combined frequency transfer functions, $H'(\omega)$, of the transducer, test cell, and receiver can be evaluated by measuring the response of a standard sample.

$$X'(\omega) = P(\omega)G_1(\omega)G_2(\omega)$$

With $X'(\omega)$ known, the material response $H(\omega)$ can then be determined.

$$H(\omega) = \frac{X(\omega)}{X'(\omega)}$$

For the data presented herein, H_2O at a temperature of 20°C was used as the test standard.

A cautionary requirement to insure the validity of the approach outlined above necessitates the use of a broad band transducer and receiver. Hence, this approach can provide a simple yet powerful technique for measuring the ultrasonic response of a material but in practice required the recent developments of sufficiently broad band transducers and receivers together with digital equipment.

Experimental Setup

The apparatus we are using to conduct these types of studies is shown in Figure 9. The transducer is controlled and monitored by a Panametrics model 5601A pulser/receiver. This component allows the signal to be conditioned in order to optimize the characterization of the sample. The signal is sent from the pulser/receiver to a one gigahertz Sonix STR81G digitizer board in the computer and then is displayed on the screen. The software used was written by Panametrics of Waltham, Massachusetts, and displays the signal in a software-based oscilloscope. The oscilloscope used determines the experimental setup that gives the best signal and allows gates and a trigger to be set up on the wave form. The trigger is set so that a

minimum energy must be achieved for the computer to record it as data and gates fix portions of the wave form to be recorded as data. The multiaxis scanning tank is controlled by the computer and allows the data collected to be matched to the exact position on the sample. The computer controls the scanning tank via a P1399 PC position match generator that is interfaced to the stepper motors on the tank via the motion controller.

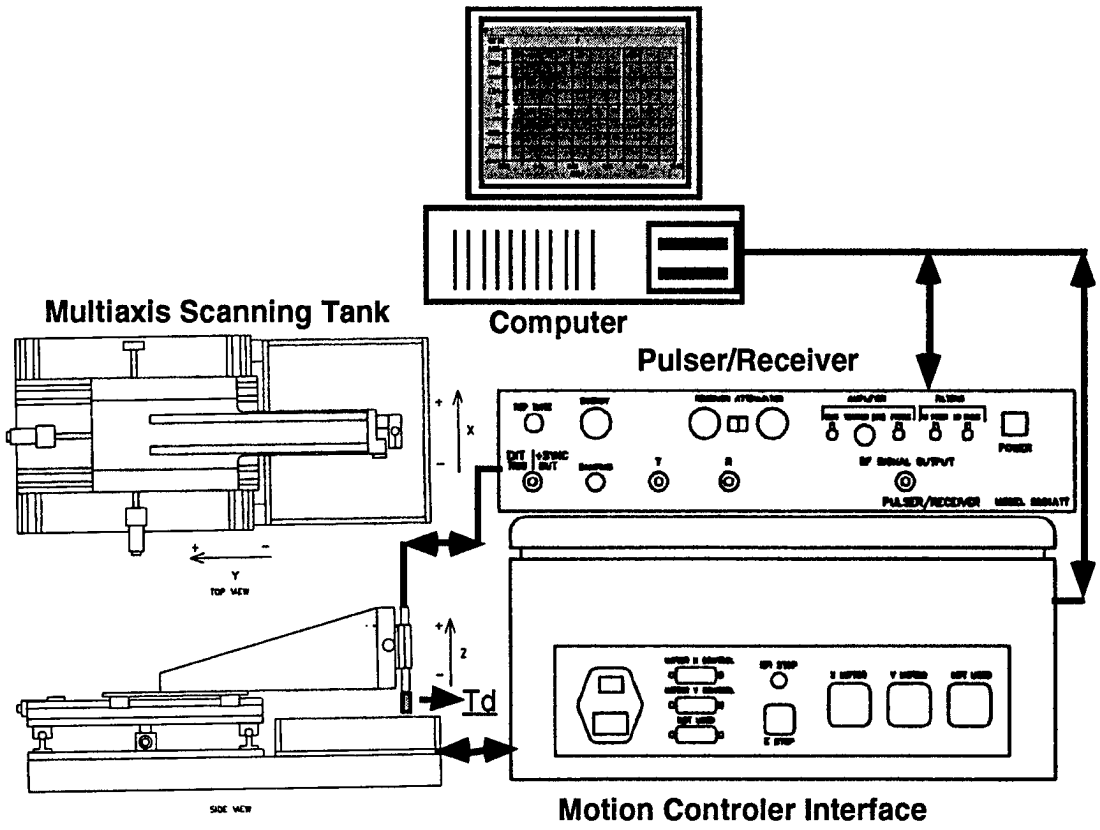

Figure 9. Ultrasonic Spectroscopy Setup. (Td = Transducer)

We are modifying this method to characterize the formation of network and heterogeneous structures. This new technique will be called Ultrasonic Spectroscopy. We are currently using the pulse echo mode to monitor the change in sound velocity during the gellation of gelatin. Figure 10 is a sketch of the apparatus we are using for these experiments. It consists of a conical glass chamber where the gelatin is placed. The chamber is surrounded by a heating/cooling jacket where liquid is circulated from a circulating heating/cooling bath. The port in the base of the apparatus allows the insertion of a transducer and is sealed in with a bushing and o-ring. The conical shape of the sample chamber is necessary to prevent reflections from the walls of the chamber convoluting experimental results. The computer system will be used as in a traditional examination of a composite laminate, but instead of saving the wave forms with a special reference across a sample, it will save them in reference to elapsed experimental time.

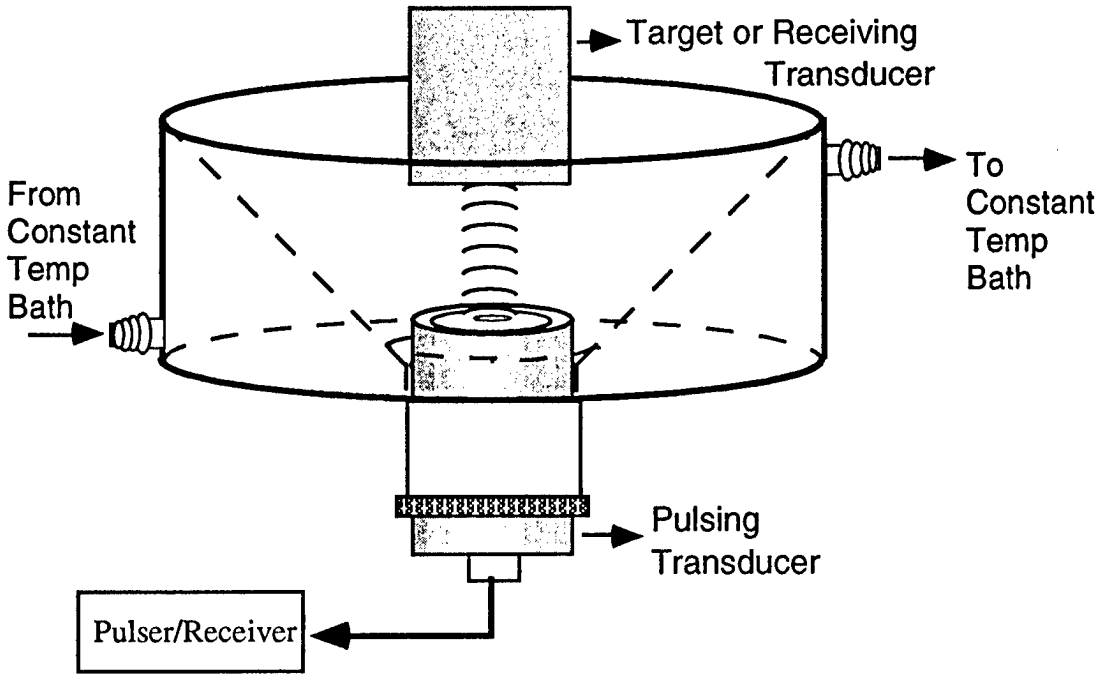

Figure 10. Ultrasonic Spectroscopy Chamber

Figure 11 illustrates the oscilloscope wave forms and respective fast Fourier transforms (FFT) from a transducer emitting a 20-MHz signal into liquid (top) and gelled (bottom) gelatin. On the left side of the oscilloscope wave forms is the initial pulse of the transducer and on the right is the reflection from the front surface of an aluminum target and then from the back surface of the target. Because sound travels slower in gelled gelatin, a shift to the right can be seen in the reflections. The FFTs of these wave forms show that in the gelled state the high frequencies are attenuated due to their absorption by the gelatin. Gelatin is an ideal model system because it is not harmful to the transducers and may be gelled and then melted over a small temperature range.

If we record the oscilloscope wave forms over the gellation and melting time periods and convert the signal intensities into a color-intensity scale, we can generate a plot that shows how the wave velocity changes during these transformations. Figure 12 shows this type of plot for gellation (top) and melting (bottom) of gelatin. The top of Figure 12 shows that there is a gradual slowing of the wave velocity as the gelatin approaches the gelled state. Upon heating, the gel network collapses to a liquid and there is a sharp increase in the wave velocity as the signal shifts to the shorter times.

Ultrasonic spectroscopy is a new technique that gives us access to a wealth of important information. It will continue to be developed in the future for analysis of viscoelastic properties, extensional and shear studies, polymerization and curing characterization, and three-dimensional mapping of heterogeneities and domains as they grow in a matrix. The apparatus currently used

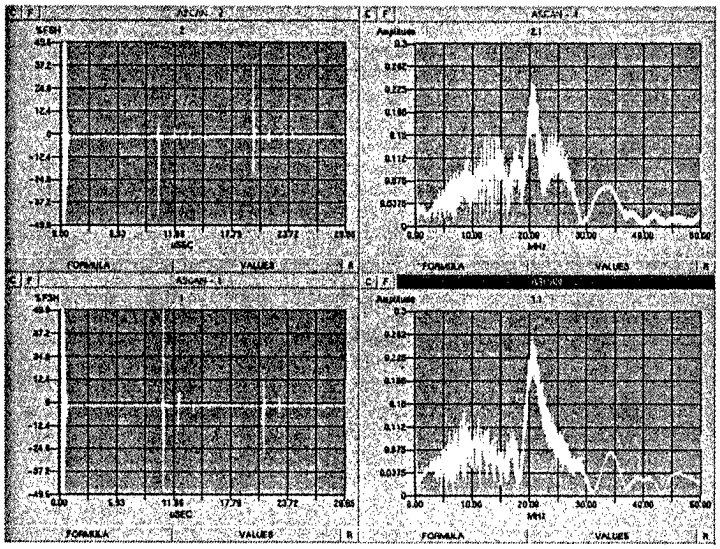

Figure 11. Top: Oscilloscope Wave Form (left) and Fast Fourier Transform (right) of Wave Form From Transducer Response of Liquid Gelatin. Bottom: Same Spectra for Gelled Gelatin.

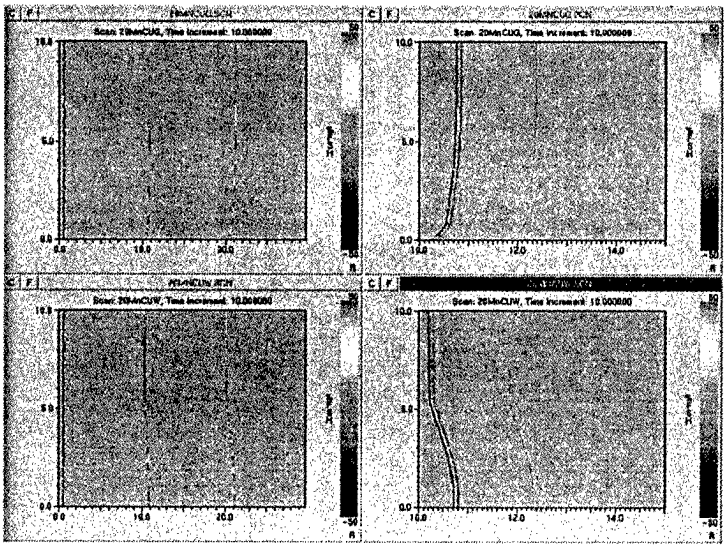

Figure 12. Plot of Oscilloscope Wave Forms Over the Gellation (top) and Melting Periods (bottom) With the Signal Intensities Converted to a Color-Intensity Scale. Left side is an expanded view of reflections from aluminum target.

(Figure 10) for the gelatin experiments is basic in design and has limited capabilities. New apparatus must be developed that will allow us to conduct the more complex experiments. A broader temperature range (-30 to 200°C) and control of the temperature ramp rate is required to examine transitions such as T_g and crystallization. The new apparatus must continue to perform pulse echo experiments and through transmission experiments that require precise alignment of the transducers. A new port must be designed to accept transducers of various types and subsequent case sizes. The transducers we will use range in frequencies from 5 to 150 MHz and depending on the application, will emit a flat face pulse or a highly focused beam of ultrasonic waves.

Data Analysis

Ultrasonic spectroscopy can be used to measure absorption spectra between different phases of material (e.g., degraded vs. bulk polymer) and the frequencies absorbed will contain information regarding the length scale of heterogeniety causing the absorption differences in the materials ability to dissipate mechanical energy (1,2). To illustrate this technique we measured the absorption spectra of the gelatin in the liquid and solid phases using the methods outlined previously. Further, the absorption spectra difference between the liquid and gelled states can be easily determined by subtracting the absorption spectra of the solid phase from that of the liquid phase. This is illustrated for the gelatin in Figure 13.

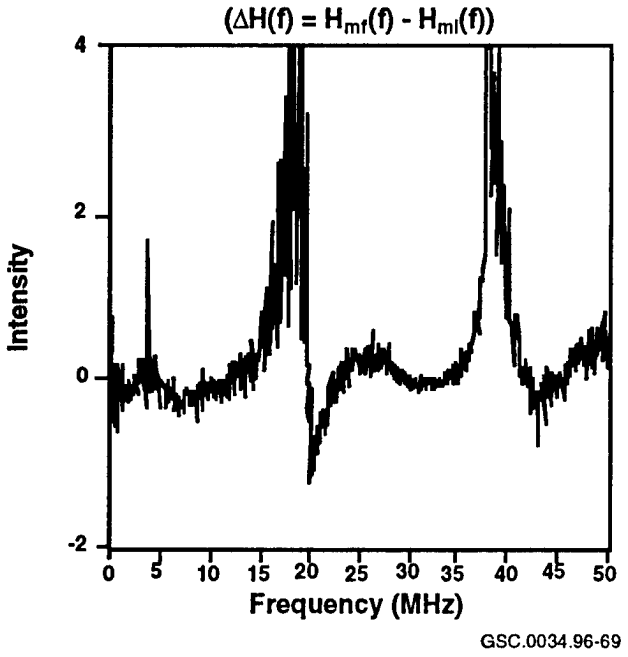

Figure 13. Absorption Spectra of Gelatin

REFERENCES

1. M. Matsushige et al. (1995) Ultrasonic Spectroscopy for Polymeric Materials, Adv. Polym. Sci., 125, 148, Springer-Verlag Berlin Heidelberg.

2. I. Alig, K. Nancke, and G.P. Johari (1996) J. Polym. Sci., Polym. Phys., 32, 1465.

A MICROSCALE COMBUSTION METHOD FOR DETERMINING FLAMMABILITY PARAMETERS OF POLYMERS

Richard N. Walters and Richard E. Lyon*
Fire Research Section, AAR-422
Federal Aviation Administration
William J. Hughes Technical Center
Atlantic City International Airport
New Jersey 08405

**Galaxy Scientific Corporation*
2500 English Creek Avenue
Egg Harbor Township, NJ 08234

A microscale flow calorimetric method has been developed to measure flammability parameters of milligram samples under conditions which approximate flaming combustion. The present work seeks to improve upon a previously published thermogravimetric technique for determining flammability characteristics of polymeric materials[1, 2] by better reproducing the solid and gas phase processes associated with the flaming combustion of solid materials. The new microscale calorimeter accomplishes these objectives by rapid (>200 K/min) heating of milligram samples to a constant, calibrated heat flux in a thermogravimetric analyzer under an inert atmosphere followed by high-temperature combustion of the pyrolyzate stream in excess oxygen. These processes correspond to the anaerobic thermolysis which occurs under non-oxidizing/reducing conditions to generate gaseous fuel and char in the pyrolysis zone of a burning solid and subsequent oxidative combustion in a diffusion flame.

Figure 1 is a schematic of the microscale flow calorimeter. The mass loss rate is continuously monitored during the test in a thermogravimetric analyzer while the sample is pyrolyzed in an inert environment. The volatilized thermal decomposition products are swept from the pyrolysis chamber in the nitrogen purge gas stream through a heated transfer line and combined with an excess of oxygen in a heated manifold at the entrance to a coiled tubular combustion chamber. The combustion furnace is maintained at several hundred degrees Centigrade, temperatures high enough to completely oxidize all of the pyrolyzed organic material. Complete oxidative combustion of the gaseous pyrolyzate occurs in the tubular reactor analogous to the combustion process in a well ventilated diffusion flame. The fuel/oxygen ratio and residence time in the combustor are controlled through purge gas and oxygen flow rate adjustments so that incomplete combustion of the pyrolyzate stream is also possible. Complete and incomplete combustion products are scrubbed from the gas stream as it exits the tubular combustor. The heat release rate (kW/g) is calculated from oxygen consumption and mass flow rate measurements of the scrubbed gas stream. The total heat released (kJ/g) is obtained by numerical integration of the heat release rate, and the char yield is determined from the residual mass in the TGA. The effective heat of combustion is calculated as the total heat divided by the mass loss, and the combustion efficiency is from the effective heat of combustion divided by the chemical heat of complete combustion as determined in an oxygen bomb calorimeter.

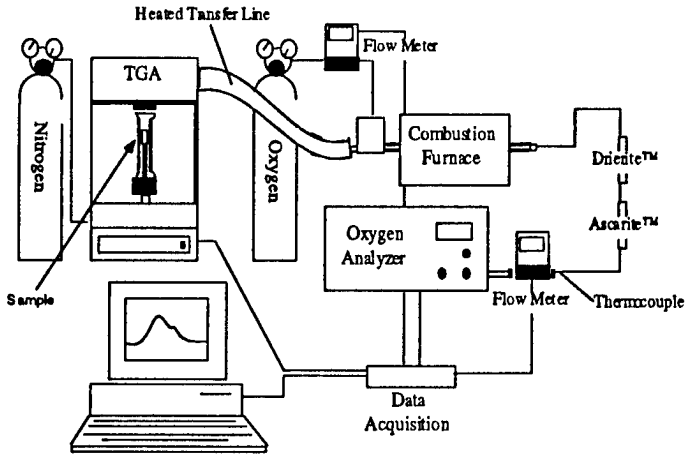

Figure 1. Schematic of Microscale Calorimeter

Figure 2 is a composite plot of the heat release rate data for some polymers tested in the microscale heat release rate device during 200 K/min heating to a 50 kW/m² incident heat flux under nitrogen in the TGA furnace. The microscale heat release rate data are expressed as kilowatts per gram of original material in order to normalize the curves since the surface area of the sample varies between tests depending on the physical form of the material (e.g., powder, film, etc.). The polymers tested show a two order of magnitude range in peak heat release rate in the microscale device between the highest and lowest values.

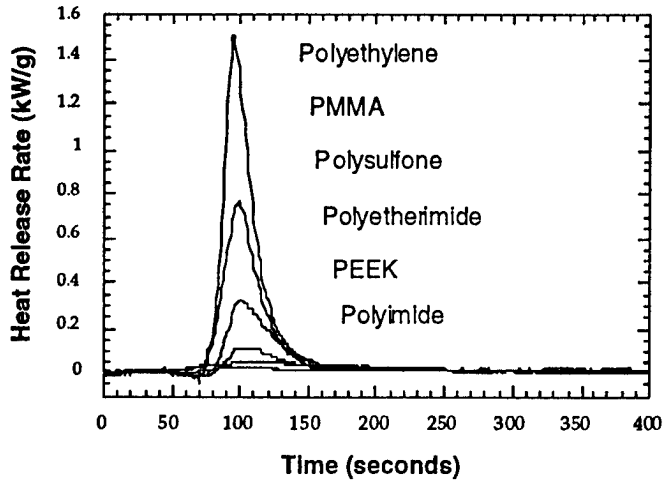

Figure 2. Heat Release Rate Curves for Various Polymers at 50 kW/m² Incident Heat Flux in the Mini Calorimeter

Figure 3 compares the peak heat release rate (HRR) data from the microscale heat release device to average heat release rate data from large (decagram) samples measured in a conventional cone calorimeter at 50 kW/m² incident heat flux for polymers where these data were available[3-7].

The cone calorimeter heat release rate values plotted in Figure 3 are steady-state or average values obtained by dividing the reported effective heat of combustion per unit area by the time of flaming combustion. Average heat release rate in the cone calorimeter is the bench-scale fire parameter which should correlate with microscale calorimetric heat release rate if the steady-state

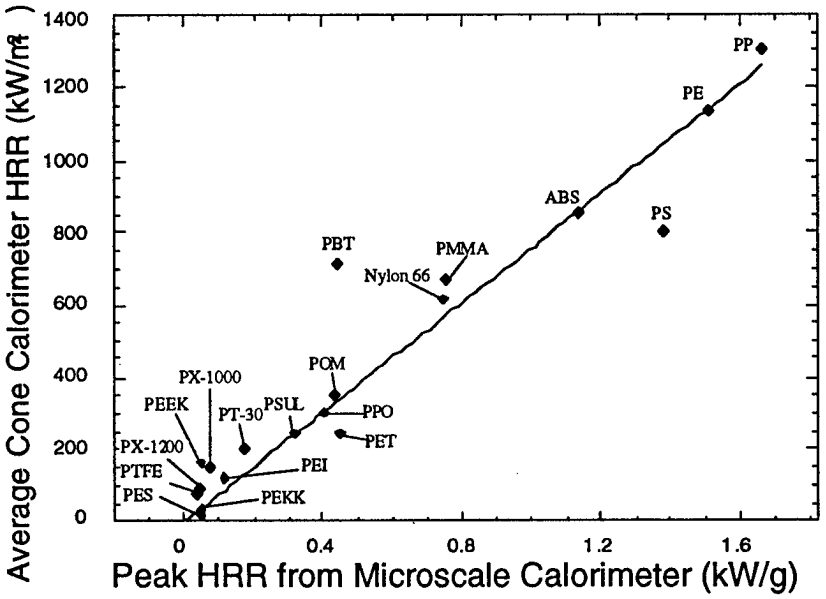

Figure 3. Correlation Between Polymer Peak Heat Release Rate (HRR) in Microscale Device and Cone Calorimeter at 50 kW/m² Incident Heat Flux

heat release of thermally thick specimens is simply a superposition along the time axis of the isothermal heat release rate of the constant thickness, constant temperature pyrolysis zone as it moves through the sample during solid flaming combustion[8].

Figure 3 indicates a good correlation between the peak heat release rates measured in the microscale device and the steady-state values measured in the bench-scale cone calorimeter. As cone calorimeter heat release rate data appears to correlate well with full-scale fire tests[9,10] microcalorimetric heat release rate should also be a good predictor of full-scale fire performance.

Separating the thermochemical and thermophysical phenomena of flaming solid combustion in the microscale calorimetric method will more accurately reproduce the local fire environment at the surface of a burning solid and should allow direct correlation with bench- and full-scale fire calorimetry tests. This is enabled by the decoupling of the intrinsic, time-dependent chemical processes of material combustion from transient effects associated with thermal diffusion in large samples. It is hoped that the new microscale combustion flow calorimeter will accelerate the development of new fire-resistant materials by providing flammability parameters which are physically meaningful for use in fire hazard evaluation and will help relate material properties to full-scale fire performance.

REFERENCES

1. T.D. Gracik and G.L. Long, "Heat Release and Flammability of a Small Specimen using Thermoanalytical Techniques," in *Fire Calorimetry*, Proceedings from the 50th Calorimetry Conference, R.E. Lyon and M.M. Hirschler Eds., Gaithersburg, MD, DOT/FAA/CT-95/46 (1995).
2. T.D. Gracik, G.L. Long, U.A.K. Sorathia, and H.E. Douglas, "A Novel Thermogravimetric Technique for Determining Flammability Characteristics of Polymeric Materials," in *Fire Calorimetry*. Proceedings from the 50th Calorimetry Conference, R.E. Lyon and M.M. Hirschler Eds., Gaithersburg, MD, DOT/FAA/CT-95/46 (1995).
3. Fire Calorimetry, R.E. Lyon and M.M. Hirschler, Eds. Proceedings from the 50th Calorimetry Conference, Gaithersburg, MD, DOT/FAA/CT-95/46 (1995).
4. M.J. Scudamore, P.J. Briggs, and F.H. Prager, "Cone Calorimetry–A Review of Tests Carried out on Plastics for the Association of Plastic Manufacturers in Europe," Fire and Materials, 15, p. 65-84 (1991).
5. T. Kashiwagi and T.G. Cleary, "Effects of Sample Mounting on Flammability Properties of Intumescent Polymers," Fire Safety Journal, 20, pp. 203-225 (1993)
6. M.M. Hirschler in Heat Release in Fires, V. Babrauskas and S. Grayson, Eds., Elsevier Applied Science, New York, (1992).
7. A. Grand, SBIR Phase I Final Report, DTRS-57-94-C-00172.
8. R.E. Lyon, "Material Properties and Flammability of Polymers," Proceedings of the 41st International SAMPE Symposium and Exhibition, Anaheim, CA, March 24-28, 1996.
9. C.P. Sarkos and R.G. Hill, "Evaluation of Aircraft Interior Panels Under Full-Scale Cabin Fire Conditions," Proceedings of the AIAA 23rd Aerospace Sciences Meeting, Reno, NV, Jan. 14-17, 1985.
10. J.G. Quintiere,V. Babrauskas, L. Cooper, M. Harkelroad, K. Steckler, and A. Tewarson, "The Role of Aircraft Panel Materials in Cabin Fires and Their Properties," DOT/FAA/CT-84/30 (June 1985).

INTEGRAL METHOD OF NONISOTHERMAL KINETIC ANALYSIS

Richard E. Lyon
Fire Safety Section, AAR-422
Federal Aviation Administration
William J. Hughes Technical Center
Atlantic City International Airport
New Jersey 08405

ABSTRACT

A new series solution for the constant heating rate Arrhenius integral is the basis of a method for determining the kinetic parameters of a single-step reaction from temperature scanning experiments. Isoconversion formulas are derived for calculating the Arrhenius activation energy and frequency factor of a reaction independent of the form of the rate law. Thermogravimetry data for pyrolysis of low-density polyethylene and differential scanning calorimetry data for the phenylethynyl curing reaction were analyzed and activation energies were determined that agreed with literature values. In contrast to existing integral methods, frequency factors for the pyrolysis and curing reaction were obtainable using the present approach without any assumptions about the reaction order or the form of the conversion function.

INTRODUCTION

Many technologically important processes and reactions occur under nonisothermal conditions and it is often desired to calculate or predict the progress of the reaction over time during transient heating. Integral methods of nonisothermal analysis utilize cumulative values of a species concentration, heat of reaction, weight loss, etc., measured in temperature scanning experiments to extract the kinetic parameters of a reacting system and determine a suitable rate law[1-13]. These powerful methods derive from the programmable heating rate capability of modern thermal analysis equipment and are useful for calculating preconversion during the heat up period in isothermal experiments[11], for testing reaction models over a broad temperature and conversion range[13], etc. Despite their utility however, integral methods have suffered from low sensitivity, a dependence on the form of the rate law, an assumption that the reaction mechanism does not change with temperature, and the somewhat cumbersome mathematics of the series approximations for the Arrhenius integral required in the analyses[3,11]. An exact solution of the Arrhenius integral is possible only for nonlinear temperature programs[3] but this capability is beyond most commercial instruments.

Since the overwhelming majority of thermal analyses are conducted at constant heating rate, the present work seeks to develop a more useful approximation for the Arrhenius integral under experimental conditions of a linear temperature program and extend these results to the unam-

biguous determination of Arrhenius kinetic parameters. It is hoped that the results of this work will aid process development of new fire-resistant thermoset resins and advance the study of polymer flammability by allowing more accurate calculation of the gasification rate in the pyrolysis zone of burning polymers[14]. Since the rate-limiting step in isothermal polymer pyrolysis is the breaking of primary chemical bonds in the molecule[15], a direct method for determining pyrolysis rate constants will facilitate the decoupling of diffusion and chemical kinetics during burning and help relate polymer structure to flammability.

BACKGROUND

Rate laws of the type

$$\frac{d\alpha}{dt} = f(\alpha,T) \tag{1}$$

are the basis for almost all of the kinetic methods used in differential thermal analysis and differential scanning calorimetry[1–13, 16]. In equation 1, T is the absolute temperature and

$$\alpha = \frac{C(t) - C(0)}{C(\infty) - C(0)}$$

is a fractional conversion in terms of the instantaneous, C(t), initial, C(0), and final, C(∞), values of a measurable reaction parameter such as a species concentration, heat of reaction, pyrolyzed mass, etc. Equation 1 is written such that α increases with time, t. The temperature dependence of f(α,T) is usually assumed to reside exclusively in a rate constant, k, which has the Arrhenius form

$$k = A \exp(-E_a/RT)$$

where A is the pre-exponential or frequency factor, E_a the activation energy for the reaction, and R the universal gas constant. These assumptions lead to the generalized reaction rate law

$$\frac{d\alpha}{dt} = k\, f(\alpha) \tag{2}$$

If k is independent of α and f(α) is independent of T, separation of variables in equation 2 gives

$$F(\alpha) \equiv \int_{\alpha_o}^{\alpha} \frac{d\alpha'}{f(\alpha')} = \int_o^t k\, dt' = \int_o^t A e^{-E_a/RT}\, dt' \tag{3}$$

where primed symbols denote variables of integration. At constant temperature, F(α) = kt, which is the basis for isothermal kinetic analyses[1, 3, 11, 13, 17]. A variety of f(α) have been assumed or derived for individual cases[1, 4, 5, 13, 17] such that a linear F(α) versus time plot is

obtained at a particular temperature having slope k(T). The Arrhenius parameters A and E_a for the reaction are determined from a number of constant temperature experiments by plotting the natural logarithm of k(T) versus 1/T over the temperature domain of interest.

The isothermal procedure based on equation 2 requires a priori knowledge of $F(\alpha)$ and the measured kinetic parameters are valid only for the temperature range examined. Usually $f(\alpha)$ and therefore $F(\alpha)$ are not known prior to the experiment so various methods have been proposed to allow determination of E_a and $f(\alpha)$ separately or in combination from a series of temperature-scanning experiments at different constant heating rates[1–3, 6–13]. For a constant heating rate, $dT/dt = \beta$, equation 3 can be written

$$F(\alpha) = \frac{A}{\beta}\int_{T_o}^{T} e^{-E_a/RT'}\,dT' \tag{4}$$

where the sample temperature is uniform but changes linearly from T_o to T over the time interval (0, t). Application of nonisothermal or integral methods to experimental data requires evaluating the exponential temperature (Arrhenius) integral on the right-hand side of equation 4. Unfortunately, the Arrhenius integral has no exact solution so numerical or approximate solutions are required.

Series solutions for the Arrhenius integral can be expressed as a polynomial, p(x), where, $x = -E_a/RT$, so that equation 4 takes the form

$$F(\alpha) = \frac{AE_a}{\beta R}\int_{x_o}^{x} \frac{e^{x'}}{x'^2}\,dx' = \frac{AE_a}{\beta R}\,p(x')\Big|_{x_o}^{x} \tag{5}$$

Several of these series solutions have been derived and Flynn and Wall provide an excellent review[3]. Typical of the series solutions for the Arrhenius integral is an asymptotic expansion of the exponential integral after a single integration by parts[18], i.e.,

$$p(x) = \frac{e^x}{x^2}\left[1 + \frac{2!}{x} + \frac{3!}{x^2} + \frac{4!}{x^3} \cdots\right] \tag{6}$$

and Schlomilch's expansion[19]

$$p(x) = \frac{e^x}{x(x-1)}\left[1 - \frac{1}{(2-x)} + \frac{2}{(2-x)(3-x)} - \frac{4}{(2-x)(3-x)(4-x)} + \cdots\right] \tag{7}$$

A property of these integral expansions is that the difference between the true value of the function and the sum of a finite number of terms in the series is essentially of the order of magnitude of the last term retained. This requires that either $-x > 30$, or that a few terms be retained in the series expansions for $-x < 10$, to achieve an accuracy greater than 95%. An empirical equation for p(x) was proposed by Doyle[6],

$$p(x) = 7.03 \times 10^{-3}\, e^{x\,B(x)} \tag{8}$$

where B(x) ranges from 1.195 to 1.034 over the domain, x = –10 to –60. An average value, B(x) = 1.052, is often used in integral methods of thermal analysis[2, 3, 6, 8, 11, 13].

Arrhenius Integral Approximation

The intractability of multiterm series approximations required for accurate evaluation of the Arrhenius integral has limited the utility of integral methods for quantitative kinetic analysis. The following derivation leads to a simple, semianalytic result which provides better accuracy than any previous single-term approximation of the constant heating rate Arrhenius temperature integral.

Begin by defining a new variable, $y = e^x/x^2$, so that equation 4 becomes

$$F(\alpha) = \frac{AE_a}{\beta R}\int_{y_o}^{y} f(y')\,dy' \tag{9}$$

with, f(y) = x/(x–2). A single integration by parts gives

$$F(\alpha) = \frac{AE_a}{\beta R}\left\{\left[\frac{e^{x'}}{x'(x'-2)}\right]\Bigg|_{x_o}^{x} + 2\int_{x_o}^{x}\frac{e^{x'}dx'}{x'^2(x'-2)^2}\right\} \tag{10}$$

Repeated integration by parts transforms the right-hand side of equation 10 to

$$F(\alpha) = \frac{AE_a}{\beta R}\frac{e^{x'}}{x'(x'-2)}\left[1 + \frac{2}{x'(x'-2)} + \frac{8}{x'(x'-2)^2} + O(x'^{-4}) + O(x'^{-5}) + \ldots\right]\Bigg|_{x_o}^{x} \tag{11}$$

which contains a new series solution for the Arrhenius integral,

$$p(x) = \frac{e^x}{x(x-2)}\left[1 + \frac{2}{x(x-2)} + \frac{8}{x(x-2)^2} + O(x^{-4}) + O(x^{-5}) + \ldots\right] \tag{12}$$

The first term of equation 12, $p(x) = e^x/(x(x–2))$, is identical to the first two terms of the Schlomilch expansion (equation 7).

For the normal temperature ranges and activation energies of scanning thermal analysis the lower limit in equation 11 can be neglected since, $-xo >> -x$. Moreover, since $-x \geq 10$ (typically), only the first term of equation 11 need be retained

$$F(\alpha) \approx \frac{AE_a}{\beta R} \frac{e^x}{x(x-2)} = \frac{ART^2}{\beta(E_a + 2RT)} e^{-E_a/RT} \tag{13}$$

By way of comparison Doyle's approximation (equation 8) leads to the single-term result

$$F(\alpha) \approx 7.03 \times 10^{-3} \frac{AE_a}{\beta R} e^{-1.052 E_a/RT} \tag{14}$$

while the first term of the asymptotic expansion (equation 7) gives

$$F(\alpha) \approx \frac{AE_a}{\beta R} \frac{e^x}{x^2} = \frac{ART^2}{\beta E_a} e^{-E_a/RT} \tag{15}$$

Equation 13 differs from equation 15 by the factor 2RT in the denominator. Because of their simplicity, equations 14 and 15 are commonly used in integral methods of thermal analysis[1–3, 6–8, 11–13].

The relative percent error associated with the use of Doyle's approximation (equation 14) and the single-term asymptotic expansion (equation 15) as solutions of the Arrhenius integral for a physically realistic domain of x are plotted in Figure 1 along with the error for the present result, equation 13. The exact value of the Arrhenius integral used for the error calculation was obtained by double precision numerical integration of equation 4 using the trapezoidal rule with a step size of 0.5K between the limits: $T_o = 300K$, T. Figure 1 shows that equation 13 is significantly more accurate than either of the single-term approximations, equation 14 or equation 15, as a solution of the Arrhenius integral. Equation 13 under predicts the true value of the Arrhenius integral by less than 1% over the domain $-x \geq 10$ normally encountered in experimental studies. Comparable accuracy requires at least three terms of the asymptotic expansion or the first two terms of the Schlomilch expansion[20].

Figure 2 is a plot of the percent relative error versus temperature using equation 13 to approximate the Arrhenius integral for a range of activation energies. An accuracy of greater than 99% is obtained for $E_a \geq 100$ kJ/mol over the temperature range normally examined in scanning thermal analyses. The positive catastrophe in Figure 2 at low temperatures is the result of neglecting the lower limit of integration in arriving at equation 13, which becomes significant as T approaches T_o.

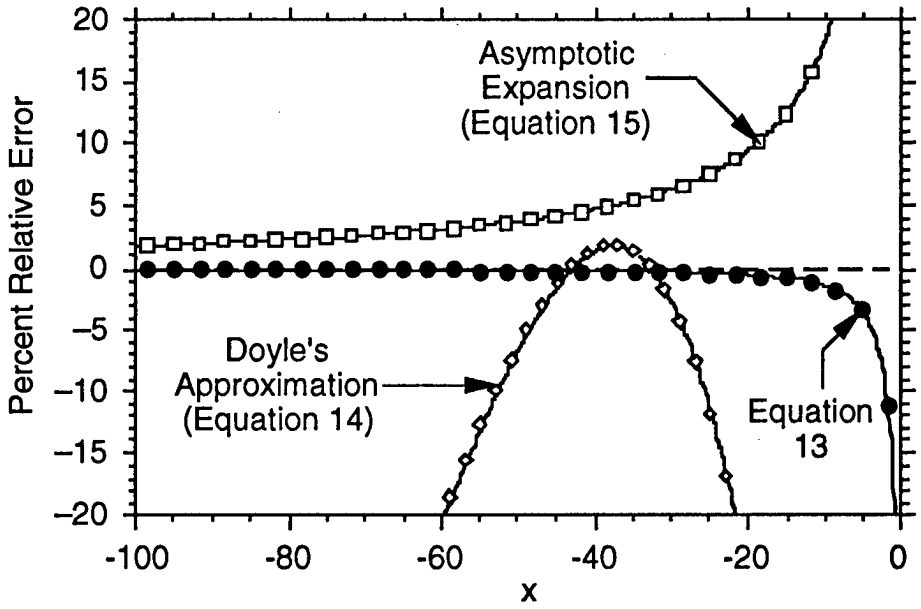

Figure 1. Percent Relative Error Versus $x = -E_a/RT$ for Equations 13, 14, and 15 as Approximations for the Arrhenius Integral

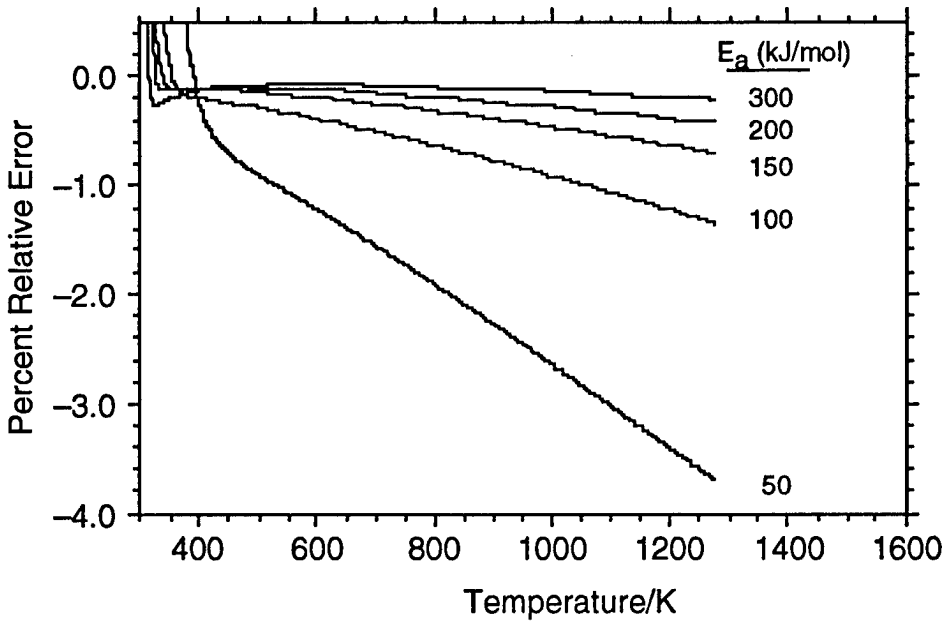

Figure 2. Percent Relative Error Versus Temperature for Equation 13 with E_a = 50, 100, 150, 200, and 300 kJ mol^{-1}

Kinetic Parameters from Constant Heating Rate Experiments

The determination of both A and E_a from isothermal or nonisothermal experiments requires a priori knowledge of $f(\alpha)$ or $F(\alpha)$. A common functional form for $f(\alpha)$ is an arbitrary (*n*-th) order reaction[1,3–13, 17, 18] which allows an analytic solution for $F(\alpha)$ and provides an additional fitting

parameter–the reaction order, n. However, while A and E_a have physical significance[14] their numerical values and the reaction order determined from three-parameter fits of *n*-th order kinetics to conversion data is questionable except in the case of a well-defined reaction mechanism[3]. To circumvent the need to assume *n*-th order reaction kinetics to extract kinetic parameters, isoconversion methods[2, 8, 11] have been developed which utilize temperature and heating rate data at a fixed value of α and thus, presumably, a fixed value of $F(\alpha)$. This eliminates the need to assume a functional form for $F(\alpha)$ to determine the activation energy of the reaction but precludes simultaneous determination of the frequency factor. Typical of the isoconversion methods is an iterative technique for determining E_a directly from conversion versus temperature data at different heating rates proposed by Wall[2]. The method is based on Doyle's approximation of the Arrhenius integral (equation 14) which can be differentiated to give

$$\frac{d\ln\beta}{d\frac{1}{T(\alpha)}} \approx -B(x)\frac{E_a}{R}$$

where $T(\alpha)$ is the temperature corresponding to a specific degree of conversion at a particular heating rate. The method requires successive approximations of E_a as the empirical coefficient $B(x)$ is incremented for each new value of $E_a/RT(\alpha)$. The activation energy thus determined is independent of $F(\alpha)$ to the extent that the assumptions used to obtain equations 1-4 are valid but the method is time consuming without computerized data analysis and is empirically based[1, 3].

An analogous but more direct method for determining E_a from constant heating rate experiments without any assumptions about the form of $f(\alpha)$ or its integral $F(\alpha)$ follows from equation 13. Taking the natural logarithms of equation 13

$$\ln[F(\alpha)] = \ln A - \ln\beta - \ln\frac{1}{T(\alpha)} - \ln(2-x) + x \qquad (16)$$

where $x = x(\alpha) = -E_a/RT(\alpha)$. If $F(\alpha)$ and A are independent of temperature and β is treated as a continuous variable, equation 16 can be differentiated with respect to the reciprocal isoconversion temperature, $1/T(\alpha)$,

$$\frac{d\ln\beta}{d\frac{1}{T(\alpha)}} = -T(\alpha)\left[2 - x - \frac{2}{2-x}\right] \qquad (17)$$

The $2/(2-x)$ term on the right-hand side of equation 17 can be neglected since it accounts for less than two percent of the bracketed quantity for $-x \geq 10$. The slope of a plot of heating rate versus the reciprocal temperature at any fixed conversion is therefore

$$\frac{d\ln\beta}{d\frac{1}{T(\alpha)}} = -\left[\frac{E_a}{R} + 2T(\alpha)\right] \qquad (18)$$

from which the activation energy at a particular conversion is

$$E_a(\alpha) = -R\left[\frac{d\ \ln\beta}{d\ 1/T(\alpha)} + 2T(\alpha)\right] \tag{19}$$

If the activation energy of the reaction is known (e.g., from equation 19) and β, $T(\alpha)$ data are available, then equation 16 is a single equation with two unknowns, A and $F(\alpha)$. Determination of a unique value for the frequency factor, A, from equation 16 therefore requires a numerical value for $F(\alpha)$. If $F(\alpha)$ satisfies the usual condition for the normalized conversion integral $F(\alpha) = 1$ at $\alpha = 1$ (c.f., references 3,17), then $\ln[F(\alpha)] = 0$ at completion of the reaction and equation 13 becomes for $T(\alpha=1) \equiv T(1)$

$$\ln[F(1)] = 0 = \ln[A] - \ln[\beta] - \ln\left[\frac{1}{T(1)}\right] - \ln\left[2 + \frac{E_a}{RT(1)}\right] - \frac{E_a}{RT(1)} \tag{20}$$

from which

$$\ln\left[\frac{\beta}{T(1)}\right] = \ln[A] - \left\{\ln[\,2 + E_a/RT(1)\,] + \frac{E_a}{RT(1)}\right\} \tag{21}$$

The frequency factor is calculable by direct substitution of E_a and β,T(1) data pairs into equation 21 after some rearrangement.

$$A = \frac{\beta\,\{E_a + 2RT(1)\}}{RT(1)^2}\, e^{E_a/RT(1)} \tag{22}$$

Alternatively, E_a may be used as a fitting parameter in equation 21 to obtain unit negative slope in a plot of $\ln[\beta/T(1)]$ versus $\{\ln[2 + E_a/RT(1)] + E_a/RT(1)\}$, yielding $\ln[A]$ as the intercept. The unit slope method allows simultaneous determination of both the global activation energy and frequency factor of an arbitrary single-step reaction from a few temperature scanning experiments without any assumptions about the reaction order or the functional form of $f(\alpha)$.

From the definition of the Arrhenius rate constant and equation 22 it follows that

$$k[T(1)] = A\exp[-E_a/RT(1)] = \frac{\beta\{E_a + 2RT(1)\}}{R\,T(1)^2} \tag{23}$$

The reaction rate constant at temperature T(1) is directly calculable from E_a and the β,T(1) data pairs obtained in temperature scanning experiments.

EXPERIMENTAL

Polyethylene Pyrolysis

Table 1 is a compilation of fractional mass loss temperatures T(α) obtained in our laboratory for anaerobic pyrolysis of 3-5 mg samples of low-density polyethylene ($M_w \approx 35{,}000$ g mol^{-1}, $M_w/M_n = 4.5$, $\rho = 906$ kg m^{-3}, Aldrich Chemical) under nitrogen flowing at 0.10 L min^{-1} in a thermogravimetric analyzer (Perkin Elmer TGA-7) at constant heating rates $\beta = 5$, 10, 20, 40, 60, and 80 K min^{-1}. Figure 3 is a composite of the data in Table 1 plotted as ln[β] versus 1/T(α) for volatile fractions $\alpha = 0.01$, 0.02, 0.05, 0.10, 0.20, 0.50, and 1.00. High-correlation coefficients ($r^2 > 0.98$) were obtained for all of the linear regression curves of ln[β] versus 1/T(α) and the slopes at each conversion were used in equation 19 to calculate the activation energies plotted in Figure 4 versus fractional conversion. Individual values for the activation energy at each conversion calculated by equation 19 were within ± 0.2% of the mean value plotted in Figure 4 indicating that E_a determined by this method is effectively independent of heating rate.

Table 1. Heating Rate and Fractional Mass Loss Temperatures for Pyrolysis of Low-Density Polyethylene

Heating Rate, β	T(0.01)	T(0.02)	T(0.05)	T(0.10)	T(0.20)	T(0.50)	T(1.0)
K min^{-1}	K	K	K	K	K	K	K
5	639	655	680	695	711	726	762
10	658	678	699	715	730	749	779
20	673	691	712	726	740	761	792
40	689	706	727	741	756	776	808
60	699	713	734	749	764	784	821
80	709	723	744	758	773	793	833

The variation in activation energy with weight loss observed in Figure 4 for low molecular weight, low-density polyethylene suggests the possibility of consecutive thermal degradation reactions or a single-step reaction with a distribution of activation energies over the conversion domain. Alternatively, F(α) or A may be temperature dependent so that their derivatives with respect to 1/T are nonzero as was assumed in deriving Equation 19. The relatively constant value, $E_a \approx 200$ kJ mol^{-1}, for conversions above about 20 percent in Figure 4 is within the range of literature values, $E_a = 192$–263 kJ mol^{-1} reported for this polymer under these experimental conditions[21].

Figure 5 is a plot of the data in Table 1 according to equation 21 for the low-density polyethylene of this study. Unit negative slope in Figure 5 was obtained for $E_a = 200$ kJ mol^{-1} in agreement with the method of equation 19 and Figure 4. The correlation coefficient for the linear regression curve was $r^2 = 0.99$. The intercept of the linear plot in Figure 5 is, $26.039 = \ln[A]$ from which $A = 2.0 \times 10^{11}$ s^{-1}, a typical value for the frequency factor or pre-exponential term in polymer thermal degradation[13].

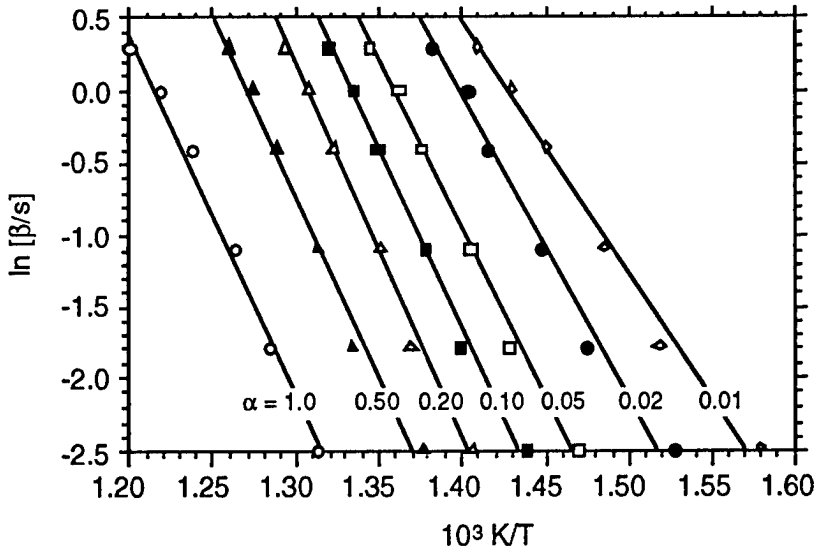

Figure 3. Plot of Natural Logarithm of Heating Rate Versus the Reciprocal Temperature for Volatile Fractions, α = 0.01, 0.02, 0.05, 0.10, 0.20, 0.50, and 1.0 for Low Molecular Weight, Low-Density Polyethylene

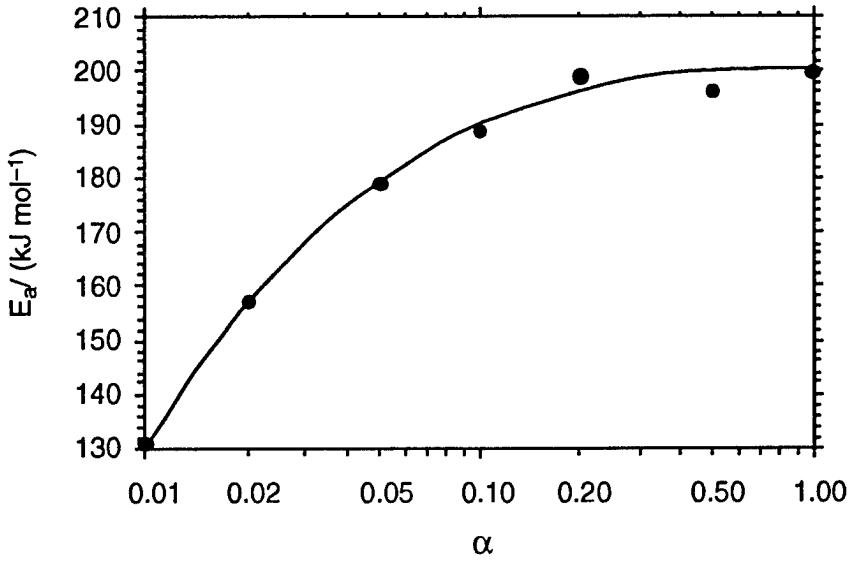

Figure 4. Activation Energy Versus Fractional Weight Loss for Low-Density Polyethylene Calculated from Equation 19

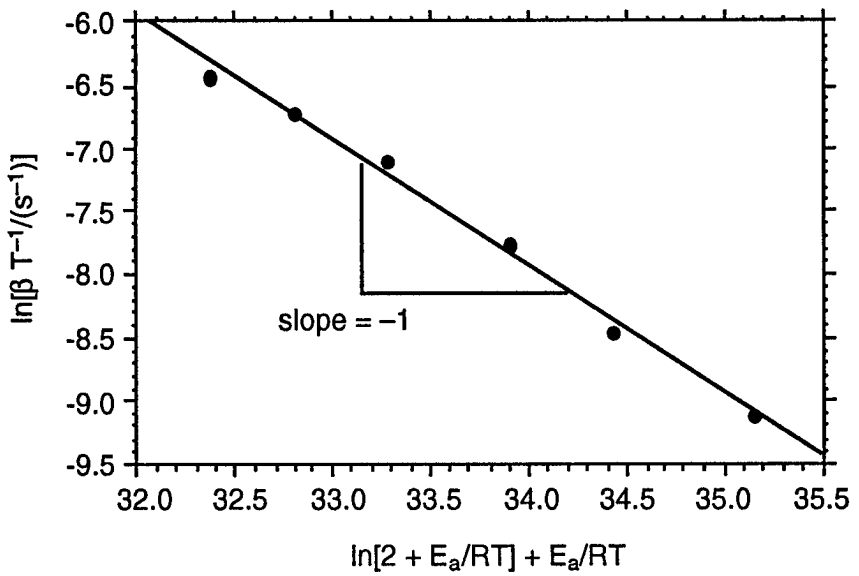

Figure 5. Plot of ln[β/T] Versus {ln[2 + E_a/RT] + E_a/RT} for Thermal Degradation of Low-Density Polyethylene at Complete Conversion According to Equation 21 With E_a = 200 kJ mol^{-1}

Phenylethynyl Curing Reaction

The present integral method of nonisothermal kinetic analysis was also applied to differential scanning calorimetry data for the curing reaction exotherm of phenylethynyl-terminated imide oligomers obtained by Hinkley[22, 23]. These phenylethynyl curing experiments were conducted on approximately 7-mg samples of the oligomer in a differential scanning calorimeter (Shimadzu DSC-50) at heating rates of 5, 20, 40, 60, and 80 K min^{-1}. Samples of fine powder were contained in open platinum pans purged with nitrogen at a flow rate of 0.03 L min^{-1} during the temperature scanning experiments. Fractional conversion, α, was calculated as the cumulative heat of reaction up to a particular temperature in the scanning experiments divided by the total heat of reaction at the incipient temperature of complete reaction according to standard methods[24]. Linear baselines were assumed.

Hinkley's analysis of these data using Wall's[2] isoconversion method and Doyle's integral approximation (equation 14) for a = 0.10, 0.30, 0.50, 0.90 yielded an average activation energy for the phenylethynyl curing reaction, E_a = 139.0 ± 3.3 kJ mol^{-1}. However, for this activation energy and temperature range x = – E_a/RT ≈ –(139 kJ mol^{-1})/(8.314 J mol^{-1} K^{-1})(800K) = –21 and the more accurate empirical constant B(x) = 1.098[2] should have been used in equation 14 in place of the average B(x) = 1.052. This single iteration of B(x) as per Wall[2] improves the activation energy estimate for the phenylethynyl curing reaction to E_a = 133.2 ± 3.2 kJ mol^{-1} which agrees well with studies by other investigators who had found E_a = 132.3 and 152.8 kJ mol^{-1} for the curing reaction of phenylethynyl-terminated model compounds[25]. Attempts by Hinkley to determine a single frequency factor for the phenylethynyl curing reaction were unsuccessful due to the presence of both F(α) and A in equation 14. Hinkley assumed n-th order kinetics with n = 3/2 and used the β-independent conversion value α ≈ 0.48 at the peak reaction rate

temperature to obtain a numerical value for F($\alpha = 0.48$). Substituting F(0.48) into equation 14 resulted in a range of frequency factors, $A = 10^5$ to 10^9 s^{-1} for the phenylethynyl curing reaction.

Phenylethynyl curing data at complete conversion not published in the original work were kindly provided by Hinkley[23] and are given in Table 2. Analysis of these data using equation 19 with the best-fit slope of the linear regression of ln[β] versus 1/T(1) gives an average $E_a = 132.8 \pm 0.6$ kJ mol^{-1}. Substituting $E_a = 132.8$ kJ mol^{-1} into equation 22 gives $A = 9.8 \pm 0.8 \times 10^6$ s^{-1} for the five data pairs. By comparison, the unit negative slope method at total conversion (equation 21) plotted in Figure 6 gives $E_a = 133.4$ kJ mol^{-1} and $A = 10.7 \times 10^6$ s^{-1} with a correlation coefficient $r^2 = 0.992$. These activation energies for the phenylethynyl curing reaction determined from equations 19 and 21 are self-consistent and in quantitative agreement with the published values, while the frequency factors for this reaction determined from equations 21 and 22 are well within the estimated range for this Arrhenius parameter.

Table 2. Heating Rate and Incipient Completion Temperatures for Phenylethynyl Curing Reaction[23]

β/(K min^{-1})	5	20	40	60	80
T(α=1)/K	726	778	795	810	821

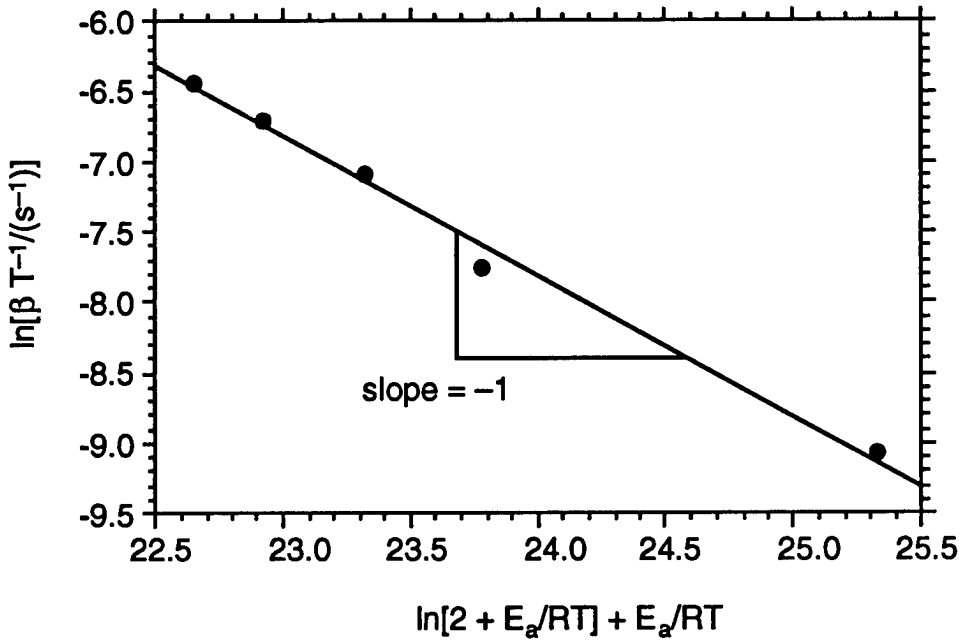

Figure 6. Plot of ln[β/T] Versus {ln[2 + E_a/RT] + E_a/RT} for Cure of Phenylethynyl-Terminated Imide Oligomer at Complete Conversion According to Equation 21 with $E_a = 133$ kJ mol^{-1}

CONCLUSIONS

A new series solution provides an accurate single-term approximation for the constant heating rate Arrhenius integral which can be used to determine the activation energy and frequency factor of an arbitrary, single-step reaction from a series of temperature scanning experiments. No assumptions about the form of the rate law are necessary to apply the present integral method to the analysis of nonisothermal reaction data. Agreement of the calculated Arrhenius activation energy and frequency factor for polyethylene pyrolysis and ethynyl curing reactions with literature values demonstrates the general utility of the present approach for determining kinetic parameters of single-step reactions from constant heating rate experiments. Determination of a physically meaningful reaction rate law from isothermal experiments is possible since the Arrhenius rate constant at complete conversion can now be obtained independent of any assumptions about reaction order or the form of the conversion function.

REFERENCES

1. W. W. Wendlandt in Thermal Methods of Analysis, 2nd Edition, John Wiley & Sons., New York, 1974, Chapter V.C.
2. J.H. Flynn and L.A.Wall, Polym. Letters, 4, (1966) p. 323.
3. Flynn and L.A. Wall, General Treatment of the Thermogravimetry of Polymers, J. Res. Natl. Bur. Stds.–A. Physics and Chemistry, 70A (6) (1966) p. 487.
4. J.D. Nam and J.C. Seferis, J.Polym.Sci.: Part B: Polym. Physics, 29 (1991) p. 601.
5. J.D. Nam and J.C. Seferis, J.Polym.Sci.: Part B: Polym. Physics, 30 (1992) p. 455.
6. C.D. Doyle, J. Appl. Polym. Sci., 6, (1962) p. 639.
7. A.W. Coates and J.P. Redfern, Nature, 201, (1964) p. 68.
8. T. Ozawa, Bul. Chem. Soc. A. Japan, 38 (11) (1965) p. 1881.
9. D.W. Van Krevelen, C. Van Heerden, and F.J. Huntjens, Fuel, 30 (1951) p. 253.
10. R.C. Turner and M. Schnitzer, Soil Science, 93 (4) (1962) p. 225.
11. B. Wunderlich, Thermal Analysis, Academic Press, Inc., New York, 1990, Chapter 2.1.3.
12. L. Reich, J. Appl. Polym. Sci., 9 (1965) p. 3033.
13. L. Reich and S.S. Stivala, Elements of Polymer Degradation, McGraw-Hill, New York, 1971, Chapter 2.
14. R. E. Lyon, in Fire and Polymers II: Materials and Tests for Hazard Prevention, G.L. Nelson, Ed., ACS Symposium Series, 599, American Chemical Society, Washington, D.C., 1995, Chapter 38, p. 618.
15. L. A. Wall, in Flammability of Solid Plastics, Vol. 7, Fire and Flammability Series, C.J. Helado, Ed., Technomic Publishing Co., Inc., Westport, CT, 1974, p. 323.
16. B. Wunderlich, in Thermal Characterization of Polymeric Materials, E.A. Turi, Ed., Academic Press, Inc., New York, NY, 1981, Chapter 2.D., p. 112.

17. M.Day, J.D. Cooney, and D.M. Wiles, Polym. Eng.Sci., 29 (1) (1989) p. 19.

18. E. Jahnke, F. Loesch, and F. Emde, Tables of Higher Functions, 6th Edition, McGraw-Hill, New York, 1960, p. 18.

19. O. Schlomilch, Vorlesungen uber hoheren Analysis, 2nd ed., Bruenschweig, 1874, p. 266.

20. C.D. Doyle, Nature, 207 (4994) (1965) p. 290.

21. N. Grassie and A Scotney, in Polymer Handbook, 2nd Edition, J Brandrup and E.H. Immergut, Eds., John Wiley & Sons, New York (1975), Chapter II.12.

22. J.A. Hinkley, J. Advanced Materials, 27(3) (1996) p. 55.

23. J.A. Hinkley, Composites and Polymers Branch, NASA Langley Research Center, Hampton, VA, private communication, June 1996.

24. R.B. Prime, in Thermal Characterization of Polymeric Materials, E.A. Turi, Ed., Academic Press, Inc., New York, NY, 1981, Chapter 5.IV, p. 532.

25. T. Takekoshi and J.M. Terry, Polymer, 35(22) (1994) p. 4874.

IN SITU FLAME CHEMISTRY BY REMOTE SPECTROSCOPY

Principal Investigator: S. Michael Angel
University of South Carolina
Department of Chemistry and Biochemistry
Columbia, SC 29208
Email: angel@psc.psc.sc.edu

Graduate Assistant: Brian M. Cullum

ABSTRACT

The purpose of this research is to use advanced in situ spectroscopic techniques to obtain relative concentration measurements of primary reactive species in the burn products of materials in order to help deduce fundamental relationships between chemical structure/composition and combustion mechanisms and to develop a better understanding of the thermal degradation of materials by measuring short-lived flammability products. Initial studies will use simple compounds such as toluene or styrene as models for more complex polymer blends. Styrene with dissolved brominated flame retardant will be studied as a surrogate for flame-retarded polystyrene. In situ optical measurements will be used to identify unknown species and confirm suspected ones especially transient species that are difficult to measure using off-line techniques.

INTRODUCTION

The purpose of this research is to use advanced in situ spectroscopic techniques to obtain relative concentration measurements of primary reactive species in the burn products of materials in order to help deduce fundamental relationships between chemical structure/composition and combustion mechanisms and to develop a better understanding of the thermal degradation of materials by measuring short-lived flammability products. Initial studies will use simple compounds such as toluene or styrene as models for more complex polymer blends. Styrene with dissolved brominated flame retardant will be studied as a surrogate for flame-retarded polystyrene. In situ optical measurements will be used to identify unknown species and confirm suspected ones especially transient species that are difficult to measure using off-line techniques. USC is being aided in this effort by a collaboration with the Research and Development Fire Retardants Division of Albemarle Corporation. Albemarle is also interested in the use of spectroscopic techniques to characterize species formed during combustion of flame-retarded materials and is supporting this project by providing guidance in experimental design and selection of target species, as well as by supplying some small pieces of experimental apparatus. Albemarle is also supplying brominated flame-retardant materials and plaques.

During the first year of this research project, our focus has been on setting up the laser-induced fluorescence (LIF) apparatus, testing the LIF setup by measuring OH radical (•OH) emission and

fluorescence excitation spectra in well-characterized systems, and using LIF to determine the effect of various flame-retardant species and synergists on •OH concentrations in methane flames. In addition we are investigating methods for introducing polymers into a flame or furnace including laser ablation. This report summarizes these preliminary results.

METHODS

Figure 1 shows a highly simplified schematic of our experimental LIF setup. A Nd:YAG-pumped tunable dye laser system is used to excite radical species in the flame or furnace. So far, most of our experiments have involved monitoring •OH fluorescence using an excitation wavelength of 281.1 nm. The •OH emission (right) and excitation (left) spectra are shown at the bottom of Figure 1. In all experiments discussed here, the •OH concentration was measured using the 314.58 nm emission band using a 1-m f/8 double monochromator (SPEX Model 1404) with a photomultiplier (PMT) detector connected to a fast digital oscilloscope (LeCroy Model 9350L) for data acquisition.

Figure 2 shows the results of a very simple experiment where the •OH concentration is measured versus the relative amount of air added to the methane burner. As expected, the •OH concentration is lowest at low air flow and increases with increasing air flow. The •OH concentration steadily increases with increasing air flow until, at pressures greater than 17 psi, the •OH concentration levels off as the probe volume becomes saturated.

For our first LIF study, we are measuring the effect of selected brominated flame retardants and synergists on the concentration of •OH and other radical species in a methane flame. The brominated species are suspected to be radical traps and these simple experiments are designed to provide information on the mechanisms by which the brominated species retard combustion.[1]

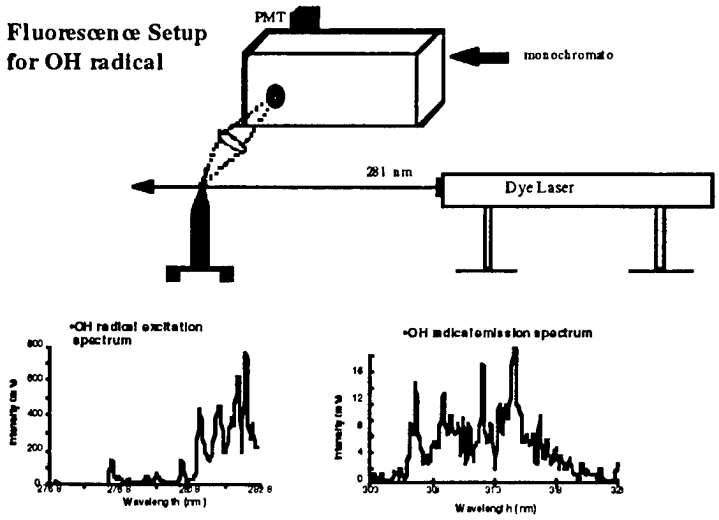

Figure 1. (Top) The Experimental LIF Setup for Measuring Radical Species in a Flame. (Bottom left) Excitation and (bottom right) Emission Spectra of •OH Measured in a Methane Flame

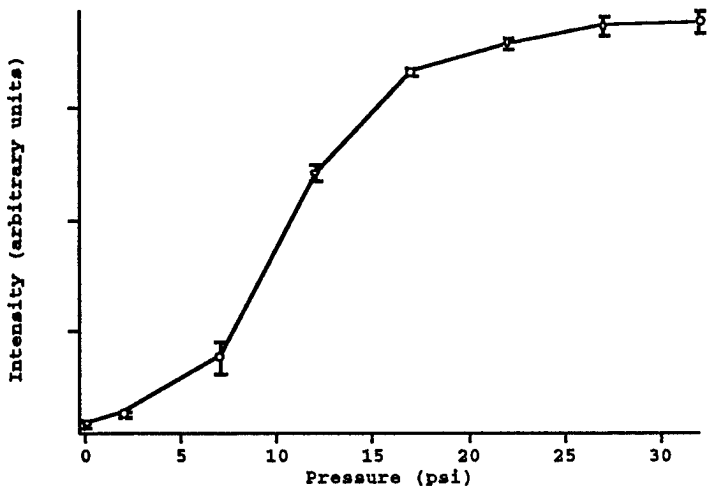

Figure 2. The Relative •OH Concentration (Fluorescence Intensity) Versus Oxidizer Flow Rate (Air) in a Methane Flame

MATERIALS

Two brominated flame retardants, a brominated aliphatic, hexabromocyclododecane or HBCD and a brominated aromatic, decabromodiphenyl oxide or DBDO, and synergsists, are being supplied by Albemarle Corp. The synergists are $SbBr_3$ and Sb_2O_3. HBCD and DBDO both act as flame retardants when used in polyvinyl chloride (PVC) and high-impact polystyrene (HIPS), respectively. The role of the synergists is not known and the exact nature of the flame-retardant species is not known. This study is being carried out to provide information concerning the roles of the various starting species. The initial experiments described here involve simply measuring the effect each species has on •OH concentrations in a flame when added alone and in combination with others.

RESULTS

All samples have been introduced into the methane flame by dissolving them in toluene and aspirating the solutions, or slurries, into the burner. The •OH fluorescence intensity was measured versus the amount of each species added to the flame. The experiments are not yet complete but preliminary results are shown in Figure 3. The middle curve (labeled HBCD) in Figure 3 shows the effect of adding HBCD to the •OH concentration that results from burning PVC in the flame. As expected, the •OH fluorescence intensity decreases with increasing concentrations of HBCD. The lower curve in Figure 3 shows the effect of adding $SbBr_3$ to the solution of PVC and HBCD. The addition of this species dramatically reduces to concentration of •OH in the flame. This is most likely due to radical trapping by •Br released in the flame. Measurements using $SbBr_3$ alone will be important in understanding the results of future experiments where this species is expected to be generated by synergsists in the flame. The addition of Sb_2O_3 to the PVC HBCD solution has no additional effect on the •OH concentration in the flame. This is not unexpected. This species has been found to act as a synergist for brominated aromatic flame retardants but should have no effect with HBCD. We also see no effect on •OH concentrations when HBr is added to the flame. This result is not completely understood since HBr has a dramatic effect on •H in H_2 flames[2]. We expect to complete this study by measuring

the effect of the Sb species on •OH and •H concentrations when used with DBDO in HIPS. In another study we also plan to determine the fluorescence lifetime of hydroxyl radicals with and without added halogenated flame retardants. This information might help verify or disprove the chemical theory (radical trap) of flame inhibition.

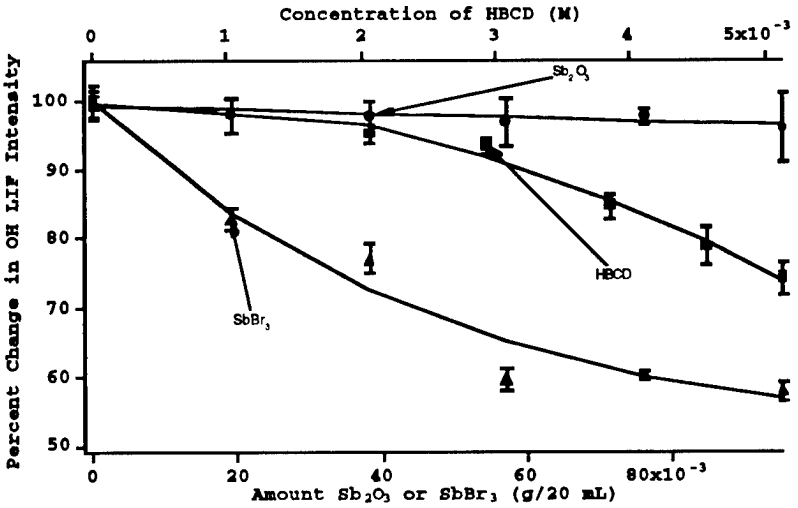

Figure 3. •OH Concentration as Measured by LIF for PVC/Toluene Aspirated into a Methane Flame with Various Additives. (Top) various amounts of Sb_2O_3 and saturated HBCD, (middle) various concentrations of HBCD, and (lower) various amounts of $SbBr_3$ and saturated HBCD.

DISCUSSION

Although the above study will likely produce useful results there are many problems associated with aspirating samples into a flame. Most importantly, it is difficult to find suitable solvents for the polymers of interest. Another inherent problem with aspiration is that the solvent might react with the chemicals prior to analysis and create erratic results. For studies involving solid polymer samples, we are investigating the use of laser ablation as a sample introduction technique. In this new technique, we use one laser to ablate particles from the polymer sample into the flame and another laser beam to excite radical fluorescence. It has been shown that high molecular weight particles are ejected from the sample surface[3,4]. We are currently characterizing this technique in terms of particle sizes, amount ejected, and particle velocities versus laser power. This information will allow us to optimize the laser ablation setup and determine the amount of material being introduced into the flame. The laser ablation setup is shown at the top of Figure 4. The laser ablation beam and fluorescence excitation beam are coincident on the polymer sample. The sample is positioned so that polymer material is ejected into the flame where it intersects the excitation beam. Particle velocities are determined by measuring the scatter of a probe beam that is placed a known distance from the solid sample (see middle and lower plots of Figure 4). Figure 5 shows an imaging setup that is being used to determine the three-dimensional spatial distribution of ejected particles as a function of laser power. Both of these studies will allow us to determine the amount of material ejected and delivered to the flame for a given laser power.

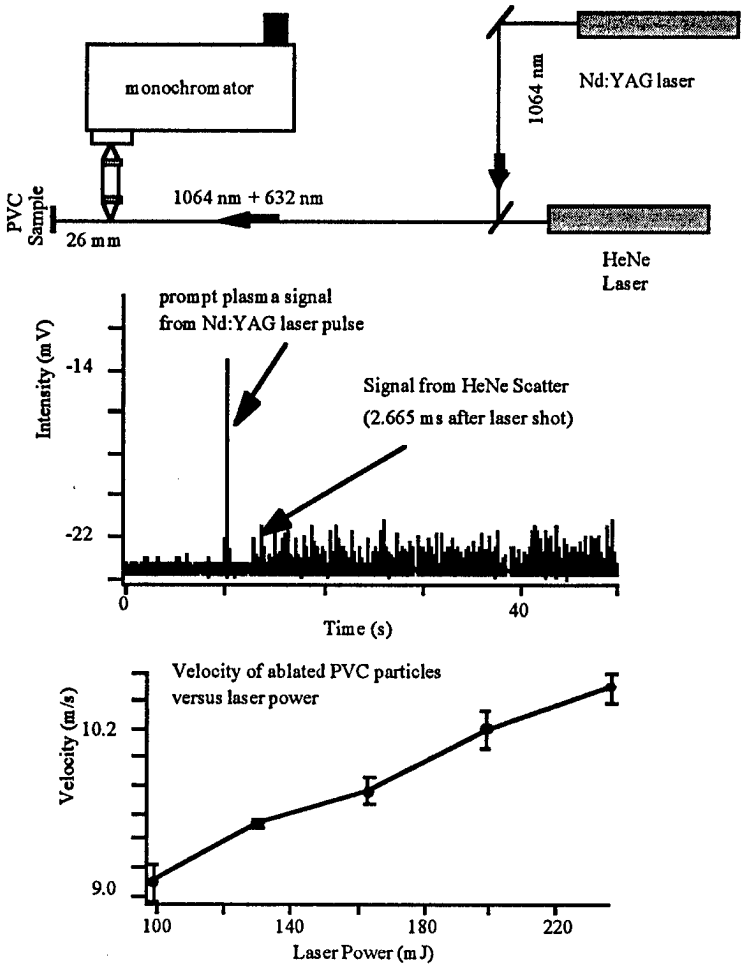

Figure 4. (Top) Experimental Setup for Laser Ablation LIF. This schematic also shows how the particle velocity measurements were made. (Lower plots) these plots show scatter data (middle) and velocity of ablated material (lower) versus laser power.

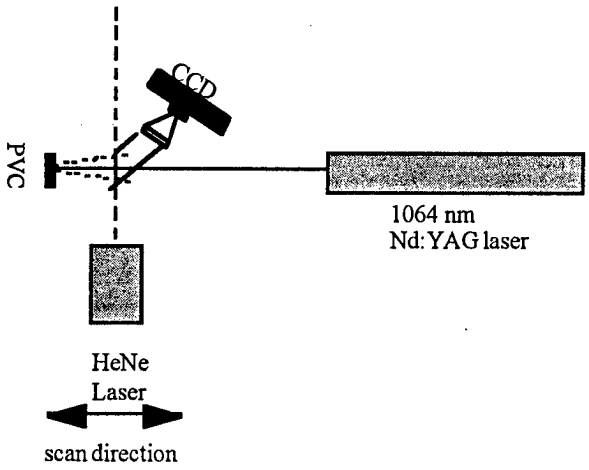

Figure 5. This Shows the Experimental Setup for the Particle Ejection Imaging

We have repeated some of the measurements shown in Figure 3 using laser ablation to introduce solid samples into a methane flame. One of these results is shown in Figure 6. Figure 6 shows that ablating HBCD blended with PVC into a flame causes a reduction in the •OH concentration in the flame. Ablation of PVC alone into the flame has little effect on the •OH concentration in the flame. This result is like that observed by aspirating HBCD/PVC solutions into the flame, showing that laser ablation is a viable sample introduction technique.

NOMENCLATURE

LIF	Laser Induced Fluorescence
PMT	Photomultiplier tube
PVC	Polyvinyl chloride
HBCD	Hexabromocyclododecane
Sb_2O_3	Antimony trioxide
$SbBr_3$	Antimony tribromide
Nd:YAG	Neodemium yttrium aluminum garnet
HeNe	Helium Neon
CCD	Charge coupled device

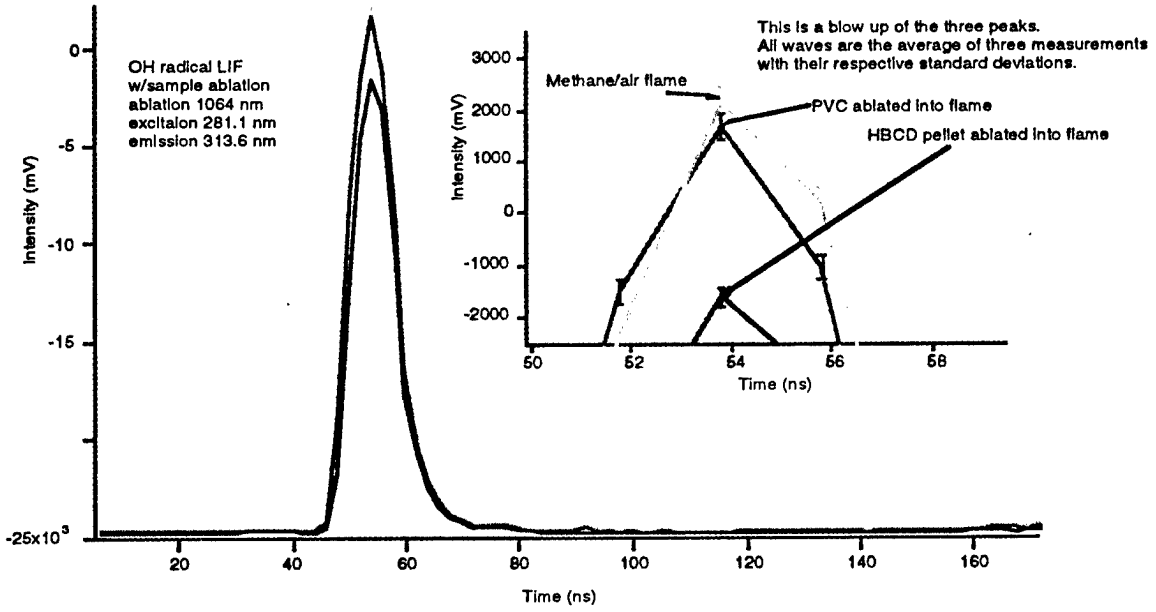

Figure 6. Shows the Experimental Results of the Laser Ablation Technique as a Sampling Technique. The temporal profile of the hydroxyl radical LIF is shown for the methane/air flame, for the flame with PVC ablated into it, and with HBCD ablated into it.

REFERENCES

1. E. Larsen, Kirk-Othmer, Encyclopedia of Chemical Technology, 10, p. 348 (1988).
2. C. Westbrook, Combustion Science and Technology, 34, p. 201 (1983).
3. E. Sutcliffe and R. Srinivasan, Journal of Applied Physics, 60 p. 3315 (1986).
4. R. Srinivasan and W. Leigh, Journal of the American chemical Society, 104, p. 6784 (1982).

FLAME-RETARDING PROPERTIES OF PHOSPHORUS CONTAINING POLY(AMIC ACID)

Byung-Wook Jo, Jin-Hae Chang**, and Richard J. Farris*
Polymer Science & Engineering, University of Massachusetts
Amherst, Ma. 01003

* Chemical Engineering Dept. Chosun University, Kwang Ju 501-759, Korea
** Polymer Science & Engineering, Kum-Oh University of Technology Kumi 730-701, Korea

ABSTRACT

Poly(amic acid) films obtained from PMDA-ODA (pyromellitic dianhydride-4,4'oxydianiline) were phosphorylated to different concentrations of phosphorus using phosphorus pentoxide. The phosphorylated poly(amic acid) films were thermally stabilized by treatment with Lithium Chloride (LiCl). The structure and properties of the resulting polymers were characterized by IR, H-NMR, elemental analysis, XRD, DSC, TGA, and dynamic mechanical analysis. The polymer films partially imidized at 140°C for 6 hr. had Limiting Oxygen Index (LOI) values in the range of 67-78. TGA results indicated char yields in the range of 54%-63% by weight at 850°C. The phosphorylated polymer films have the potential to be used as a fire-safe material in heterocyclic precursor polymers.

INTRODUCTION

Polymers with low combustion heats and high gasification heats are relatively poor sources of fuel. Therefore, thermally stable polymers with aromatic or heterocyclic structures form a viable class of fire-safe materials which offers opportunities for fundamental research as well as commercial applications. Most thermoplastics usually degrade to produce little char and high volatiles. Some of the newer, high-performance polymers, such as polysulfones, polybenzoxazoles, polyimides and polyetherketones, give high char yields with low heat release rates[1]. The scaling relationships between thermal parameters and flame retardation of idealized polymeric materials have been established by Lyon[2]. A similar relationship, however, between thermal stability and flammability for polymeric flame retardants is not universal. It is well known that char formation to give a thermally insulating, top layer on the surface of the polymeric materials prevents the heat transfer to the underlying layer of the bulk material.

Flame retardancy of organic polymers having a phosphorous group is well established[3-7]. The phosphorus containing flame retardants mainly influence the reactions occurring in the condensed phase, while other flame retardants, such as those containing halogen moieties, act in the gas phase[1]. The former is particularly effective in polymers with high oxygen and/or nitrogen content. A retardant of this type is converted by thermal decomposition to phosphoric acid which, in the condensed phase, extracts water vapor endothermically from the pyrolyzing

substrate, thereby diluting flammable gases and quenching the flame and causing the substrate to char[1,8]. The nitrogen containing groups can promote the formation of a frothy layer by forming gaseous decomposition products, which protect the substrate effectively against the intense radiation heat from the combustion zone[1,9].

Polyimides have high thermal and chemical resistance as well as excellent mechanical properties. Consequently, they have been used for a wide variety of applications such as matrix resins, coatings, and adhesives for high-temperature applications in aerospace and electronics industries. For these reasons, in the present study we have introduced phosphorus oxide into a poly(amic acid), poly(4,4-oxydiphenylene pyromellitamic acid) (PAA), to produce phosphorylated poly(amic acid) (PPAA). The PPAA was subsequently treated with an ionic salt, lithium chloride, to retard the thermally initiated cyclization reaction. We hypothesized that the uncyclized or partially cyclized PPAA would subsequently convert to a polyimide, and would release water as a byproduct, during a fire. This would lead to a frothy layer and a considerable absorption of heat.

EXPERIMENTAL

Materials

PAA was supplied by DuPont as a 15 wt% stock solution in N,N- dimethylacetamide (DMAc) with an intrinsic viscosity of 2.01 dL/g. Phosphorus pentoxide (Fisher Scientific, 99.4%), lithium chloride (Aldrich Co.), dehydrated ethanol (Pharmco Co.), and methanol (Aldrich Co.) were used without further purification. DMAc was dried over calcium hydride followed by distillation under vacuum.

Phosphorylation and Film Preparation

Phosphorus pentoxide was added to a 15% solution of PAA (in DMAc) in different molar ratios for 14 hr. at room temperature under continuous stirring. The molar ratio was varied from 0.2 ~ 2.0 in P_2O_5/PAA.

The resulting polymer solutions were coated onto glass plates, followed by drying at 60°C for 2 hr. The dried PPAA films were immersed into alcoholic LiCl solution (5% in ethanol) and kept for 10 hr. in a refrigerator. Thereafter, the films, while still on the glass plates, were cleaned in an ultrasonic cleaner five times in a 30-min. cycle. These were later dried at 80°C under vacuum, no higher than 0.5 mm Hg, for 2 hr. A pure PAA film, without phosphorus, was prepared by the same method as well as by casting from DMAc. These were spin coated to thicknesses of 4 to 6 μm and later imidized isothermally at 140, 150, and 180°C.

Characterization

Chemical structure and molecular ordering of the polymer films were characterized by IR, H-NMR, and X-ray diffractometry. The thermal stability and flammability behavior were evaluated by Thermogravimetric Analysis (TGA), Differential Scanning Calorimetry (DSC), and

Limiting Oxygen Index (LOI) data. A dynamic mechanical analyzer and IR spectrophotometer were employed to monitor the degree of cyclization reaction. IR absorption of n-imide band at 725 cm^{-1} was monitored in reference to an aromatic ring vibration band at 925 cm^{-1}, which is not present in the solvent but exists both in PPAA and polyimide[10]. Elemental analysis was carried out at the Microanalytical Laboratory of University of Massachusetts.

Limiting Oxygen Index (LOI)

Thin film samples (140 mm x 60 mm x ca 0.3 mm) were first heat treated by heating at a rate of 5°C/min. to 140°C and then kept at that temperature for 6 hr. A Stanton Redcroft flame meter was subsequently used to determine their LOI values. The conversion to cyclized imide ring of the PPAAs was in the range of 35% to 39%. The O_2 concentration in the glass chimney of the flame meter was set initially to 25% and the total flow rate of the mixed gas ($N_2 + O_2$) was always kept at 18 liter/min. The LOI was located in each case by replacing the partly burned sample with a fresh sample of the same size.

RESULTS AND DISCUSSION

The preparation of phosphorus-containing polymers was conducted by reacting PAA with P_2O_5 in DMAc (Scheme 1). The PPAA was treated with alcoholic LiCl to retard the thermally induced imide ring closure.

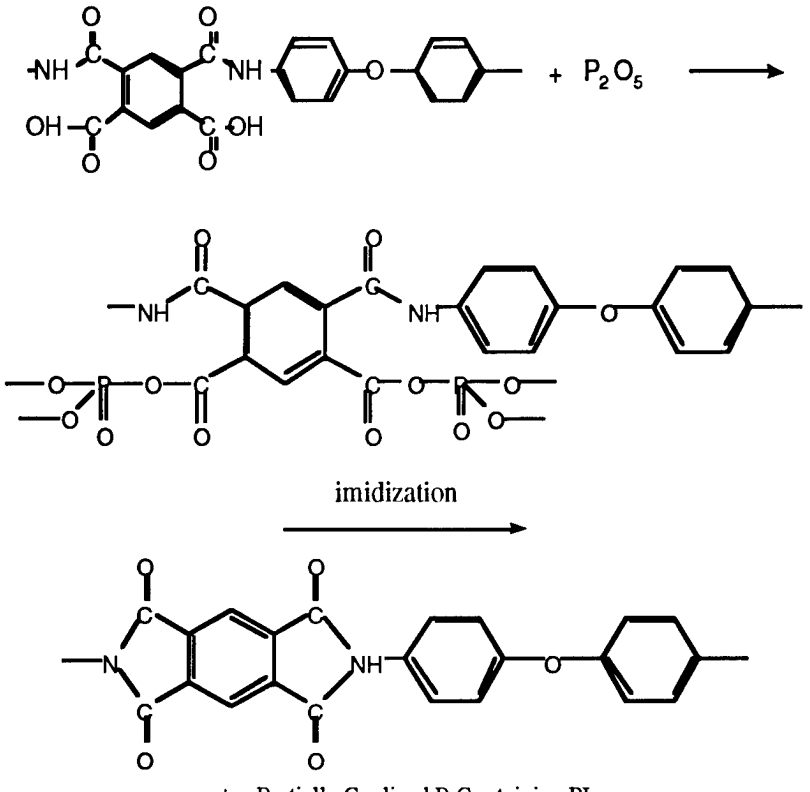

Scheme 1. Phosphorylation of Poly(amic acid)

The PPAA films with variable phosphorus contents were obtained through varying feed ratios of P_2O_5/PAA. Some analytical data of the resulting PPAAs are summarized in Table 1. Phosphorus elemental analysis of the PPAAs is consistent with the values calculated from the predicted compositions in all cases, except for those phosphorylated by a feed ratio of more than 1.0 (P_2O_5/PAA). The phosphorus contents in the latter were much lower than the calculated values. It is assumed that PAA probably reacts with P_2O_5 adequately in a one-to-one molar ratio. Sadikov et al.[11] reported that P_2O_5 quickly reacted with a model poly(amic acid) in a one-to-one mole ratio in NMP under room temperature.

Table 1. Characterization of Phosphorylated Poly(amic acid)

PPAA	Feed Ratio P_2O_5 : PAA	Phosphorus Content	
		Calculated	Found
PA-1	2.0 : 1.0	18.13	12.35
PA-2	1.5 : 1.1	15.17	11.05
PA-3	1.0 : 1.0	11.44	10.82
PA-4	0.5 : 1.0	6.46	6.30
PA-5	0.2 : 1.0	2.80	2.62

The PPAAs were treated with alcoholic lithium chloride to retard the cyclization of carboxyamic fragments in PPAAs. The chloride ion reduces the electrophilicity of carboxylic carbon atoms which are exposed upon nucleophilic attack. And the lithium ion protects amide nitrogen atoms from electrophilic attack for imide ring formation.

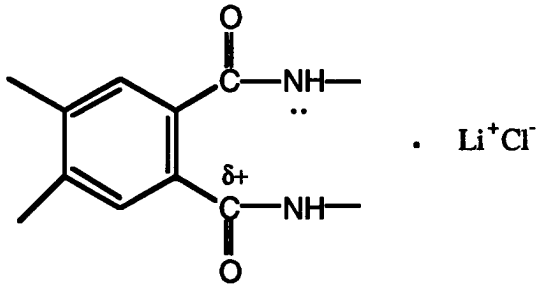

Although the formation of the PPAA complex with LiCl was not clearly detected by IR and NMR spectrometry, elemental analysis showed lithium contents of around 0.5% in samples treated with the alcoholic LiCl solution. This value is very close to that calculated from a one-to-one complex of LiCl and PPAA.

IR spectra of PPAA (sample, PA-3) show an absorbance at 1050 ~ 820 cm^{-1} characteristic of the P-O-C (aromatic) stretch in aromatic phosphates (Figure 1B) which does not appear in the spectrum of PAA (Figure 1A). Also, the strong absorbance at 1686 cm^{-1} of PAA, arising from C=O stretch, is decreased in intensity in the spectrum of PA-3. The spectrum of PA-3 treated with alcoholic LiCl show changes in intensities in the range of 1620 ~1780 cm^{-1} that corresponds to carboxyl C=O and amide C-N stretches (Figure 1C). All of the PPAAs show spectra similar to those of PA-3. This reveals the formation of the phosphate structure and some

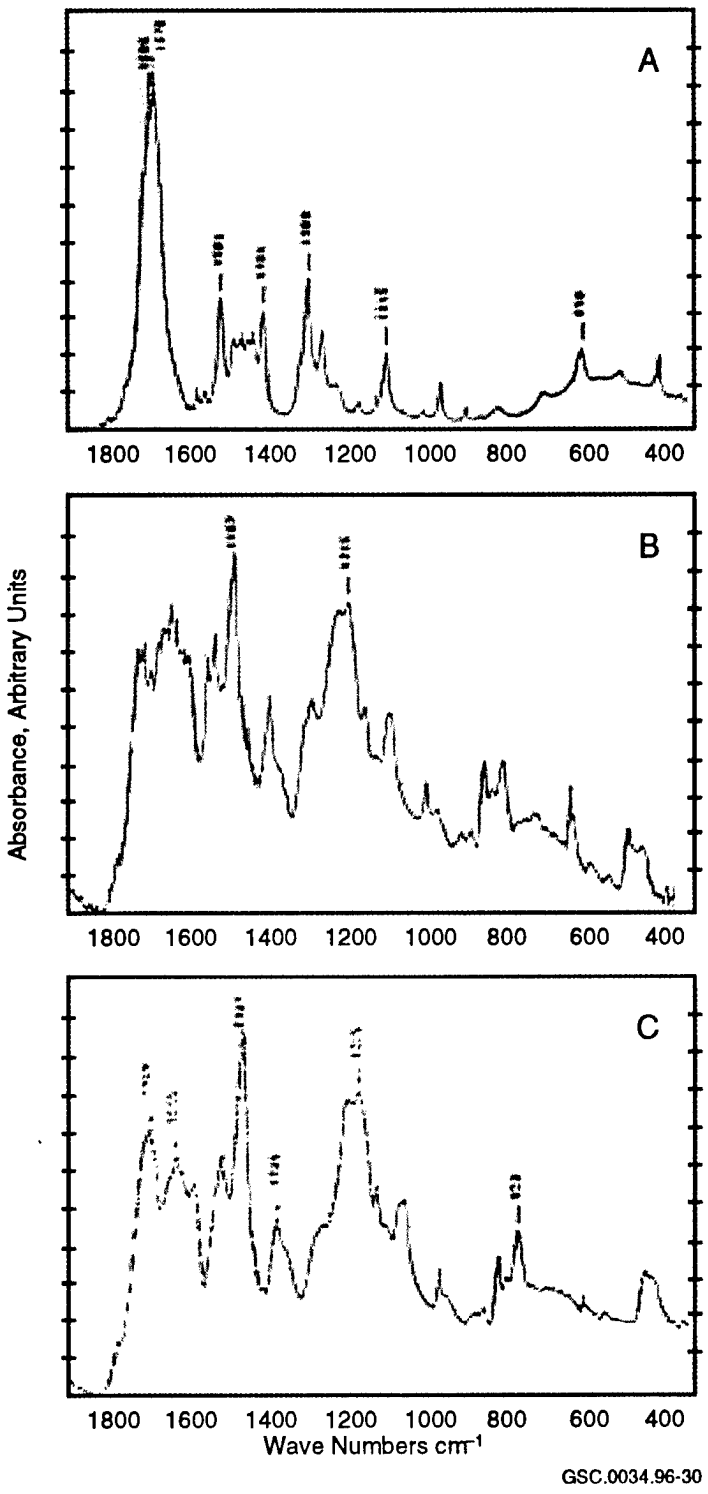

Figure 1. IR Spectra of (A) PAA, (B) Neat PA-3, and (C) PA-3 Treated With LiCl

protection of carbonyl and amide groups in a PPAA. The structure was also confirmed by H-NMR. The peak at d=9.8 ppm corresponding to the carboxylic protons disappears after phosphorylation (Figure 2). Chemical shifts of all proton signals under influence of electron density dislocation in the side of strong fields are also observed.

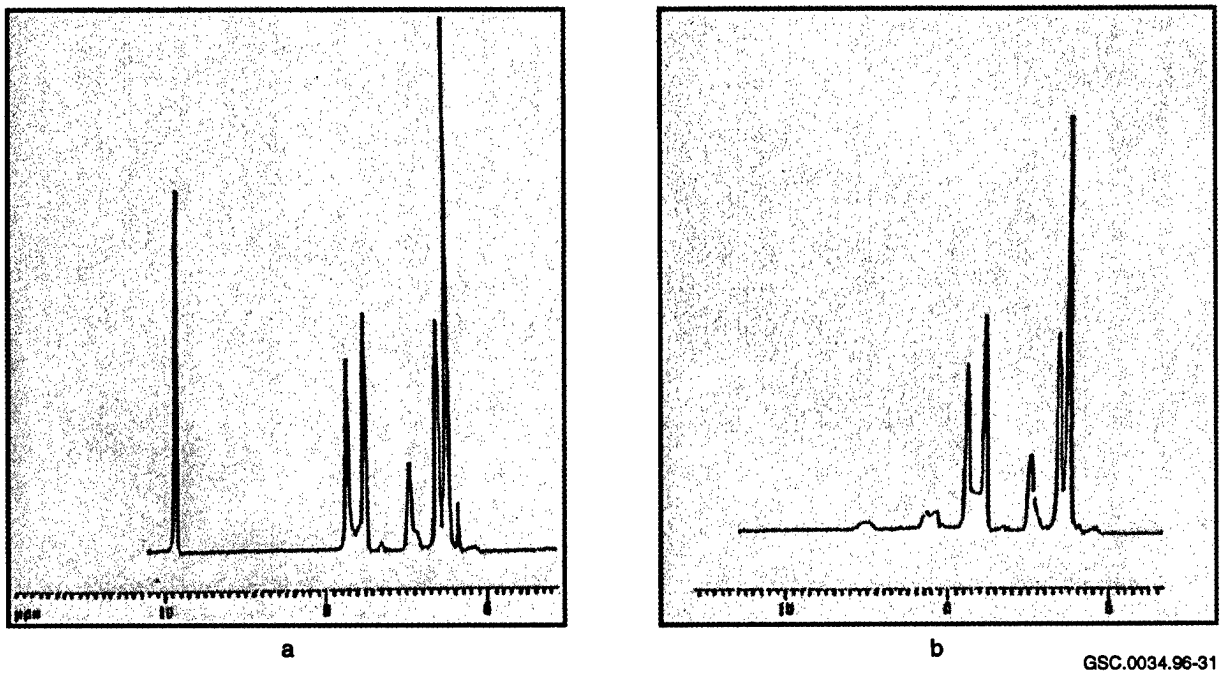

Figure 2. H-NMR Spectra of PAA Before (a) and After (b) Phosphonylation

Thermogravimetric analysis of PA-3 film cast from DMAc shows a weight loss of 30% on the first step (Figure 3). IR spectra show about 60% conversion to cyclized imide ring closure after the heat treatment on the TGA. Therefore, the weight losses are attributed to the removal of both solvent and water of cyclization, which by itself, could amount only to 6.5% by weight. The theoretical value of DMAc on this basis is 28.2%, which implies that it would lose 34.7% of its initial weight after 100% conversion. It further indicates that in the PPAA film cast from DMAc, one mole DMAc is associated with each carboxyl group. Kreuz et al.[12] reported that there were weight losses of 19% to 32% in the temperature range of 170°C ~ 200°C which agreed with the one-to-one complex formation between DMAc and poly(amic acid) (PMDA-ODA).

TGA traces of the PAAs, before and after phosphorylation in N2, are shown in Figure 4. For PAA, weight losses at 120°C and a rapid degradation is observed at 570°C which depends on the amount of solvent retained and the heating rate. Weight losses in PAA, of the order of 22%, are likely due to a sensitive moisture absorbing characteristic of the amic acid. After being phosphorylated, for example, the polymer film, PA-5, begins to lose weight at 175°C followed by a second step weight loss at 595°C. On the thermograms (Figure 4) for the PPAAs, the weight loss of the first stage does not show a dependency on the phosphorus content of the PPAAs, whereas the char yield ratio increases with the phosphorus content. Char yields of 63% in PA-1, 60% both in PA-2 and PA-3, 56% in PA-4, and 54% in PA-5 are observed in TGA under a heating rate of 20°C/min. These high char yields, compared with that of PAA (39%), are probably due to the formation of phosphorus-nitrogen-carbon bonds and subsequent cross-linking carbonization of the char at the second step of degradation[7-13]. The LOI values of PAA, PA-1, PA-2, PA-3, PA-4, and PA-5 are 62, 78, 75, 70, 68, and 67 respectively (Table 2).

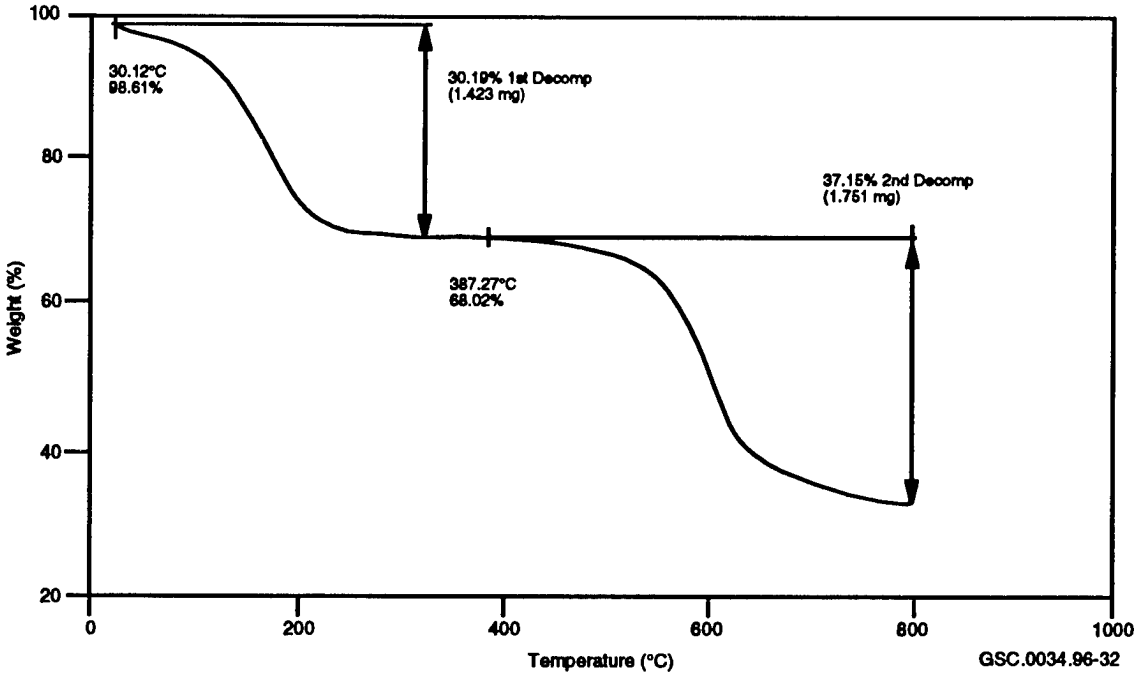

Figure 3. TGA Thermogram of PA-3 Obtained From DMAc Solution

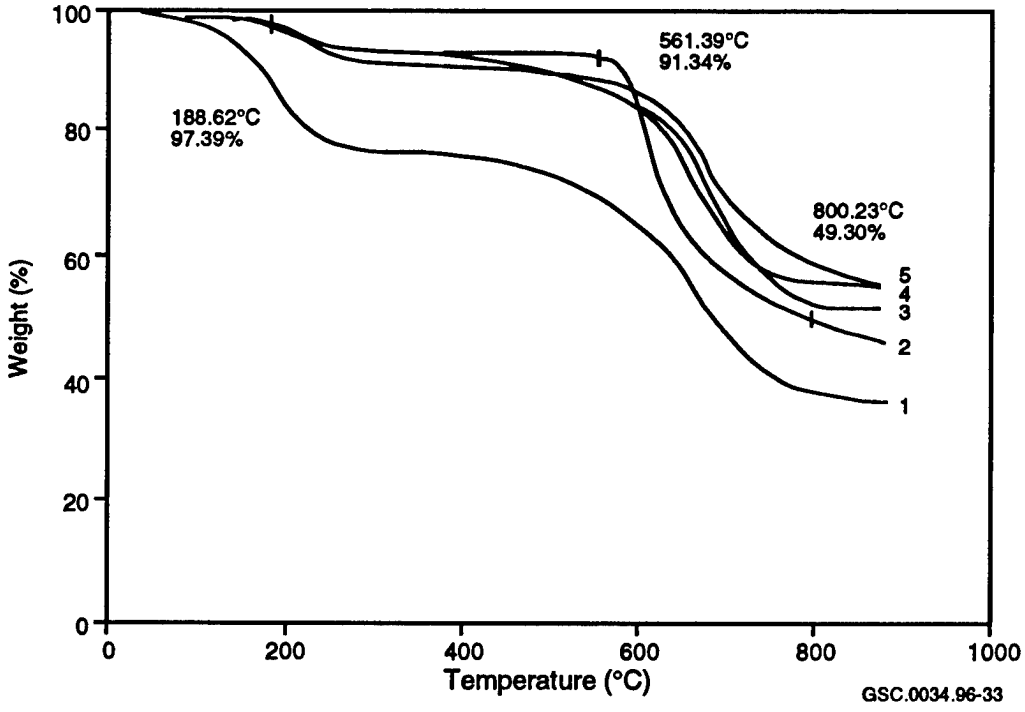

Figure 4. TGA Thermograms of (1) PAA, (2) PA-5, (3) PA-4, (4) PA-3, and (5) PA-2

Table 2. Thermogravimetric and LOI of PAA and PPAA

Samples	Onset Temp. of Wt. Loss (°C)		Char % at 850°C	LOI
	Step 1	Step 2		
PAA	142	440	39	62
PA-1	165	540	63	78
PA-2	164	520	60	75
PA-3	167	505	60	70
PA-4	160	510	56	68
PA-5	162	506	54	67

A higher ratio of phosphorylation leads to a higher char yield and a higher LOI value. However, P_2O_5 feed ratios of one or more make the corresponding PAA films very brittle. The corresponding DSC results in Figure 5 also confirm the solvent removal and the endothermic character of cyclization reaction to produce an imide ring.

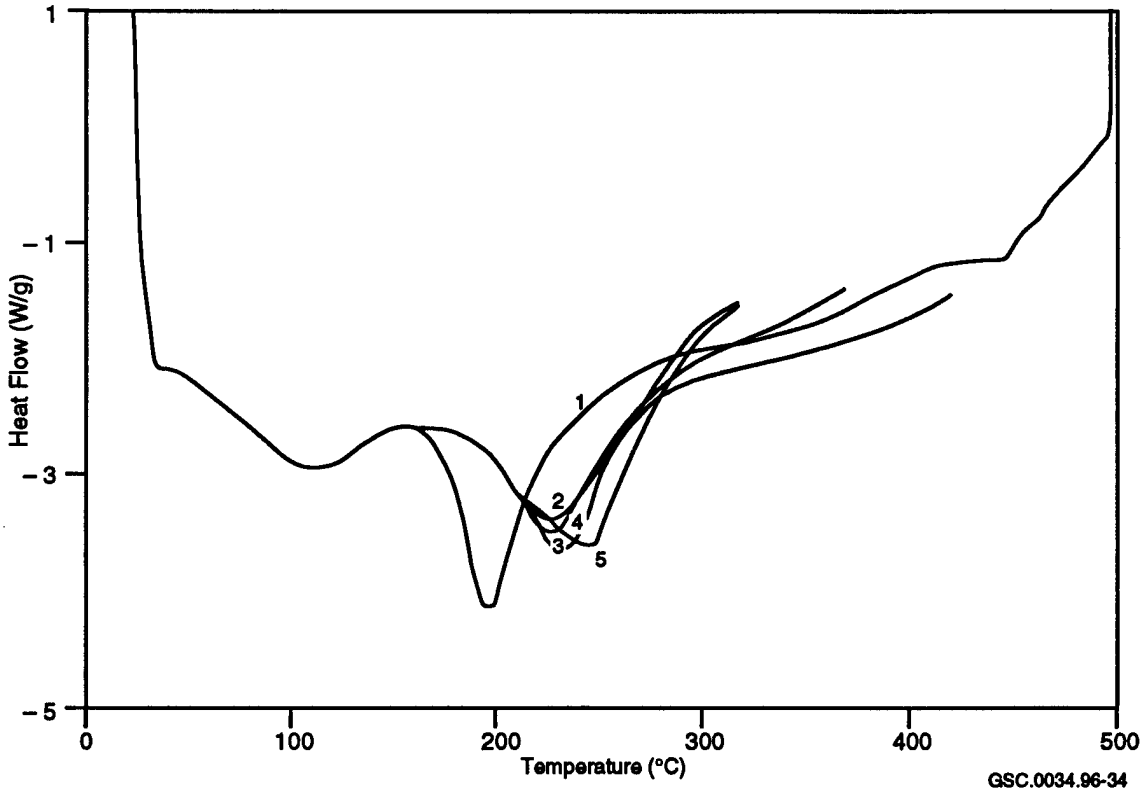

Figure 5. DSC Thermograms of (1) PAA, (2) PA-5, (3) PA-4, (4) PA-3, and (5) PA-2

The cyclization rate and extent of cure of the PPAAs appeared to be dependent both on temperature and film thickness in our preliminary experiments of the cyclization reactions. Therefore, the film thickness of the samples in the subsequent kinetic experiments was set to an almost constant value of 4 to 6 μm. Figure 6 shows the imide conversion rates of PA-3 obtained at isothermal temperatures, 140°C, 159°C, and 180°C. The slope of the graphs in Figure 6 tindicates an initial rapid rate followed by a more gradual conversion. The conversion rates of the PPAAs including PA-3, however, are much lower than that of PAA(PMDA-ODA). Ginsburg and Susko[10] reported that the PAA (PMDA-ODA) films of 4.6 μm in thickness show more than 70% conversion at 150°C after 40 min. On the other hand, PA-3 shows about 18% conversion even after 60 min. at the same temperature.

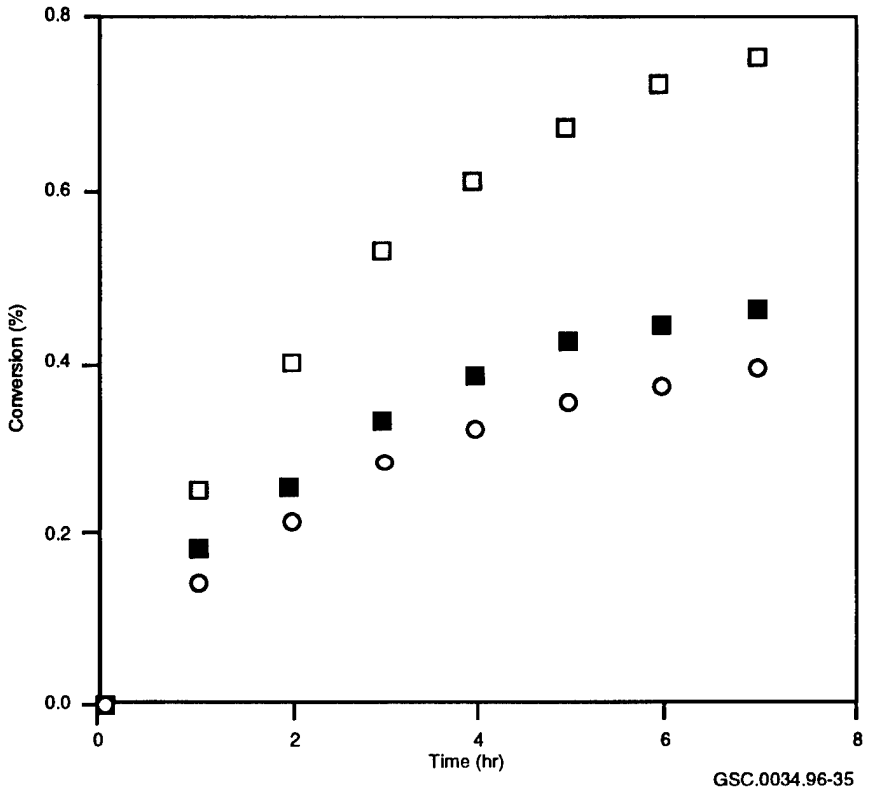

Figure 6. Kinetic Plots of PA-3 Cyclization Under Different Isothermal Temperatures, 140°C (○) and 150°C (■) and 180°C (□)

X-ray diffraction patterns of PPAAs were obtained by a Siemens (D500) diffractometer with CuKa radiation. Figure 7 shows a sharp peak at 2θ=5.9 (repeat period of 13.4Å). Since this is smaller than the projected length of the monomer unit, 18Å[14], we associate this peak with the interchain repeat distance likely due to a polar interaction between the introduced phosphate group and amide/acid group. A broad peak occurs centered at 2θ=19.2° corresponding to a repeat period of 4.95Å, which can be associated with the mean width of PPAA and therefore with the interchain spacing between adjoining parallel polymer chains. These repeat periods are slightly different than those of the PAA (d=13.9Å and 4.8Å)[15] due to stronger intrachain interaction and bulkier side groups.

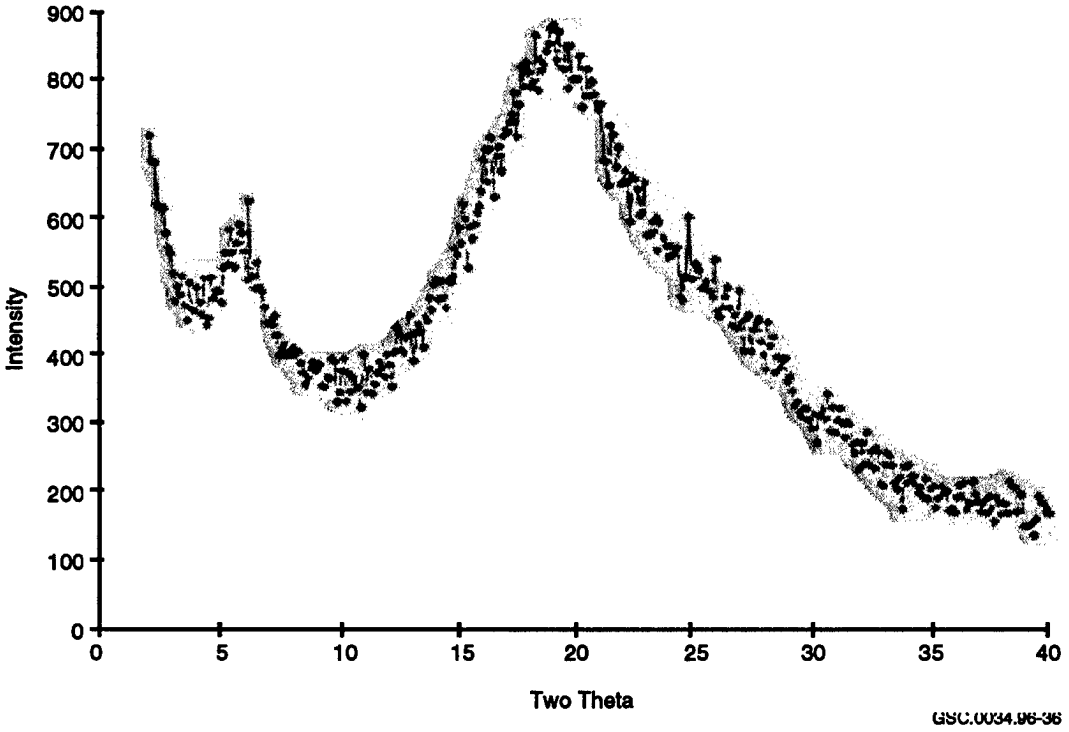

Figure 7. X-Ray Diffractogram of PA-3

Figure 8 shows tanδ, storage modulus(E′), and displacement traces of the PAA, PA-3 treated with LiCl, and PA-3 without LiCl treatment versus temperature at a heating rate of 0.2°C/min. at different frequencies (0.1, 1.0, 20, 90 Hz). All of the mechanical spectra clearly show the drop of E′ and increase of tanδ, probably due to plasticizing effects of the residual solvent and water. Further heating leads to a maximum in tanδ and a minimum in E′ reflecting the highest plasticizing action. The modulus is increased both by the evaporation of solvent and water as well as by the imidization reaction. The displacements increase rapidly during plasticizing, and then contract during cyclization in all of the samples. The temperature of a maximum in tanδ and a minimum in E′ increase for PA-3 treated with LiCl, PAA, and PA-3 without LiCl treatment in that order, reflecting the thermal stability of the amic acids. There is no strong frequency dependency of the observed transition indicating that the activation energy of these transitions would likely be high.

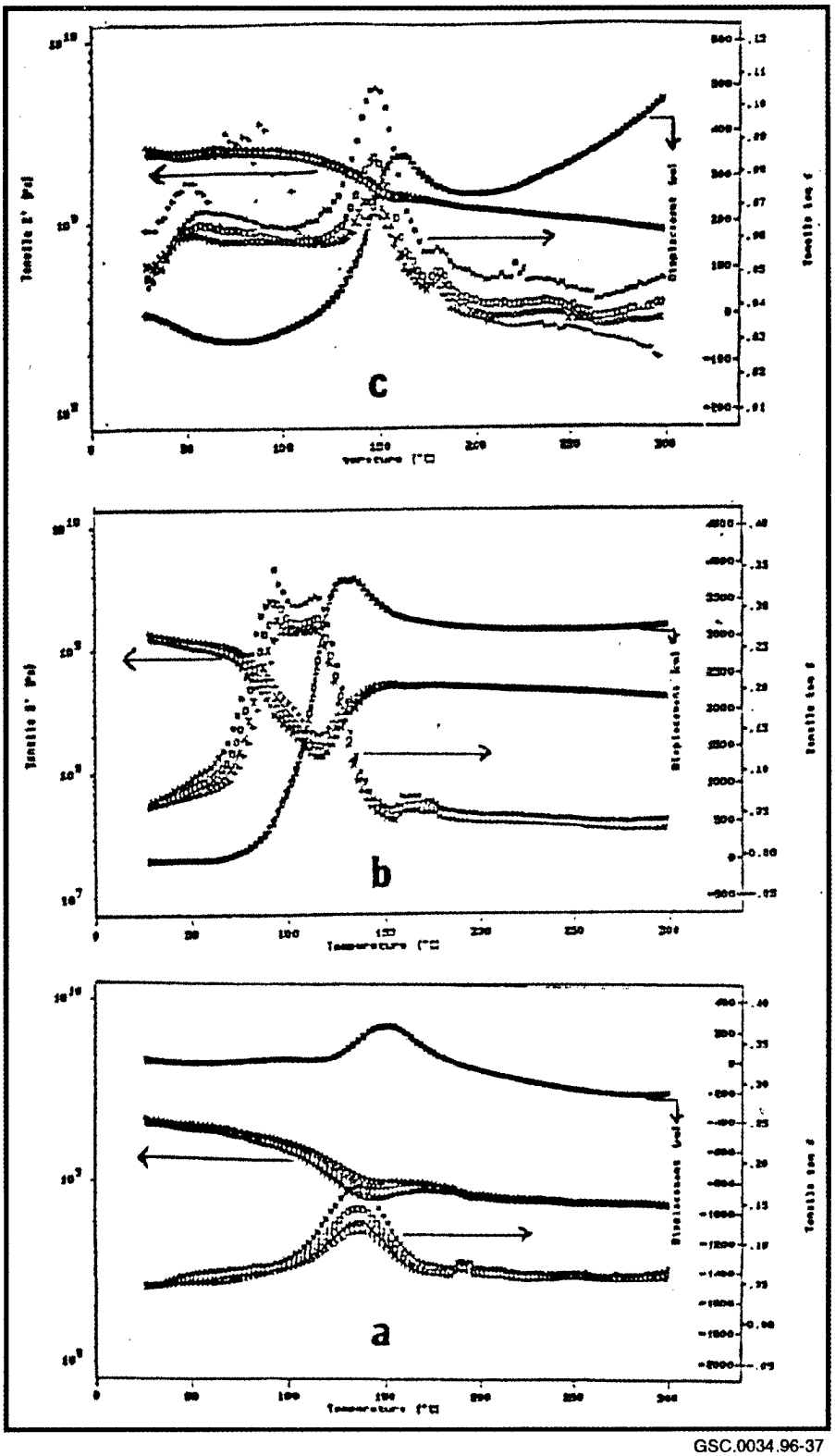

Figure 8. Dynamic Mechanical Thermograms of (a) PAA, (b) PA-3 Treated Without LiCl, and (c) with LiCl

CONCLUSION

The incorporation of phosphorus into poly (4,4-oxydiphenylene-pyromellitamic acid) was achieved through a simple chemical modification of the PAA by means of P_2O_5. The phosphorus content of the PPAAs could be tailored within 1/1 mole ratio of P_2O_5/PAA or less. These polymers exhibit high char yields and LOI values. PPAAs show a synergistic effect on improving the flame retardancy of a heterocyclic polymer composed of phosphorus, nitrogen, and carbon. The phosphorylated poly (amic acid)s are thermally stabilized by means of LiCl treatment. The resulting polymer films could be utilized as a fire safe material in heterocyclic precursor polymers.

ACKNOWLEDGMENTS

This work was supported by the Federal Aviation Administration (FAA) and the Center for UMass-Industrial Research on Polymers (CUMIRP). B.W. Jo wishes to offer special thanks the YonAm Foundation (Korea) for partial support.

REFERENCES

1. J. Troitzsch, International Plastics Flammability Handbook, Hanser Publishers, Munchen (1982).
2. R.E. Lyon, "Recent Advances in Flame Retardancy of Polymeric Materials," The 6th Annual BCC Conference on Flame Retardancy, Stamford, Connecticut, May 23-25, 1995, USA.
3. P. Kannan, Gangadhara and K. Kishore, Polymer, 32, p. 1909 (1991).
4. M. Richard, B.I. Dahiyat, D.M. Arm, S.Lin, and K.W. Leong, J. Polym. Sci., Part A, 29, p. 1157 (1991).
5. M. Banks, J.R. Ebdon, and M Johnson, Polymer, 34, p. 4547 (1993).
6. ibid. 35, p. 3470 (1994).
7. Y.-L. Liu, G.-H. Hsiue, Y.-S. Chieu, R.-J. Jeng, and C. Ma, J. Appl. Polym. Sci., 59, p. 1619 (1996).
8. E.D. Weil, R.H. Hansen, and N. Patel, in "Fire and Polymers," G.L. Nelson, Eds., A.C.S., Washington, D.C. (1990).
9. K.S. Annakutty and K. Kishore, Polymer, 29, p. 1273 (1988).
10. R. Ginsburg and J.R. Susko, in "Polyimides," vol. 1, p. 237, Plenum Press, New York (1984).
11. B.B. Sadikov, N.Yu. Shpilman, Yu.A. Dubitsky, and B.A. Zhuvanov, in "Polyimide and Other High Temperature Polymers," M.J.M. Aladie and B.Sillion, eds., Elsevier Science Publishers, Amsterdam (1991).
12. J.A. Kreuz, A.L. Endrey, F.P. Gay, and C.E. Sroog, J. Polym. Sci., Part A-1, 4, p. 2607 (1966).

13. C.P.R. Nair, G. Clouet, and Y. Guilbert, Polym. Degrad. Stab., 26, p. 305 (1989).
14. T.M. Birshtein, Polym. Sci. USSR, 19, p. 63 (1977).
15. N. Takahashi, Do Y. Yoon, and W. Parrish, Macromolecules, 17, p. 2583 (1984).

FIRE CALORIMETRY OF FLAME-RETARDED POLYMERS

D.J. Priest
Omega Point Laboratories
Elmendorf, TX

INTRODUCTION

A Phase II SBIR (Small Business Innovation Research) program regarding fire calorimetry investigations on fire-retardant polymer systems began in August of 1998. The completed Phase I study will be described in this section, with the proposed objectives of the Phase II program.

Some of the most important characteristics that should be determined in the investigation of fire performance of materials and products include heat release rate, ignition delay time, mass loss rate, smoke release rate, effective heat of combustion, and release rates of toxic gases. The test methods that permit measurement of such parameters are sometimes called fire calorimetry methods and range in size from bench-scale to real-scale devices. These particular studies utilized the bench-scale device known as the cone calorimeter (ASTM E1354/ISO 5660). This method utilizes oxygen consumption methodology for determining the heat release rate. Heat release rate (HRR) as a function of time (including peak, average, and total heat release) is probably the single most important parameter for appraising the fire performance and potential fire hazard of a material or product.

This Phase I SBIR program was intended to be exploratory in nature, with the major research and development objectives to be undertaken in Phase II. The objective for Phase I was to evaluate the performance of a number of fire-retardant (FR) polymers under temperature and heat flux conditions that might exist in real fires. The evaluations were undertaken on a laboratory scale, using apparatuses and test procedures that are recognized by the fire community. While it is understood that many of the polymer-FR systems utilized in this study were not designed to withstand the more severe exposure conditions applied to them, the purpose was to gain some fundamental information on the suitability of bench-scale test methods to evaluate such systems and an understanding of how these materials would perform under the simulated conditions.

MATERIALS

Specimens of commercial FR and non-FR polymers were supplied by companies in the business of producing such products. For the purposes of this paper it was not considered necessary to identify the FR agents in any specific polymer system. Therefore, although the types of agents will be described below, the fire-retarded polymers will be identified only with the added descriptor FR. It is believed that all of the FR products were UL94 V-0 materials in the thickness supplied. These specimens were not intended to represent all of the products of a given category; they were selected for purposes of study and illustration.

The fire-retardant agents incorporated in the polymer systems included the following: bromine and chlorine, incorporated into organic molecules; phosphorus, either alone or as part of an organic molecule, sometimes in combination with bromine; antimony, as Sb_2O_3, only in combination with a bromine compound; and metal oxide hydrates (e.g., alumina trihydrate, $Al_2O_3 \cdot 3H_2O$, or other metal hydrate). The polymers included the following (in alphabetical order, with abbreviations used in the text): acrylonitrile-butadiene-styrene (ABS), high-impact polystyrene (HIPS), polybutylene terephthalate (PBT), polycarbonate-ABS copolymer (PC/ABS), polyethylene terephthalate (PET), rigid polyurethane/polyisocyanurate foam (RPU), unsaturated (thermoset) polyester (UPT), and cross-linked polyethylene (XPE).

METHODS

There are a number of common flammability test methods that are used to evaluate fire-retardant polymers. Many of the bench-scale methods are intended only to evaluate ignitability and therefore rely on exposure of the specimen to an open flame under ambient conditions. Results of these tests are generally based on the time and extent of burning and many of them contain simple pass/fail criteria. Thus, little additional information on the nature of the burning is obtained from such tests. Other methods account for the specimen size and exposure conditions and produce results that can be extrapolated to other fire scenarios.

Among the tests applicable to FR polymers is the UL94 test to which most of the specimens studied herein had been previously evaluated. The V-0 classification is common among FR engineering plastics used for electrical applications (e.g., appliance housings). This test method entails ignition of a specimen under relatively mild test conditions, compared to those of a room-size fire. The Oxygen Index test (ASTM D2863), the FAR 25.853 (Part b), and the NFPA 701 tests all are used for various FR materials; however, the results generally are of limited use in extrapolating the potential flammability of products to real fire scenarios.

Other test methods are available that have been utilized for evaluating FR polymers and provide the opportunity to obtain additional data for extrapolation to larger-scale scenarios. Included are the cone calorimeter (ASTM E1354, ISO 5660), the OSU HRR calorimeter (ASTM E906 and 14 CFR Part 25/Appendix F/Part IV), and the ASTM E662 Smoke Chamber. The cone calorimeter method was the one selected for this study.

The cone calorimeter apparatus has been described in numerous papers and in the standard test methods ASTM E1354 and ISO 5660; therefore, it will not be described here. The method is based on the principle of oxygen consumption calorimetry where the primary measurements are oxygen concentration and flow rate in the exhaust stream. The standard procedure used involves exposing specimens measuring 100 mm x 100 mm (3.9 in. x 3.9 in.) and up to 50 mm (2 in.) thick in a horizontal orientation to an external radiant heat flux of up to 100 kW/m^2. The high heat fluxes represent moderate to severe fire test conditions. Ignition is accomplished with a high-voltage spark igniter. Generally, the specimens were run only wrapped in aluminum foil; however, the rigid polyurethane foam specimens were run using the metal edge frame to reduce burning on the sides of the specimens. In some cases, two to four thin, stainless steel wires were wrapped around the specimen and the holder in order to reduce warping. Continuous measurements were taken of mass loss, visible smoke, and gaseous products including oxygen, carbon monoxide, and carbon dioxide.

RESULTS

Each of the specimens received was tested at one or more external heat flux levels using the cone calorimeter. Several of the specimens were evaluated at up to three heat flux levels. A summary of some of the heat release results obtained in this study are reported in Table 1. The results listed include time to flash ignition, time to sustained ignition, peak heat release rate, average heat release for 60 seconds following ignition, and effective heat of combustion.

Table 1. Summary of Cone Calorimeter Heat Release Results (Average of at Least Two Tests)

Specimen ID	Heat Flux (kW/m^2)	Flash (s)	t_{ig} (s)	Peak HRR (kW/m^2)	Avg. HRR Ign+60s (kW/m^2)	Eff. Hc (MJ/kg)
ABS-FR	25	98	120	439.2	211.0	10.3
ABS-FR	50	27	34	413.5	247.2	10.0
ABS-FR	75	15	17	493.5	289.3	10.0
ABS-NFR	25	---	111	670.8	382.8	29.0
ABS-NFR	50	---	38	1005.4	538.4	28.3
ABS-NFR	75	14	17	1215.4	691.3	29.4
HIPS-FR	25	149	304	303.7	232.2	11.0
HIPS-FR	50	40	106	252.0	210.5	10.2
HIPS-FR	75	20	25	301.2	220.0	9.8
HIPS-NFR	25	176	206	834.2	331.7	29.8
HIPS-NFR	50	---	52	1038.9	473.6	28.2
HIPS-NFR	75	21	24	1217.7	615.2	26.4
PCABS-FR	25	211	267	351.1	226.4	17.8
PCABS-FR	50	51	53	320.7	259.8	18.4
PCABS-FR	75	26	28	453.1	313.3	17.0
PCABS-NFR	25	---	189	436.1	316.9	22.4
PCABS-NFR	50	---	49	468.8	339.6	22.4
PCABS-NFR	75	---	21	590.3	416.4	22.2
UPT-FR	25	---	ni	~10	<10	2.8
UPT-FR	50	150	159	110.7	73.9	15.8
UPT-FR	75	37	79	125.1	102.8	14.3
UPT-NFR	25	107	119	568.4	367.8	23.2
UPT-NFR	50	40	42	941.6	600.8	23.8
XPE-FR	25	155	162	227.1	77.8	20.0
XPE-FR	50	61	63	293.1	221.7	22.0
XPE-FR	75	33	37	493.8	324.1	20.7
XPE-NFR	25	---	86	931.0	322.2	36.1
XPE-NFR	50	33	37	1517.0	891.1	39.9

Flash = time to onset of flashing
t_{ig} = time to sustained ignition
Avg. HRR = average over 60 s after t_{ig}
Eff. Hc = effective heat of combustion

Additional results obtained during this study (but not reported herein) included Specific Extinction Areas (smoke density normalized to specimen mass loss), average CO (carbon monoxide) and CO_2 (carbon dioxide) yields, and the CO/CO_2 ratios. These results relate to the completeness of combustion of the respective FR and non-FR polymer samples.

The response of specimens to a range of external heat fluxes can produce valuable information for characterization of the thermal properties of a material. For example, the relationship of ignition time and external heat flux contains the term $k\rho c$, often called the thermal response parameter. This includes the thermal conductivity (k), the density (ρ), and the specific heat (c).

$$t_{ig} = \frac{\pi k\rho c}{4}\left[\frac{\Delta T}{\dot{Q}''_{ext}}\right]^2 \tag{1}$$

where

t_{ig} = Time to sustained ignition (s)
$k\rho c$ = Thermal response parameter [(kW/m^2-K)^2-s]
ΔT = Ignition temperature minus ambient temperature (K)
$\dot{Q}''_{ext}$ = Applied external heat flux (kW/m^2)

Inverting equation 1 and taking the square root, the relationship is the following:

$$\frac{1}{\sqrt{t_{ig}}} = \sqrt{\frac{4}{\pi k\rho c}}\,\frac{\dot{Q}''_{ext}}{\Delta T} \tag{2}$$

Plotting $(t_{ig})^{-1/2}$ vs. $\dot{Q}''_{ext}$ gives a straight line, and the reciprocal of the slope (S) is directly proportional to the thermal response parameter:

$$1/S = \Delta T\sqrt{\frac{\pi k\rho c}{4}} \tag{3}$$

This treatment of the data to determine thermal response parameters was applied to the specimens run at three heat flux levels. Ignition temperatures were determined for several of these materials using the procedure of ASTM D1929 (Ignition Properties of Plastics). These results are presented in Table 2.

Table 2. Thermal Response Parameters

Specimen ID	Slope[a]	TRP[b]	t_{ig}, °C[c]	$k\rho c$
ABS-FR	0.00303	330	420	0.878
ABS-NFR	0.00295	339	410	0.970
HIPS-FR	0.00285	351	390	1.16
HIPS-NFR	0.00269	372	410	1.17
PCABS-FR	0.00256	391	440	1.12
PCABS-NFR	0.00291	344	440	0.861
UPT-FR	0.00133	752[d]	(e)	(f)
UPT-NFR	0.00251	398[d]	(e)	(f)
XPE-FR	0.00172	581	(e)	(f)
XPE-NFR	0.00226	442[d]	(e)	(f)

Notes to Table 2:
(a) Slope $(t_{ig})^{-1/2}$ vs. Q_{ext} (b) Reciprocal of slope (c) Flash ign. temp., per ASTM D1929
(d) Only 2 data points (e) Not determined (f) Not calculated

DISCUSSION

Ignition and Heat Release of FR vs. Non-FR Materials

The potential fire hazard of any material or product is dependent on many factors, generally including ignitability, rate of surface flame spread, heat release rate (which is generally proportional to mass loss rate), peak heat release rate, smoke evolution, and toxicity of the smoke. The results from the testing performed in the cone calorimeter address most of these factors, either directly (e.g., heat release rate) or indirectly (e.g., ignition time and HRR as functions of external heat flux, an indicator of flame spread potential). Further, the data from the cone calorimeter are presented in engineering terms which are conducive to extrapolation to other size fires and other fire scenarios. Thus, one of the potential benefits of bench-scale testing using the cone calorimeter includes the ability to assess potential fire hazard.

Ignitability and heat release data are presented in Table 1 and in the graphs in this report. The ignition data generally are reported as time to sustained ignition, which is defined as ignition without the assistance of the spark igniter for a period of 4 seconds or more. In Table 1, values are given for flash ignition time, which is the time at which some ignition occurred, but one that would not have continued without the sparker being present (this conclusion having been drawn by observation and experimentation with numerous tests). Although many specimens (not necessarily FR materials) flash for a few seconds prior to ignition, the longer duration of flashing or transient flaming in these tests (up to several minutes) is one of the complications in testing fire-retardant materials. Some judgment is required to determine when sustained ignition has occurred. The onset of transient flaming in the FR ABS and HIPS specimens started prior to that of the non-FR specimens (see Table 1 and Figures 1 and 2). Heat was released during the flashing/nonsustained ignition portion of the experiment; therefore, the comparative plots of FR and non-FR HIPS (Figure 2), for example, give the appearance that the FR specimen ignited earlier than the non-FR (which, in some respects, it did).

Several of the FR polymers shown in Table 1 did not have significantly increased times to sustained ignition (t_{ig}), compared to the non-FR specimens. The sustained ignition times for FR-ABS were essentially the same as those for non-FR ABS, while the FR versions of HIPS, PC/ABS, and cross-linked polyethylene had ignition delay times somewhat longer than their non-FR counterparts (and nearly identical at the highest heat flux tested, 75 kW/m^2). The particular FR polyester tested in this study exhibited more dramatic results for times to ignition than many of the other specimens, especially at the lowest heat flux level (25 kW/m^2), where the FR specimen did not ignite over a 10 minute period.

From the data in Table 1 it was observed that the FR polymers generally exhibited significantly reduced heat release rates compared to the non-FR polymers. This phenomenon also can be seen from the plots in Figures 1–6. The reduction in heat release (peak, average, or total) for the FR polymers was sometimes 50 percent or more compared to the non-FR polymers. This effect was present for all of the heat fluxes examined; in fact, the percent decrease was generally greater at higher heat fluxes. The lower heat release rates for the FR specimens compared to the non-FR specimens also led to lower effective heats of combustion.

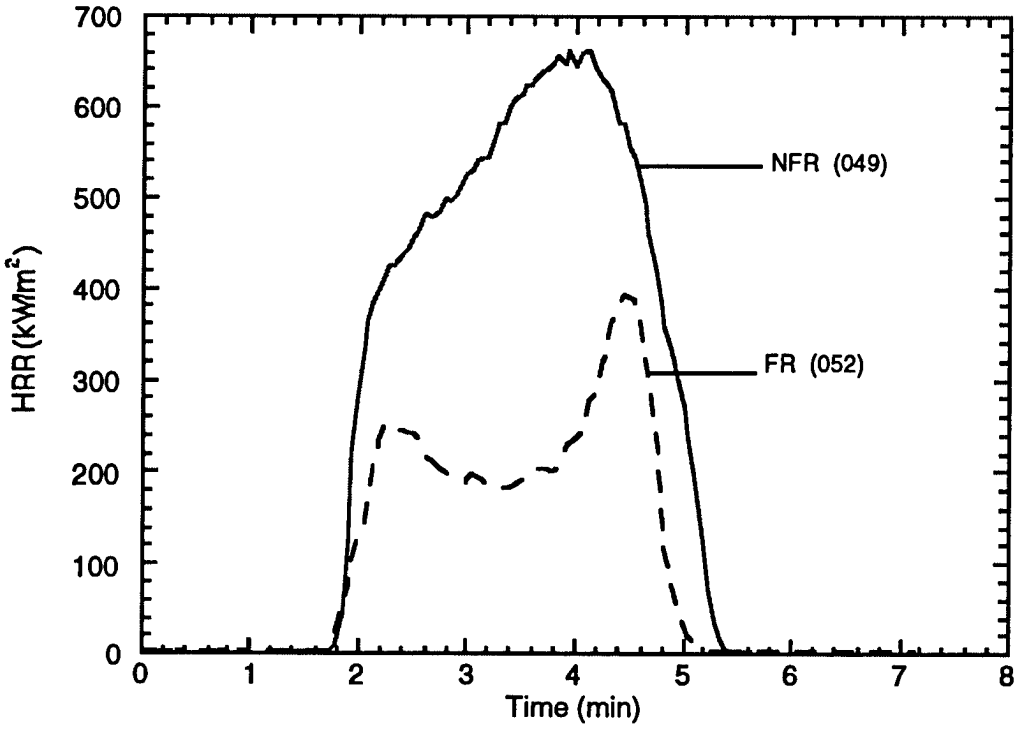

Figure 1. Heat Release Rate Curves for FR and Non-FR ABS (25 kW/m²)

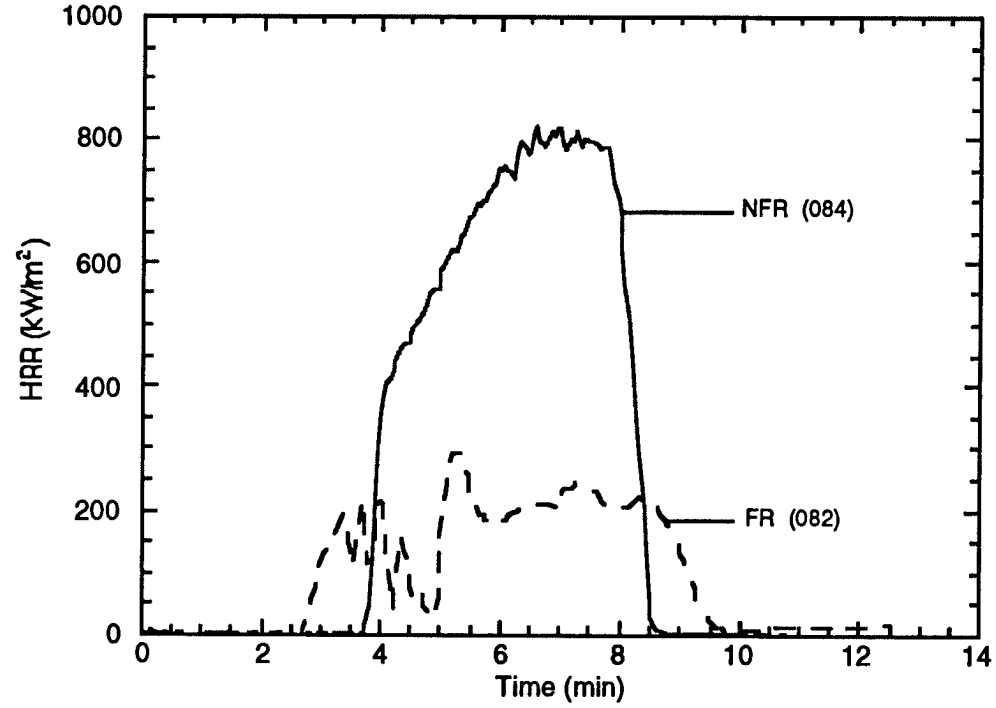

Figure 2. Heat Release Rate Curves for FR and Non-FR HIPS (25 kW/m²)

In contrast to the substantial effect on HRR due to the addition of the FR agents shown in Table 1, several other FR polymers exhibited little or no differences in times to ignition or heat release results compared to the non-FR materials (data not shown). A full explanation of the anomaly presented by these specimens is not readily apparent. It is significant to note that these particular fire-retardant specimens, that had met certain flammability criteria for marketability, had little apparent advantage in ignitability or rate of burning compared to the non-FR specimens under the heat flux conditions tested.

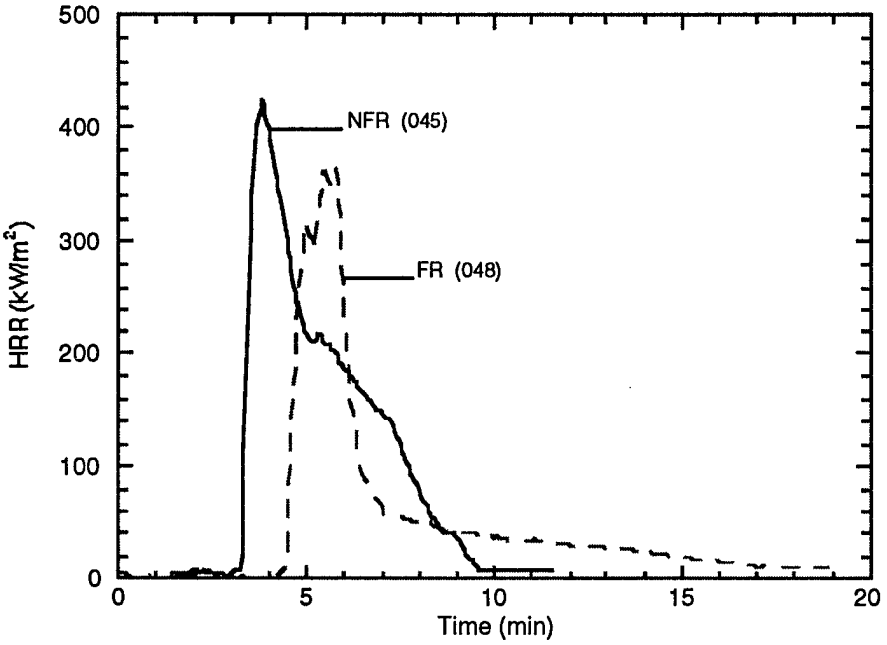

Figure 3. Heat Release Rate Curves for FR and Non-FR PC/ABS (25 kW/m²)

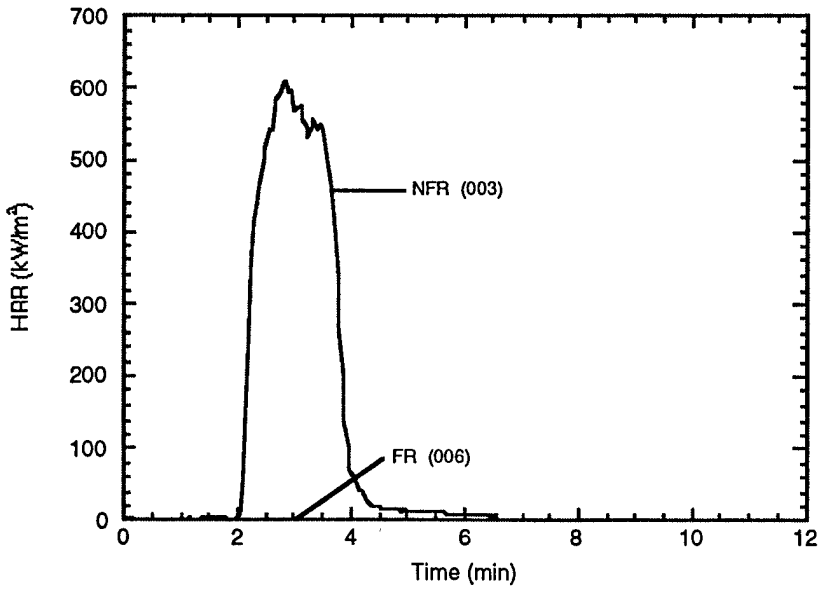

Figure 4. Heat Release Rate Curves for FR and Non-FR UPT (25 kW/m²)

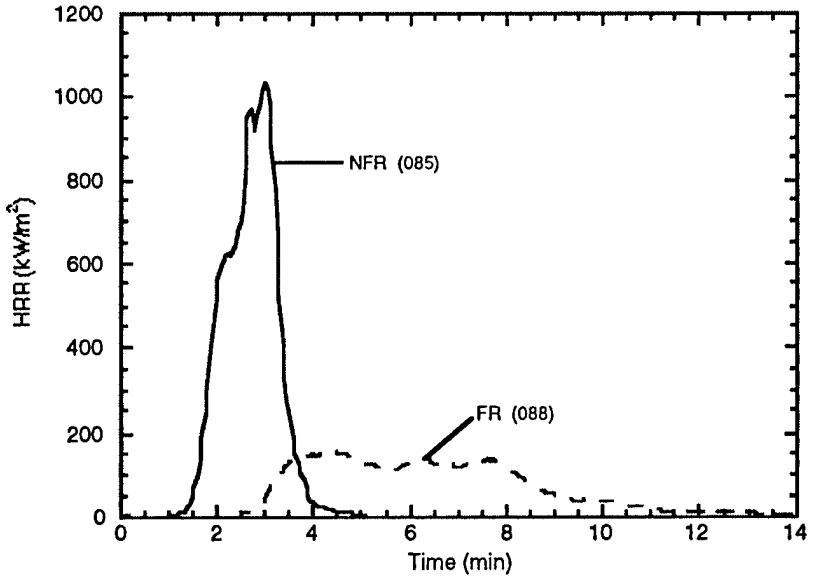

Figure 5. Heat Release Rate Curves for FR and Non-FR XPE (25 kW/m²)

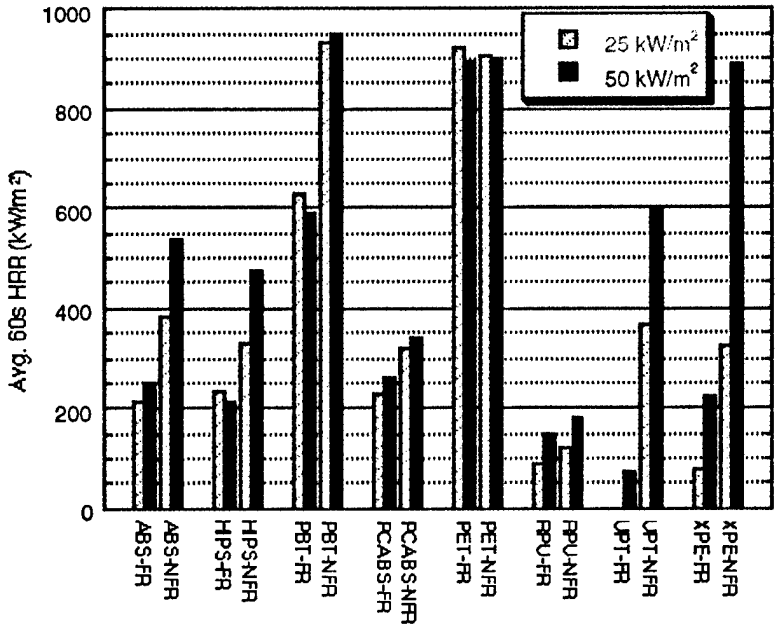

Figure 6. Avg. (60 s) HRR for FR and NFR Specimens at Two Heat Fluxes

The effect of external heat flux on heat release rate is apparent from the plots in Figures 7 and 8. These sets of curves exhibit the effects of increasing heat flux: a reduction in times to ignition and an increase in heat release rate (with generally shorter times of burning). Exceptions to this were the FR-PC/ABS specimens (Figure 8), whose peak HRR values at 50 kW/m² and at 25 kW/m² were not very different from one another. The total heat release values for any given specimen were not very different over the three heat fluxes tested. Thus, since most of the

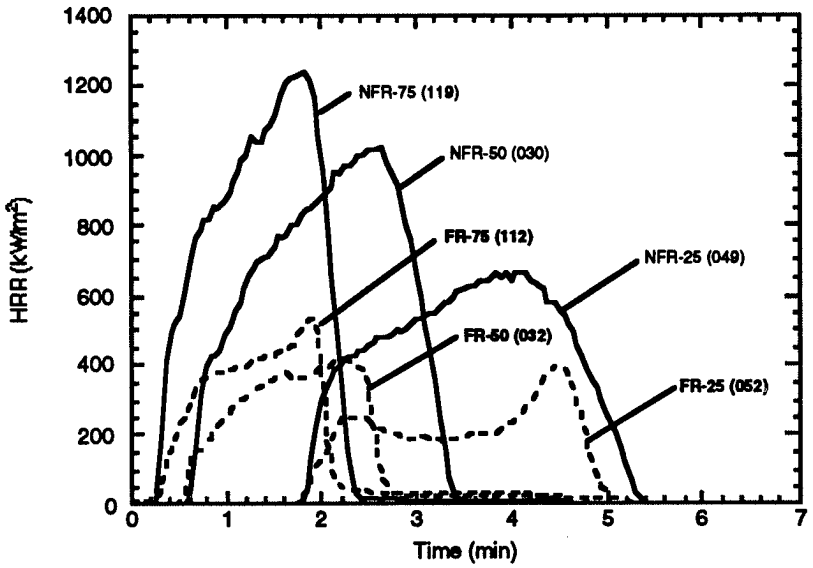

Figure 7. Heat Release Rate Curves for FR and NFR ABS at 25, 50, and 75 kW/m² Heat Flux

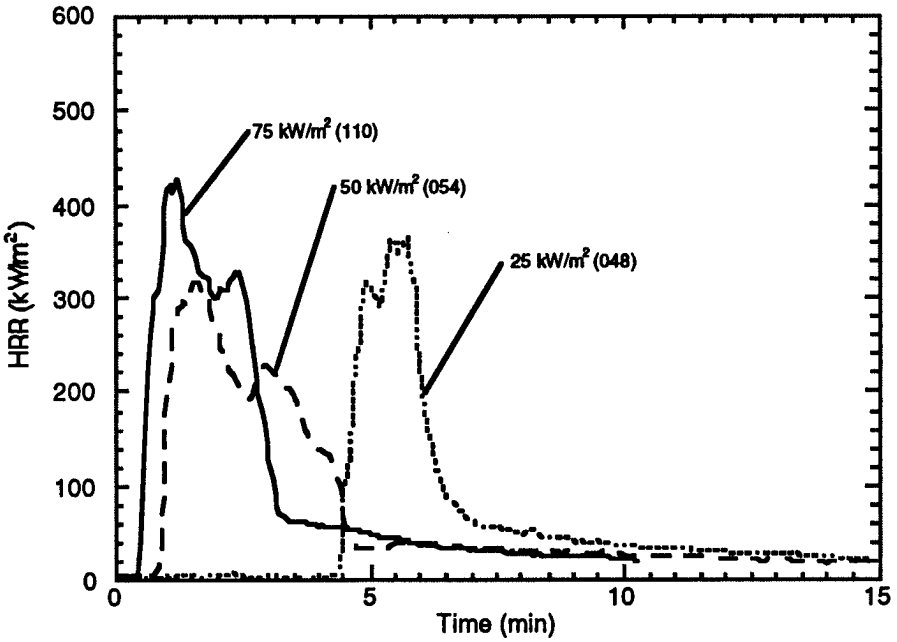

Figure 8. Heat Release Rate Curves for FR PC/ABS at 25, 50, and 75 kW/m² Heat Flux

specimens burned up totally over the duration of the experiment, the effective heats of combustion for any given sample were not substantially different over the heat flux range tested.

Mention should be made of the thicknesses of the specimens evaluated in this study. For the plaques sent to us, the thicknesses ranged from 2.5 to 7 mm. Whiteley[1] reported a study on the effect of specimen thickness on heat release results, in which he concluded that steady state burning (i.e., from a thermally thick specimen) required specimens of about 6 mm or more in

thickness. For our study, we accepted specimens in whatever thickness supplied, which was generally that of the usual commercial product. However, it should be noted that the thinner specimens may have HRR curves that will be substantially different from thicker ones and that they do not represent steady-state conditions. In any event, the comparisons in this study were all performed within a polymer/FR polymer group with the same specimen thicknesses.

Ignition and Heat Release as Functions of External Heat Flux

As previously described, the relationship between ignition delay time and external heat flux contains the term $k\rho c$, the thermal response parameter. This value is dependent on the response of a substance to heat and should be valuable in assessing the potential fire hazard of a substance. The reciprocal of the square root of the sustained ignition time was plotted against the external heat flux for several different materials ($k\rho c$ being proportional to the reciprocal of the slope).

An example of such a plot is shown in Figure 9. The results of the analysis of these data are presented in Table 2. Tewarson[2] has recommended using the reciprocal of the slope alone, which he calls the TRP, instead of $k\rho c$, so that one need not independently determine the ignition temperature. Both the TRP and the $k\rho c$ values (where we had determined ignition temperatures) are shown in the table.

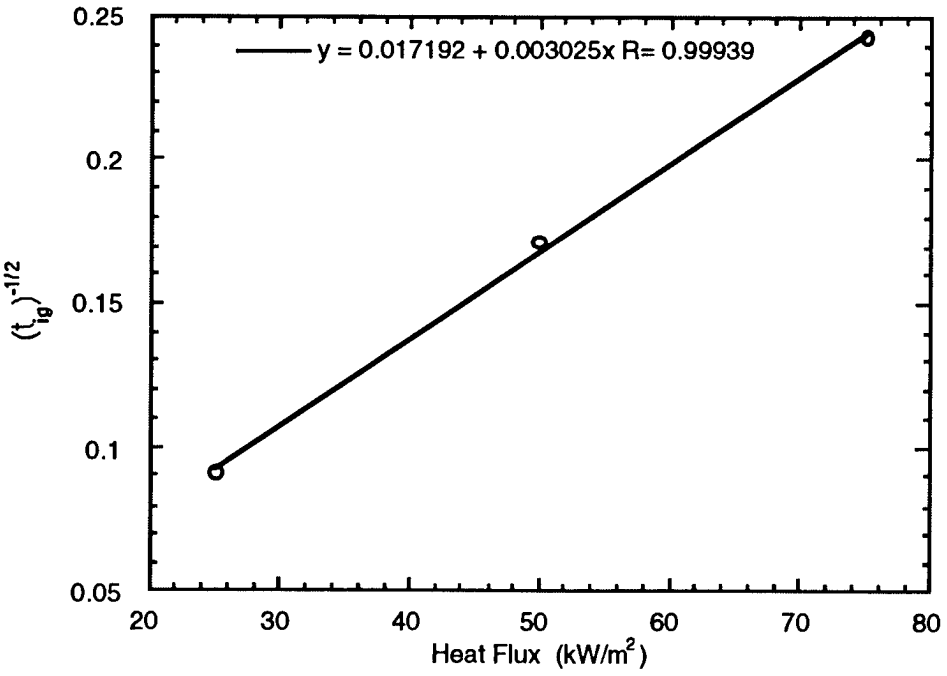

Figure 9. Ignition Delay Time as a Function of External Heat Flux for FR ABS

Apparently, there was very little difference in the thermal response parameter between the FR and non-FR ABS, HIPS, and PCABS. This was an unexpected result because one would anticipate that the FR polymers would perform better than the non-FR polymers in such an analysis. On the other hand, it is not a surprising result if one considers the lack of difference in ignition delay times. Further, the ignition temperatures of the FR and non-FR samples were not

substantially different. For the FR UPT and XPE specimens, however, the TRP values were significantly higher than for the non-FR materials. At this time, with a relatively limited database, it is uncertain whether or not the thermal response parameter actually reflects a lack of difference between certain FR and non-FR materials, or whether the thermal response parameter is an inadequate measure of the performance of such materials.

Although space precludes presentation of data on smoke and CO evolution from these products (data that were collected and analyzed as part of this program), it was felt that a brief note and an example plot (Figure 10) would be appropriate. Many FR agents have a tendency to increase the smoke evolution, as illustrated by the figure, compared to the non-FR polymer. Generally, this is thought to be due to the flame suppressing influence of the FR agent. Along with increased smoke evolution, one often sees increased evolution of carbon monoxide (CO), for the same reasons as the increase in smoke. In a hazard analysis, visible smoke and CO would offset some of the benefits of resistance to ignition and lowering of heat release rate. Not all of the FR agents showed an increase in smoke and CO, in fact those parameters were reduced for several of the specimens tested.

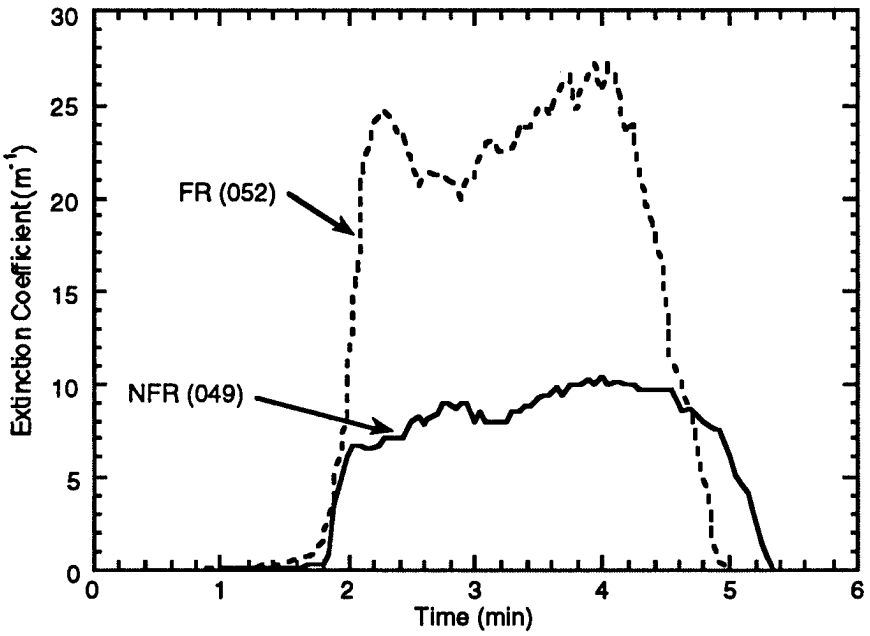

Figure 10. Smoke Extinction Coefficient for FR and Non-FR ABS

Additional analyses that may be performed on the data obtained from the cone calorimeter include plots of the 60 s avg. HRR values as a function of external heat flux. From these data one can obtain values that relate to the ease with which a material might continue burning in the absence of an external flux and to the minimum heat flux required to sustain combustion of the material. Another useful plot of the data from the cone calorimeter is that of mass loss rate (MLR) as a function of external heat flux. From such data, the heat of gasification may be estimated[3,4,5]. Also, information on the tendency for a material to char may be derived from such data. These analyses will be continued in the Phase II program.

The potential utility of cone calorimeter data obtained over a range of external heat fluxes has not been sufficiently explored by most researchers. It is possible that fundamental characteristics of burning materials may be derived from analysis of such data, which would allow the prediction of fire performance based on chemical structure and physical properties.

CONCLUSIONS

- The standard cone calorimeter apparatus and protocol proved to be very useful for evaluating the effectiveness of fire-retarded (FR) polymers under laboratory-simulated real fire conditions (elevated heat fluxes). Furthermore, with appropriate analysis of the results, it is an appropriate bench-scale test protocol for evaluating the unique contribution of FR additives under real-scale fire conditions.

- Common fire-retarded polymer systems, designed for today's markets, generally ignited and burned readily under flammability test conditions that more nearly reflect real fire scenarios. Although a hazard analysis assessment was not performed, it might be concluded from these results that the fire hazard of many of the FR polymers under simulated real fire conditions would not be substantially different from that of the non-FR polymers, taking into consideration ignition delay, heat release rate, and smoke and CO evolution.

FUTURE WORK

The primary objective of the future work study is to develop highly fire-resistant polymer systems that consist of thermally stable polymers combined with appropriate fire-retardant agents. These polymer systems will be developed to withstand high-temperature and high heat flux conditions in the presence of an ignition source. The polymers will be designed to possess good fire performance properties, including low ignitability, reduced heat release, and low smoke evolution; while maintaining sufficiently good physical properties to be useful in real applications.

A second objective, related to the primary one, is to compare the results among the fire test methods currently used or anticipated for future use in the evaluation of fire-resistant polymeric materials. A comparison among these fire test methods is essential to permit selection of the best tests for evaluating products for developmental purposes and to insure that the primary test methodology produces results that can be extrapolated to different fire scenarios. A fire hazard classification system will be recommended to bring together the efficacy of the fire-resistant polymer and the potential fire hazard associated with its proposed use.

There is enormous potential utility for truly fire-resistant polymeric materials in many areas of commerce, the military, and other government agencies. Any application where polymeric products are desirable but fire is a problem will benefit from this technology. New avenues for applicability will also become evident. Use of FR polymers could include commercial and military aircraft and ships (i.e., under the auspices of the FAA, Coast Guard, and military departments); aerospace; military fighting vehicles; and the interiors of buildings for commercial or military use.

Traditionally, the role of fire-retardant additives has been to slow the ignition of a flammable polymeric material under low heat flux conditions, as in a scenario where such a material is the first item ignited. Future applications of FR polymers, however, may require more stringent tests that can only be accommodated by combinations of additive or reactive fire-retardant chemicals in a thermally stable polymer.

REFERENCES

1. Whiteley, R. H., M. D. Sawyer, and M. J. McLoughlin, "Cone Calorimeter Studies of the Flame-Retardant Effects of Decabromodiphenyl Ether and Antimony Trioxide in Cross-Linked Polyethylene," Flame-Retardants '94, Interscience Communications Ltd., London, 1994.
2. Tewarson, A. "Flammability Parameters of Materials: Ignition, Combustion, and Fire Propagation," J. Fire Sciences, v. 12, July/August 1994, pp 329-356.

☆U.S. GOVERNMENT PRINTING OFFICE: 1998–704-401